

The Chemistry of Platinum Complexes and Hydrosilation

By

Danny Chan

A thesis submitted for the degree of
Doctor of Philosophy

University of York
Department of Chemistry

August 1999

**PAGE
NUMBERING
AS
ORIGINAL**

ABSTRACT

This thesis describes the study of a series of platinum complexes, with particular emphasis towards hydrosilation.

Platinum bis(phosphine) azodicarbonyl complexes $\text{Pt}(\text{PR}^1_3)_2(\text{R}^2\text{OCNNCOR}^2)$ ($\text{R}^1 = \text{Ph, Me}$; $\text{R}^2 = \text{Ph, Me, OEt, Pr}^i$) were synthesised and studied. Multinuclear NMR spectroscopy on $\text{Pt}(\text{PR}^1_3)_2(\text{R}^2\text{OCNNCOR}^2)$ revealed that the dicarbonyl substituted azo ligand is co-ordinated asymmetrically, consistent with a five membered, Pt-N-N-C-O ring. The crystal structure of $\text{Pt}(\text{PPh}_3)_2(\text{Pr}^i\text{O}_2\text{CNNCO}_2\text{Pr}^i)$ shows that the co-ordination sphere of platinum is essentially square planar and co-planar with the five-membered, Pt(1)-O(1)-C(5)-N(2)-N(1) ring. The $\text{Pt}(\text{PR}^1_3)_2(\text{R}^2\text{OCNNCOR}^2)$ complexes show sensitivity towards chlorinated solvents (CH_2Cl_2 , CHCl_3) under photolysis conditions forming the corresponding platinum bis(phosphine) dichloride complexes; the same products are formed in a slower thermal reaction but only for complexes with azodicarboxylate ligands. Complexes with azodicarboxylate ligands also react photochemically with ethylene in d_8 -THF yielding $\text{Pt}(\text{PPh}_3)_2(\text{C}_2\text{H}_4)$ but the azodiacyl analogues are inert in this respect.

Azodicarboxylate compounds $\text{RO}_2\text{CNNCO}_2\text{R}$ ($\text{R} = \text{Et, Pr}^i, \text{Bu}^t$) are inhibitors of the catalytic activity of $[(\text{Pt}\{\eta^4\text{-(CH}_2\text{=CHSiMe}_2)_2\text{O}\})_2\{\mu\text{-(CH}_2\text{=CHSiMe}_2)_2\text{O}\}]$ for the hydrosilation reaction. The inhibited species can be decomposed thermally or photochemically to give active hydrosilation catalysts. It was found that the bulky azo compound $\text{Bu}^t\text{O}_2\text{CNNCO}_2\text{Bu}^t$ was the least effective inhibitor of $[(\text{Pt}\{\eta^4\text{-(CH}_2\text{=CHSiMe}_2)_2\text{O}\})_2\{\mu\text{-(CH}_2\text{=CHSiMe}_2)_2\text{O}\}]$.

The photochemistry of platinum bis(phosphine) malonates and phthalates was found to be limited, and their reactivities were much lower compared to the analogous oxalate complexes.

Silyl hydride complexes, *cis*- $\text{Pt}(\text{PCy}_3)_2(\text{H})(\text{SiR}_3)$, were synthesised from the reaction of $\text{Pt}(\text{PCy}_3)_2$ and the corresponding silane. These complexes undergo dynamic exchange in solution. Two exchange processes were identified; the first involves mutual phosphine exchange, *i.e.* positional interchange between the hydride and the silyl ligands. The second process occurs at higher temperatures (above 290 K) and involves the elimination and re-addition of the silane ligand HSiR_3 . Thermodynamic and activation parameters are obtained for *cis*- $\text{Pt}(\text{PCy}_3)_2(\text{SiR}_3)$ ($\text{R} = \text{Ph, SiR}_3 = \text{SiMe}_2\text{CH}_2\text{CH=CH}_2, \text{SiMe}_2\text{Et}$). The reaction of $\text{Pt}(\text{PCy}_3)_2$ with the disilane $\text{HSiMe}_2(1,2\text{-C}_6\text{H}_4)\text{SiMe}_2\text{H}$ is thought to form a Pt(IV) bis(silyl) dihydride trigonal bipyramidal species of the form, $\text{Pt}(\text{PCy}_3)_2(\text{H})_2[\text{SiMe}_2(1,2\text{-C}_6\text{H}_4)\text{SiMe}_2]$, where the hydride ligands are in the axial positions. All of the platinum silyl hydride complexes studied degrade thermally to form *trans*- $\text{Pt}(\text{PCy}_3)_2(\text{H})_2$ at, or above, room temperature.

TABLE OF CONTENTS

Acknowledgements	vii
List of abbreviations	viii
CHAPTER 1: INTRODUCTION	
1.1 GENERAL BACKGROUND	3
1.2 THE HYDROSILATION REACTION	3
1.2.1 The Chalk-Harrod Mechanism for Hydrosilation	4
1.2.2 The modified Chalk-Harrod Mechanism for Hydrosilation	9
1.2.3 The Seitz-Wrighton Mechanism for Hydrosilation	10
1.2.4 The Two Silicon Cycle for Hydrosilation	11
1.2.5 Direct Evidence for Silyl Migration in the hydrosilation reaction	12
1.2.6 Ruthenium catalysed hydrosilation; formation of Si-C bond <i>via</i> both reductive elimination and silyl migration	15
1.2.7 Hydrosilation reactions involving colloidal platinum	17
1.2.8 Theoretical investigation of the hydrosilation reaction	20
1.3 SILANE ACTIVATION	21
1.3.1 Comparison between C-H and Si-H activation	22
1.3.2 Bonding in metal silyl hydride and η^2 -silane complexes	22
1.3.3 Fluxional behaviour of silyl hydride complexes	28
1.4 PHOTOACTIVATED HYDROSILATION CATALYSTS	29
1.4.1 Azo complexes	30
1.4.2 Oxalate complexes	31
1.5 OUTLINE OF THESIS	33
1.6 REFERENCES	34
CHAPTER 2: PLATINUM AZODICARBONYL COMPLEXES	
2.1 INTRODUCTION	41
2.2 RESULTS	43
2.2.1 Preparation of $\text{Pt}(\text{PR}^1_3)_2(\text{R}^2\text{OCNNCOR}^2)$ complexes [$\text{R}^1 = \text{R}^2 = \text{Ph}$ (1); $\text{R}^1 = \text{Me}, \text{R}^2 = \text{Ph}$ (3); $\text{R}^1 = \text{R}^2 = \text{Me}$ (4)]	43
2.2.2 NMR characterisation of $\text{Pt}(\text{PR}^1_3)_2(\text{R}^2\text{OCNNCOR}^2)$ complexes [$\text{R}^1 = \text{R}^2 = \text{Ph}$ (1); $\text{R}^1 = \text{Me}, \text{R}^2 = \text{Ph}$ (3); $\text{R}^1 = \text{R}^2 = \text{Me}$ (4)]	43

2.2.3 UV/VIS and IR spectroscopic data of 1 , 3 and 4	51
2.2.4 Preparation of Pt(PPh ₃) ₂ (R ² OCNNCOR ²) complexes [R ² = OEt (2), OPr ⁱ (5)]	54
2.2.5 NMR characterisation of Pt(PPh ₃) ₂ (R ² OCNNCOR ²) complexes [R ² = OEt (2) OPr ⁱ (5)]	55
2.2.6 UV/VIS and IR spectroscopic data of 2 and 5	55
2.2.7 Crystal Structure of Pt(PPh ₃) ₂ (Pr ⁱ O ₂ CNNCO ₂ Pr ⁱ)·(C ₆ H ₆) 5	55
2.2.8 Preparation of Pt(dppe)(R ² OCNNCOR ²) [R ² = OEt (6), OPr ⁱ (7)]	61
2.2.9 Reactions of Pt(PR ¹) ₂ (R ² OCNNCOR ²) complexes (R ¹ = Me, Ph; R ² = Me, Ph, OEt, OPr ⁱ)	62
2.3 DISCUSSIONS	62
2.3.1 Preparation of Pt(PR ¹) ₂ (R ² OCNNCOR ²) (R ¹ = Me, Ph; R ² = Me, Ph, OEt, OPr ⁱ) complexes containing a Pt–N–N–C–O metallacycle	62
2.3.2 Structure and bonding in azo complexes	63
2.3.2a Structure and bonding in azo carbonyl complexes	64
2.3.3 The <i>trans</i> -influence of the metallacycle in 1-7	68
2.3.4 Photochemical reactions of azodicarbonyl metallacycles	72
2.4 CONCLUSIONS	74
2.5 REFERENCES	74
CHAPTER 3: AZO-INHIBITED PLATINUM HYDROSILATION CATALYSTS	
3.1 INTRODUCTION	81
3.2 RESULTS	84
3.2.1 Preparation of [(Pt{η ⁴ -(CH ₂ =CHSiMe ₂) ₂ O}) ₂ (μ-(CH ₂ =CHSiMe ₂) ₂ O)] 8	84
3.2.2 Inhibition of [(Pt{η ⁴ -(CH ₂ =CHSiMe ₂) ₂ O}) ₂ (μ-(CH ₂ =CHSiMe ₂) ₂ O)] 8	87
3.2.2a Characterisation of azodicarboxylate inhibited 8	87
3.2.2b Photolysis of compounds 9-11 in THF	95
3.2.3 Hydrosilation using azo-inhibited 8	97
3.2.3a Model hydrosilation system	97
3.2.3b Photoactivation of azo-inhibited 8 in a model hydrosilation system	98
3.3 DISCUSSIONS	
3.3.1 Preparation of [(Pt{η ⁴ -(CH ₂ =CHSiMe ₂) ₂ O}) ₂ (μ-(CH ₂ =CHSiMe ₂) ₂ O)] 8	104
3.3.2 Inhibition of [(Pt{η ⁴ -(CH ₂ =CHSiMe ₂) ₂ O}) ₂ (μ-(CH ₂ =CHSiMe ₂) ₂ O)] 8	107
3.3.3 Effectiveness of EtO ₂ CNNCO ₂ Et, Pr ⁱ O ₂ CNNCO ₂ Pr ⁱ and Bu ^t O ₂ CNNCO ₂ Bu ^t as inhibitors of 8	109
3.4 CONCLUSIONS	110

CHAPTER 4: PLATINUM CARBOXYLATE COMPLEXES

4.1 INTRODUCTION	115
4.2 RESULTS	115
4.2.1 Preparation of platinum(II) carboxylate complexes	115
4.2.2 NMR characterisation of platinum(II) carboxylate complexes	116
4.2.3 IR characterisation of platinum(II) carboxylate complexes	121
4.2.4 Photolysis of platinum(II) carboxylate complexes	123
4.3 DISCUSSIONS	124
4.3.1 Preparation of platinum(II) carboxylate complexes	124
4.3.2 Reactivity of platinum(II) carboxylate complexes	124
4.4 CONCLUSIONS	127
4.5 REFERENCES	127

CHAPTER 5: PLATINUM SILYL HYDRIDE COMPLEXES

5.1 INTRODUCTION	131
5.1.1 Transition Metal Silyl Hydride complexes	131
5.1.2 Dynamic Processes Platinum Metal Silyl Hydride complexes	131
5.2 RESULTS	133
5.2.1 Preparation of <i>cis</i> -Pt(PCy ₃) ₂ (H)(SiR ₃) complexes	133
5.2.2 ¹ H and ³¹ P { ¹ H} NMR characterisation of <i>cis</i> -Pt(PCy ₃) ₂ (H)(SiR ₃)	134
5.2.3 Fluxional behaviour of <i>cis</i> -Pt(PCy ₃) ₂ (H)(SiR ₃)	138
5.2.3a Reversible silane dissociation in <i>cis</i> -Pt(PCy ₃) ₂ (H)(SiR ₃)	143
5.2.3b Exchange between <i>cis</i> -Pt(PCy ₃) ₂ (H)(SiR ₃) and free silane	146
5.2.4 Thermodynamic parameters for the free silane exchange process in <i>cis</i> -Pt(PCy ₃) ₂ (H)(SiR ₃)	149
5.2.4a Standard enthalpy and entropy of reaction for the dissociation of <i>cis</i> -Pt(PCy ₃) ₂ (H)(SiPh ₃) to Pt(PCy ₃) ₂ and HSiPh ₃	150
5.2.4b Standard enthalpy and entropy of reaction for the dissociation of <i>cis</i> -Pt(PCy ₃) ₂ (H)(SiMe ₂ CH ₂ CH=CH ₂) to Pt(PCy ₃) ₂ and HSiMe ₂ CH ₂ CH=CH ₂	151
5.2.4c Standard enthalpy and entropy of reaction for the dissociation of <i>cis</i> -Pt(PCy ₃) ₂ (H)(SiMe ₂ Et) to Pt(PCy ₃) ₂ and HSiMe ₂ Et	152
5.2.5 Activation parameters for the dynamic processes of <i>cis</i> -Pt(PCy ₃) ₂ (H)(SiR ₃) in solution	154

5.2.6 DNMR-SIM	154
5.2.6a Main Parameters	154
5.2.6b Configuration	155
5.2.6c Rate Constants	156
5.2.6d Population Levels	157
5.2.6e Comparison between simulated and observed spectra	157
5.2.7 Simulation of dynamic NMR spectra	157
5.2.7a Simulations of the dynamic NMR spectra of <i>cis</i> -Pt(PCy ₃) ₂ (H)(SiPh ₃) ₂	157
5.2.7b Simulations of the dynamic NMR spectra of <i>cis</i> -Pt(PCy ₃) ₂ (H)(SiMe ₂ CH ₂ CH=CH ₂)	161
5.2.7c Simulations of the dynamic NMR spectra of <i>cis</i> -Pt(PCy ₃) ₂ (H)(SiMe ₂ Et)	163
5.2.8 Thermal reactions of <i>cis</i> -Pt(PCy ₃) ₂ (H)(SiR ₃)	168
5.2.9 Photochemical reactions of <i>cis</i> -Pt(PCy ₃) ₂ (H)(SiR ₃)	170
5.2.9a Photolysis of <i>trans</i> -Pt(PCy ₃) ₂ (H) ₂ with HSiR ₃	171
5.2.10 Reaction of Pt(PCy ₃) ₂ with disilanes	173
5.3 DISCUSSIONS	175
5.3.1 Preparation of platinum silyl hydride complexes	175
5.3.2 Dynamic exchange in <i>cis</i> -Pt(PCy ₃) ₂ (H)(SiR ₃)	177
5.3.3 Photochemistry of <i>trans</i> -Pt(PCy ₃) ₂ (H) ₂ and <i>cis</i> -Pt(PCy ₃) ₂ (H)(SiR ₃)	184
5.3.4 Reactions of Pt(PCy ₃) ₂ with disilanes	185
5.4 CONCLUSIONS	188
5.5 REFERENCES	189
CHAPTER 6: EXPERIMENTAL	
6.1 GENERAL METHODS	193
6.2 SYNTHESIS AND REACTIONS OF PLATINUM BIS(PHOSPHINE) AZO DICARBONYL COMPLEXES	194
6.2.1 Preparation of Pt(PPh ₃) ₂ (PhOCNNCOPh) 1	194
6.2.2 Preparation of Pt(PPh ₃) ₂ (EtO ₂ CNNCO ₂ Et) 2	195
6.2.3 Preparation of Pt(PMe ₃) ₂ (PhOCNNCOPh) 3	195
6.2.4 Preparation of Pt(PMe ₃) ₂ (MeOCNNCOMe) 4	196
6.2.5 Preparation of Pt(PPh ₃) ₂ (Pr ⁱ O ₂ CNNCO ₂ Pr ⁱ) 5	196
6.2.6 Preparation of Pt(dppe)(EtO ₂ CNNCO ₂ Et) 6	197
6.2.7 Preparation of Pt(dppe)(Pr ⁱ O ₂ CNNCO ₂ Pr ⁱ) 7	197
6.2.8 X-ray crystallographic study of 5	197

6.2.9 Photolysis of Pt(PPh ₃) ₂ (PhOCNNCOPh) 1 , Pt(PMe ₃) ₂ (PhOCNNCOPh) 3 and Pt(PMe ₃) ₂ (MeOCNNCOMe) 4 with ethene or diphenylacetylene in C ₆ D ₆	197
6.2.10 Photolysis of Pt(PPh ₃) ₂ (PhOCNNCOPh) 1 , Pt(PMe ₃) ₂ (PhOCNNCOPh) 3 and Pt(PMe ₃) ₂ (MeOCNNCOMe) 4 with ethene or diphenylacetylene in CDCl ₃	198
6.2.11 Photolysis of Pt(PPh ₃) ₂ (EtO ₂ CNNCO ₂ Et) 2 and Pt(PPh ₃) ₂ (Pr ⁱ O ₂ CNNCO ₂ Pr ⁱ) 5 with ethene or diphenylacetylene in C ₆ D ₆	198
6.2.12 Thermal reactions of Pt(PPh ₃) ₂ (EtO ₂ CNNCO ₂ Et) 2 and Pt(PPh ₃) ₂ (Pr ⁱ O ₂ CNNCO ₂ Pr ⁱ) 5 with ethene or diphenylacetylene in C ₆ D ₆	198
6.3 SYNTHESIS AND REACTIONS OF AZO-INHIBITED PLATINUM HYDROSILATION CATALYSTS	198
6.3.1 Synthesis of [(Pt{η ⁴ -(CH ₂ =CHSiMe ₂) ₂ O}) ₂ (μ-(CH ₂ =CHSiMe ₂) ₂ O)] 8	198
6.3.2 Synthesis of PtCl ₂ (CH=CHPh) ₂	199
6.3.3 Synthesis of 8 with PtCl ₂ (CH=CHPh) ₂	199
6.3.4 Inhibition of 8 with RO ₂ CNNCO ₂ R to form 9 (R = Et), 10 , (R = Pr ⁱ) and 11 (R = Bu ^t)	199
6.3.5 Model hydrosilation system using 1-octene and 1,1,1,3,5,5,5-heptamethyl-trisiloxane	199
6.4 SYNTHESIS AND REACTIONS OF PLATINUM BIS(PHOSPHINE) CARBOXYLATE COMPLEXES	200
6.4.1 Preparation of Pt(dppe)(O ₂ CCH ₂ CO ₂) 12	200
6.4.2 Preparation of Pt(PMe ₃) ₂ [O ₂ C(1,2-C ₆ H ₄)CO ₂] 13	201
6.4.3 Preparation of Pt(COD)(O ₂ CCH ₂ CO ₂) 14	201
6.4.4 Photolysis of Pt(dppe)(O ₂ CCH ₂ CO ₂) 12	201
6.4.5 Photolysis of Pt(PMe ₃) ₂ [O ₂ C(1,2-C ₆ H ₄)CO ₂] 13	201
6.5 SYNTHESIS AND REACTIONS OF PLATINUM BIS(PHOSPHINE) SILYL HYDRIDE COMPLEXES	202
6.5.1 Preparation of Pt(PCy ₃) ₂	202
6.5.2 Preparation of <i>trans</i> -Pt(PCy ₃) ₂ (H) ₂	202
6.5.3 Preparation of <i>cis</i> -Pt(PCy ₃) ₂ (H)(SiPh ₃) 15	203
6.5.4 Preparation of <i>cis</i> -Pt(PCy ₃) ₂ (H)(SiMe ₂ CH ₂ CH=CH ₂) 16	203
6.5.5 Preparation of <i>cis</i> -Pt(PCy ₃) ₂ (H)(SiMe ₂ Et) 17	203
6.5.6 Preparation HSiMe ₂ OCH ₂ C(Me)=CH ₂	204
6.5.7 Preparation of <i>cis</i> -Pt(PCy ₃) ₂ (H)[SiMe ₂ OCH ₂ C(Me)=CH ₂] 18	204
6.5.8 Preparation of <i>cis</i> -Pt(PCy ₃) ₂ (H)[Si(OMe) ₂ CH ₂ CH=CH ₂] 19	204
6.5.9 Preparation of <i>cis</i> -Pt(PCy ₃) ₂ (H)(SiPh ₂ OSiPh ₂ H) 20	205
6.5.10 Reaction of Pt(PCy ₃) ₂ with HSiMe ₂ (1,2-C ₆ H ₄)SiMe ₂ H	205
6.5.11 Thermolysis of <i>cis</i> -Pt(PCy ₃) ₂ (H)(SiMe ₂ CH ₂ CH=CH ₂) 16	205

6.5.12 Photolysis of <i>cis</i> -Pt(PCy ₃) ₂ (H)(SiR ¹ ₂ R ²) [R ¹ = R ² = Ph (15); R ¹ = Me, R ² = CH ₂ CH=CH ₂ (16)]	206
6.5.13 Photolysis of <i>trans</i> -Pt(PCy ₃) ₂ (H) ₂ with HSiMe ₂ Et	206
6.5.14 Thermodynamic and kinetic measurements of dynamic processes in <i>cis</i> -Pt(PCy ₃) ₂ (H)(SiR ¹ ₂ R ²) [R ¹ = R ² = Ph (15); R ¹ = Me, R ² = CH ₂ CH=CH ₂ (16); R ¹ = Me, R ² = Et (17)]	207

ACKNOWLEDGEMENTS

I would first like to thank my two supervisors Robin Perutz and Simon Duckett for their guidance and encouragement during my DPhil. I am also extremely grateful to Dow Corning for a CASE studentship and I would like to especially acknowledge Peter Hupfield who made my stay at Dow Corning a very rewarding experience. Thanks also goes to Sylviane Sabo-Etienne and her group for the opportunity to visit the CNRS laboratories in Toulouse, special thanks go to Fabien Delpéch who acted as my constant guide (and translator) during my stay. I would also like to thank Leroy Cronin for the crystallographic work in chapter 2.

A big thank you also goes to past and present members of C121 and they are (in alphabetical order): Adelle, Aysin, Carmen, Cath, Catherine, Dave, Jeremy, Mike, Marisa, Naser, Ralf, Steve, Thomas and Virginia. A special mention is needed again for Naser for his “endless” supply of platinum. I would also like to thank Derek, John and Steve, my long suffering housemates, for putting up with all my mad stunts for the past four years.

Thanks also go to members of the technical and workshop staff for providing an excellent service. They are Barry, Davor and Roy (electronic workshop), Steve and Brian (glassblowing workshop), Barbara (NMR service) and Terry (Mechanical workshop) and Steve (Stores).

I would also like to thank all the totally insane but lovely people in the University of York Fencing club for providing welcome distractions and someone to stab.

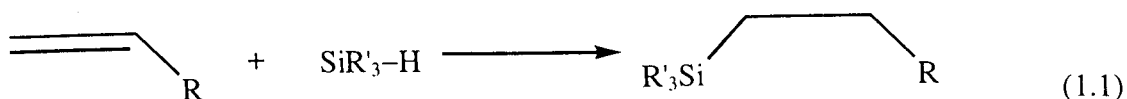
Finally I would like to thank my family for all their support throughout my studies.

CHAPTER 1

INTRODUCTION

1.1 GENERAL BACKGROUND

The hydrosilation, or hydrosilylation, reaction involves the addition of the Si–H bond across an unsaturated bond and plays an immensely important role in industry. Commercially, the hydrosilation reaction most commonly involves an unsaturated hydrocarbon, and leads to the formation of a new Si–C bond (Equation 1.1). This reaction can be used to generate a diverse range of novel organosilanes, cross-linked silicone polymers and cross-linked silicone co-polymers with organic monomers, some of its many applications being in silicone gels, rubbers and paper coatings.¹



In this thesis, we explore the thermal and photochemical reactivity of a variety of platinum complexes, the roles they play in the hydrosilation reaction and the type of interaction formed between the platinum metal centre and the Si–H bond of various silanes.

1.2 THE HYDROSILATION REACTION

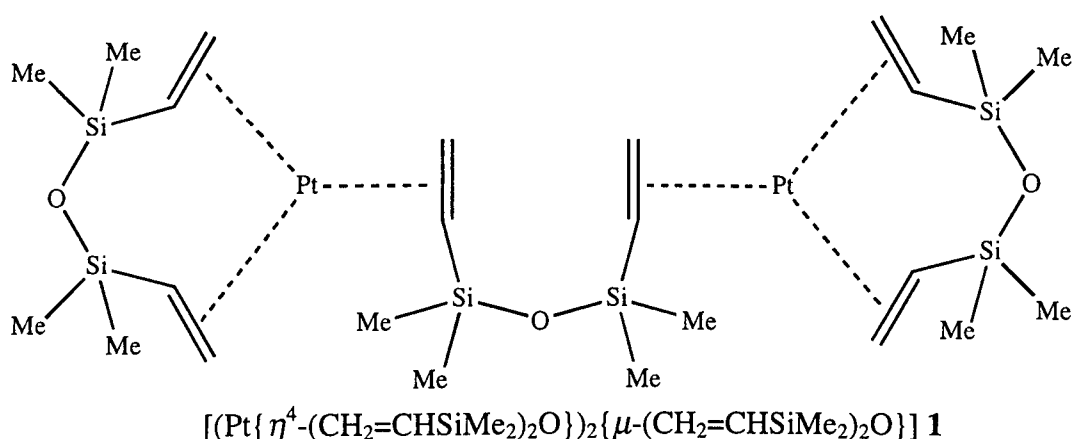
The hydrosilation reaction can take place by two distinct routes. The first route to be developed involved a free radical chain mechanism,^{2,3} and was initiated either thermally (*ca.* 300 °C),⁴ with UV or γ radiation,^{5,6} or with the use of a radical initiator, *e.g.* the decomposition of acyl peroxides⁷ or azonitriles.⁸ However, the main drawback of this pathway is that complex functional groups attached to the unsaturated hydrocarbon are rarely tolerant of the harsh conditions employed. Not surprisingly, these methods find little use in the industries of today.

The second pathway utilises transition metals to catalyse the hydrosilation reaction, and it is the method of choice today. The use of transition metal catalysts allows the hydrosilation reaction to proceed more smoothly, at lower temperatures and in higher yields. Speier pioneered the first commercially successful transition metal hydrosilation catalyst in the 1950s and prompted tremendous interest in the subject.⁹ In 1957, Speier showed chloroplatinic acid, H₂PtCl₆, also known as Speier's Catalyst, to be an extremely effective hydrosilation catalyst precursor,¹⁰ with as little as 10⁻⁵-10⁻⁸ moles of H₂PtCl₆ required per mole of Si–H function.¹¹

The catalytic hydrosilation reaction cycle was generally assumed to proceed initially *via* a platinum(0) species derived from a HSiR₃ induced reduction of H₂PtCl₆.¹² However, Lewis and co-workers have suggested that Speier's catalyst and other highly active platinum catalysts require the formation of colloidal platinum for hydrosilation.¹³

Lewis also offers an explanation for the induction period and oxygen sensitivity³ often observed for the catalysed hydrosilation reaction. This is discussed in Section 1.2.6.

In more recent years, Karstedt's catalyst, or solution, has been used most widely to catalyse the hydrosilation reaction. This catalyst is formed by the reaction of H_2PtCl_6 with vinylsiloxane.¹⁴ Lappert and co-workers found that reacting $\text{Pt}(\text{COD})_2$ with *sym*-tetramethyldivinylsiloxane, $(\text{H}_2\text{C}=\text{CHSiMe}_2)_2\text{O}$, yielded a catalytically active solution which has the same ^1H , ^{29}Si $\{^1\text{H}\}$ and ^{195}Pt $\{^1\text{H}\}$ NMR features as obtained for the reaction between H_2PtCl_6 and $(\text{H}_2\text{C}=\text{CHSiMe}_2)_2\text{O}$.¹⁵ They have also determined the crystal structure of the precursor to the active catalyst which corresponds to the species $[(\text{Pt}\{\eta^4\text{-(CH}_2=\text{CHSiMe}_2)_2\text{O}\})_2\{\mu\text{-(CH}_2=\text{CHSiMe}_2)_2\text{O}\}]$ **1**, with one bridging and two chelating $(\text{H}_2\text{C}=\text{CHSiMe}_2)_2\text{O}$ ligands.

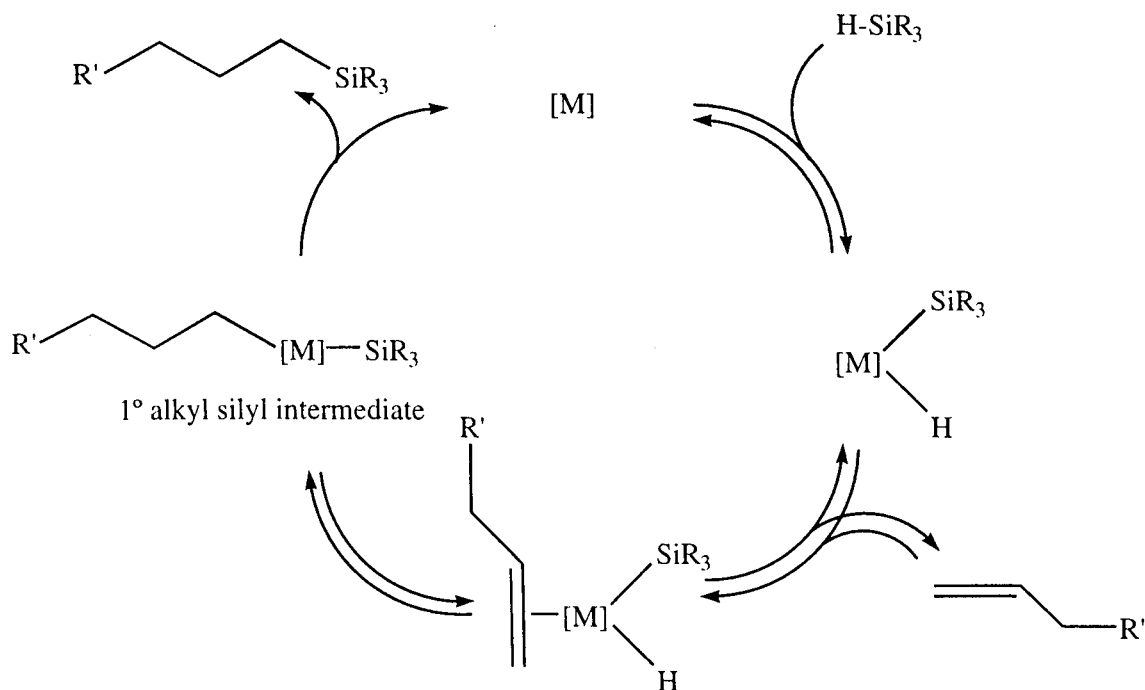


Besides platinum, complexes of other transition metals have also been found to be active as hydrosilation catalysts. These include Rh, Co, Ru, Pd and Ni,^{3,11} and the studies on these and other metals have led to the identification of key intermediates. This has helped to construct a more detailed and accurate understanding of the individual steps involved in the hydrosilation mechanism for a homogeneous system catalysed by transition metals.

1.2.1 The Chalk-Harrod Mechanism for Hydrosilation

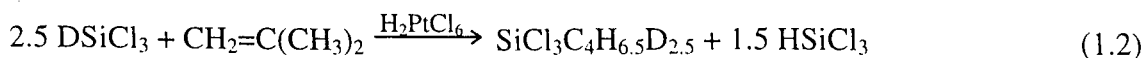
The first and most widely accepted mechanism for the transition metal catalysed hydrosilation reaction was proposed by Chalk and Harrod in 1965. In their studies of the reaction between 1-hexene and various silanes initiated by platinum(II) and rhodium(I) olefin complexes,¹⁶ they proposed a mechanism which initially involves the oxidative addition of the Si-H bond to a catalytically active transition metal centre, yielding a metal silyl hydride intermediate. This is then followed by alkene addition and hydride transfer to form a metal alkyl silyl intermediate. The final step of the catalytic cycle sees

the reductive elimination of the alkyl and silyl groups to produce the organosilane product, regenerating the active transition metal catalyst in the process (Scheme 1.1).



Scheme 1.1 The Chalk-Harrod mechanism for olefin hydrosilylation.¹⁷

Studies by Speier *et al.* on the addition of DSiCl_3 to a series of terminal olefins have shown that extensive exchange occurs between the Si–D group of the deuterated silane and the C–H group of the alkene, along with alkene isomerisation (Equation 1.2).¹⁸

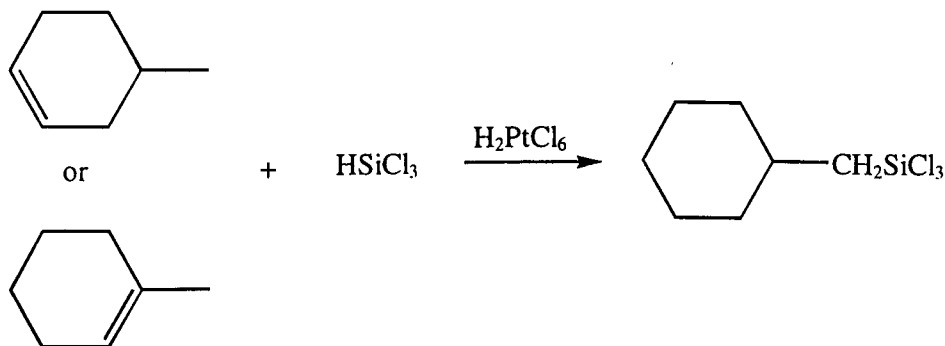


Speier also reacted isobutene with DSiCl_3 in the presence of H_2PtCl_6 and found the product, isobutyltrichlorosilane, was 70 % deuterated at the tertiary position and deuterium was found in every other possible position so that an average of 2.5 deuterium atoms were present in each molecule of the product.¹⁸ This observation supports the reversibility of the steps shown in Schemes 1.1 and 1.3.

Interestingly, isomerisation of alkenes often occurs during hydrosilylation with long chain terminal alkenes converting to internal alkenes which are thermodynamically more favourable and often unreactive to hydrosilylation.^{19,20} Haszeldine *et al.* studied the hydrosilylation of 1-hexene with various silanes using Wilkinson's complex, $\text{Rh}(\text{PPh}_3)_3\text{Cl}$, to catalyse the reaction. They found that when using HSiPh_3 , 100 % conversion to the *n*-hexylsilane was obtained but only 70 % and 8 % *n*-hexylsilane was formed when HSiEt_3 and HSiCl_3 were used, respectively. The rest of the 1-hexene had

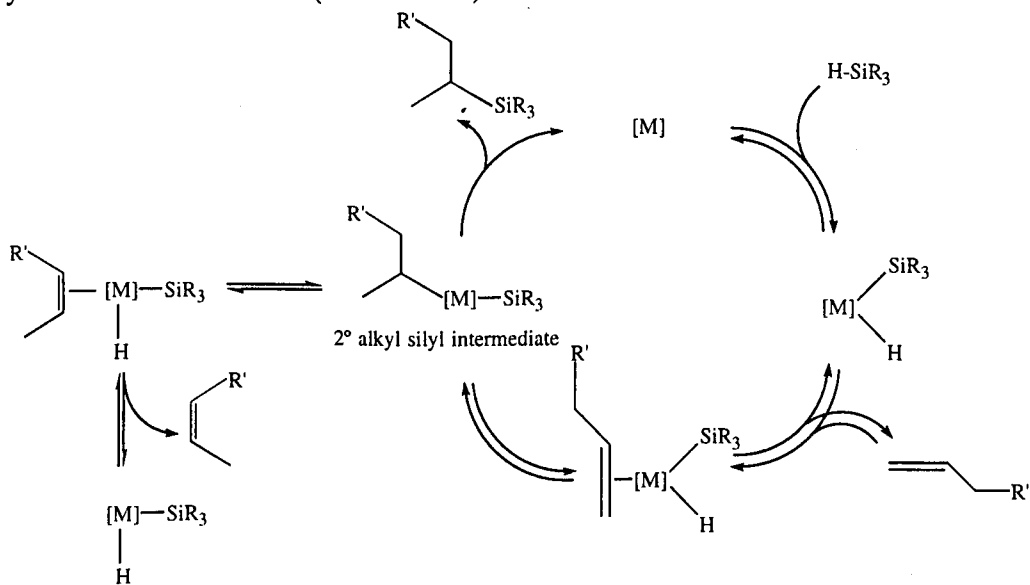
undergone complete isomerisation to internal hexenes. From this observation it would appear that alkene isomerisation is in direct competition with hydrosilation.

Internal alkenes have been reported to undergo hydrosilation, but only after isomerisation of the alkene. Speier reacted a series of methylcyclohexenes with HSiCl_3 to form $\text{SiCl}_3(\text{C}_7\text{H}_{13})$ (Scheme 1.2).^{18,21} This study demonstrated that the preferred location of the silyl group is at the terminal alkene positions over any internal positions.



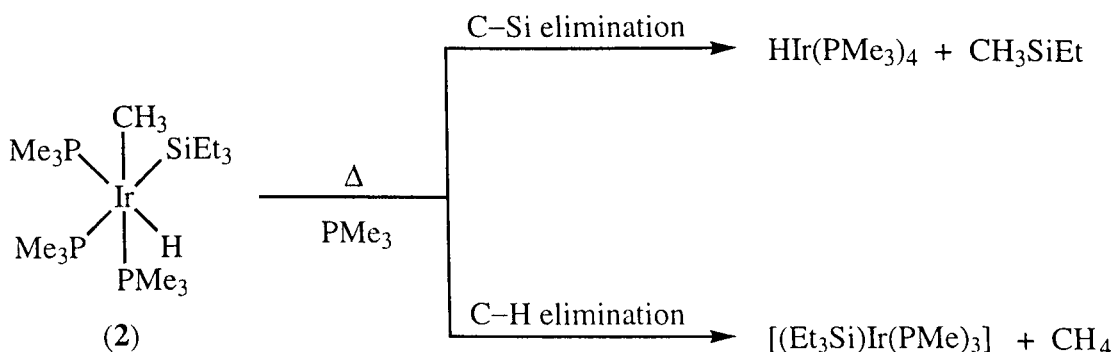
Scheme 1.2 Hydrosilation of methylcyclohexenes with trichlorosilane.

The proposed mechanisms for the isomerisation of alkenes generally involves either a metal alkyl hydride or an η^3 -allyl metal intermediate.²² Chalk and Harrod proposed that the isomerisation of alkenes during the hydrosilation reaction can occur after the formation of the metal silyl hydride alkene intermediate (Scheme 1.3).¹⁶ This can go on to form either the primary (1°) or secondary (2°) alkyl silyl intermediate. If alkene isomerisation occurs, then the 2° alkyl silyl intermediate either reductively eliminates to form a 3° organosilane product or undergoes β -hydride elimination to yield an internal alkene (Scheme 1.3).



Scheme 1.3 Chalk-Harrod mechanism for alkene hydrosilation, involving alkene isomerisation.¹⁷

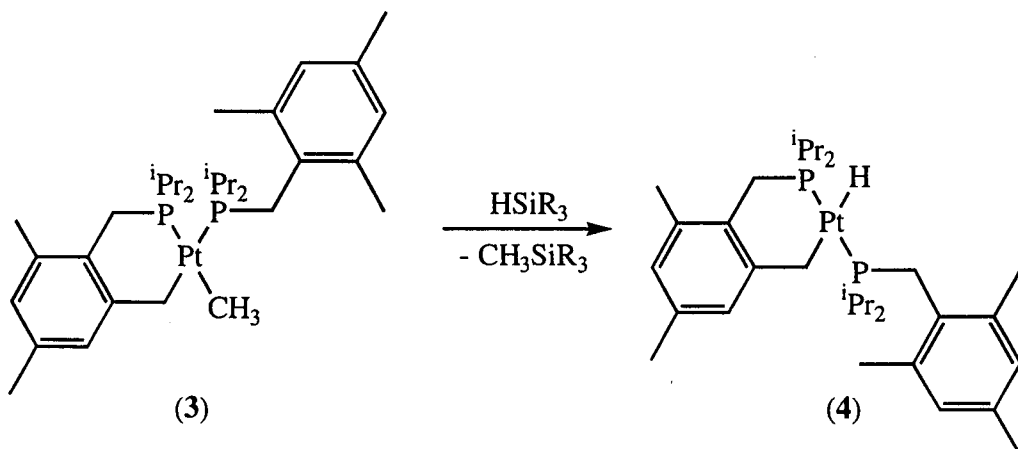
It should be noted, however, that alkyl silyl reductive elimination is not a common process and only a few examples have been documented. The first stoichiometric example was reported by Gladysz and co-workers.²³ They found that $\text{Fe}(\text{CO})_4(\text{SiMe}_3)\text{R}$ ($\text{R} = \text{alkyl}$) decomposed slowly at room temperature to yield RSiMe_3 . Later Milstein and co-workers demonstrated that competitive C–H and Si–C reductive elimination occurs in the Ir(III) complex, $\text{Ir}(\text{PMe}_3)_3(\text{H})(\text{SiEt}_3)(\text{CH}_3)$ **2**, to form CH_4 or SiMeEt_3 (Scheme 1.4).²⁴



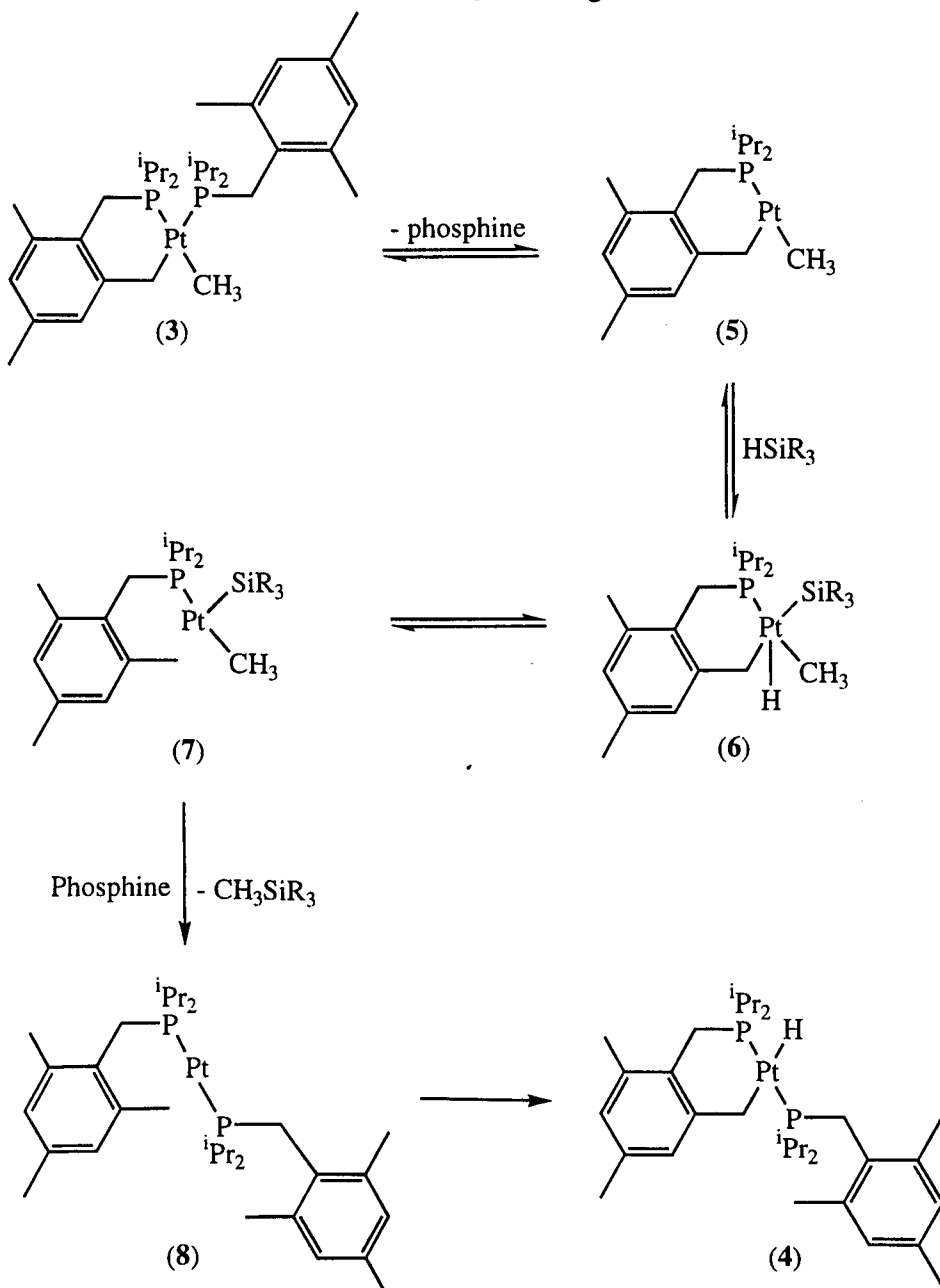
Scheme 1.4 Competitive C–H and C–Si elimination in $\text{Ir}(\text{PMe}_3)_3(\text{H})(\text{SiEt}_3)(\text{CH}_3)$ **2**.²⁴

More recently, Milstein and co-workers were able to demonstrate exclusive Si–C bond formation from the reaction of a platinum(II) alkyl complex **3**, with various silanes (Scheme 1.5), but they were uncertain of the explanation for this observation.²⁵ However, they did propose that phosphine can dissociate from **3** to form **5** (Scheme 1.6). This was said to be due to the strong *trans*-influence of the σ -benzyl ligand and the steric hindrance of the cyclometallated ligand. Si–H oxidative addition to the coordinatively unsaturated metal centre in **5** would then afford **6**, a Pt(IV) species. Three possible pathways are available from **6**, the first is Si–H reductive elimination, the second is C–H reductive elimination and the third is Si–C reductive elimination. They argued that because of the strong *trans*-influence of silyl ligands, which is comparable with or even higher than that of hydride ligands,²⁶ $\text{ArCH}_2\text{–H}$ formation, a reverse cyclometallation process to **7**, might be preferred over CH_4 or CH_3SiR_3 formation.²⁷ This would then allow Si–C reductive elimination to yield the Pt(0) species **8**, which can undergo cyclometallation to form the final product **4**.

Ozawa *et al.* have also demonstrated that facile Si–C reductive elimination occurs in *cis*- $\text{PtMe}(\text{SiPh}_3)(\text{PMePh}_2)_2$ **9** to give MeSiPh_2 and a platinum(0) species.²⁸ This was an unexpected result since *cis*- $\text{PtMe}_2(\text{PMePh}_2)_2$ **10** is thermally inactive towards reductive elimination.²⁹



Scheme 1.5 Reaction of **3** with HSiR_3 resulting in exclusive Si–C bond formation.²⁵



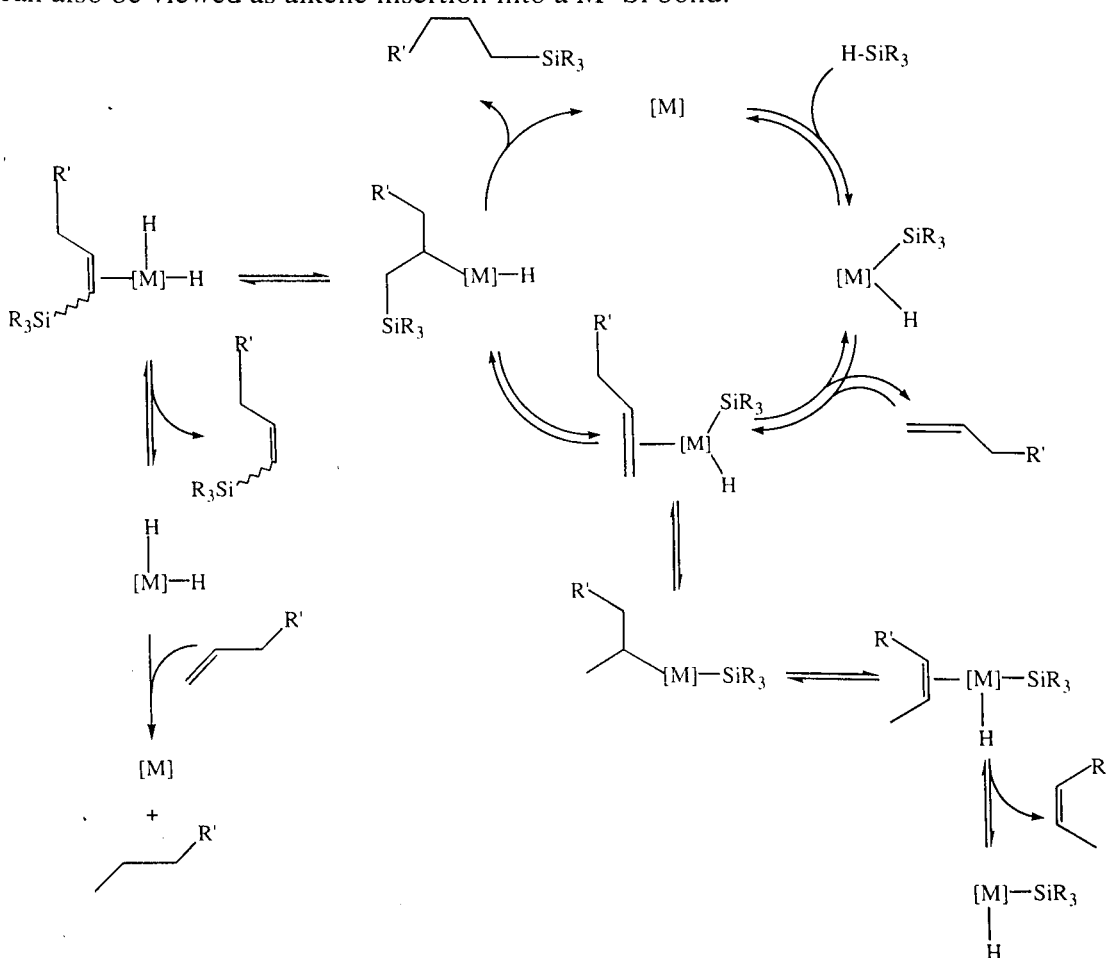
Scheme 1.6 Possible pathway for Si–C formation in the reaction between **3** and HSiR_3 .²⁵

1.2.2 The modified Chalk-Harrod Mechanism for Hydrosilation

Wrighton *et al.* were the first to propose a modified version of the Chalk-Harrod mechanism¹⁶ which identified a pathway for Si–C bond formation³⁰ other than Si–C reductive elimination.^{23,24,25,28} Their modified Chalk-Harrod mechanism also provides a plausible pathway for the silation reaction, *i.e.* formation of vinyl silanes (Equation 1.3),³¹ which sometimes occurs during hydrosilation.



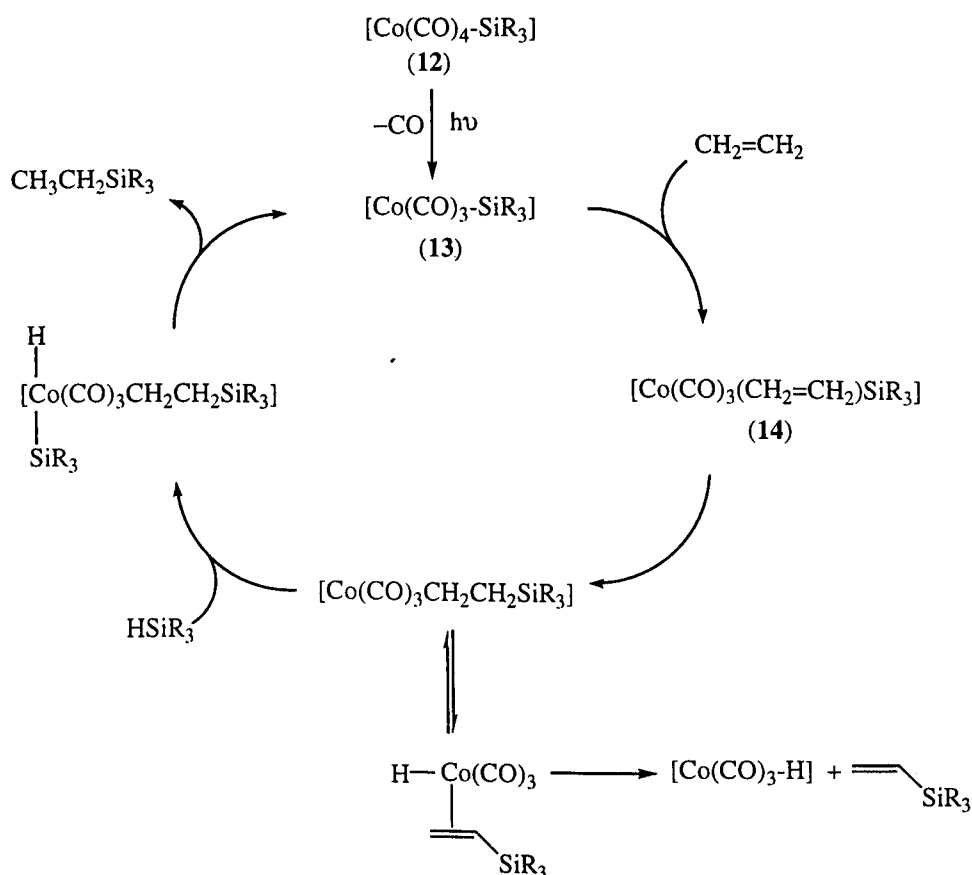
Wrighton studied the catalytic activities of $\text{Fe}(\text{CO})_5$ **11** under irradiation in the presence of an alkene and various silanes and found good conversion to a mixture of alkane, alkylsilane and vinylsilane products.³⁰ They proposed that a silyl group migration, instead of a hydride migration, was the step responsible for the formation of the Si–C bond (Scheme 1.7). Subsequent C–H reductive elimination leads to the hydrosilation product, whilst β -hydride elimination forms a vinylsilane and an alkane (Scheme 1.7). It is important to note that the classification between migration and insertion reactions is subjective and generally has no mechanistic implications. According to Braunstein and Knorr, silyl group migration onto a co-ordinated alkene can also be viewed as alkene insertion into a M–Si bond.³²



Scheme 1.7 The modified Chalk-Harrod Mechanism.¹⁷

1.2.3 The Seitz-Wrighton Mechanism for Hydrosilation

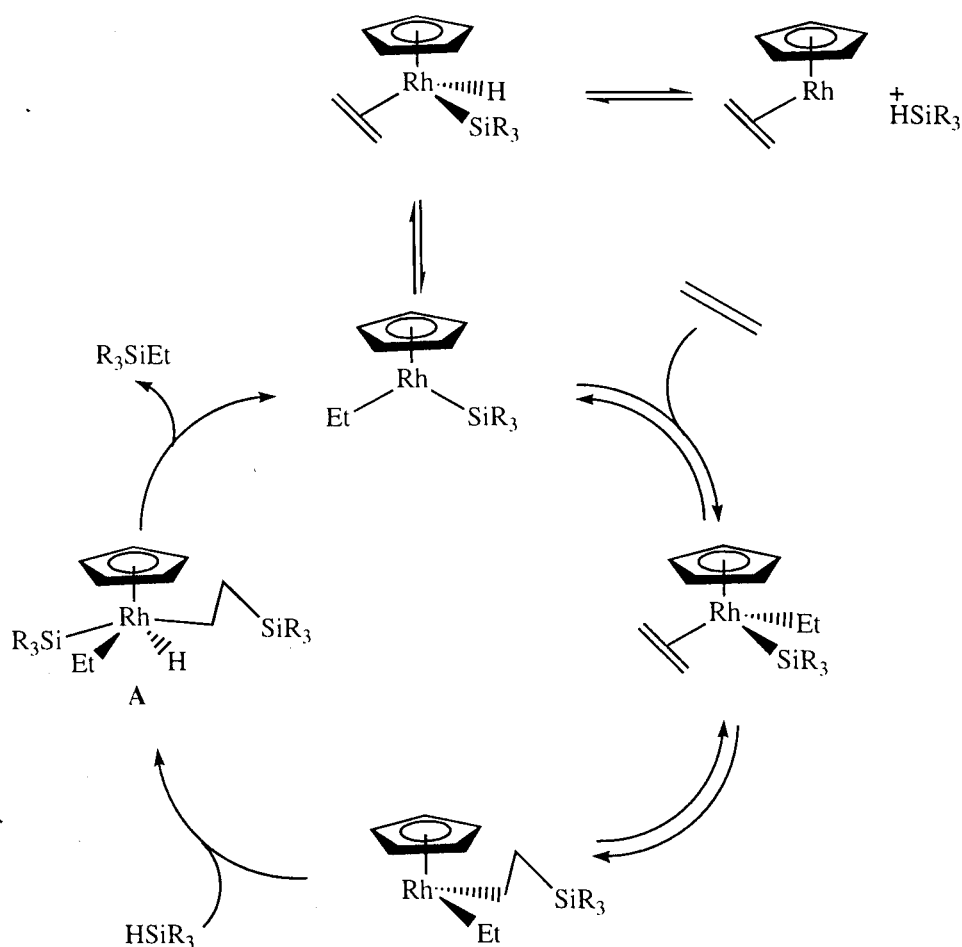
Seitz and Wrighton later produced more evidence that silyl migration could occur during hydrosilation by establishing that $\text{Co}(\text{CO})_4(\text{SiEt}_3)$ **12**, an effective hydrosilation catalyst, undergoes alkene insertion into the Co–Si bond upon photolysis in the presence of silane, and under an atmosphere of ethene (Scheme 1.8).³³ In Seitz and Wrighton's mechanism (Scheme 1.8), **12** loses CO upon photolysis to generate the co-ordinatively unsaturated 16-electron species, $\text{Co}(\text{CO})_3(\text{SiEt}_3)$ **13**, which can be observed by FTIR in a methylcyclohexane or ethene matrix at 77 K.³⁴ The next step sees the co-ordination of ethene to the unsaturated complex to form $\text{Co}(\text{CO})_3(\text{CH}_2=\text{CH}_2)(\text{SiR}_3)$ **14**, observable by ^1H NMR spectroscopy, and it is then followed by insertion of ethene into the Co–Si bond in the presence of silane. The silane then oxidatively adds to the cobalt centre and a C–H reductive elimination completes the cycle. Unlike the modified Chalk-Harrod mechanism in Scheme 1.7, the catalytic cycle proposed by Seitz and Wrighton (Scheme 1.8) does not involve the formation of a metal ethene silyl hydride and silyl migration occurs before oxidative addition of the silane to the metal. Studies by Wrighton on the iron complex, $(\eta^5\text{-C}_5\text{Me}_5)(\text{CO})_2\text{Fe}(\text{SiR}_3)$ **15**, have also provided similar evidence supporting the mechanism in Scheme 1.8.³⁵



Scheme 1.8 The Seitz-Wrighton Mechanism for Hydrosilation.³³

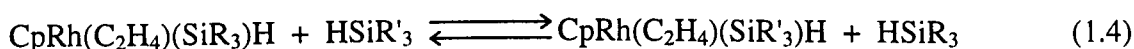
1.2.4 The Two Silicon Cycle for Hydrosilation

Perutz and co-workers have shown that on photolysing the rhodium(I) complex, $\text{CpRh}(\text{C}_2\text{H}_4)_2$ **16**, in the presence of various silanes, the rhodium(III) complex $\text{CpRh}(\text{C}_2\text{H}_4)(\text{SiR}_3)\text{H}$ is formed, as are various hydrosilation and silation products.³⁶ $\text{CpRh}(\text{C}_2\text{H}_4)(\text{SiR}_3)\text{H}$ was found to catalyse the hydrosilation reaction and contains all the ligands for the key intermediate found in the Chalk-Harrod mechanism (Scheme 1.1 and 1.3).¹⁶ Duckett and Perutz later demonstrated, through deuterium labelling, cross-alkene and cross-silane experiments, that silyl migrations were operative in their system and concluded that $\text{CpRh}(\text{C}_2\text{H}_4)(\text{SiR}_3)\text{H}$ is actually a catalyst precursor and lies outside the catalytic cycle.³⁷ They proposed that the active catalytic species in their system is in fact $\text{CpRh}(\text{C}_2\text{H}_5)\text{SiR}_3$, where the ethyl group is only a spectator in the hydrosilation reaction. Like Seitz and Wrighton's mechanism,³³ the "Two Silicon Cycle", proposed by Duckett and Perutz, has the key feature of alkene inserting into the metal silicon bond and an intermediate **A** containing two SiR_3 groups (Scheme 1.9). In fact, this cycle is equivalent to that of Seitz and Wrighton's³³ with $\text{Co}(\text{CO})_3$ replaced by CpRhEt . Although silation products were present in the hydrosilation system studied by Duckett and Perutz, no mechanistic pathway was proposed for their formation.



Scheme 1.9 The "Two Silicon Cycle" for Hydrosilation.³⁷

Duckett and Perutz found that the hydrosilation of C_2D_4 in the presence of $CpRh(C_2H_4)(SiEt_3)H$ **17** failed to produce significant quantities of $CpRh(C_2D_4)(SiEt_3)H$ **18** and concluded that the ethene ligand in the rhodium(III) complex is not directly involved in the hydrosilation reaction. The silyl group in $CpRh(C_2H_4)(SiR_3)H$, however, does play a part in the hydrosilation reaction since hydrosilation of ethene with $HSiR'_3$ resulted in the formation of $CpRh(C_2H_4)(SiR'_3)H$. However, reductive elimination of SiR_3H and oxidative addition of SiR'_3H to rhodium is another possible pathway for silane exchange (Equation 1.4).³⁸ Duckett and Perutz demonstrated that hydrosilation of ethene and $HSi[CH_2CH(CH_3)_2]_3$ with $CpRh(C_2H_4)(SiMe_3)H$ **19** produced 30 % $CpRh(C_2H_4)\{Si[CH_2CH(CH_3)_2]_3\}H$ **20** after 7 days whereas a mixture of $HSi[CH_2CH(CH_3)_2]_3$ and **19** produced only 10 % **20** after 9 days.

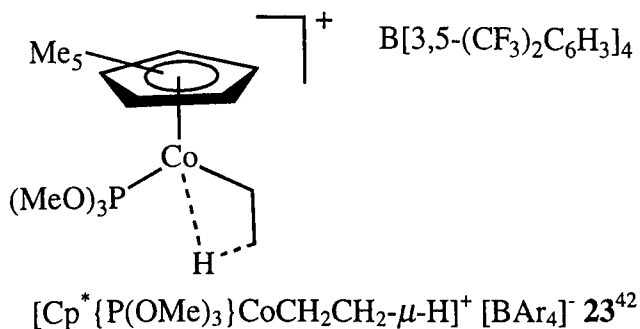


The formation of the $CpRh(C_2H_4)$ **21** fragment³⁹ in the catalytic cycle was ruled out by Duckett and Perutz because of the high Rh(I)/Rh(III) product ratio (1.0:0.6), generated during the hydrosilation of ethene and $HSiPr^i_3$ with $CpRh(C_2H_4)(SiEt_3)H$ **17**. Laser flash photolysis studies have demonstrated that $HSiEt_3$ reacts much faster with **21** than ethene which is contrary to the observations made by Duckett and Perutz if **21** is involved in the hydrosilation reaction.³⁹

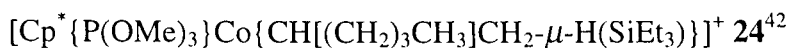
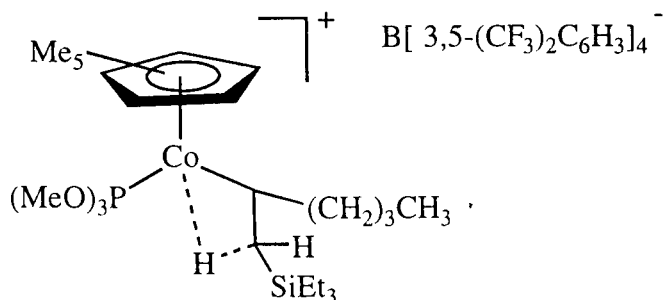
According to Duckett and Perutz, the formation of the rhodium(V) intermediate, $CpRh(SiR_3)_2(H)_2$, in their mechanism (Scheme 1.9) was plausible because this oxidation state is accessible and has been known to catalyse the hydrosilation reaction, *e.g.* $Cp^*Rh(SiEt_3)_2(H)_2$ **22**.⁴⁰

1.2.5 Direct Evidence for Silyl Migration in the hydrosilation reaction

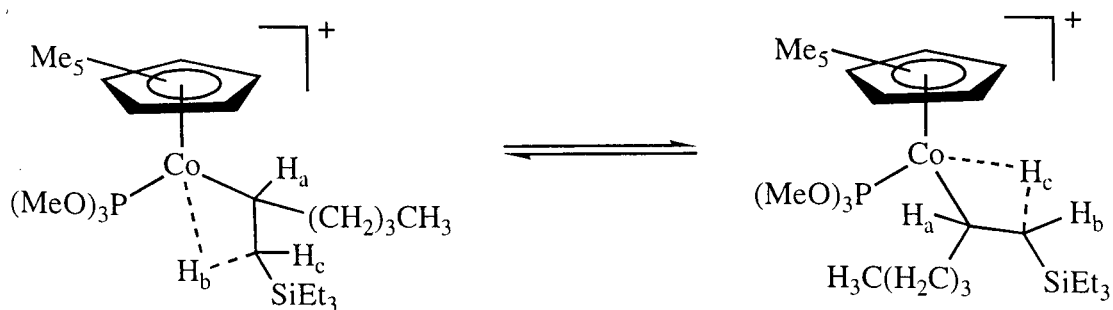
Brookhart *et al.*'s studies on alkene polymerisation and oligomerisation⁴¹ catalysed by the electrophilic Co(III) complex, $[Cp^*\{P(OMe)_3\}CoCH_2CH_2-\mu-H][BAr_4]$ **23**, led them to investigate the hydrosilation of alkenes.⁴²



Brookhart found the hydrosilation of 1-hexene with HSiEt_3 catalysed by **23** yielded exclusively $\text{Et}_3\text{Si}(\text{CH}_2)_5\text{CH}_3$ in 75 % yield. Low temperature ^1H NMR spectroscopy of the working catalyst solution revealed the formation of ethane in the early stages of the hydrosilation reaction between 1-hexene and HSiEt_3 . Also, an intermediate formed *in situ*, at low temperature, during hydrosilation was identified by Brookhart as $[\text{Cp}^*\{\text{P}(\text{OMe})_3\}\text{Co}\{\text{CH}[(\text{CH}_2)_3\text{CH}_3]\text{CH}_2-\mu\text{-H}(\text{SiEt}_3)\}]^+$ **24**.



The identity of the intermediate **24** has provided direct evidence for silyl migration during the cobalt catalysed hydrosilation reaction. Brookhart has also shown by dynamic ^1H NMR spectroscopy that **24** undergoes inversion at the cobalt centre (Scheme 1.10).⁴²

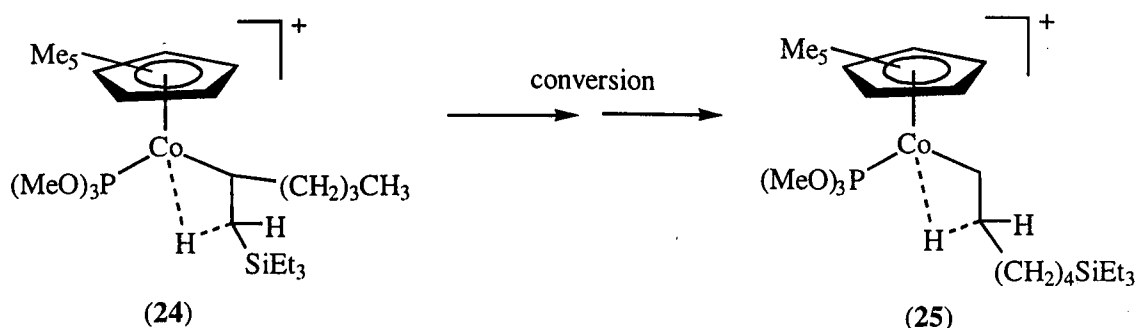


Scheme 1.10 Inversion at Co in **24**.⁴²

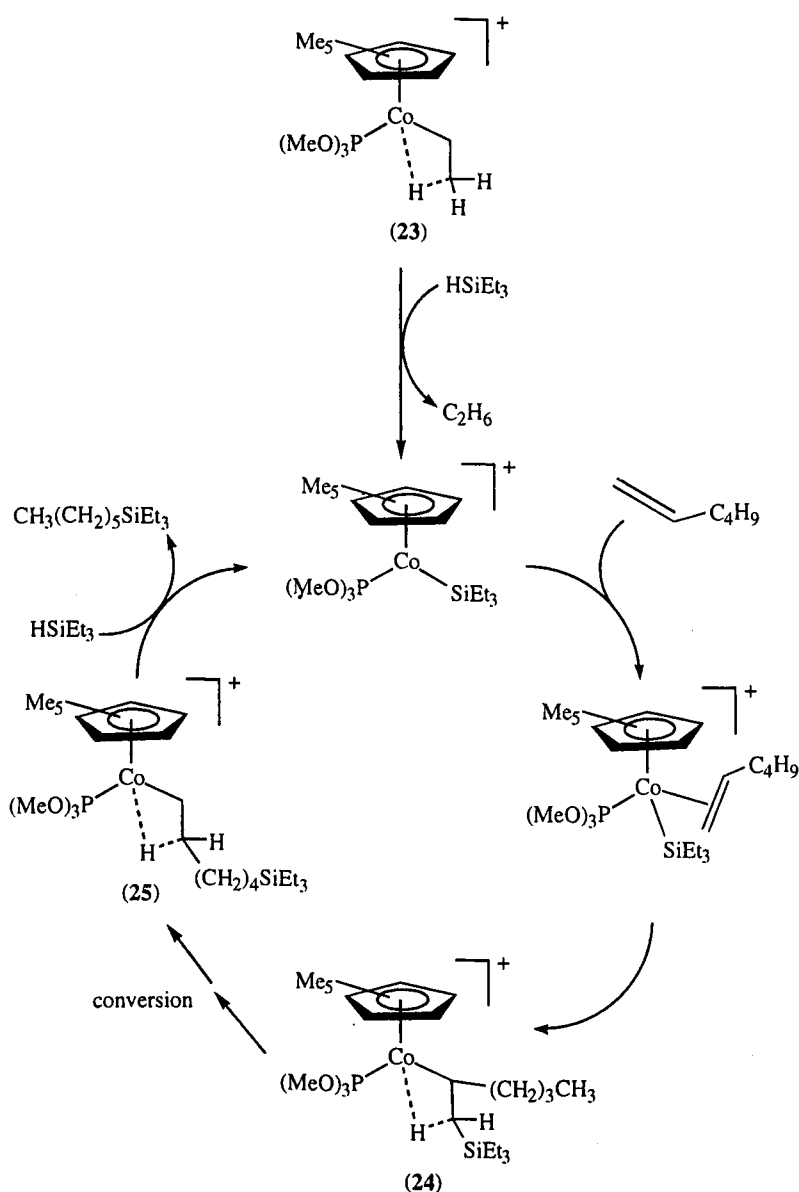
From further low temperature ^1H NMR studies, Brookhart found that the intermediate **24** undergoes a number of β -elimination/migratory insertion steps to form a series of alkyl substituted agostic species. One of these species, **25**, was determined to be part of the catalytic cycle from deuterium labelling experiments (Scheme 1.11). The overall pathway proposed by Brookhart can be seen in Scheme 1.12.

The mechanisms proposed by Brookhart *et al.*,⁴² Duckett and Perutz,³⁸ and Seitz and Wrighton³³ are all very similar in that all three mechanisms have silyl migration, or alkene insertion, as the key step in the formation of the Si-C bond. Also, these

mechanisms do not have a metal alkene silyl hydride intermediate as part of the catalytic cycle which is found in Chalk and Harrod's mechanism and its variant.^{16,30}



Scheme 1.11 Conversion of **24** to **25** during the hydrosilation of 1-hexene with HSiEt_3 .⁴²

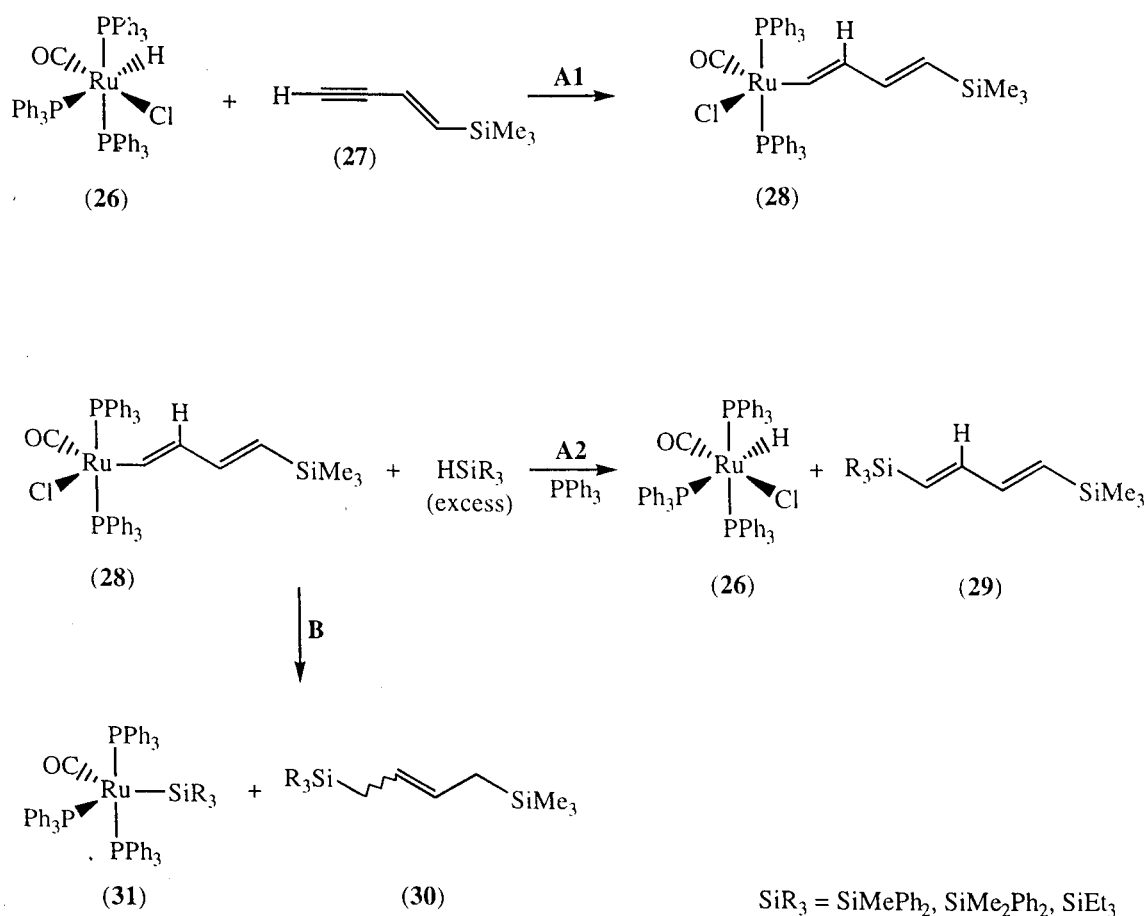


Scheme 1.12 Overall pathway for the hydrosilation of 1-hexene using **23**.⁴²

1.2.6 Ruthenium catalysed hydrosilation, formation of Si–C bond *via* both reductive elimination and silyl migration.

Ozawa and co-workers⁴³ have recently proposed that Si–C bond formation during hydrosilation can occur *via* both reductive elimination and silyl migration in the same system. This incorporates all the key steps found in the Chalk-Harrod and variants of the Chalk-Harrod mechanism, *ie.* Si–C reductive elimination and alkene insertion, or silyl migration.^{16,30,33,35,37,42} Ozawa and co-workers found that the ruthenium hydride complex, $\text{RuHCl}(\text{CO})(\text{PPh}_3)_3$ **26**, was able to catalyse the hydrosilation of 1-(trimethylsilyl)-1-butene-3-yne **27** with various silanes.

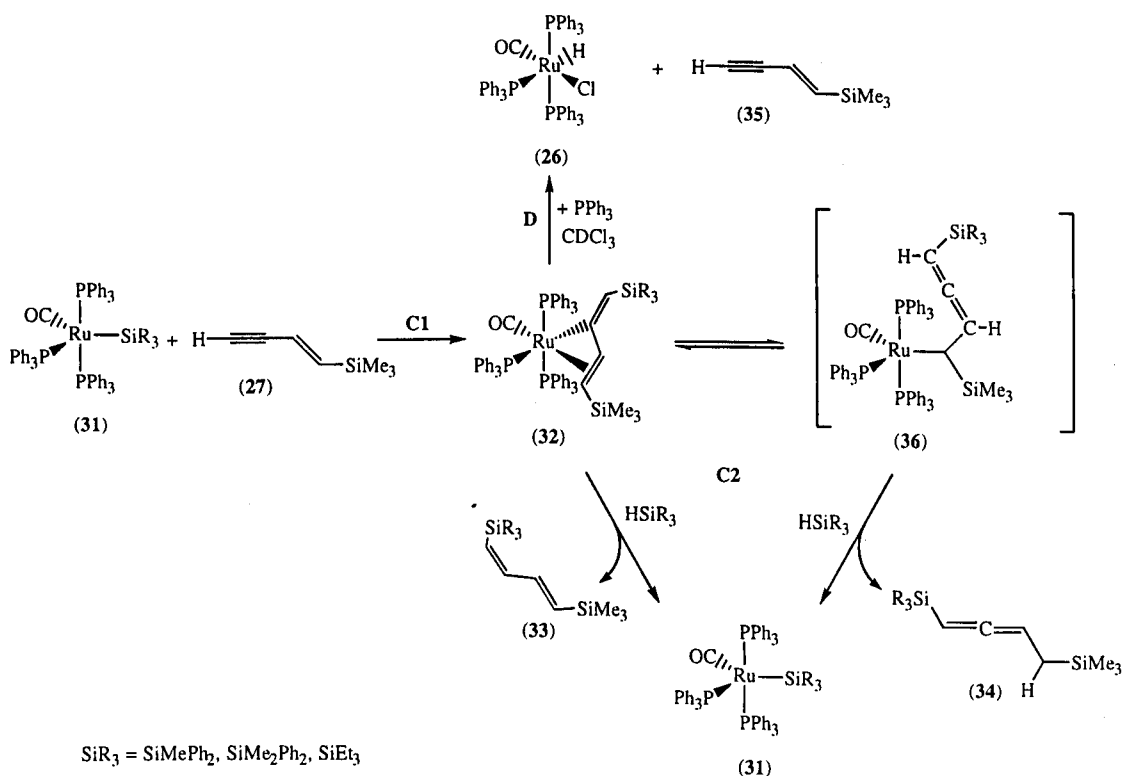
Complex **26** itself was inactive towards silanes but readily reacts with 1-(trimethylsilyl)-1-butene-3-yne **27** to form the ruthenium dienyl complex, $\text{Ru}(\text{CH}=\text{CH}-\text{CH}=\text{CHSiMe}_3)\text{Cl}(\text{CO})(\text{PPh}_3)_2$ **28** *via* pathway **A1** (Scheme 1.13).⁴³ Reaction of **28** with excess silanes, HSiR_3 ($\text{SiR}_3 = \text{SiMePh}_2$, SiMe_2Ph and SiEt_3), yielded hydrosilation products $\text{SiR}_3\text{CH}=\text{CH}-\text{CH}=\text{CHSiMe}_3$ **29** and $\text{SiR}_3\text{CH}_2\text{CH}=\text{CH}-\text{CH}_2\text{SiMe}_3$ **30**, as well as forming the ruthenium silyl complex **31** and regenerating the hydride **26** (Scheme 1.13).



Scheme 1.13 Reaction of **26** with **27** (pathway **A1**). Reaction of **28** with HSiR_3 (pathway **A2** and **B**).⁴³

From the product ratios observed for the reaction shown in Scheme 1.13, Ozawa concluded that two reaction pathways are present, **A2** and **B**. According to Ozawa, pathway **A2** yields **26** and **29** *via* C–Si and Ru–H bond formation, *ie.* the Chalk-Harrod Mechanism.¹⁶ In the second pathway, **B**, C–H and Ru–Si bond formation occurs, leading to the ruthenium silyl complex **31** and 1-(trimethylsilyl)-1,3-butadiene, which is then apparently hydrosilated to form **30** (Scheme 1.13). More details of this pathway are described below.

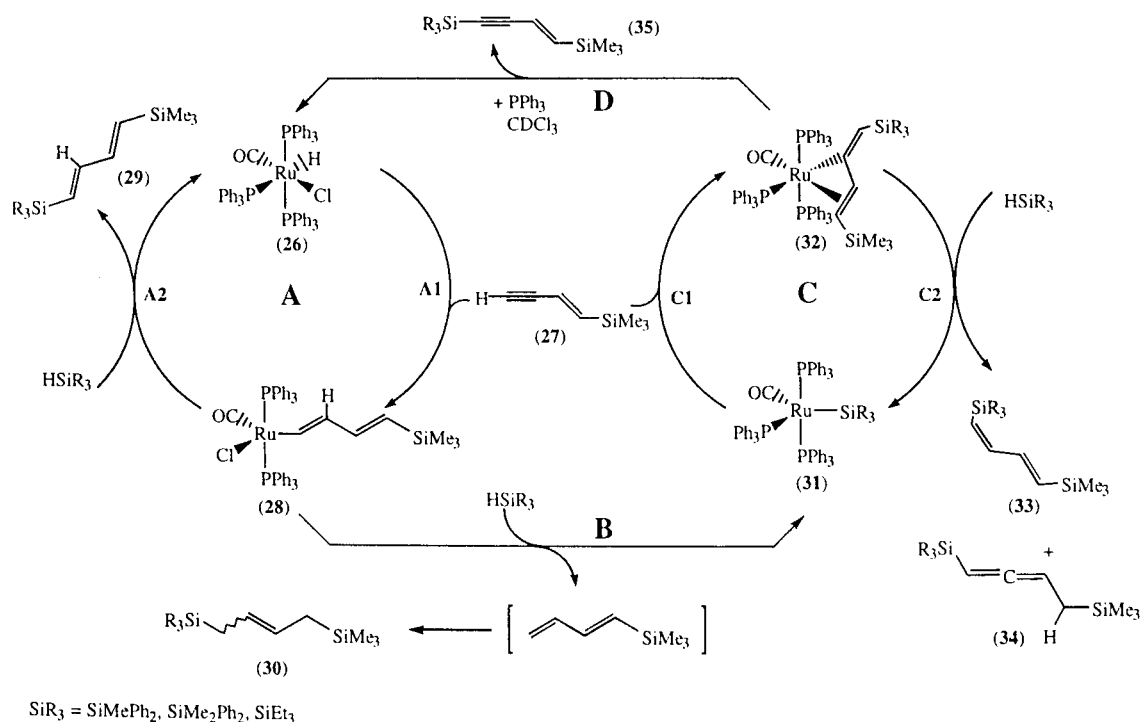
Ozawa showed that the reaction of the ruthenium silyl complex **31** with **27** formed the insertion product **32** *via* pathway **C1** (Scheme 1.14). Complex **32** can react with various silanes *via* pathway **C2** to give two types of hydrosilation product, **33** and **34**, but the presence of PPh₃ inhibits this reaction and leads to the formation of the ruthenium hydride **26** and the silylation product SiR₃C≡C–CH=CHSiMe₃ **35** *via* pathway **D** (Scheme 1.14). According to Ozawa, hydrosilation product **34** derives from the allenylmethylruthenium species **36** which is formed from a 1,3-hydride shift of the dienyl ligand in **32** (Scheme 1.14, pathway **C2**).



Scheme 1.14 Reaction of the ruthenium silyl complex **31** with **27** in the presence of PPh₃ (pathways **C1** and **D**) and in the absence of PPh₃ (pathways **C1** and **C2**).⁴³

In summary, Ozawa's mechanism for hydrosilation of 1-(trimethylsilyl)-1-butene-3-yne **27** with HSiR₃ by the ruthenium hydride **26** contains two major pathways, **A** (**A1** and **A2** in Scheme 1.13) and **C** (**C1** and **C2** in Scheme 1.14). Pathway **A** can be seen as the traditional Chalk-Harrod mechanism,¹⁶ whereas pathway **C** represents the silyl

migration mechanism.^{30,33,35,37,42} Pathways **A** and **C** are connected by processes **B** and **D**. The overall mechanism for the hydrosilation reaction proposed by Ozawa using the ruthenium hydride **26** is summarised in Scheme 1.15.



Scheme 1.15 Mechanism for hydrosilation by ruthenium-based catalyst $\text{RuHCl}(\text{CO})\text{-(PPh}_3)_3$ **26**.⁴³

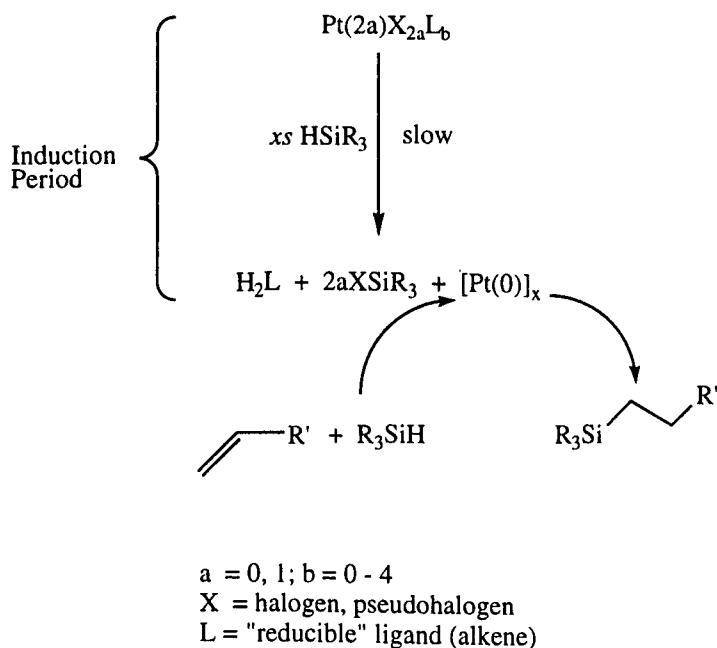
1.2.7 Hydrosilation reactions involving colloidal platinum

Lewis and co-workers were the first to demonstrate, with light scattering, TEM and ESCA, that platinum colloid formation occurs in Speier's catalyst, H_2PtCl_6 , and other highly active platinum hydrosilation catalysts, *e.g.* $\text{Pt}(\text{COD})\text{Cl}_2$ **37**, $\text{Pt}(\text{COD})_2$ **38** and Karstedt's catalyst **1**.¹³

Crabtree⁴⁴ and Whitesides⁴⁵ have shown that elemental mercury can selectively poison heterogeneous based catalysts, whilst homogeneous based catalysts are unaffected. Crabtree has also used dibenzo[a,e]cyclooctetraene (DBCOT) as a selective poison for homogeneous transition metal catalysts.⁴⁴ Lewis and co-workers showed that Speier's catalyst, **37** and **38**, were poisoned upon addition of elemental mercury.¹³ This demonstrates that H_2PtCl_6 , **37** and **38**, require the formation of colloidal platinum as a key step in the hydrosilation reaction.

The mechanism which Lewis proposed for the formation of colloidal platinum requires the compound to form a platinum(0) species which is free of ligands (Scheme 1.13). According to Lewis, Speier's catalyst and **37** were reduced to platinum(0) by the silanes present in the hydrosilation reaction. This was offered as an explanation of the

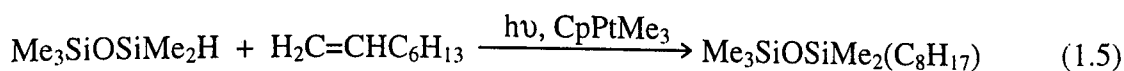
initial induction period often observed for these catalysts during the hydrosilation reaction.³



Scheme 1.16 Proposed mechanism for platinum colloid formation during hydrosilation.¹³

It has been observed that both Speier's and Karstedt's catalysts require the presence of oxygen to drive the hydrosilation reaction to completion.^{46,47} Lewis suggested that oxygen acts as a weakly co-ordinating ligand to the platinum colloids formed during hydrosilation, preventing irreversible aggregation to larger colloids, since larger particle colloids would have reduced activity.⁴⁸ Lewis has observed that if the oxygen is depleted in a typical hydrosilation reaction, the reaction stops and large platinum colloids are formed.⁴⁹

Broadman showed that photolysis of the platinum(IV) complex, CpPtMe_3 **39**, formed an active species which catalysed the hydrosilation of 1-octene with $\text{HMe}_2\text{SiOSiMe}_3$ (Equation 1.5).⁵⁰

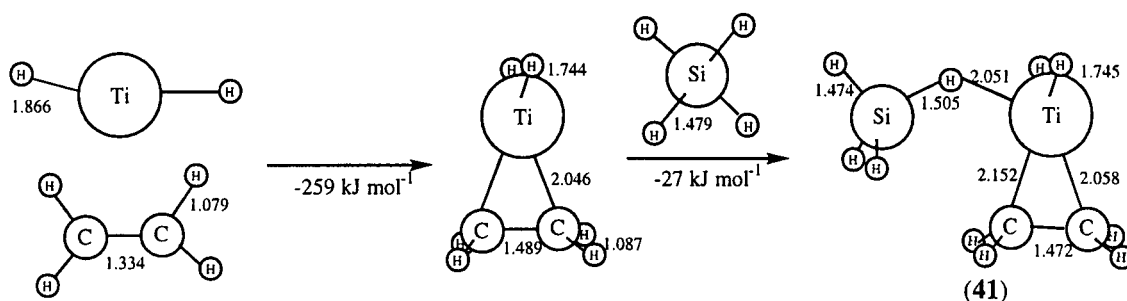


Broadman demonstrated that the active species formed in the reaction were colloidal in nature and elemental mercury deactivated the catalysts, whilst dibenzo[a,e]cyclooctetraene (DBCOT) had no effect.⁵⁰ Analysis by TEM provided evidence that platinum colloids are formed upon photolysis of **39**. Irradiation of **39** with only the silane, $\text{HMe}_2\text{SiOSiMe}_3$, yielded a bis(silyl) hydride species, $\text{CpPt}(\text{SiMe}_2\text{OSiMe}_3)_2\text{H}$ **40** (Scheme 1.17). Broadman compared the activities of **39** and

1.2.8 Theoretical investigation of the hydrosilation reaction

Harrod and co-workers^{51,52} have shown in the past that organotitanium compounds can act as catalysts for the hydrosilation reaction and the polymerisation of primary organosilanes *via* dehydrogenative coupling of organosilanes. Recent *ab initio* calculations of the hydrosilation reaction by Bode *et al.* have shown that titanium(II) is an effective catalyst for this process.⁵³ Using TiH_2 as the simplest model catalyst for the hydrosilation of C_2H_4 and SiH_4 , Bode *et al.* calculated that the catalysed reaction proceeds *via* a reaction pathway that is barrierless, whilst the uncatalysed reaction has an activation barrier of 326 kJ mol^{-1} .⁵³

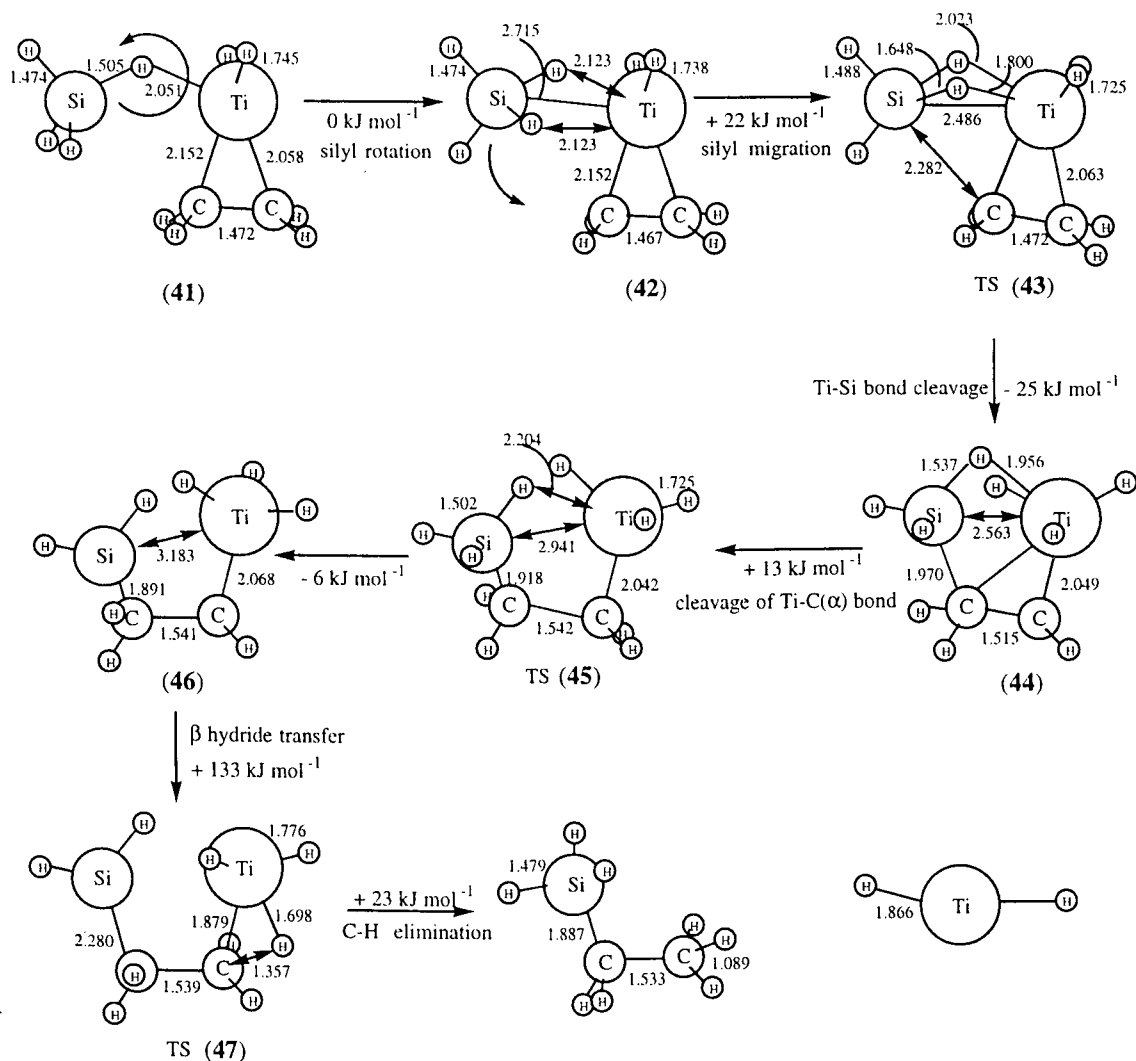
In their calculations, Bode *et al.* showed that ethene adds to TiH_2 to form a three-membered metallacycle (Scheme 1.19). This process was shown to be exothermic by 259 kJ mol^{-1} , and is followed by silane addition to form **41** which is also exothermic by 27 kJ mol^{-1} . Overall the formation of species **41** is exothermic by 286 kJ mol^{-1} (Scheme 1.19). Alternatively, silane addition to TiH_2 followed by ethene addition can occur which also results in the formation of **41**. The very large drop in energy due to the initial formation of **41** was said to be the driving force of the whole reaction (Scheme 1.19).⁵³



Scheme 1.19 Formation of **41** from TiH_2 , C_2H_4 and SiH_4 as the driving force for the hydrosilation reaction (bond lengths in Å).⁵³

Scheme 1.20 shows Bode *et al.*'s calculated minimum energy pathway for ethylsilane formation from **41**.⁵³ Silyl ligand migration to the α carbon (**41** to **46**), is followed by hydrogen transfer from Ti to the β carbon (**46** to **47**), and removal of the TiH_2 catalyst. They calculated the overall process (Schemes 1.19 and 1.20) to be exothermic by 117 kJ mol^{-1} .

Bode *et al.* noted, however, that although the calculations for the simple TiH_2 model catalyst system might be very accurate, they do not take into account electronic or steric factors if the substituents on the Ti catalyst were anything but hydrogen, *e.g.* TiCl_2 or TiCp_2 .⁵³



Scheme 1.20 Formation of ethylsilane from C_2H_4 and SiH_4 using TiH_2 as catalyst. Structures shown are calculated for the minimum energy pathway (TS = transition state).⁵³

1.3 SILANE ACTIVATION

The activation of silanes by transition metal centres to form metal silyl species has been widely studied since they have been shown to be key intermediates in hydrosilation. One of the most convenient routes to transition metal silyl complexes is *via* the oxidative addition of a Si-H bond to a co-ordinatively unsaturated metal centre. Examples of the oxidative addition of a Si-H bond are known for nearly all of the transition metals.^{3,54,55}

Addition of Si-X (X = Cl, C, Si) bonds to transition metals occurs less readily and is less common. Oxidative addition of Si-X bonds is normally found with the later transition metals, *e.g.* Rh, Pd and Pt.⁵⁶

1.3.1 Comparison between C–H and Si–H activation

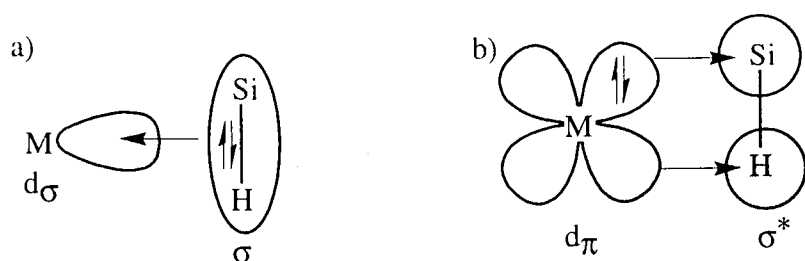
The interaction of silanes with transition metal centres is often a facile process when compared to C–H activation. *Ab initio* calculations by Sakaki⁵⁷ have shown that Si–H oxidative addition of SiH₄ to Pt(PH₃)₂ proceeds more easily when compared to C–H oxidative addition of CH₄ to Pt(PH₃)₂. Sakaki showed that the calculated activation barrier for SiH₄ addition to Pt(PH₃)₂ is much smaller and the process is exothermic ($\Delta H^\ddagger = 2.9 \text{ kJ mol}^{-1}$; $\Delta H^\circ = -110.5 \text{ kJ mol}^{-1}$) whilst for CH₄ the barrier is large and the process is endothermic ($\Delta H^\ddagger = 120 \text{ kJ mol}^{-1}$; $\Delta H^\circ = 27.2 \text{ kJ mol}^{-1}$). Sakaki concluded that the driving force for Si–H activation arises from the formation of a Pt–SiH₃ bond which is stronger [$D(\text{Pt–SiH}_3)_{\text{calc.}} = 257.3 \text{ kJ mol}^{-1}$], compared with a Pt–CH₃ bond [$D(\text{Pt–CH}_3)_{\text{calc.}} = 166.1 \text{ kJ mol}^{-1}$].⁵⁷

Puddephatt provided the first experimental estimation of a Pt–Si bond energy using differential scanning calorimetry (DSC).⁵⁸ The estimated Pt–Si bond energy, $D(\text{Pt–SiMe}_3)$, of PtIme₂(SiMe₃)(bpy) (bpy = 2,2'-bipyridine) **48** was found to be $233 \pm 14 \text{ kJ mol}^{-1}$. Values of 137 and 129 kJ mol^{-1} have been found for Pt–Me bonds in *cis*-PtMe₄(MeCN)₂ **49** and *cis*-PtMe₄(2,6-Me₂C₆H₃NC)₂ **50**, also by Puddephatt using DSC.⁵⁹

Experimental evidence from Puddephatt^{58,59} and *ab initio* calculations by Sakaki⁵⁷ both showed that a Pt–Si bond is approximately 100 kJ mol^{-1} stronger than a Pt–C bond. Furthermore, the Si–H bond of SiH₄ [$D(\text{Si–H}) = 378 \text{ kJ mol}^{-1}$]⁶⁰ is weaker than the C–H bond of CH₄ [$D(\text{C–H}) = 438 \text{ kJ mol}^{-1}$].⁶¹ However, it must be noted that Si–H bond strengths of HSiR₃ will vary depending on the substituent R.⁶²

1.3.2 Bonding in metal silyl hydride and η^2 -silane complexes

In general, oxidative addition of an Si–H bond to a transition metal centre can result in either full cleavage of the Si–H bond to give a product with a classical 2-centre 2-electron interaction, or an η^2 -Si–H σ complex with a non-classical 3-centre 2-electron interaction. In the non-classical 3-centre 2-electron situation, two types of bonding interaction can take place. Firstly, the Si–H σ bonding orbital can interact with the metal *d*-orbital and secondly the metal *d_π*-orbital can interact with the Si–H σ^* -antibonding orbital (Scheme 1.21). Sufficient π backbonding from the metal centre would result in the full oxidative addition of the Si–H bond. Therefore the extent of σ -donor and σ^* -acceptor ability of the Si–H bond can be tuned by varying the substituents on the silicon atom.



Scheme 1.21 Non classical 3-centre 2-electron bonding interaction between Si–H and the metal, M. (a) σ -bonding interaction. (b) metal π -backbonding interaction.

An η^2 -Si–H σ bonded complex can be considered as an arrested state in the course of the oxidative addition pathway and is, in some ways, analogous to the bonding found in π -complexes. Since the substituents at either the silicon or the metal centre will have a dramatic impact on the oxidative addition pathway of the Si–H bond to the metal, the stage at which the oxidative addition process is stopped can be tuned by altering the substituents on the silicon or the metal. Structural evidence of the first σ -bonded Si–H complex was first obtained by Graham for $\text{Cp}(\text{OC})_2\text{Mn}(\text{HSiPh}_3)$ **51** by X-ray diffraction.⁶³ A more accurate analysis by Schubert was later performed using neutron diffraction techniques on $(\eta^5\text{-C}_5\text{H}_4\text{Me})(\text{OC})_2\text{Mn}(\text{HSiFPh}_2)$ **52** in which a Si–H bond distance of 1.8 Å was observed.^{64,65} This is about 0.3 Å longer than the covalent Si–H bond lengths found in normal tetrahedral silanes (1.5 Å).⁶⁶

NMR spectroscopy is by far the most convenient tool in determining if a 3-centre 2-electron interaction is present in a M–H–Si system. The magnitude of the coupling constant $J(\text{SiMH})$ is a reliable indicator of the strength of any Si–H interaction. In the upper limit, where the silicon is directly bonded to the hydride, $J(\text{SiH})$ is of the magnitude of about 200 Hz.⁶⁶ In the lower limit, where there is no bonding interaction between the silicon atom and the hydride, $^2J(\text{SiH})$ can be found in the range of 3.5–20 Hz.^{67,68,69}

In Schubert's review of η^2 -Si–H σ complexes,⁶⁶ the M–H–Si 3-centre 2-electron bonding interactions in the complexes of the type $(\eta^5\text{-C}_5\text{H}_4\text{Me})(\text{CO})_2\text{Mn}(\text{H})(\text{SiR}_3)$ were discussed in detail.⁶⁵ Firstly, Schubert examined the effect of changing the substituent on the silicon atom. This had the effect of reducing the $J(\text{SiMnH})$ value as more electronegative groups are present next to the silicon atom. For example, $(\eta^5\text{-C}_5\text{H}_4\text{Me})(\text{CO})_2\text{Mn}(\text{H})(\text{SiHPh}_2)$ **53** has a $J(\text{SiMnH})$ value of 65.4 Hz, whereas $(\eta^5\text{-C}_5\text{H}_4\text{Me})(\text{CO})_2\text{Mn}(\text{H})(\text{SiCl}_3)$ **54** has a $J(\text{SiMnH})$ value of 54.8 Hz. This could be explained by the fact that the more electronegative chlorine atoms are promoting π -metal backbonding to the Si–H σ^* -antibonding orbital and thereby decreasing the Si–H bond character. Schubert also demonstrated that altering the substituents on the metal itself can have a dramatic effect on the Si–H bond interaction. On substituting one of

the CO ligands for the more electron donating PMe_3 ligand, the complex $(\eta^5\text{-C}_5\text{H}_4\text{Me})\text{-}(\text{CO})(\text{PMe}_3)\text{Mn}(\text{H})(\text{SiCl}_3)$ **55** has an even lower value of $J(\text{SiMnH})$ (20.0 Hz). Here the Si–H bond character is said to be negligible because the σ -donating PMe_3 ligand is enriching the metal centre with electron density, thus enhancing the metal π -backbonding to the Si–H σ^* -antibonding orbital. Data from molecular orbital calculations and from PE (Photo-Electron) spectra support this idea.⁶⁶

Kubas and co-workers have shown that $\eta^2\text{-Si-H}$ σ -interactions can also be found in the molybdenum complexes of $\text{Mo}(\text{CO})(\text{PP})_2(\eta^2\text{-HSiR}_3)$ (PP = depe, dppe), e.g. $\text{Mo}(\text{CO})(\text{depe})_2(\eta^2\text{-HSiHPh}_2)$ **56**, which are analogous to the $\eta^2\text{-H}_2$ molybdenum complexes, e.g. $\text{Mo}(\text{CO})(\text{dppe})_2(\text{H}_2)$ **57** (Figure 1.1). Interestingly, the molybdenum silane complex **56** has the Si–H moiety *cis* to the carbonyl, whereas the dihydrogen complex has the H_2 ligand *trans* to the carbonyl (Figure 1.1).

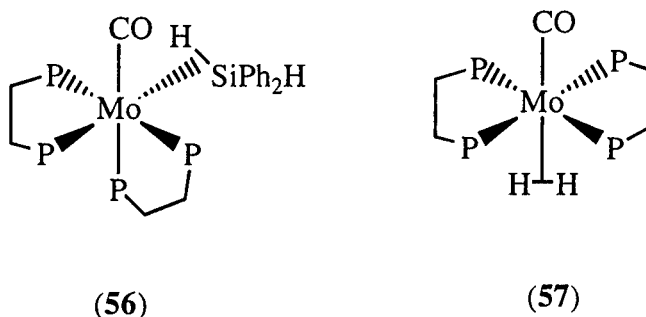
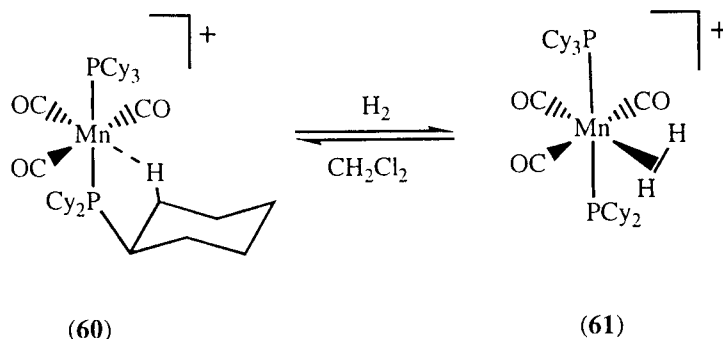


Figure 1.1 *cis* vs. *trans* co-ordination of H–X (X = SiR_3 , H) in the silane complex **56** and the dihydrogen complex **57**.⁷⁰

Ab initio calculations by Lin and co-workers on the model complex $\text{Mo}(\text{CO})(\text{PH}_3)_4(\eta^2\text{-HSiH}_3)$ **58** have shown that the *cis* isomer of **58** is 41.4 kJ mol^{-1} lower in energy than the *trans* isomer of **58**. Lin and co-workers pointed out that in dihydrogen, the H–H σ^* -antibonding orbital lies quite high in energy, whereas in silanes the H–Si σ^* -antibonding orbital lies lower in energy. This would mean that in the dihydrogen complexes, the dihydrogen ligand is less susceptible to metal to H–H σ^* -backbonding, whereas for η^2 -silane complexes metal to σ^* -backbonding is more pronounced. Lin then argued that if η^2 -silane molybdenum complexes, e.g. **56**, have the silane ligand *trans* to the carbonyl ligand, both the silane and the carbonyl ligand would be sharing the same d -orbital, and there will be competition between the two ligands for the metal d -electrons. Hence, the presence of the H–Si moiety would destabilise the *trans* configuration due to the better σ^* -accepting ability of Si–H function. The dihydrogen complex **57** on the other hand has a H–H distance of approximately 0.8 \AA which is only slightly larger than that of molecular dihydrogen.⁷¹ This further reinforces Lin's argument that there is little π backbonding from the metal to the H–H σ^* -antibonding orbital, and the reason why dihydrogen is found *trans* to the carbonyl

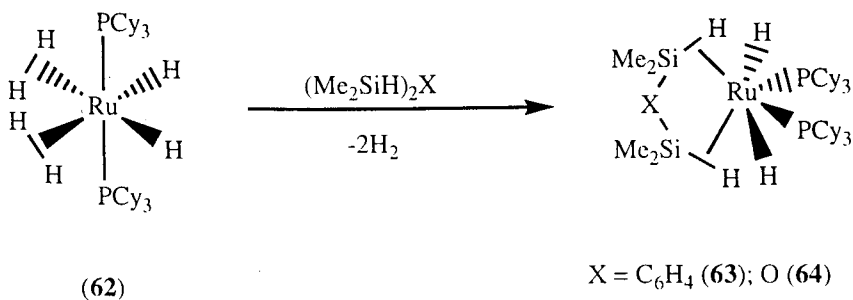
ligand. Interestingly, for classical molybdenum dihydride complexes, *e.g.* $\text{Mo}(\text{H})_2(\text{depe})_2(\text{CO})$ **59** a 7-co-ordinate pentagonal bipyramidal complex, the hydride ligands are *cis* to the carbonyl ligand.⁷²

Kubas and co-workers have recently demonstrated the versatility of dihydrogen as a ligand.⁷³ In their work, the highly electrophilic cationic manganese complex, $[\text{Mn}(\text{CO})_3(\text{PCy}_3)_2][\text{B}\{\text{C}_6\text{H}_3(3,5\text{-CF}_3)_2\}_4]$ **60**, was found only to bind with H_2 and very weakly with SO_2 (Scheme 1.22). Ligands like N_2 , ethene and silanes which are normally reliant on a large amount of metal π -backbonding, *e.g.* $\text{M} \rightarrow \sigma^*$ and $\text{M} \rightarrow \pi^*$, did not bind to **60** in solution. This demonstrates again that dihydrogen complexes favour H–H-to-metal σ -bonding interaction over metal-to-H–H σ^* -antibonding interaction.



Scheme 1.22 Reversible binding of dihydrogen to **60**.⁷³

Sabo-Etienne and co-workers isolated the first mono-nuclear transition metal complex containing two co-ordinated η^2 -Si–H σ -bonds.⁷⁴ They showed that the reaction of the ruthenium bis(dihydrogen) complex, $\text{RuH}_2(\text{H}_2)_2(\text{PCy}_3)_2$ **62**, with the disilanes $(\text{HSiMe}_2)_2\text{X}$ [$\text{X} = \text{C}_6\text{H}_4$, O] yielded the complex $\text{RuH}_2[(\eta^2\text{-HSiMe}_2)_2\text{X}](\text{PCy}_3)_2$ [$\text{X} = \text{C}_6\text{H}_4$ (**63**), O (**64**)] as determined from their crystal structures (Scheme 1.23).⁷⁴

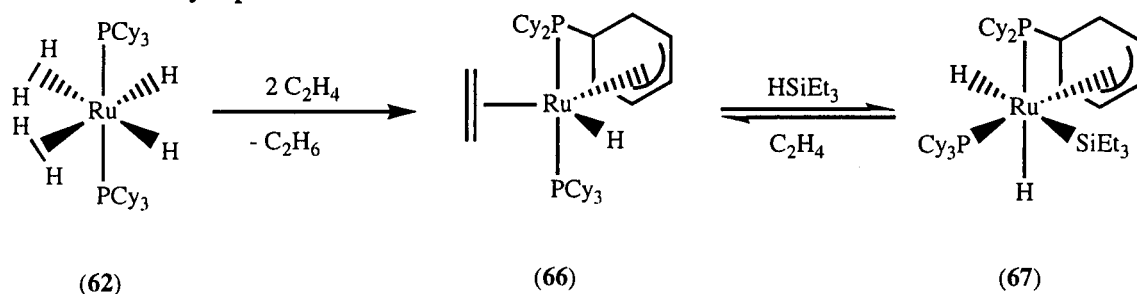


Scheme 1.23 Synthesis of $\text{RuH}_2[(\eta^2\text{-HSiMe}_2)_2\text{X}](\text{PCy}_3)_2$ [$\text{X} = \text{C}_6\text{H}_4$ (**61**), O (**62**)].⁷⁴

Sabo-Etienne and co-workers said that the chelating effect of the disilane $(\text{HSiMe}_2)_2\text{X}$ was responsible for the stabilisation of **63** and **64**. It was also observed that the flexible disiloxane ligand in **64** is more susceptible to substitution reactions than **63** which contains the more rigid disilane ligand $(\text{HSiMe}_2)_2\text{C}_6\text{H}_4$. For example, bubbling

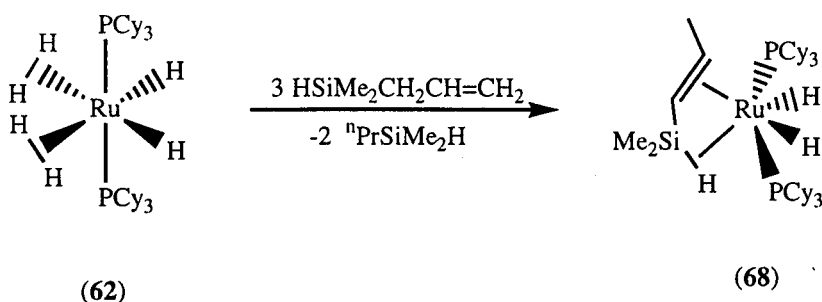
H₂ and CO through a solution of **64** yielded **62** and RuH₂(CO)₂(PCy₃)₂ **65** respectively, whereas for **63** no such ligand substitution reaction was observed.

The ruthenium bis(dihydrogen) complex **62** has been found to be an effective silylation catalyst of ethene.³¹ Sabo-Etienne and co-workers reported that **62** can selectively catalyse the reaction between HSiEt₃ and ethene to give the vinylsilane CH₂=CHSiEt₃ in 97% yield. The catalytic resting state for this reaction is said to be RuH[(η³-C₆H₈)P(C₆H₁₁)₂](C₂H₄)(PCy₃) **66** formed on reacting **62** with ethene. Complex **62** then reacts with HSiEt₃ to form the formally Ru(IV) complex Ru(H)₂(SiEt₃)[(η³-C₆H₈)P(C₆H₁₁)₂](C₂H₄)(PCy₃) **67** (Scheme 1.24). Sabo-Etienne and co-workers observed **66** during all of their catalytic studies and this species was the only detected complex after total conversion of HSiEt₃. Complex **67** was also reported to be an effective catalyst precursor.



Scheme 1.24 Formation of the catalytic resting state **65** during the silylation of ethene.³¹

Sabo-Etienne and co-workers have recently studied the interaction of the ruthenium bis(dihydrogen) complex **62** with the allylsilane CH₂=CHCH₂SiMe₂H, in an attempt to evaluate the competition between the co-ordination of the alkene function and the Si–H function.⁷⁵ In their work, reaction of **62** with CH₂=CHCH₂SiMe₂H yielded the ruthenium(II) dihydride complex, Ru(H)₂[η⁴-HSiMe₂(CH=CHMe)](PCy₃)₂ **68** (Scheme 1.25), where the vinylsilane ligand co-ordinates to ruthenium *via* an η²-Si–H σ-bond and an η²-C=C π-bond as characterised from its crystal structure. The η⁴-co-ordinated vinylsilane ligand in **67** is only weakly bound and can be easily displaced with H₂, CO or C₂H₄ to form **62**, **65** and **66**, respectively. This is also reflected in the large *J*(SiRuH) coupling constant of 105 Hz, indicating that the Si–H bond is only weakly activated and suggests a reduced metal to Si–H σ*-backbonding interaction.



Scheme 1.25 Synthesis of Ru(H)₂[η⁴-HSiMe₂(CH=CHMe)](PCy₃)₂ **68**.⁷⁵

Sabo-Etienne and co-workers have shown that **62** catalyses the reaction between ethene and the allylsilane $\text{HSiMe}_2\text{CH}_2\text{CH}=\text{CH}_2$ to give initially a variety of hydrosilation and silation products (Table 1.1).⁷⁵ They have also observed that redistribution around the silicon atom occurs once all the allylsilane has been consumed in the reaction, resulting mainly in the conversion of $(\text{CH}_2=\text{CHCH}_2)\text{Me}_2\text{Si}(\text{CH}=\text{CH}_2)$ to $\text{Me}_2\text{Si}(\text{CH}=\text{CH}_2)_2$. Complex **68** was found to possess similar catalytic activities to **62**, whereas the ethene silation catalyst, $\text{RuH}[(\eta^3\text{-C}_6\text{H}_8)\text{P}(\text{C}_6\text{H}_{11})_2](\text{C}_2\text{H}_4)(\text{PCy}_3)$ **66**,³¹ had reduced catalytic activities in this reaction and redistribution at the silicon atom was not as significant.

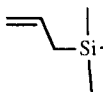
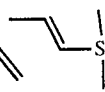
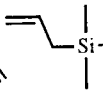
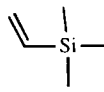
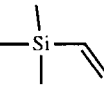
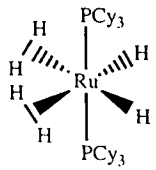
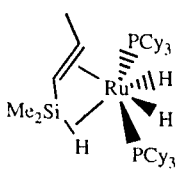
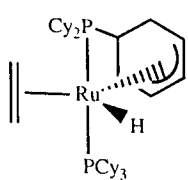
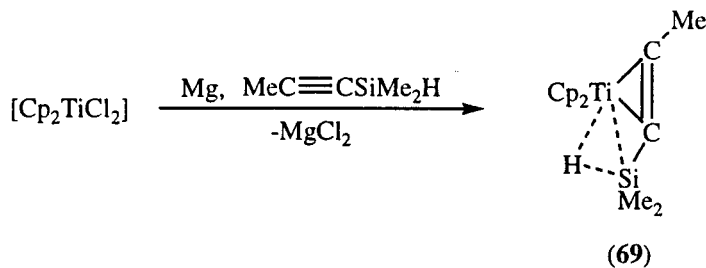
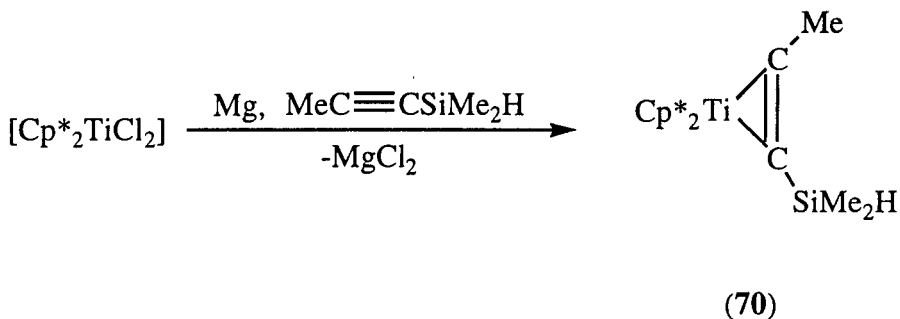
		Product / %				
						
	20 min ^a	28	10	36	5	8
	60 min	1	10	36	27	12
(62)						
	20 min ^a	16	10	37	12	10
	60 min	1	10	37	25	12
(68)						
	70 min ^{a,b}	28	5	37	8	11
(66)						

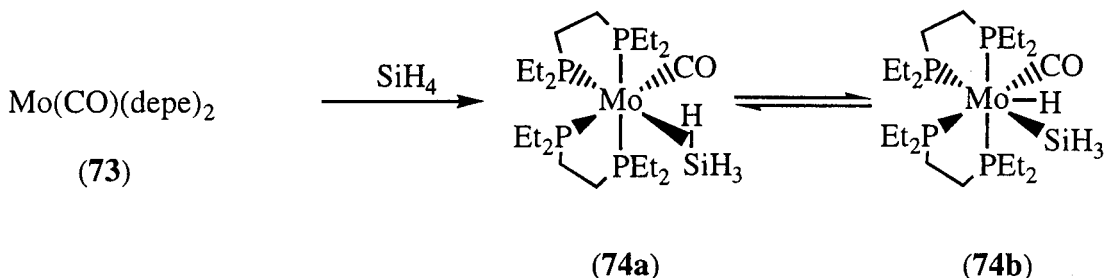
Table 1.1 Reaction of ethene with $\text{HSiMe}_2\text{CH}_2\text{CH}=\text{CH}_2$ catalysed by **62**, **66** or **68**. *a* Time after which $\text{HSiMe}_2\text{CH}_2\text{CH}=\text{CH}_2$ is totally consumed. *b* No more reaction after 70 min.⁷⁵

The Si–H bond can sometimes interact with the metal centre intramolecularly even though the silicon atom is not directly attached to the metal centre. Baumann and Rosenthal have recently shown that the reduction of the titanocene dichloride, $[\text{Cp}_2\text{TiCl}_2]$, with magnesium in the presence of the alkynylsilane, $\text{MeC}\equiv\text{CSiMe}_2\text{H}$, yielded the titanocene complex $\text{Cp}_2\text{Ti}(\text{MeC}\equiv\text{CSiMe}_2\text{H})$ **69**, which contains a β agostic Si–H interaction (Scheme 1.26).⁷⁶ However, it was found that if the cyclopentadienyl ligands on the titanium were replaced by pentamethylcyclopentadienyl ligands to form $\text{Cp}^*\text{Ti}(\text{MeC}\equiv\text{CSiMe}_2\text{H})$ **70** then no β agostic Si–H interaction was observed (Scheme 1.27).

Scheme 1.26 Synthesis of **69**.⁷⁶Scheme 1.27 Synthesis of **70**.⁷⁶

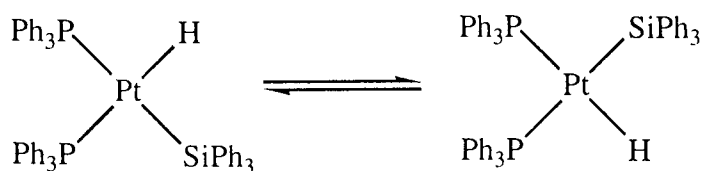
1.3.3 Fluxional behaviour of silyl hydride complexes

Transition metal silyl hydride complexes are often found to exhibit fluxional behaviour at room temperature. For example, Kubas and co-workers demonstrated that the reaction of SiH_4 with the formally 16-electron molybdenum complex, $\text{Mo}(\text{CO})(\text{dppe})_2$ **71**, yielded the six co-ordinate *cis*- $\text{Mo}(\eta^2\text{-HSiH}_3)(\text{CO})(\text{dppe})_2$ **72** octahedral complex. However, on changing the phosphine ligand from dppe to depe, Kubas found that reacting *cis*- $\text{Mo}(\text{CO})(\text{depe})_2$ **73** with SiH_4 yielded the tautomers *cis*- $\text{Mo}(\eta^2\text{-H-SiH}_3)(\text{CO})(\text{depe})_2$ **74a** and $\text{MoH}(\text{SiH}_3)(\text{CO})(\text{depe})_2$ **74b** which are in equilibrium with one another at room temperature (Scheme 1.28).⁷⁹ This is presumably because the more σ -donating phosphine in **74** populates the σ^* -antibonding orbital of the silane to favour the oxidative addition product, **74b**, whereas in **72** only π -acceptor ligands are bound to molybdenum, favouring only the $\eta^2\text{-Si-H}$ σ -complex.

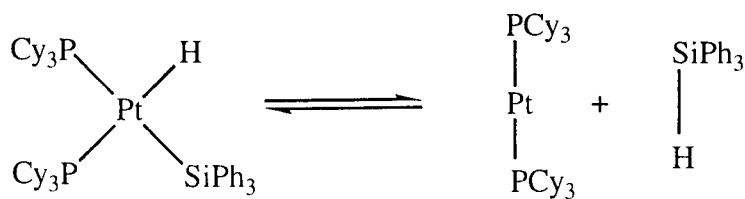
Scheme 1.28 Reaction of $\text{Mo}(\text{CO})(\text{depe})_2$ **73** with SiH_4 to form the tautomers **74a** and **74b**.⁷⁹

Kubas found that the ratio between **74a** and **74b** is temperature dependent and the thermodynamic parameters for conversion of **74a** to **74b** were $\Delta H^\circ = -2.55 \pm 0.8 \text{ kJ mol}^{-1}$ and $\Delta S^\circ = -8.8 \pm 3.0 \text{ J mol}^{-1} \text{ K}^{-1}$.⁷⁹

Pidcock and co-workers have shown the platinum complex, *cis*-Pt(PPh₃)₂(H)(SiPh₃) **75**, exhibits mutual phosphine exchange. It can also alternatively be viewed as the interchange of position between the silyl and hydride ligand (Scheme 1.29).⁸⁰ Pidcock and co-workers deduced from the variable temperature hydride NMR spectra of **75** that the exchange of phosphines occurs without dissociation of silane. Clark and Hampden-Smith later showed that the more sterically demanding analogue, *cis*-Pt(PCy₃)₂(H)(SiPh₃) **76**, displays the same type of mutual phosphine exchange, plus, reductive elimination and re-addition of the silane (Scheme 1.30).⁸¹ The dynamic processes present in **76** and other silyl hydride derivatives will be discussed in more detail in Chapter 5.



Scheme 1.29 Mutual phosphine exchange in *cis*-Pt(PPh₃)₂(H)(SiPh₃) **75**.⁸⁰

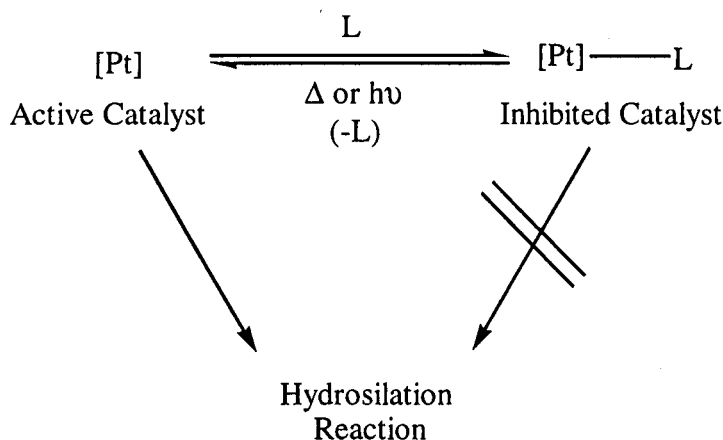


Scheme 1.30 Reversible oxidative addition/reductive elimination of silane in *cis*-Pt(PCy₃)₂(H)(SiPh₃) **76**.⁸¹

1.4 PHOTOACTIVATED HYDROSILATION CATALYSTS

Hydrosilation catalysts are often inhibited commercially in order to exert control on catalyst activities. It has been shown that maleates and fumarates displace the labile bridging vinylsiloxane ligand in Karstedt's catalyst **1** to form species which are inactive toward the hydrosilation reaction (Scheme 1.31).^{15,82} Reactivation of the latent catalyst is then achieved *in situ* by heating the hydrosilation reaction mixture. An alternative method for activation of latent hydrosilation catalysts would be by photochemical

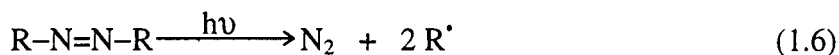
means. This latter method has the advantage of being less energy intensive compared to the more conventional thermal activation methods. Several examples of photoactivated hydrosilation systems have already been encountered in this chapter. For instance, Wrighton and co-workers have shown both $\text{Fe}(\text{CO})_5$ **11** and $\text{Co}(\text{CO})_4(\text{SiEt}_3)$ **12** eject CO upon photolysis to form a 16-electron species which is highly active towards the hydrosilation reaction.^{30,33} However, no photoactivated hydrosilation catalysts have yet been found which are suitable for commercial application.



Scheme 1.31 Inhibition and reactivation of a platinum hydrosilation catalyst.

1.4.1 Azo complexes

Azo, or diazene, ligands are known to degrade on photolysis or thermolysis, usually resulting in the elimination of a dinitrogen molecule and a radical pair (Equation 1.6).⁸³



Heaton identified the azo series as potential photo-sensitive inhibitor ligands, where azo-inhibited hydrosilation catalysts can be reactivated photochemically.⁸⁴ In Heaton's work, Karstedt's catalyst **1** was reacted with various azo ligands to test for catalyst inhibition. Heaton found that only the azo ligands with adjacent carbonyl groups, *ie.* $\text{RCON}=\text{NCOR}$, were effective as inhibitors and adequate inhibition of catalytic activities was achieved only when the concentration of the azo inhibitors was in excess of the catalyst. Reactivation of the azo inhibited catalyst was reported to be attainable either thermally or photochemically. However, the co-ordination mode of the azo ligand to the platinum metal centre in Heaton's system was unclear.⁸⁴

Three possible co-ordination modes to the metal centre are open to the azo ligand, RCONNCOR . The first possibility would involve the co-ordination of one of the lone pairs on the azo nitrogen to the metal centre to form a σ -complex [Figure 1.2 (a)], the second possibility would involve the formation of an η^2 -azo complex [Figure 1.2 (b)],

and the final possibility has the carbonyl group directly involved in the binding of the azo dicarbonyl ligand to the metal centre [Figure 1.2 (c)]. Numerous examples of compounds exhibiting the binding mode shown in Figure 1.2 (a) are discussed in detail in a review by Kisch and Holzmeier.⁸⁵ There are relatively few well documented η^2 -azo complexes of the type shown in Figure 1.2 (b); some examples include the azobenzene⁸⁶ and diazofluorene⁸⁷ complexes of nickel(0), *e.g.* $\text{Ni}(\text{}^t\text{BuNC})_2(\text{PhN=NPh})$ **77**.⁸⁶ However, in the complexes found with co-ordination modes displayed in Figures 1.2 (a) and (b), the ligated azo ligand does not contain an adjacent carbonyl group. Indeed the co-ordination mode shown in Figure 1.2 (c) is generally observed for the azo ligand of the type ROCNNCOR , as first demonstrated by Ibers and Ittel in the complex $\text{Pt}(\text{PPh}_3)_2(\text{PhOCNNCOPh})$ **78**.⁸⁸

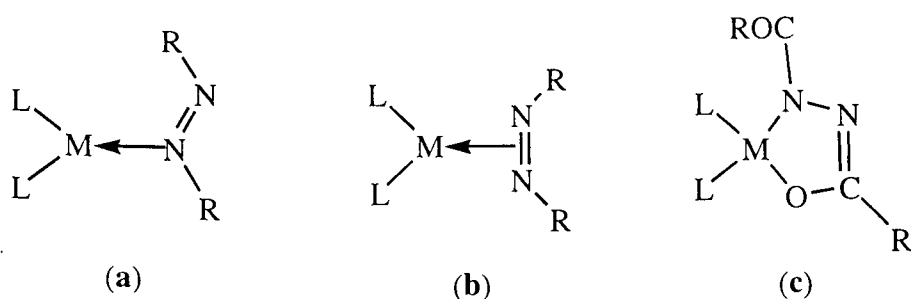
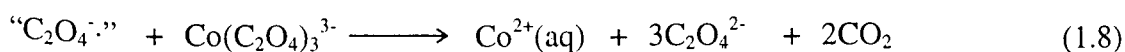
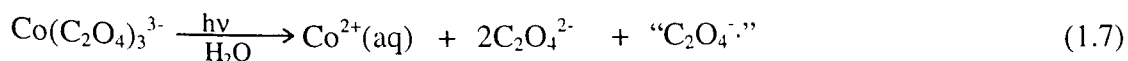


Figure 1.2 Possible metal-azo co-ordination modes. (a) σ azo complex, (b) η^2 -azo complex, (c) metallacyclic azo complex if an adjacent CO is present.

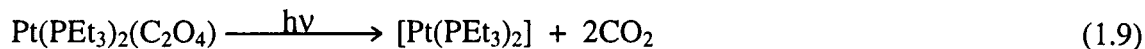
The co-ordination mode and photochemistry of several azo diacyl, ROCNNCOR , and azo dicarboxylate, $\text{RO}_2\text{CNNCO}_2\text{R}$, model platinum phosphine complexes, $\text{Pt}(\text{PR}_3)_2(\text{R}'\text{OCNNCOR}')$ and $\text{Pt}(\text{PR}_3)_2(\text{R}'\text{O}_2\text{CNNCO}_2\text{R}')$, are investigated in detail in Chapter 2.

1.4.2 Oxalate complexes

It has been shown that irradiation of transition metal oxalate complexes leads to the fragmentation of the oxalate dianion to form two molecules of carbon dioxide.⁸⁹ The process is thought to occur *via* a two-electron transfer to two metal centres. A well known example is $\text{Co}(\text{C}_2\text{O}_4)_3^{3-}$ **79**, where photolysis leads to reduction of two metal centres and the formation of Co(II) (Equation 1.7 and 1.8).⁸⁹



Trogler and co-workers observed that photolysis of the platinum oxalate complex, $\text{Pt}(\text{PEt}_3)_2(\text{C}_2\text{O}_4)$ **80**, leads to the formation of a highly reactive 14-electron bis(phosphine)platinum fragment and two molecules of carbon dioxide (Equation 1.9).⁹⁰



Although the 14-electron species was not observed directly, its presence was inferred from reaction with ethene and diphenylacetylene to form $\text{Pt}(\text{PEt}_3)_2(\text{C}_2\text{H}_4)$ **81** and $\text{Pt}(\text{PEt}_3)_2(\text{PhC}\equiv\text{CPh})$ **82**, respectively.

According to Trogler, on photolysis of **80**, rapid transfer of two electrons from the oxalate ligand to one metal occurs. Trogler argued that a successive, or simultaneous, transfer of two electrons would yield the more stable Pt(0) oxidation state, whereas transfer of one electron to the metal centre would produce the relatively unstable Pt(I) oxidation state.

Later, Trogler demonstrated that the reactive 14-electron bis(phosphine)platinum fragment formed on photolysis of **80** and the silica supported analogue (Figure 1.3) proved to be effective as a hydrosilation catalyst.⁹¹

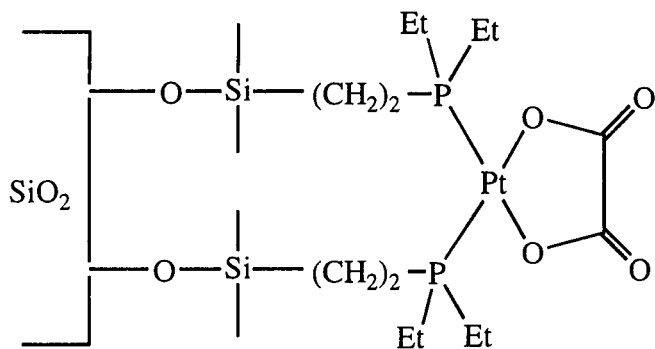


Figure 1.3 Silica supported $\text{Pt}(\text{PEt}_3)_2(\text{C}_2\text{O}_4)$ **80**.⁹¹

As expected Trogler found marked differences between the unsupported and supported bis(phosphine)platinum oxalates as hydrosilation catalysts. Irradiation of unsupported **80** resulted in a long and variable induction period for the hydrosilation reaction of 1-heptene and HSiMeCl_2 , whereas for silica supported **80**, the rate of reaction was more consistent. Furthermore, the presence of elemental mercury does not appear to poison the catalytic activity of the photoactivated supported **80** but the presence of oxygen or co-ordinating solvent does. Unfortunately, the effect of elemental mercury on unsupported **80** was not discussed. Trogler's explanation was that unsupported **80** can form cluster compounds upon irradiation in the presence of silane,⁹² and these clusters may be catalytically inactive towards the hydrosilation reaction. This is not dissimilar to the observation made by Lewis on platinum colloid formation during

the hydrosilation process for Speier's and Karstedt's catalyst (Section 1.2.6).^{48,49} Since the photo-generated active metal sites in supported **80** cannot interact with each other, Trogler argued that metal cluster formation was not possible and hydrosilation proceeds *via* monomeric active sites on the silica support.

Anderson and co-workers later studied the photochemical reactions of some platinum chelate phosphine oxalate complexes.⁹³ MO model calculations have shown that a bent 14-electron ML_2 metal fragment is more reactive than a linear ML_2 fragment and is isolobal with CH_2 .⁹⁴ Indeed, Whitesides demonstrated that the bent $Pt(dcpe)$ fragment [$dcpe = 1,2$ -bis(dicyclohexylphosphino)ethane], formed by thermolysis of $Pt(dcpe)(H)(CH_2CMe_3)$ **83**, is reactive towards the oxidative addition of C–H bonds.⁹⁵ In Anderson's work photolysis of $Pt(dppe)(C_2O_4)$ **84** with $PhC\equiv CPh$ yielded a mixture of $Pt(dppe)(PhC\equiv CPh)$ **85** and $Pt(dppe)(Ph)(C\equiv CPh)$ **86**, which is consistent with the formation of a 14-electron $Pt(dppe)$ fragment and two equivalents of CO_2 . However, photolysis of **84** in the absence of substrate in CH_3CN/C_6H_6 yielded two species, one of which was identified as $Pt(dppe)(CO_3)$ **87**; the other species remained unidentified. It was suggested by Anderson that two possible pathways were responsible for this observation, (i) photolysis of **84** initially generates the $Pt(dppe)$ fragment and CO_2 , the photogenerated CO_2 then reacts with the $Pt(dppe)$ fragment to form **87** and CO , or (ii) photolysis of **84** gives **87** and CO .

1.5 OUTLINE OF THESIS

The first part of this thesis investigates various ways in which platinum-based hydrosilation catalysts can be activated on photolysis. The latter part of this thesis investigates the interaction of the platinum metal centre with various silanes in a sterically crowded environment.

In Chapter 2, the structure and reactivities of several platinum azodicarbonyl complexes, $Pt(PR_3)_2(R'OCNNCOR')$ ($R = Ph, Me$; $R' = Ph, Me, OEt$ and O^iPr) are investigated. Here, we examine the role that the carbonyl group has on the co-ordination mode of the azodicarbonyl ligand to the platinum centre. The photochemistry of these compounds is also discussed in this chapter.

In Chapter 3, photoactivation of azo-inhibited Karstedt's catalyst **1** is examined. In this chapter, azo dicarboxylates of the form RO_2CNNCO_2R ($R = Et, ^iPr$ and tBu) are used to inhibit the catalytic activities of **1**. The effect of the R group on the azo-inhibited catalyst is investigated.

In Chapter 4, the synthesis and photochemistry of platinum complexes of malonate ($O_2CCH_2CO_2$) and phthalate ($O_2CC_6H_4CO_2$) are examined.

In Chapter 5, dynamic processes of $cis\text{-Pt}(\text{PCy}_3)_2(\text{H})(\text{SiR}_3)$ are studied. In this chapter, we examine the interaction between the Si—H bond of various silanes with the platinum centre by variable temperature NMR spectroscopy.

1.6 REFERENCES

- 1 W. Noll, *Chemistry and Technology of Silicones*, New York, Academic, 1968.
- 2 J. R. Falender, F. O. Stark and A. P. Wright, *Comprehensive Organometallic Chemistry*, Eds. G. Wilkinson, F. G. A. Stone and E. W. Abel, Oxford, Pergamon, 1982, **2**, 305.
- 3 J. L. Speier, *Adv. Organomet. Chem.*, 1979, **17**, 407.
- 4 A. J. Barry, L. DePree, J. W. Gilkey and D. E. Hook, *J. Am. Chem. Soc.*, 1947, **69**, 2916.
- 5 A. V. Topchiev, N. S. Nametkin and O. P. Solovova, *Dokl. Akad. Nauk. SSSR*, 1952, **86**, 965.
- 6 A. M. El-Abbady and L. C. Anderson, *J. Am. Chem. Soc.*, 1958, **80**, 1737.
- 7 L. H. Sommer, E. W. Pietrusza and F. C. Whitmore, *J. Am. Chem. Soc.*, 1947, **69**, 188.
- 8 R. V. Lipscomb, U.S. Patent 2,570,462, 1951.
- 9 B. Marciniak, J. Gulinski, W. Urbaniak and Z. W. Kornetka, *Comprehensive Handbook on Hydrosilylation*, Ed. B. Marciniak, Oxford, Pergamon, 1992.
- 10 G. H. Barnes, J. L. Speier and J. A. Webster, *J. Am. Chem. Soc.*, 1957, **79**, 974.
- 11 I. Ojima, *The Chemistry of Organic Silicon Compounds*, Eds. S. Patai and Z. Rappoport, Wiley, 1989, 1479.
- 12 W. Kiggen and F. Vögtle, *Angew. Chem. Int. Ed. Engl.*, 1984, **23**, 714.
- 13 L. N. Lewis and N. Lewis, *J. Am. Chem. Soc.*, 1986, **108**, 7228.
- 14 B. D. Karstedt, U.S. Patent 3,775,452, 1973.
- 15 P. B. Hitchcock, M. F. Lappert and N. J. Warhurst, *Angew. Chem. Int. Ed. Engl.*, 1991, **30**, 438.
- 16 A. J. Chalk and J. F. Harrod, *J. Am. Chem. Soc.*, 1965, **87**, 16; A. J. Chalk and J. F. Harrod, *J. Am. Chem. Soc.*, 1965, **87**, 1183.
- 17 S. H. Bergen, P. Noheda, J. Whelan, B. Bosnich, *J. Am. Chem. Soc.*, 1992, **114**, 2128.
- 18 J. W. Ryan and J. L. Speier, *J. Am. Chem. Soc.*, 1964, **86**, 895.
- 19 R. N. Haszeldine, R. V. Parish and D. J. Parry, *J. Chem. Soc. (A)*, 1969, 683.
- 20 H. M. Dickers, R. N. Haszeldine, L. S. Malkin, A. P. Mather and R. V. Parish, *J. Chem. Soc., Dalton Trans.*, 1980, 308.
- 21 J. Saam and J. L. Speier, *J. Am. Chem. Soc.*, 1961, **83**, 1351.

- 22 R. H. Crabtree, *The Organometallic Chemistry of Transition Metals*, 2nd Edition, Wiley, New York, 1994.
- 23 A. J. Blakeney and J. A. Gladysz, *Inorg. Chim. Acta*, 1980, **53**, L25; K. C. Brinkman, A. J. Blakeney, W. Krone-Schimdt and J. A. Gladysz, *Organometallics*, 1984, **3**, 1325.
- 24 M. Aizenberg and D. Milstein, *Angew. Chem. Int. Ed. Engl.*, 1994, **33**, 317; M. Aizenberg and D. Milstein, *J. Am. Chem. Soc.*, 1995, **117**, 6456.
- 25 M. E. van der Boom, J. Ott and D. Milstein, *Organometallics*, 1998, **17**, 4263.
- 26 R. N. Haszeldine, R. V. Parish and J. H. Setchfield, *J. Organomet. Chem.*, 1973, **57**, 279.
- 27 D. L. Thorn, *Organometallics*, 1998, **17**, 348.
- 28 F. Ozawa, T. Hikida, K. Hasebe and T. Mori, *Organometallics*, 1998, **17**, 1018; F. Ozawa, T. Hikida and T. Hayashi, *J. Am. Chem. Soc.*, 1994, **116**, 2844.
- 29 J. J. Low and W. A. Goddard, *J. Am. Chem. Soc.*, 1986, **108**, 6115.
- 30 J. C. Mitchener and M. S. Wrighton, *J. Am. Chem. Soc.*, 1981, **103**, 975; M. A. Schroeder and M. S. Wrighton, *J. Organomet. Chem.*, 1977, **128**, 345.
- 31 M. L. Christ, S. Sabo-Etienne and B. Chaudret, *Organometallics*, 1995, **14**, 1082.
- 32 P. Braunstein and M. Knorr, *J. Organomet. Chem.*, 1995, **500**, 21.
- 33 F. Seitz and M. S. Wrighton, *Angew. Chem. Int. Ed. Engl.*, 1988, **27**, 289.
- 34 F. R. Anderson and M. S. Wrighton, *J. Am. Chem. Soc.*, 1984, **106**, 995.
- 35 C. L. Randolph and M. S. Wrighton, *J. Am. Chem. Soc.*, 1986, **108**, 3366.
- 36 D. M. Haddleton and R. N. Perutz, *J. Chem. Soc., Chem. Commun.*, 1985, 1372.
- 37 S. B. Duckett and R. N. Perutz, *Organometallics*, 1992, **11**, 90.
- 38 S. B. Duckett and R. N. Perutz, *J. Chem. Soc., Chem. Commun.*, 1991, 28.
- 39 S. D. Belt, *D. Phil Thesis*, University of York, 1989.
- 40 A. Millan, M. -J. Fernandez, P. Bentz and P. M. Maitlis, *J. Mol. Catal.*, 1984, **26**, 89.
- 41 G. F. Schmidt and M. Brookhart, *J. Am. Chem. Soc.*, 1985, **107**, 1443; M. Brookhart, A. F. Volpe, D. M. Lincoln, I. T. Horváth and J. M. Millar, *J. Am. Chem. Soc.*, 1990, **112**, 5634.
- 42 M. Brookhart, B. Grant and A. F. Volpe, *Organometallics*, 1992, **11**, 3920.
- 43 Y. Maruyama, K. Yamamura, I. Nakayama, K. Yoshiuchi and F. Ozawa, *J. Am. Chem. Soc.*, 1998, **120**, 1421.
- 44 R. H. Crabtree, M. F. Mellea, J. M. Mihelcic and J. M. Quirk, *J. Am. Chem. Soc.*, 1982, **104**, 6994; D. R. Anton and R. H. Crabtree, *Organometallics*, 1983, **2**, 855.

- 45 G. M. Whitesides, M. Hackett, R. L. Brainard, J. P. M. Lavalleye, A. F. Sowinski, A. N. Izumi, S. S. Moore, D. W. Brown and E. M. Staudt, *Organometallics*, 1985, **4**, 1819.
- 46 J. F. Harrod and A. J. Chalk, *Organic Synthesis via Metal Carbonyls*, Eds. I. Wender and P. Pino, Wiley, New York, 1997, 673.
- 47 A. Onopchenko and E. T. Sabourin, *J. Org. Chem.*, 1987, **52**, 4118.
- 48 L. N. Lewis, *J. Am. Chem. Soc.*, 1990, **112**, 5998.
- 49 L. N. Lewis, J. R. Uriarte and N. Lewis, *J. Mol. Cat.*, 1991, **127**, 67.
- 50 L. D. Boardman, *Organometallics*, 1992, **11**, 4194.
- 51 C. Aitken, J. F. Harrod and E. Samuel, *J. Organomet. Chem.*, 1985, **279**, C11.
- 52 J. F. Harrod and S. S. Yun, *Organometallics*, 1987, **6**, 1381.
- 53 B. M. Bode, P. Day and M. S. Gordon, *J. Am. Chem. Soc.*, 1998, **120**, 1552.
- 54 T. D. Tilley, *Transition-Metal Silyl Derivatives*, Eds. S. Patai and Z. Rappoport, Wiley, New York, 1977, 673.
- 55 U. Schubert, *Transition Met. Chem.*, 1991, **16**, 136.
- 56 H. K. Sharma and K. H. Pannell, *Chem. Rev.*, 1995, **95**, 1351; U. Schubert, *Angew. Chem. Int. Ed. Engl.*, 1994, **33**, 419.
- 57 S. Sakaki and M. Ieki, *J. Am. Chem. Soc.*, 1993, **115**, 2373.
- 58 C. J. Levy and R. J. Puddephatt, *Organometallics*, 1995, **14**, 5019.
- 59 S. Roy, R. J. Puddephatt and J. D. Scott, *J. Chem. Soc., Dalton Trans.*, 1989, 2121.
- 60 A. M. Doncaster and R. Walsh, *Int. J. Chem. Kinet.*, 1981, **13**, 503.
- 61 D. M. Golden and S. W. Benson, *Chem. Rev.*, 1969, **69**, 125.
- 62 R. Walsh, *The Chemistry of Organic Silicon Compounds*, Eds. S. Patai and Z. Rappoport, Wiley, New York, 1989, Chapter 5.
- 63 W. G. A. Graham, *J. Organomet. Chem.*, 1986, **300**, 81.
- 64 K. Ackermann, U. Schubert and B. Wörle, *J. Am. Chem. Soc.*, 1982, **104**, 7378.
- 65 K. Ackermann, J. Müller, G. Scholz, U. Schubert and B. Wörle, *J. Organomet. Chem.*, 1986, **306**, 303.
- 66 U. Schubert, *Adv. Organomet. Chem.*, 1990, **30**, 151.
- 67 W. A. G. Graham and W. Jetz, *Inorg. Chem.*, 1971, **10**, 1159.
- 68 P. M. Bailey, P. O. Bentz, M. J. Fernandez, T. F. Koetzle and P. M. Maitlis, *J. Am. Chem. Soc.*, 1984, **106**, 5458.
- 69 A. Schenkel and U. Schubert, *Chem. Ber.*, 1988, **121**, 939.
- 70 M. Fan, G. Jia and Z. Lin, *J. Am. Chem. Soc.*, 1996, **118**, 9915.
- 71 G. J. Kubas, R. R. Ryan, B. I. Swanson, P. J. Vergamini and H. J. Wasserman, *J. Am. Chem. Soc.*, 1984, **106**, 451.

- 72 G. J. Kubas, R. R. Ryan and C. J. Unkefer, *J. Am. Chem. Soc.*, 1987, **109**, 8113.
- 73 A. Toupadakis, G. Kubas, W. A. King B. L. Scott and J. Huhmann-Vincent, *Organometallics*, 1998, **17**, 5315.
- 74 F. Delpech, S. Sabo-Etienne, B. Chaudret and J. Daran, *J. Am. Chem. Soc.*, 1997, **119**, 3167.
- 75 F. Delpech, S. Sabo-Etienne, B. Donnadiou and B. Chaudret, *Organometallics*, 1998, **17**, 4926.
- 76 N. Peulecke, A. Ohff, P. Kosse, A. Tillack, A. Spannenberg, R. Kempe, W. Baumann, V. V. Burlakov and U. Rosenthal, *Chem. Eur. J.*, 1998, **4**, 1852.
- 77 M. Sato, T. Tatsumi, T. Kodama, M. Hidai, T. Uchida and Y. Uchida, *J. Am. Chem. Soc.*, 1978, **100**, 4447.
- 78 X. Luo, G. J. Kubas, J. C. Bryan, C. J. Burns and C. J. Unkefer, *J. Am. Chem. Soc.*, 1994, **116**, 10312.
- 79 X. Luo, G. J. Kubas, J. C. Bryan, C. J. Burns and C. J. Unkefer, *J. Am. Chem. Soc.*, 1995, **117**, 1159.
- 80 H. Azizian, K. R. Dixon, C. Eaborn, A. Pidcock, N. M. Shuaib and J. Vinaixa, *J. Chem. Soc., Chem. Commun.*, 1982, 1020.
- 81 H. C. Clark and M. J. Hampden-Smith, *Co-ord. Chem. Rev.*, 1987, **79**, 229.
- 82 P. Y. K. Lo, Patent, US-4774111, 1987; S. S. D. Brown, R. G. Taylor and P. Y. K. Lo, Patent, DE-4204305, 1992.
- 83 P. S. Engel, *Chem. Rev.*, 1980, **80**, 99.
- 84 S. N. Heaton, *D.Phil Thesis*, University of York, 1995.
- 85 H. Kisch and P. Holzmeier, *Adv. Organomet. Chem.*, 1992, **34**, 67.
- 86 R. S. Dickson and J. A. Ibers, *J. Am. Chem. Soc.*, 1972, **94**, 2988.
- 87 A. Nakamura, T. Yoshida, M. Cowie, S. Otsuka and J. A. Ibers, *J. Am. Chem. Soc.*, 1977, **99**, 2108.
- 88 S. D. Ittel and J. A. Ibers, *Inorg. Chem.*, 1973, **12**, 2290.
- 89 A. W. Adamson, W. L. Waltz, E. Zinato, D. W. Watts, P. D. Fleischauer and R. D. Lindholm, *Chem. Rev.*, 1968, **68**, 541.
- 90 R. S. Paonessa, A. L. Prignano and W. C. Trogler, *Organometallics*, 1985, **4**, 647.
- 91 A. L. Prignano and W. C. Trogler, *J. Am. Chem. Soc.*, 1987, **109**, 3586.
- 92 M. Ciriano, M. Green, J. A. K. Howard, J. Proud, J. L. Spencer, F. G. A. Stone and C. A. Tsipis, *J. Chem. Soc., Dalton Trans.*, 1978, 801.
- 93 G. K. Anderson, G. J. Lumetta and J. W. Siria, *J. Organomet. Chem.*, 1992, **434**, 253.
- 94 J. Y. Saillard and R. Hoffmann, *J. Am. Chem. Soc.*, 1984, **106**, 2006; P. Hoffman, H. Heiss and G. Müller, *Z. Naturforsch.*, 1987, **B42**, 395.

- 95 M. Hackett, J. A. Ibers, P. Jernakoff and G. M. Whitesides, *J. Am. Chem. Soc.*, 1986, **108**, 8094; M. Hackett, J. A. Ibers and G. M. Whitesides, *J. Am. Chem. Soc.*, 1988, **110**, 1436; M. Hackett and G. M. Whitesides, *J. Am. Chem. Soc.*, 1988, **110**, 1449.

CHAPTER 2

PLATINUM AZODICARBONYL COMPLEXES

2.1 INTRODUCTION

Heaton has shown that azo, or diazene, compounds with carbonyl groups adjacent to the azo function can inhibit the activities of Karstedt's catalyst.¹ As discussed in Chapter 1 (Section 1.4.1), Heaton demonstrated that after inhibition by azodicarbonyl ligands, Karstedt's catalyst can be reactivated thermally or photochemically. However, the co-ordination mode of the azodicarbonyl compound to the platinum centre in Karstedt's catalyst has not been clearly identified.

There are, in general, two ways in which an azo ligand can co-ordinate to transition metals.² The usual mode requires the azo group to utilise its lone pair(s) on the nitrogen atom(s), often the HOMO, to form σ bond(s) with the metal. This method of co-ordination can generate both mononuclear and binuclear complexes (Figure 2.1).^{2,3}

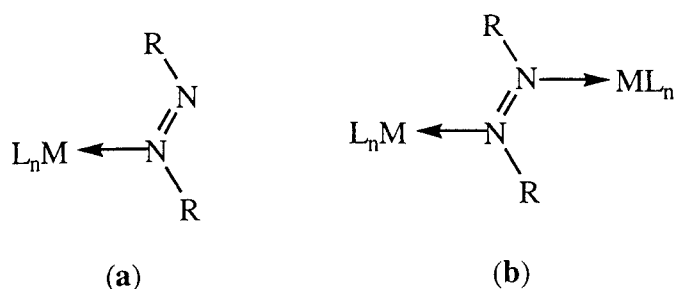


Figure 2.1 (a) Mononuclear azo transition metal σ complex. (b) Binuclear azo transition metal σ complex.

The second mode of co-ordination involves the symmetrical binding of the azo moiety to the metal by the transfer of electron density from the $N=N$ π -bonding molecular orbital to the metal and from the metal to the $N=N$ π^* -antibonding molecular orbital (Figure 2.2).⁴ Both of these bonding methods will be discussed in more detail in Section 2.3.2.

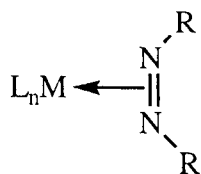
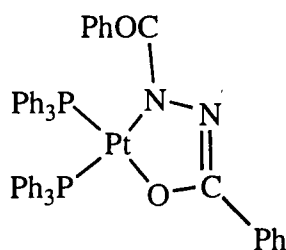


Figure 2.2 η^2 -azo transition metal complex.

Introduction of substituents other than simple alkyl or aryl groups into the azo compound can provide additional co-ordination sites for the metal. A carbonyl-substituted azo compound, for instance, can bind through oxygen as well as nitrogen.^{5,6} Ittel and Ibers have shown by X-ray crystallography that the azo ligand in the complex

$\text{Pt}(\text{PPh}_3)_2(\text{PhOCNNCOPh})$ **1** co-ordinates to the metal as a metallacycle, binding to the metal through one oxygen and one nitrogen atom to form a five-membered ring.⁷

Bond lengths from the crystal structure of **1** revealed that the $\text{N}=\text{N}$ double bond had lengthened to that of a single bond and one of the $\text{C}-\text{N}$ single bonds had shortened to that of a $\text{C}=\text{N}$ double bond when compared to the free ligand. Thus, this form can be described as a $\text{Pt}(\text{II})$ complex with a substituted hydrazido ligand.⁷



(1)

Stone and co-workers in the late 1960s postulated that $\text{Pt}(\text{PPh}_3)_2(\text{EtO}_2\text{CNNCO}_2\text{Et})$ **2** adopts a symmetrical structure, where the azodicarboxylate ligand is co-ordinated to the metal in an η^2 -fashion (Figure 2.2).⁸ Cenini and co-workers later revealed that **2** in fact contains two inequivalent phosphorus nuclei,⁹ indicating that the azodicarboxylate ligand in **2** co-ordinates to platinum in the same way as the azo-dibenzoyl ligand found in **1**.

It is also important to note that transition metal complexes of diazo $\text{RNNR}(0)$, diazenido $\text{NNR}(0)$ and hydrazido $\text{NRNR}_2(1-)$ or $\text{NNR}_2(2-)$, represent important stages of dinitrogen activation by transition metals.^{10,11} This is of special relevance to nitrogen fixation in biological systems where molecular dinitrogen is converted to ammonia by the enzyme nitrogenase. The active site of nitrogenase, believed to be responsible for the co-ordination and activation of dinitrogen, was found to contain Fe and Mo atoms.¹² Extensive research in this area has produced a wide variety of dinitrogen complexes many of which can be protonated to form hydrazines and/or ammonia. For example, the complexes $\text{M}(\text{N}_2)_2\text{P}_4$ [$\text{M} = \text{Mo}$ or W ; $\text{P} = \text{mono}(\text{phosphine})$ or $\text{P}_2 = \text{bis}(\text{phosphine})$] have been shown to react with halogen acid or HBF_4 to yield the diazenido or hydrazido metal complex with chelating phosphine attached to the metal, or ammonia with monophosphine attached to the metal.^{13,14} The ultimate aim of this area of research is to produce an efficient catalytic system which mimics the biological system.

In this chapter, the full characterisation of $\text{Pt}(\text{PMe}_3)_2(\text{PhOCNNCOPh})$ **3** and $\text{Pt}(\text{PMe}_3)_2(\text{MeOCNNCOMe})$ **4**, the trimethylphosphine analogues of **1**, is reported. New routes to the platinum azodicarboxylate complexes $\text{Pt}(\text{PPh}_3)_2(\text{EtO}_2\text{CNNCO}_2\text{Et})$ **2** and $\text{Pt}(\text{PPh}_3)_2(\text{Pr}^i\text{O}_2\text{CNNCO}_2\text{Pr}^i)$ **5** have also been developed. A crystal structure of **5** has been obtained, which provides unambiguous evidence on the binding mode of the

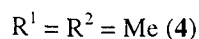
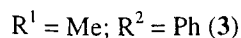
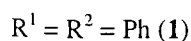
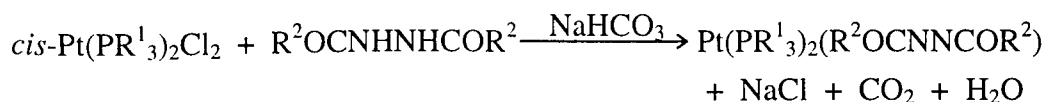
azodicarboxylate ligand to the platinum centre. These compounds were synthesised in order to test their photochemical properties.

2.2 RESULTS

2.2.1 Preparation of $\text{Pt}(\text{PR}^1_3)_2(\text{R}^2\text{OCNNCOR}^2)$ complexes [$\text{R}^1 = \text{R}^2 = \text{Ph}$ (1); $\text{R}^1 = \text{Me}, \text{R}^2 = \text{Ph}$ (3); $\text{R}^1 = \text{R}^2 = \text{Me}$ (4)]

The procedure reported by Dilworth and Kasenally¹⁵ for the preparation of the complex $\text{Pt}(\text{PPh}_3)_2(\text{PhOCNNCOPh})$ **1** was used to synthesise the two analogues, $\text{Pt}(\text{PMe}_3)_2(\text{PhOCNNCOPh})$ **3** and $\text{Pt}(\text{PMe}_3)_2(\text{MeOCNNCOMe})$ **4**. Reaction of the *cis*-platinum bisphosphine dichloride complex with the appropriate diacyl hydrazine in refluxing ethanol, in the presence of NaHCO_3 , yielded air-stable crystals of the azo platinum complex after work up (60-70 % yield, Equation 2.1).

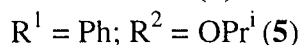
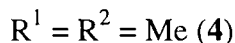
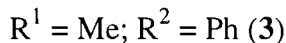
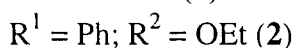
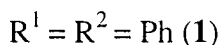
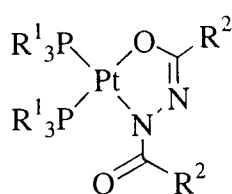
Complex **1** was also synthesised by the same method as shown in Equation 2.1 in order to obtain comparative spectroscopic data. Complexes **1**, **3** and **4** are all highly soluble in benzene, THF and chlorinated solvents.



(2.1)

2.2.2 NMR characterisation of $\text{Pt}(\text{PR}^1_3)_2(\text{R}^2\text{OCNNCOR}^2)$ complexes [$\text{R}^1 = \text{R}^2 = \text{Ph}$ (1); $\text{R}^1 = \text{Me}, \text{R}^2 = \text{Ph}$ (3); $\text{R}^1 = \text{R}^2 = \text{Me}$ (4)]

Multinuclear NMR spectroscopy of complexes **1**, **3** and **4** (Tables 2.1-2.4) indicates that the co-ordination of the azo ligand $\text{R}^2\text{OCNNCOR}^2$ ($\text{R}^2 = \text{Me}, \text{Ph}$) to the platinum centre is *via* the oxygen and nitrogen atoms (Scheme 2.1) as in the crystal structure of **1**.⁷



Scheme 2.1 The complexes $\text{Pt}(\text{PR}^1_3)_2(\text{R}^2\text{OCNNCOR}^2)$, showing the binding mode of the azodicarbonyl ligand.

The ^{31}P $\{^1\text{H}\}$ NMR spectrum of **4** in CDCl_3 shows two inequivalent phosphorus nuclei that are mutually coupled and possess ^{195}Pt satellites (Figure 2.3). The two $^1J(\text{PtP})$ coupling constants of **4** differ by about 400 Hz. Generally, a phosphorus nucleus *trans* to an oxygen donor has a larger $^1J(\text{PtP})$ value compared to a phosphorus *trans* to a nitrogen donor;¹⁶ this is discussed in more detail in Section 2.3.1. Following this trend we can assign the resonance at $\delta_{\text{P}} -37.0$ [$^1J(\text{PtP}) = 3448$ Hz] to the phosphorus nucleus *trans* to the oxygen donor and the resonance at $\delta_{\text{P}} -28.0$ [$^1J(\text{PtP}) = 3010$ Hz] to the phosphorus nucleus *trans* to the nitrogen donor. The phosphorus resonances for complexes **1-7** have been assigned in the same fashion (Table 2.2).

The ^1H NMR spectrum of **4** (Figure 2.4) in CD_2Cl_2 shows two methyl resonances on the azodiacyl ligand as a singlet at $\delta_{\text{H}} 2.08$ and a doublet at $\delta_{\text{H}} 1.91$ [$^5J(\text{PH}) = 0.9$ Hz]. The two PMe_3 groups appear as separate doublets at $\delta_{\text{H}} 1.62$ and $\delta_{\text{H}} 1.72$, each possessing overlapping ^{195}Pt satellites. On selective phosphorus decoupling at $\delta_{\text{P}} -37$, phosphorus *trans* to oxygen, the doublet resonances at $\delta_{\text{H}} 1.91$ (COMe) and $\delta_{\text{H}} 1.72$ (PMe_3) in the ^1H NMR spectrum collapse into singlets. On selective phosphorus decoupling at $\delta_{\text{P}} -28$, phosphorus *trans* to nitrogen, only the doublet resonance at $\delta_{\text{H}} 1.62$ (PMe_3) in the ^1H NMR spectrum collapses into a singlet. Hence the resonance at $\delta_{\text{H}} 1.62$ is due to the PMe_3 *trans* to nitrogen and the resonance at $\delta_{\text{H}} 1.72$ is due to the PMe_3 *trans* to oxygen. On changing the solvent to C_6D_6 we observe a substantial downfield shift of the azodiacyl methyl resonances and an upfield shift of the PMe_3 doublets, with increased separation between them (Figure 2.5).

The ^{13}C $\{^1\text{H}\}$ NMR spectrum of **4** (Figure 2.6) shows two CO resonances at $\delta_{\text{C}} 175.4$ and $\delta_{\text{C}} 165.4$, the former resonance being a doublet [$J(\text{PC}) = 3$ Hz] with ^{195}Pt satellites [$J(\text{PtC}) = 67$ Hz] and the latter a doublet of doublets [$J(\text{PC}) = 9$ and 4 Hz] without detectable ^{195}Pt satellites (Figure 2.7). The azodiacyl methyl carbon atoms can be detected as two doublet resonances at $\delta_{\text{C}} 22.1$ [$J(\text{PC}) = 4$ Hz] and $\delta_{\text{C}} 16.5$ [$J(\text{PC}) = 5$ Hz] (Figure 2.8).

The ^{195}Pt $\{^1\text{H}\}$ NMR spectrum of **4** (Figure 2.9, Table 2.4) confirms the presence of two inequivalent phosphine ligands attached to the platinum centre. In Figure 2.9, we see a set of doublet of doublets whose $J(\text{PtP})$ values roughly correspond to the $J(\text{PtP})$ values obtained from the ^{31}P $\{^1\text{H}\}$ spectrum of **4** (Figure 2.3, Table 2.2).

Compound	δ (J / Hz)
Pt(PPh ₃) ₂ (PhOCNNCOPh) 1^a	7.00-8.00 (m, Ph)
Pt(PPh ₃) ₂ (EtO ₂ CNNCO ₂ Et) 2^b	1.14 (3 H, br. t, CH ₂ CH ₃) 1.35 [3 H, t, CH ₂ CH ₃ , <i>J</i> (HH) = 7.0] 4.12 (2 H, br., CH ₂ CH ₃) 4.57 [2 H, quart, CH ₂ CH ₃ , <i>J</i> (HH) = 7.0] 7.00-8.00 (30 H, m, Ph)
Pt(PMe ₃) ₂ (PhOCNNCOPh) 3^a	1.80 [9 H, d, PCH ₃ , ² <i>J</i> (PH) = 11.0] ^c 1.90 [9 H, d, PCH ₃ , ² <i>J</i> (PH) = 11.3] ^c 7.00-8.00 (10 H, m, Ph)
Pt(PMe ₃) ₂ (MeOCNNCOMe) 4^d	1.62 [9 H, d, PCH ₃ , ² <i>J</i> (PH) = 10.7] ^c 1.72 [9 H, d, PCH ₃ , ² <i>J</i> (PH) = 11.2] ^c 1.91 [3 H, d, COCH ₃ , ⁵ <i>J</i> (HH) = 0.9] 2.08 (3 H, s, COCH ₃)
Pt(PPh ₃) ₂ (Pr ¹ O ₂ CNNCO ₂ Pr ¹) 5^e	0.75 [6 H, d, CH(CH ₃) ₂ , <i>J</i> (HH) = 6.2] 1.06 [6 H, d, CH(CH ₃) ₂ , <i>J</i> (HH) = 6.2] 4.08 [1 H, sept, CH(CH ₃) ₂ , <i>J</i> (HH) = 6.2] 4.12 [1 H, sept, CH(CH ₃) ₂ , <i>J</i> (HH) = 6.2] 7.00-8.00 (30 H, m, Ph)
Pt(dppe)(EtO ₂ CNNCO ₂ Et) 6^b	0.97 [3 H, t, CH ₂ CH ₃ , <i>J</i> (HH) = 7.2] 1.23 [3 H, t, CH ₂ CH ₃ , <i>J</i> (HH) = 7.2] 4.00 [2 H, d, CH ₂ CH ₃ , <i>J</i> (HH) = 7.2] 4.62 [2 H, d, CH ₂ CH ₃ , <i>J</i> (HH) = 7.2]
Pt(dppe)(Pr ¹ O ₂ CNNCO ₂ Pr ¹) 7^b	1.10 [6 H, d, CH(CH ₃) ₂ , <i>J</i> (HH) = 6.2] 1.36 [6 H, d, CH(CH ₃) ₂ , <i>J</i> (HH) = 6.2] 4.79 [1 H, sept, CH(CH ₃) ₂ , <i>J</i> (HH) = 6.2] 5.40 [1 H, sept, CH(CH ₃) ₂ , <i>J</i> (HH) = 6.2] 7.00-8.00 (30 H, m, Ph)

Table 2.1 ¹H (300.13 MHz, 295 K) NMR spectroscopic data for complexes **1-7**. P^O indicates phosphorus *trans* to oxygen and P^N indicates phosphorus *trans* to nitrogen. *a* In CDCl₃. *b* In C₆D₆. *c* Contain overlapping ¹⁹⁵Pt satellites. *d* In CD₂Cl₂. *e* In [²H₈]THF.

Compound	δ (J / Hz)
Pt(PPh ₃) ₂ (PhOCNNCOPh) 1^a	17.5 [d, P ^N , ² J(PP) = 22, J(PtP) = 3261] 3.1 [d, P ^O , ² J(PP) = 22, J(PtP) = 3685]
Pt(PPh ₃) ₂ (EtO ₂ CNNCO ₂ Et) 2^b	6.2 [br. d, P ^O , J(PtP) \approx 3790] 16.6 [d, P ^N , ² J(PP) = 23, J(PtP) = 3166]
Pt(PMe ₃) ₂ (PhOCNNCOPh) 3^a	-10.9 [d, P ^N , ² J(PP) = 26, J(PtP) = 3028] -20.1 [d, P ^O , ² J(PP) = 26, J(PtP) = 3435]
Pt(PMe ₃) ₂ (MeOCNNCOMe) 4^c	-28.0 [d, P ^N , ² J(PP) = 27, J(PtP) = 3010] -37.0 [d, P ^O , ² J(PP) = 27, J(PtP) = 3448]
Pt(PPh ₃) ₂ (Pr ⁱ O ₂ CNNCO ₂ Pr ⁱ) 5^d	5.8 [d, P ^O , ² J(PP) = 23, J(PtP) = 3859] 16.5 [d, P ^N , ² J(PP) = 23, J(PtP) = 3158]
Pt(dppe)(EtO ₂ CNNCO ₂ Et) 6^b	31.1 [d, P ^O , ² J(PP) = 11, J(PtP) = 3839] 38.1 [d, P ^N , ² J(PP) = 11, J(PtP) = 3041]
Pt(dppe)(Pr ⁱ O ₂ CNNCO ₂ Pr ⁱ) 7^b	31.0 [d, P ^O , ² J(PP) = 12, J(PtP) = 3843] 38.1 [d, P ^N , ² J(PP) = 12, J(PtP) = 3023]

Table 2.2 ³¹P {¹H} (121.49 MHz, 295 K) NMR spectroscopic data for complexes **1-7**. Couplings to Pt refer to the satellites from ¹⁹⁵Pt. P^O indicates phosphorus *trans* to oxygen and P^N indicates phosphorus *trans* to nitrogen. *a* In CDCl₃. *b* In C₆D₆. *c* In CD₂Cl₂. *d* In [²H₈]THF.

Compound	δ (J / Hz)
Pt(PPh ₃) ₂ (PhOCNNCOPh) 1^a	127.1-135.2 (Ph) 163.2 [dd, $\underline{\text{C}}\text{O}$, $J(\text{PC}) = 10, 3$] 171.7 [d, $\underline{\text{C}}\text{O}$, $J(\text{PC}) = 4$]
Pt(PMe ₃) ₂ (PhOCNNCOPh) 3^a	16.6 [d, $\underline{\text{P}}\underline{\text{C}}\text{H}_3$, $J(\text{PC}) = 38$, ${}^2J(\text{PtC}) = 33$] 19.7 [dd, $\underline{\text{P}}\underline{\text{C}}\text{H}_3$, $J(\text{PC}) = 44, 2$; ${}^2J(\text{PtC}) = 43$] 124.2-131.8 (Ph) 163.4 [dd, $\underline{\text{C}}\text{O}$, $J(\text{PC}) = 9, 3$] 174.6 [d, $\underline{\text{C}}\text{O}$, $J(\text{PC}) = 4$]
Pt(PMe ₃) ₂ (MeOCNNCOMe) 4^b	16.3 [d, $\underline{\text{P}}\underline{\text{C}}\text{H}_3$, $J(\text{PC}) = 38$, ${}^2J(\text{PtC}) = 33$] 16.5 [d, $\underline{\text{C}}\text{H}_3$, $J(\text{PC}) = 5$] 19.6 [dd, $\underline{\text{P}}\underline{\text{C}}\text{H}_3$, $J(\text{PC}) = 45, 2$; ${}^2J(\text{PtC}) = 45$] 22.1 [d, $\underline{\text{C}}\text{H}_3$, $J(\text{PC}) = 4$] 165.4 [dd, $\underline{\text{C}}\text{O}$, $J(\text{PC}) = 9, 4$] 175.4 [d, $\underline{\text{C}}\text{O}$, $J(\text{PC}) = 3$, $J(\text{PtC}) = 67$]
Pt(PPh ₃) ₂ (Pr ⁱ O ₂ CNNCO ₂ Pr ⁱ) 5^c	23.8 (s, $\underline{\text{C}}\text{H}_3$) 24.1 (s, $\underline{\text{C}}\text{H}_3$) 67.6 (s, $\underline{\text{C}}\text{H}$) 71.2 (s, $\underline{\text{C}}\text{H}$) 128.8-136.6 (Ph)

Table 2.3 ${}^{13}\text{C}$ { ${}^1\text{H}$ } (75.47 MHz, 295 K) NMR spectroscopic data of complexes **1** and **3-5**. Couplings to Pt refer to satellites from ${}^{195}\text{Pt}$. *a* In CDCl_3 . *b* In $[\text{}^2\text{H}_8]\text{THF}$, no CO resonances were detected.

Compound	δ (J / Hz)
Pt(PPh ₃) ₂ (PhOCNNCOPh) 1^a	-4291 [dd, $J(\text{PtP}^{\text{O}}) = 3680$, $J(\text{PtP}^{\text{N}}) = 3302$]
Pt(PMe ₃) ₂ (PhOCNNCOPh) 3^a	-4257 [dd, $J(\text{PtP}^{\text{O}}) = 3458$, $J(\text{PtP}^{\text{N}}) = 3028$]
Pt(PMe ₃) ₂ (MeOCNNCOMe) 4^a	-4260 [dd, $J(\text{PtP}^{\text{O}}) = 3446$, $J(\text{PtP}^{\text{N}}) = 3010$]
Pt(PPh ₃) ₂ (Pr ⁱ O ₂ CNNCO ₂ Pr ⁱ) 5^b	-4168 [dd, $J(\text{PtP}^{\text{O}}) = 3871$, $J(\text{PtP}^{\text{N}}) = 3118$]

Table 2.4 ${}^{195}\text{Pt}$ { ${}^1\text{H}$ } (107.52 MHz, 300 K) NMR spectroscopic data of complexes **1** and **3-5**. P^O indicates phosphorus *trans* to oxygen and P^N indicates phosphorus *trans* to nitrogen. *a* In CD_2Cl_2 . *b* In $[\text{}^2\text{H}_8]\text{THF}$.

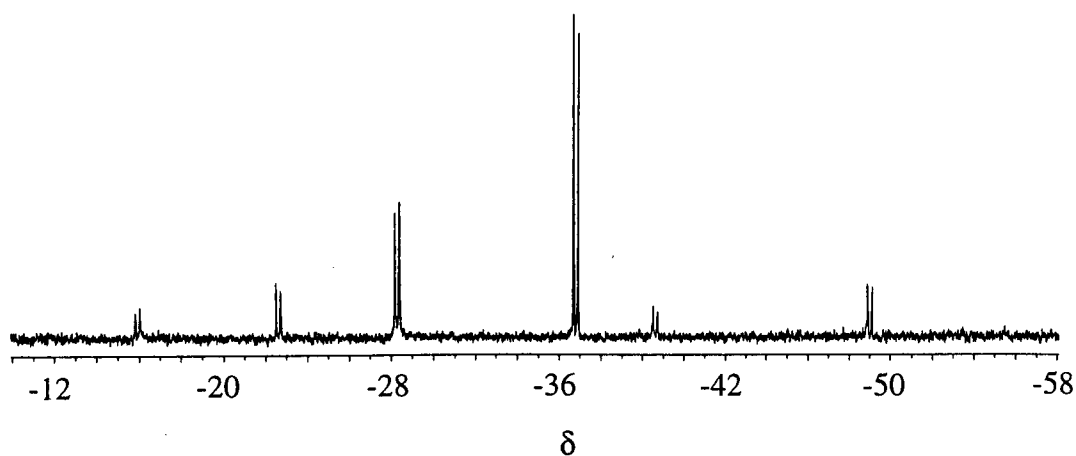


Figure 2.3 ^{31}P $\{^1\text{H}\}$ (121.49 MHz) NMR spectrum of $\text{Pt}(\text{PMe}_3)_2(\text{MeOCNNCOMe})$ **4** in CDCl_3 (295 K) consisting of two mutually coupled doublets, each with ^{195}Pt satellites.

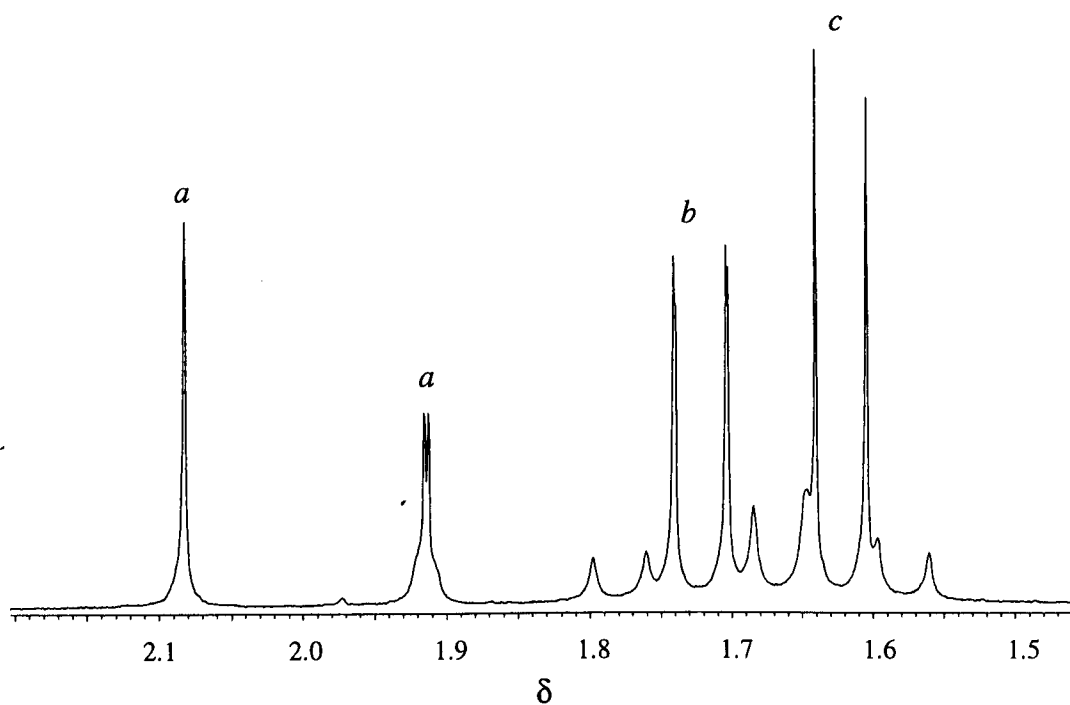


Figure 2.4 ^1H (300.13 MHz) NMR of $\text{Pt}(\text{PMe}_3)_2(\text{MeOCNNCOMe})$ **4** in CD_2Cl_2 (295 K). *a* COCH_3 . *b* PCH_3 (*trans* to nitrogen). *c* PCH_3 (*trans* to oxygen).

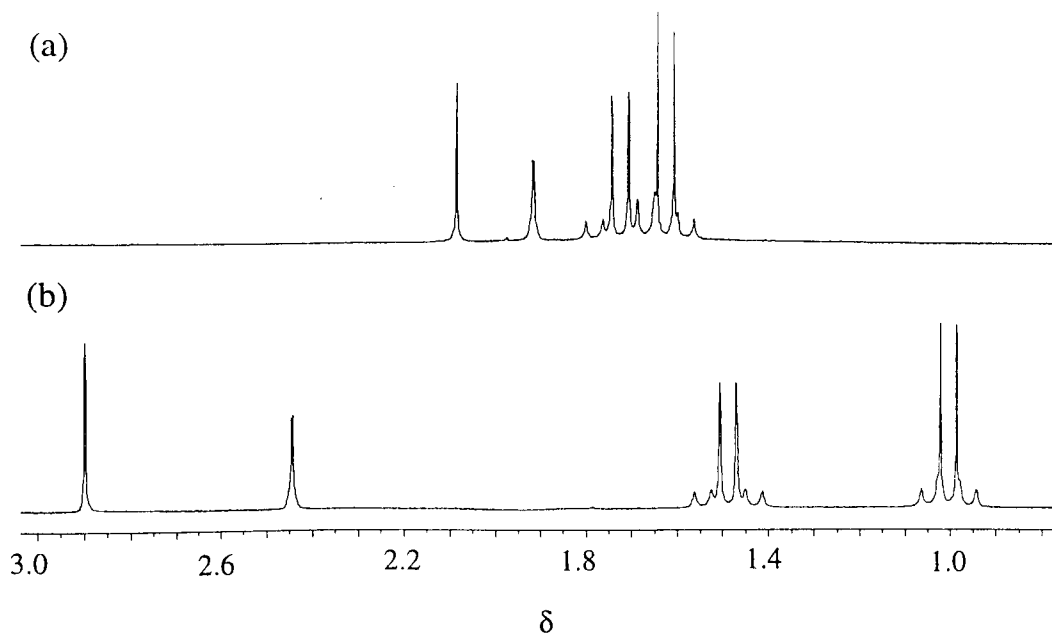


Figure 2.5 ^1H (300.13 MHz, 295 K) NMR spectrum of $\text{Pt}(\text{PMe}_3)_2(\text{MeOCNNCOMe})$ **4**. (a) in CD_2Cl_2 . (b) in C_6D_6 .

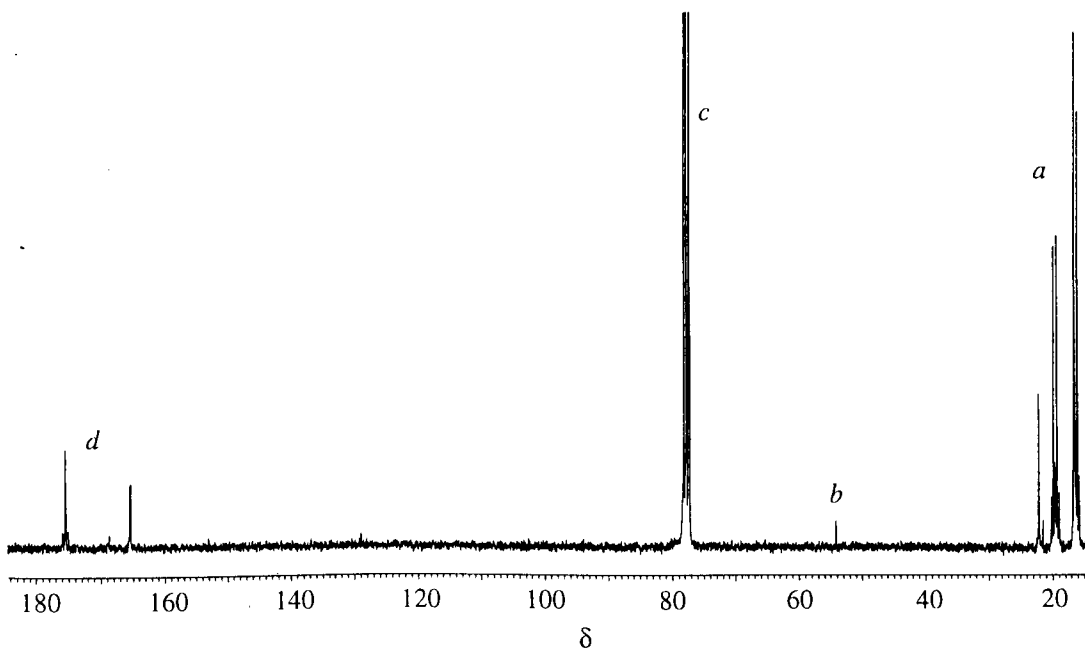


Figure 2.6 ^{13}C (^1H) (75.47 MHz, 295 K) NMR spectrum of **4** in CDCl_3 . *a* CH_3 resonances from PMe_3 and azodiacyl ligands. *b* impurities. *c* CDCl_3 . *d* CO resonances from azodiacyl ligand.

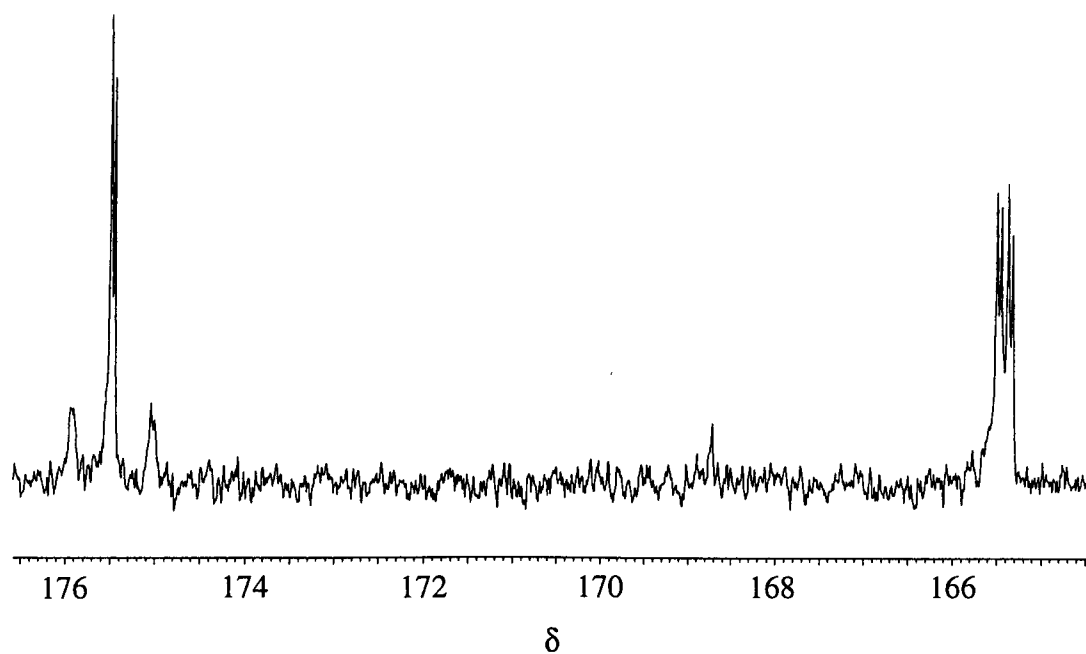


Figure 2.7 ^{13}C $\{^1\text{H}\}$ (75.47 MHz, 295 K) NMR spectrum of **4** in CDCl_3 , showing the azodiacyl CO resonances.

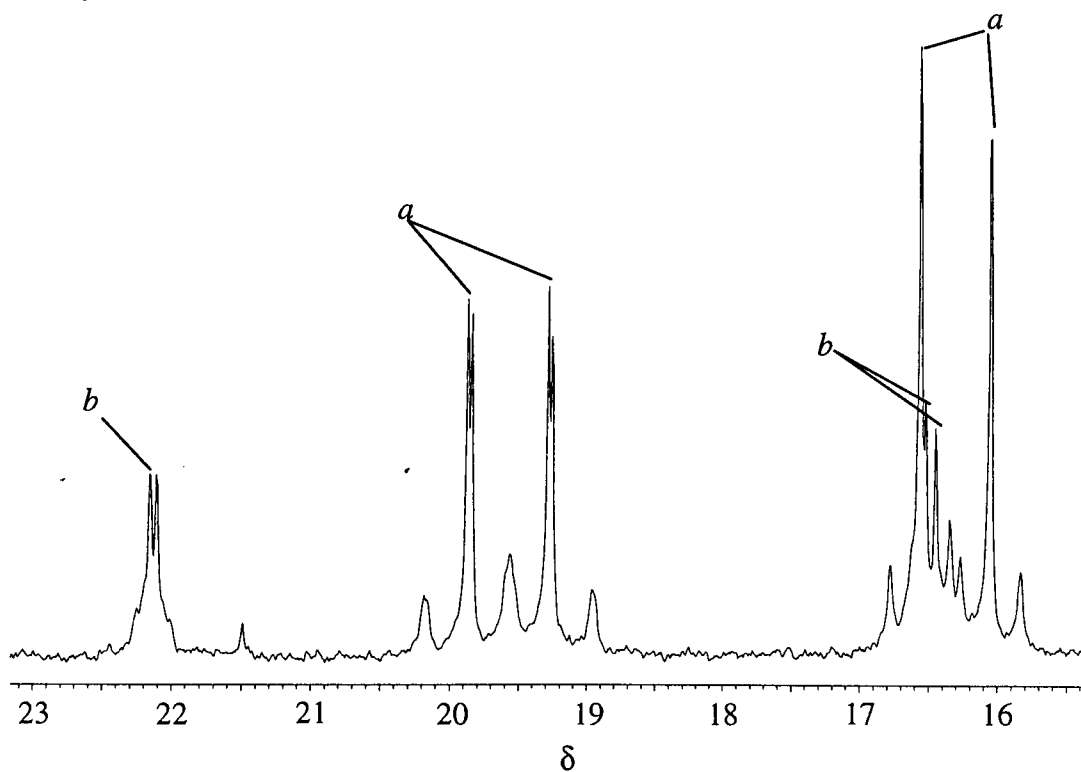


Figure 2.8 ^{13}C $\{^1\text{H}\}$ (75.47 MHz, 295 K) NMR spectrum of **4** in CDCl_3 , showing the methyl resonances of the PMe_3 and azodiacyl ligands. *a* $\text{P}\underline{\text{C}}\text{H}_3$ with ^{195}Pt satellites. *b* $\text{CO}\underline{\text{C}}\text{H}_3$.

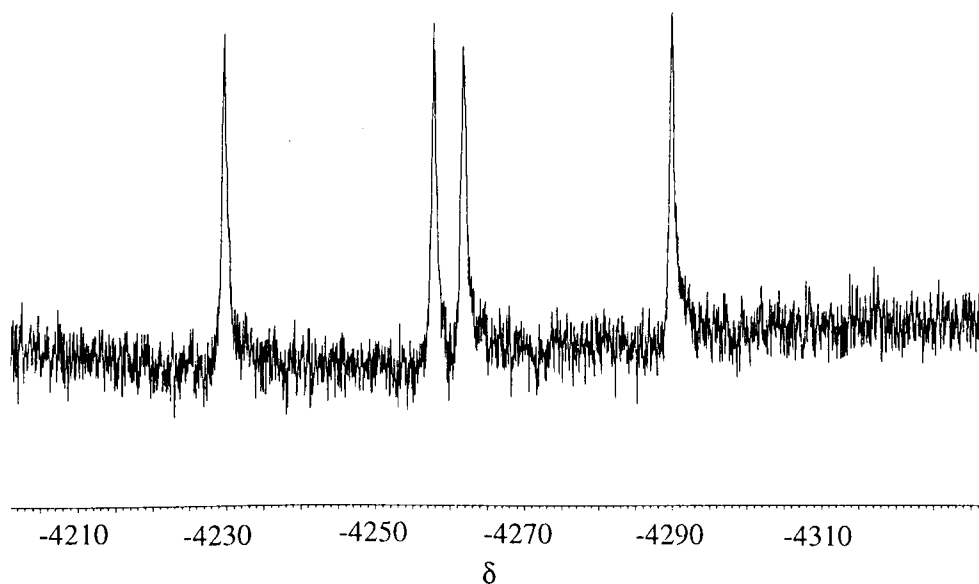


Figure 2.9 $^{195}\text{Pt} \{^1\text{H}\}$ (107.52 MHz, 300 K) NMR spectrum of **4** in CD_2Cl_2 . Complexes **1** and **3** show similar features.

2.2.3 UV/VIS and IR spectroscopic data of **1**, **3** and **4**

The UV/VIS spectra of complexes **1**, **3** and **4** show a prominent low-energy band at around 300 nm (Figure 2.8 and Table 2.5). Both complexes **1** and **3** show a band maximum at *ca.* 320 nm, whereas the band for **4** is shifted 15 nm to higher energy. This effect is observed on changing the azo from the aryl PhOCNNCOPh ligand to the alkyl MeOCNNCOMe ligand. No such effects are observed on changing the phosphine ligand from PPh_3 to PMe_3 . Since the crystal structure of **1** shows a conjugated metallacycle,⁷ this band is assigned as a transition of the metallacycle, rather than attempting to distinguish intra-ligand transitions from charge-transfer transitions.

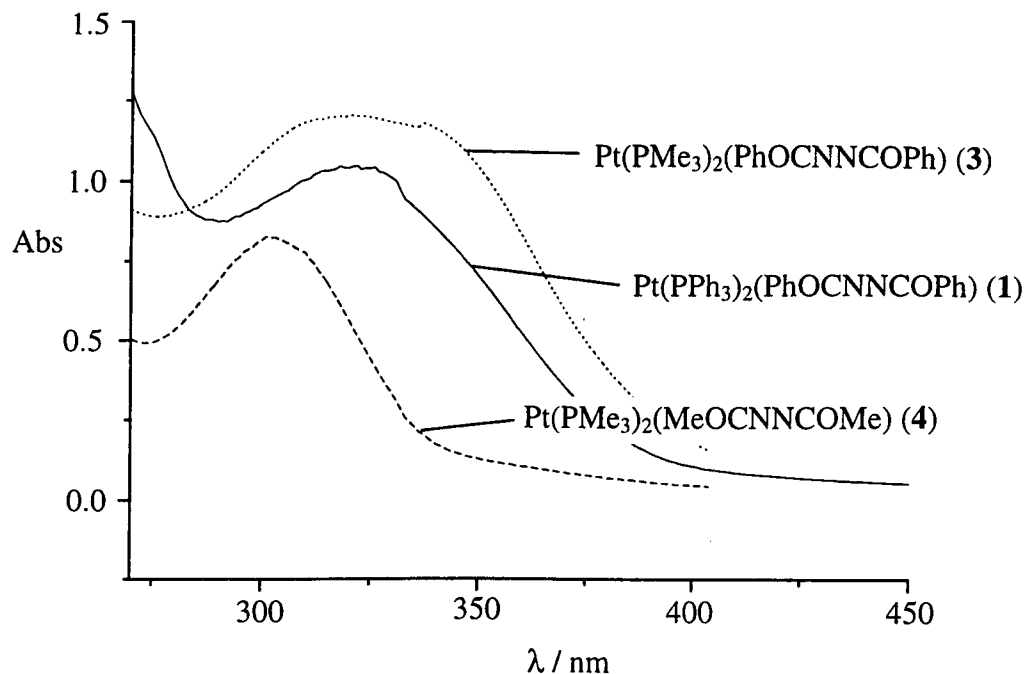


Figure 2.8 UV/VIS spectra of **1**, **3** and **4** in THF, showing the band assigned as the transition of the metallacycle. Complexes **1**, **3** and **4** are of different concentration.

The IR spectra of **1**, **3** and **4** show two broad bands in the region of 1560-1600 cm^{-1} (Figure 2.9 and Table 2.5), which were assigned as $\nu(\text{C}=\text{O})$ and $\nu(\text{C}=\text{N})$ and agree with Kasenally and Dilworth's observations.¹⁵ However, from the appearance of the spectra in Figure 2.9, other smaller peaks are evidently present, which could be due to a number of different CO/CN stretching bands present in the solid state.

Compound	UV/VIS in THF λ / nm ($\epsilon / \text{dm}^3 \text{mol}^{-1} \text{cm}^{-1}$)	IR, $\nu(\text{CO})$, $\nu(\text{CN})$ ν / cm^{-1}
Pt(PPh ₃) ₂ (PhOCNNCOPh) 1	318 (12000)	1565 ^a 1595 ^a
Pt(PPh ₃) ₂ (Et ₂ OCNNCO ₂ Et) 2	333 (3100) 463 (400)	1618 ^b 1642 ^b 1610 ^c 1621 ^c 1629 ^c 1648 ^c 1668 ^c
Pt(PMe ₃) ₂ (PhOCNNCOPh) 3	319 (8700)	1561 ^a 1586 ^a
Pt(PMe ₃) ₂ (MeOCNNCOMe) 4	303 (4500)	1576 ^a 1612 ^a
Pt(PPh)(Pr ⁱ ₂ OCNNCO ₂ Pr ⁱ) 5	337 (3100) 465 (400)	1613 ^c 1635 ^c

Table 2.5 UV/VIS and IR data for complexes **1-5**. *a* in KBr pellet. *b* in CH₂Cl₂. *c* in Nujol.

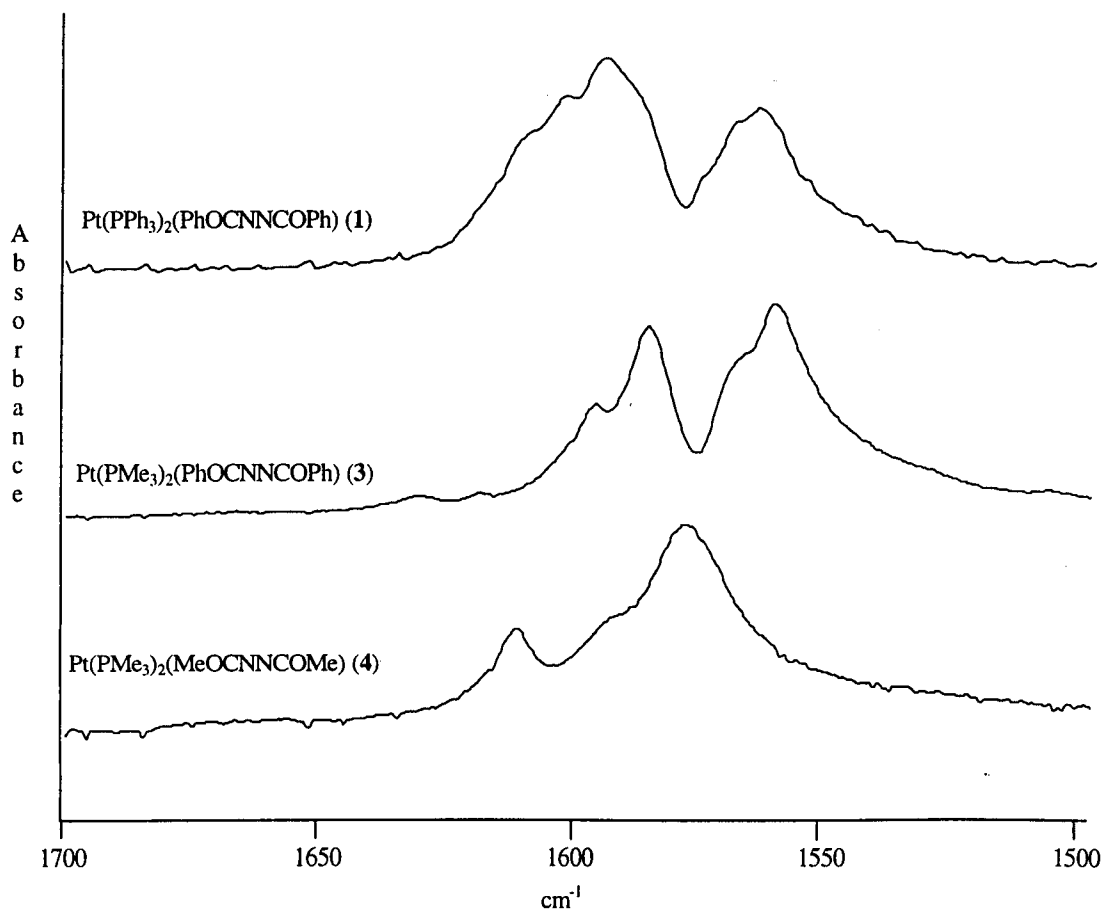
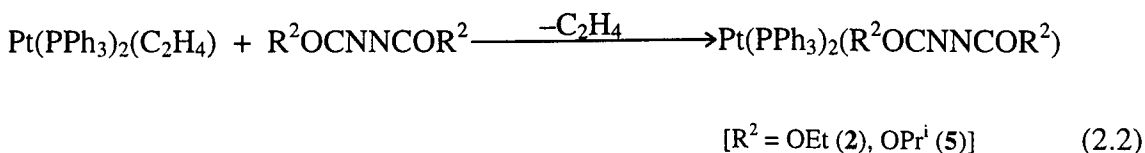


Figure 2.9 IR spectra of 1, 3-4 in KBr pellets.

2.2.4 Preparation of $\text{Pt}(\text{PPh}_3)_2(\text{R}^2\text{OCNNCOR}^2)$ complexes [$\text{R}^2 = \text{OEt}$ (2), OPr^i (5)]

Reaction of $\text{Pt}(\text{PPh}_3)_2(\text{C}_2\text{H}_4)$ with an equivalent amount or excess (up to threefold) of $\text{R}^2\text{OCNNCOR}^2$ ($\text{R}^2 = \text{OEt}$, OPr^i) in benzene at room temperature in the absence of light yields $\text{Pt}(\text{PPh}_3)_2(\text{R}^2\text{OCNNCOR}^2)$ [$\text{R}^2 = \text{OEt}$ (2), OPr^i (5)] and ethene gas (Equation 2.2).



These compounds are yellow/orange in colour and relatively stable as solids. Both 2 and 5 are slightly soluble in benzene, with 5 being more soluble in THF. Based on the evidence of Cenini *et al.*⁹ and our own work, the binding mode of the azo ligand in 2 corresponds to that found in complexes 1, 3 and 4, co-ordinating *via* the nitrogen and oxygen atoms to form a metallacycle.

2.2.5 NMR characterisation of Pt(PPh₃)₂(R²OCNNCOR²) complexes [R² = OEt (**2**), OPrⁱ (**5**)]

Multinuclear NMR spectra of Pt(PPh₃)₂(EtO₂CNNCO₂Et) **2** and Pt(PPh₃)₂(PrⁱO-OCNNCO₂Prⁱ) **5** confirm that both complexes have inequivalent phosphorus atoms as well as inequivalent alkyl groups on the azo ligand (Tables 2.1-2.4). Due to solubility problems suitable ¹³C {¹H} and ¹⁹⁵Pt {¹H} NMR spectra of complex **2** could not be obtained. Furthermore no CO resonances were observed in the ¹³C {¹H} NMR spectrum of **5** even after long periods of acquisition.

2.2.6 UV/VIS and IR spectroscopic data of **2** and **5**

The IR spectra of **2** and **5** show CO/CN stretching bands in the 1610-1670 cm⁻¹ region, which are higher in wavenumbers and more intense compared to the CO/CN bands assigned to **1**, **3-4** (Table 2.5). In the IR spectrum of **2**, two broad peaks are observed at around 1600 cm⁻¹ in dichloromethane, but in Nujol we can observe up to five peaks in the same region. The UV/VIS spectra of **2** and **5** contain low-energy shoulders at *ca.* 330 and 460 nm (Table 2.5).

2.2.7 Crystal Structure of Pt(PPh₃)₂(PrⁱO₂CNNCO₂Prⁱ)·(C₆H₆)₂ **5**

Crystals of **5** suitable for X-ray data collection were grown by slow evaporation of a 2:1 THF-benzene solution of **5** at room temperature. The crystal data were collected and refined by Leroy Cronin at the University of York. The structure of **5** consists of monomolecular units of the complex with two molecules of benzene per unit cell (Figure 2.10). Crystallographic details are summarised in Table 2.6. The structure of **5** in Figure 2.11 and 2.12 clearly shows that the azo ligand co-ordinates to the platinum centre through the oxygen atom of one carbonyl group and the nitrogen atom of the azo function remote from the co-ordinated carbonyl.

The principal bond lengths and angles (Figure 2.13) follow a very similar pattern to that reported for **1** and related azodiacyl metal complexes.^{5,6,7} The platinacycle contains O–C and N–N bonds which are extended relative to those of the free ligand, while the C–N bond is shortened.⁷ The platinacycle containing Pt, O1, C5, N2 and N1 is planar within 0.012 Å (Plane 1) and essentially co-planar with the co-ordinated atoms P1, P2, O1 and N1 which are planar within 0.028 Å (Plane 2). The exocyclic carbon atom C4 is co-planar with the metallacycle, atoms Pt1, N1, N2 and C4 are planar within 0.001 Å (Plane 3). Calculations of least-squares planes 1, 2 and 3 are summarised in Tables 2.7 and 2.8. The phosphorus-metal bond lengths differ only slightly [$\delta r(\text{Pt-P}) =$

0.012 Å], but there is a substantial difference in the angles to adjacent ligands: P1–Pt–N1 = 97.5(1)°, P2–Pt–O1 = 87.1(1)°.

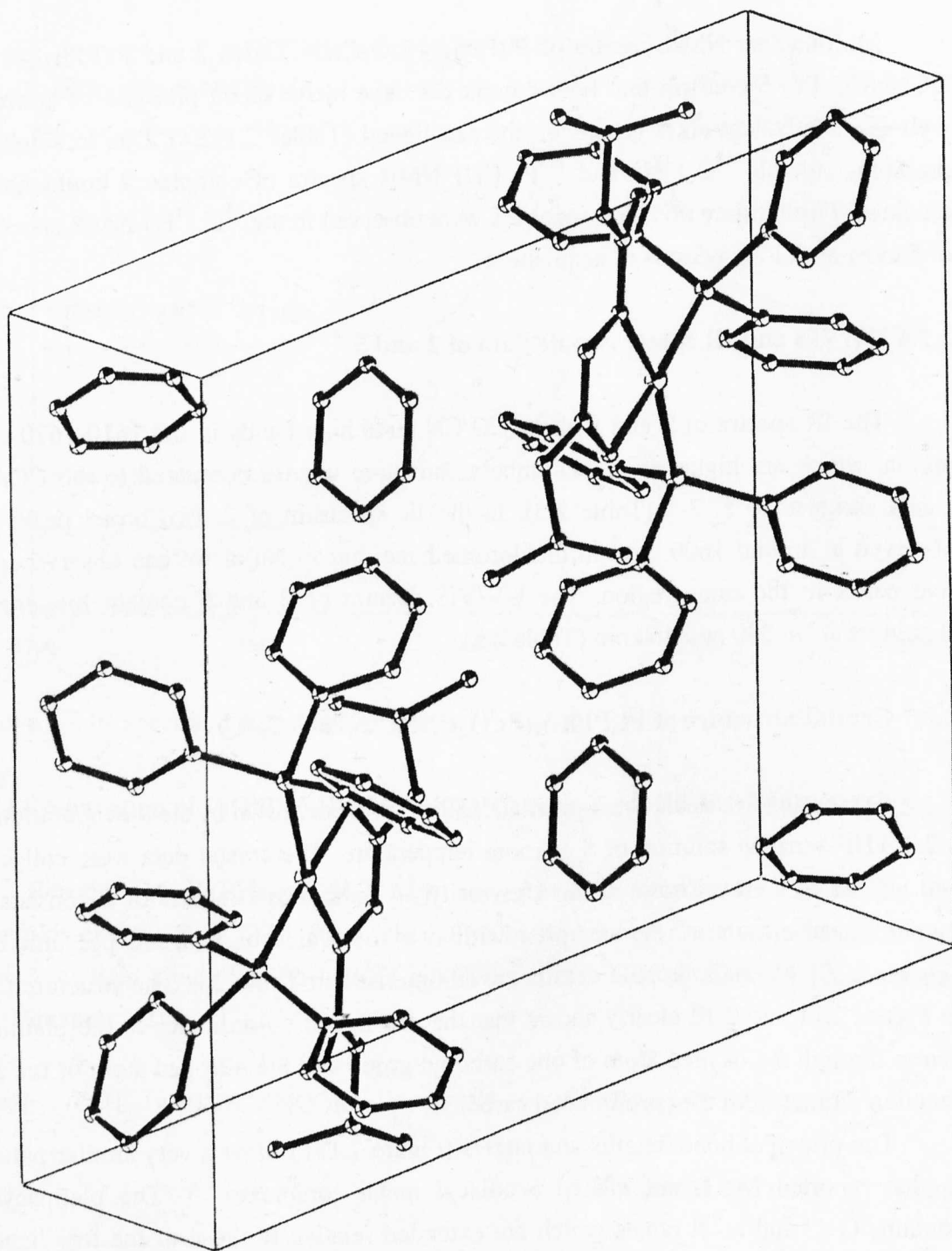


Figure 2.10 Packing arrangement in a unit cell of Pt(PPh₃)₂(PrⁱO₂CNCNCO₂Prⁱ) (5), showing two molecules of benzene of crystallisation.

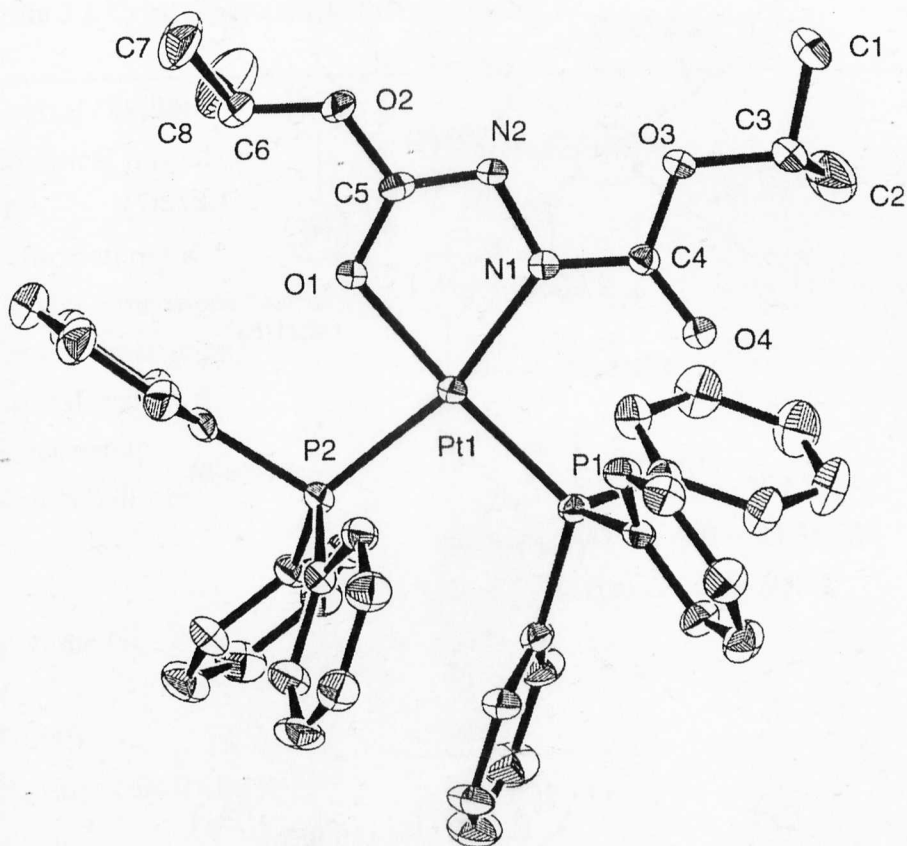


Figure 2.11 ORTEP¹⁷ drawing of $\text{Pt}(\text{PPh}_3)_2(\text{Pr}^i\text{O}_2\text{C}\text{N}\text{N}\text{CO}_2\text{Pr}^i)$ (**5**) showing non-hydrogen atoms with thermal ellipsoids at the 30 % probability level. The two molecules of benzene of crystallisation are not shown.

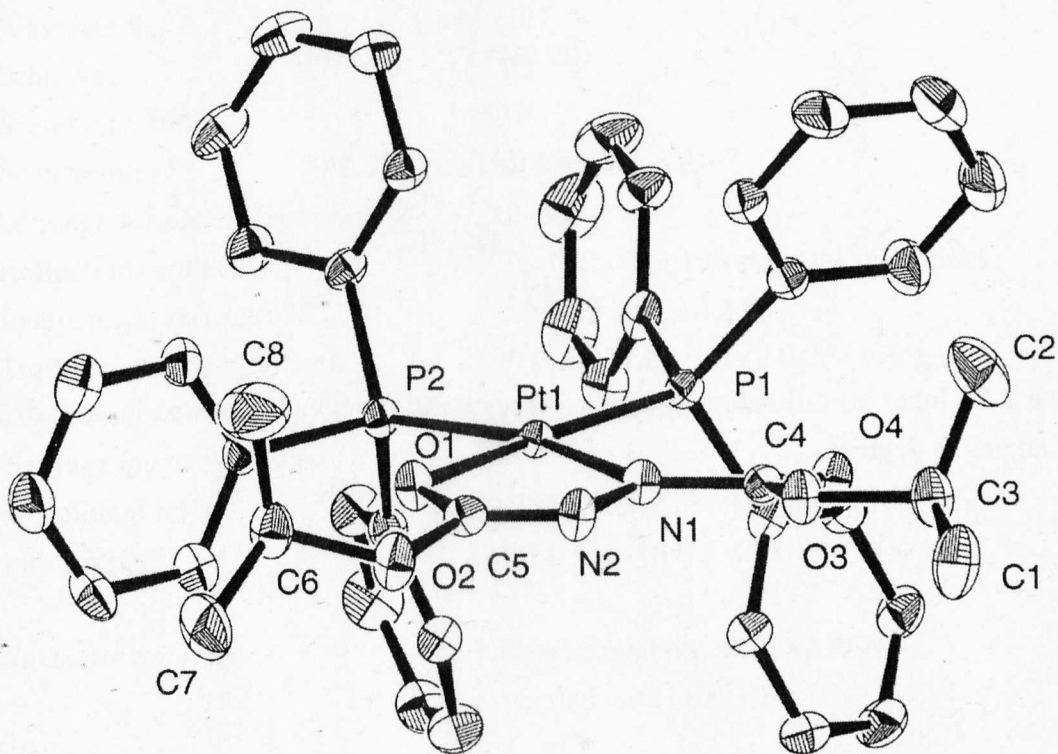


Figure 2.12 ORTEP¹⁷ drawing of **5** from an alternative perspective.

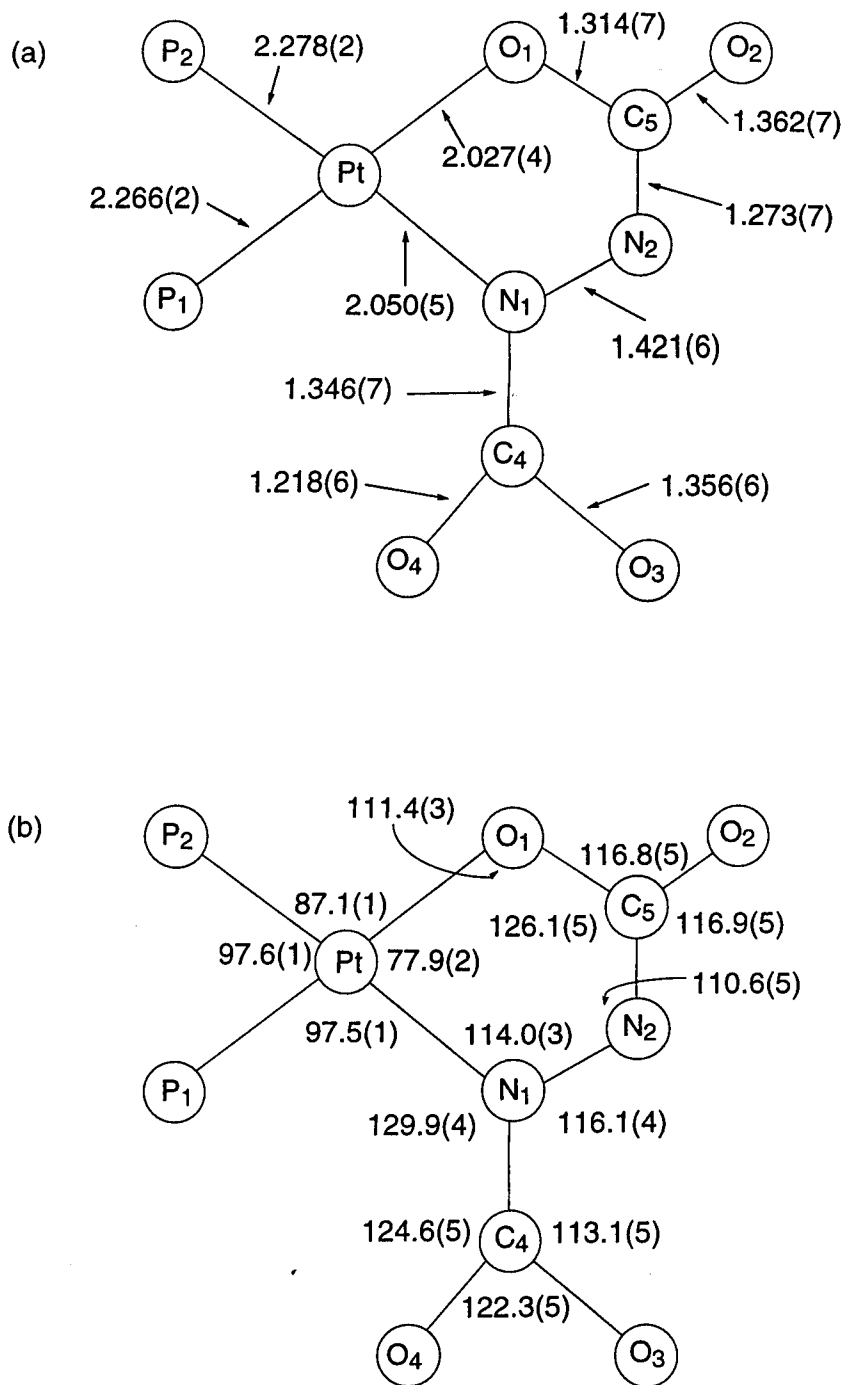


Figure 2.13 Inner co-ordination sphere of **5**, showing (a) bond distances in Å and (b) bond angles in degrees.

Table 2.6 Crystallographic data for complex **5**.

<i>Crystal Data</i>	
Empirical formula	C ₅₆ H ₅₆ N ₂ O ₂ P ₂ Pt
<i>M</i>	1078.06
Temperature / K	293(2)
Crystal dimensions / mm	0.4 x 0.4 x 0.4
Crystal description	Brown block
Crystal system	Triclinic
Space group	$\overline{P1}$ (No. 2)
Unit cell dimensions ^a	$a = 15.395(10) \text{ \AA}$ $\alpha = 104.86(3)^\circ$ $b = 15.8857(7) \text{ \AA}$ $\beta = 95.38(3)^\circ$ $c = 11.481(2) \text{ \AA}$ $\gamma = 66.95(3)^\circ$
Volume / \AA^3	2497(2)
<i>Z</i>	2
<i>F</i> (000)	1092
Density (calcd) / g cm ⁻³	1.434
μ / cm ⁻¹	29.21
<i>Data Collection</i>	
Diffractometer	Rigaku AFC6S
Radiation	MoK α , graphite monochromated
Wavelength / \AA	0.7107
Scan type	ω -2 θ
Scan rate / min ⁻¹	16.0°
Scan width / °	(1.21 + 0.30 tan θ)
2 θ range for data collection / °	5.18–50.02
Reflections collected	9336 (including 195 standard reflections)
Independent reflections ^b	8783 [<i>R</i> %(int) = 3.12]
Transmission co-efficients	0.90 (min), 1.00 (max), 0.96 (average)
Data corrections	Lorentz-polarisation
Average intensity change of standard reflx:	–0.9 % (3 reflx checked every 150 data)
Index ranges	0 ≤ <i>h</i> ≤ 18, –16 ≤ <i>k</i> ≤ 18, –13 ≤ <i>l</i> ≤ 13
<i>Structure Solution</i>	Patterson methods with SAPI91 ^c expanded with DIRDIF ^d

Table 2.6 (cont.)

<i>Refinement method</i>	Full-matrix least squares on F^2 with SHELXL93 ^c
Non-hydrogen atoms	Anisotropic
Hydrogen atoms	Riding model, isotropic
Weighting scheme	$w = [\sigma^2(F_o^2) + (0.0457P)^2]^{-1}$ $P = [\max(I_{\text{obs}}, 0) + 2F_c^2] / 3$
Data ^f / restraints / parameters	8783 / 0 / 586
Data-to-parameter ratio	14.98
Goodness-of-fit ^g on F^2	1.00
$R(\%)^h$ indices	
$[I_o > 2\sigma(I_o)]$	$R1 = 0.0391, wR2 = 0.0854$
All data	$R1 = 0.0650, wR2 = 0.0932$
Final difference map	
Largest diff. peak ⁱ and hole / $e \text{ \AA}^{-3}$	0.77 and -0.64
Largest shift / esd in final cycle	0.00

a Unit cell parameters and their esds were determined from a least-squares fitting of the setting angles of 20 reflections in the range $13.96^\circ \leq 2\theta \leq 15.82^\circ$. *b* $R(\text{int}) = \Sigma|F_o^2 - F_o^2(\text{mean})|/\Sigma[F_o^2]$; 358 reflections measured twice. *c* Ref. 18(a). *d* Ref. 18(b). *e* Ref. 18(c). *f* Zero reflections suppressed in the refinement. *g* $\text{GOF} = \{\Sigma[w(F_o^2 - F_c^2)^2]/(n - p)\}^{1/2}$ where p = number of parameters, n = number of data. *h* $R1 = \Sigma|F_o^2| - |F_o^2|/\Sigma|F_o^2|$. $wR1 = \{\Sigma[w(F_o^2 - F_c^2)^2]/\Sigma[w(F_o^2)^2]\}^{1/2}$. *i* Located 1.10 Å away from Pt1.

Plane	A	B	C	D
1	13.35(1)	-1.41(1)	-1.62(2)	8.14(1)
2	13.64(2)	-0.80(4)	-1.65(2)	8.80(4)
3	13.90(2)	-0.26(4)	-1.59(2)	9.41(5)

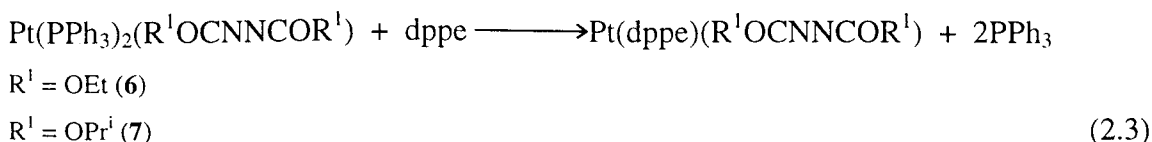
Table 2.7 Least-squares planes of: Pt1, P1, P2, N1 (Plane 1), Pt1, O1, C5, N2, N1 (Plane 2) and Pt1, N1, N2, C4 (Plane 3). Plane equation is defined as $Ax + By + Cz = D$, where x, y, z are the crystal co-ordinates.

	Plane 1	Plane 2	Plane 3
Pt1	0.047(2) ^a	0.008(2) ^a	-0.001(1) ^a
P1	0.005(1) ^a		
P2	-0.020(1) ^a		
O1	0.093(6)	-0.002(3) ^a	
N1	-0.022(1) ^a	-0.016(3) ^a	0.003(4) ^a
N2		0.018(4) ^a	-0.001(1) ^a
C4			-0.001(2) ^a
C5		-0.009(4) ^a	

Table 2.8 Deviations from the calculated least-squares planes (Plane 1, 2 and 3). (Plane 1)[⊥](Plane 2) = 2.3(2)°, (Plane 2)[⊥](Plane 3) = 2.1(2)°. ^a Atoms used to define the plane.

2.2.8 Preparation of Pt(dppe)(R¹OCNNCOR¹) [R¹ = OEt (6); R¹ = OPrⁱ (7)]

On addition of excess 1,2-bis(diphenylphosphino)ethane (dppe) to complex **2** or **4**, a new singlet resonance was observed in the ³¹P {¹H} NMR spectrum at δ -4.7 (free PPh₃) and two new doublet resonances at *ca.* δ 38.1 and δ 31.1, both with ¹⁹⁵Pt satellites, which have been assigned to the complex Pt(dppe)(EtO₂CNNCO₂Et) **6** (Tables 2.1 and 2.2). The complex Pt(dppe)(PrⁱO₂CNNCO₂Prⁱ) **7** is formed by the same method (Equation 2.3).



The displacement of triphenylphosphine with dppe is not uncommon in platinum complexes; for example, addition of dppe to *cis*-Pt(PPh₃)₂Cl₂ in chloroform produces Pt(dppe)Cl₂ in quantitative yield.¹⁹

2.2.9 Reactions of $\text{Pt}(\text{PR}^1_3)_2(\text{R}^2\text{OCNNCOR}^2)$ complexes ($\text{R}^1 = \text{Me, Ph}$; $\text{R}^2 = \text{Me, Ph, OEt, OPr}^i$)

Complexes **1**, **3** and **4** show no reactivity towards ethene or diphenyl acetylene when photolysed in $[\text{}^2\text{H}_8]\text{THF}$. Photolysis of complexes **1**, **3-4** in CDCl_3 resulted in the formation of the corresponding *cis*-platinum bis(phosphine) dichloride complexes $\text{Pt}(\text{PR}^1_3)_2\text{Cl}_2$ ($\text{R}^1 = \text{Ph, Me}$).

Both complexes **2** and **5** react thermally with chlorinated solvents at room temperature to give *cis*- $\text{Pt}(\text{PPh}_3)_2\text{Cl}_2$ as the major product, with **5** being more readily converted to *cis*- $\text{Pt}(\text{PPh}_3)_2\text{Cl}_2$. UV irradiation in CHCl_3 generated the same products more rapidly. Irradiation of **5** with ethene or diphenylacetylene in $[\text{}^2\text{H}_8]\text{THF}$ resulted in the formation of $\text{Pt}(\text{PPh}_3)_2(\eta^2\text{-C}_2\text{H}_4)$ ($\delta_{\text{H}} 2.2$, $J(\text{PtH}) = 62$ Hz) or $\text{Pt}(\text{PPh}_3)_2(\text{PhC}\equiv\text{CPh})$ [$\delta_{\text{P}} 35$, $J(\text{PtP}) = 3000$ Hz].²⁰ However, the same outcome can be achieved if the mixture is heated at 70 °C in the absence of light.

In addition to the organometallic species some organic photoproducts are observed on irradiation of **5** in $[\text{}^2\text{H}_8]\text{THF}$. Their ^1H NMR spectra exhibit similar features to the ^1H NMR data of the photoproducts from the free diazene ligand $\text{Pr}^i\text{O}_2\text{CNNCO}_2\text{Pr}^i$. In general, azo compounds initially undergo photochemically induced *trans-cis* isomerisation prior to degradation, involving liberation of molecular N_2 and formation of a radical pair.²¹ Azodicarbonyl compounds are reported to form the corresponding diketone upon extrusion of N_2 on photolysis.²²

2.3 Discussions

2.3.1 Preparation of $\text{Pt}(\text{PR}^1_3)_2(\text{R}^2\text{OCNNCOR}^2)$ ($\text{R}^1 = \text{Ph, Me}$; $\text{R}^2 = \text{Ph, Me, OEt, OPr}^i$) complexes containing a Pt–N–N–C–O metallacycle

The complex $\text{Pt}(\text{PR}^1_3)_2(\text{R}^2\text{O}_2\text{CNNCO}_2\text{R}^2)$ was prepared by two methods. The first method involved the reaction between *cis*- $\text{Pt}(\text{PR}_3)_2\text{Cl}_2$ ($\text{R} = \text{Ph}$ or Me) with the diacyl hydrazine ROCNHNHCOR (Ph or Me) which is deprotonated in the presence of NaHCO_3 under reflux conditions. The second method involved the displacement of the ethene ligand in $\text{Pt}(\text{PPh}_3)_2(\eta^2\text{-C}_2\text{H}_4)$ with the azodicarboxylate ligand $\text{RO}_2\text{CNNCO}_2\text{R}$. Both methods resulted in a structure where the azodicarbonyl ligand is N,O-bonded to platinum, forming a Pt–N–N–C–O metallacycle.

2.3.2 Structure and bonding in azo complexes

As discussed previously in Section 2.1, azo transition metal complexes can coordinate to the metal in two ways when the substituents on the azo function are simple alkyl or aryl groups, the first involves the HOMO of the nitrogen atom to form a σ -bond and in the second method, the azo function co-ordinates to the metal in an η^2 -fashion, utilising its π - and π^* -molecular orbitals to interact with the d_{σ} - and d_{π} -orbitals on the metal (Figures 2.1-2.2). The molecular orbital description of the azo compound reveals that there are n_1 - and n_2 -molecular orbitals present from the combination of the two sp^2 nonbonding n -orbitals on the two nitrogen atoms.² n_1 is the antibonding combination (HOMO) and n_2 is the bonding combination of the n -orbitals where the energy difference between n_1 and n_2 is said to be sensitive to the NNX (X = substituent) bond angle.²³ Figure 2.14 shows the n - and π -orbitals of the *cis*- and *trans*-azo function. In most circumstances, the order of orbitals going from the highest occupied down is n_1 , π then n_2 .²³

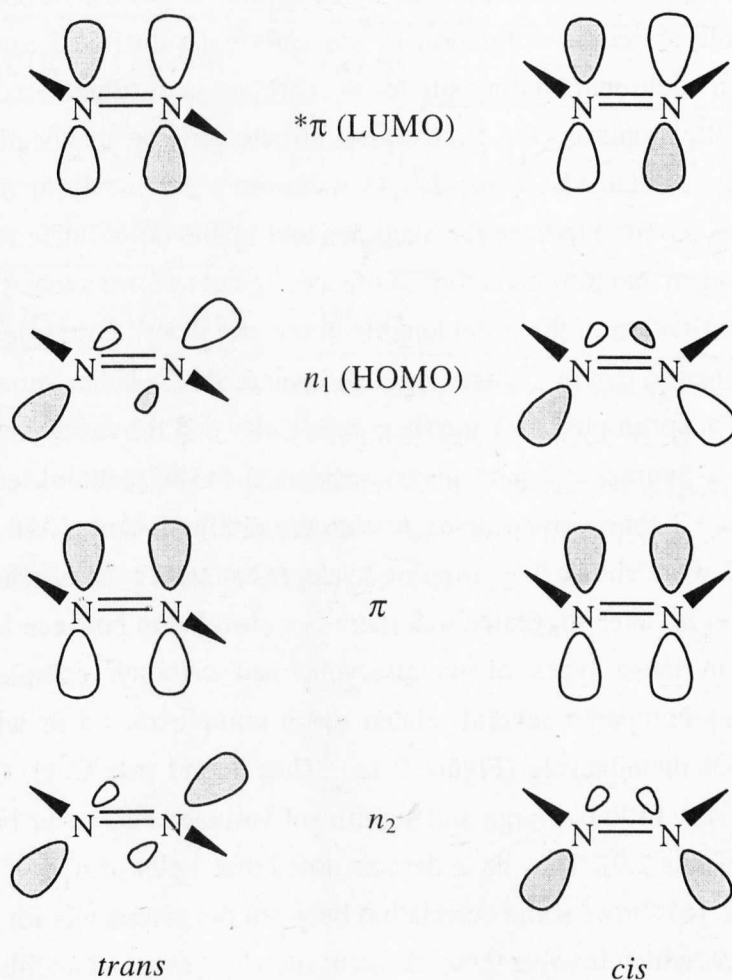


Figure 2.14 Molecular orbitals description of the *trans*- and *cis*-azo function.²

The ability of an azo compound to co-ordinate to a metal centre relies mainly on the interaction of the HOMO (n_1) of the azo function to form a mononuclear σ -complex. Additional involvement from the n_2 -orbital generates a binuclear system. The formation of π -complexes involving the N=N function is rare. Examples of N=N π -complexes are found when the metal centre is electron rich (a poor σ -acceptor) and the azo ligand is a good π -acceptor and a poor σ -donor, *e.g.* $\text{Ni}(\text{Bu}^1\text{NC})_2(\text{PhN}=\text{NPh})$ and $\text{Ni}(\text{Bu}^1\text{NC})_2$ - (diazofluorene).^{24,25}

2.3.2a Structure and bonding in azo carbonyl complexes

In cases where the azo ligand has a carbonyl adjacent to the azo function, the carbonyl groups should, according to Bent's rule,²⁶ draw π -electrons away from the N=N function, increasing the s -character of the n_1 - and n_2 -orbitals, making them less available for σ -donation to the metal centre. The electron withdrawing nature of the carbonyl group should enable the azo function to act as a better π -acceptor, promoting η^2 -co-ordination of the azo function to the metal centre. In fact the carbonyl group plays a more direct role in the co-ordination of the carbonyl substituted azo ligand and is found to act as an additional binding site for the carbonyl-substituted azo ligand.

Ibers and Ittel reported the first crystal structure of an azodicarbonyl platinum complex, $\text{Pt}(\text{PPh}_3)_2(\text{PhOCNNCOPh})$ **1**.⁷ As mentioned previously in Section 2.1, the structure of **1** was reported to have the azodibenzoyl ligand co-ordinated to the platinum centre *via* the oxygen and nitrogen atom of the azo ligand to form a metallacycle.

Closer examination of the bond lengths in the metallacycle revealed that the N=N bond has lengthened to that of a single bond and one of the C-N has shortened to that of a double bond. This prompted Ittel and Ibers to identify that the azodibenzoyl ligand has been reduced to a hydrazido ligand on co-ordination to the platinum centre, and now formally carries a -2 charge in complex **1**, with the platinum centre in the +2 oxidation state. Our current work shows that complex **5** adopts the same type of structure

Marabella *et al.* later suggested that there is a correlation between M-N and M-O bond distances in these types of metallacyclic azo carbonyl complexes.⁵ In their investigation, they compared several related metal complexes, all of which contained the M-O-C-N-N metallacycle (Figure 2.15). They found that C-O, C-N and N-N distances varied very little but large and significant variations do occur in the M-N and M-O distances (Table 2.9). They have demonstrated that a plot of $r(\text{M-N}) - r(\text{M-O})$ vs. $r(\text{M-N})$ (Figure 2.16) shows some correlation between the parameters for the complexes found in Table 2.9, which involve three different metals, a range of ancillary ligands and a variety of co-ordination geometries (4, 6 and 7).

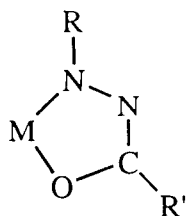


Figure 2.15 Metallacycles investigated by Marabella *et al.*⁵ [R = H, C₆H₄CH₃, C(CH₃)₂, COPh; R' = Ph].

	Bond lengths					
	R	M–N, Å	M–O, Å	N–N, Å	C–N, Å	C–O, Å
1 ⁷	COPh	2.047 (6)	2.016 (5)	1.401 (9)	1.286 (10)	1.318 (10)
5	CO ₂ Pr ⁱ	2.050 (5)	2.027 (4)	1.421 (6)	1.273 (7)	1.314 (7)
A ⁵	COPh	2.119 (18)	2.054 (14)	1.418 (14)	1.295 (10)	1.314 (11)
B ²⁷	C ₆ H ₄ CH ₃	1.984 (8)	2.110 (7)	1.38 (1)	1.30 (1)	1.30 (1)
C ²⁸	H	1.945 (8)	2.131 (7)	1.41 (1)	1.33 (1)	1.27 (1)
D ²⁹	Ph	2.030 (17)	2.159 (12)	1.38 (2)	1.35 (3)	1.24 (3)
E ³⁰	C(CH ₃) ₂	2.127 (10)	2.013 (7)	1.41 (1)	1.31 (2)	1.32 (1)

Table 2.9 Examples of transition metal complexes containing the M–O–C–N–N metallacycle, adapted from ref. 5. **1**-Pt(PPh₃)₂(PhOCNNCOPh), **5**-Pt(PPh₃)₂(PrⁱO₂C–NNCO₂Prⁱ), **A**-MoO(S₂CNMe₂)₂(PhOCNNCOPh), **B**-Mo(NC₆H₄CH₃)Cl₂(PMe₂Ph)–(PhOCNNC₆H₄CH₃), **C**-Mo(NNCOPh)Cl(PMe₂Ph)₂(PhCONNH), **D**-[MoOCl₃(Cl–PhOCNNPh)][–], **E**-ReOCl₂(PPh₃)[PhOCNN=C(CH₃)₂].

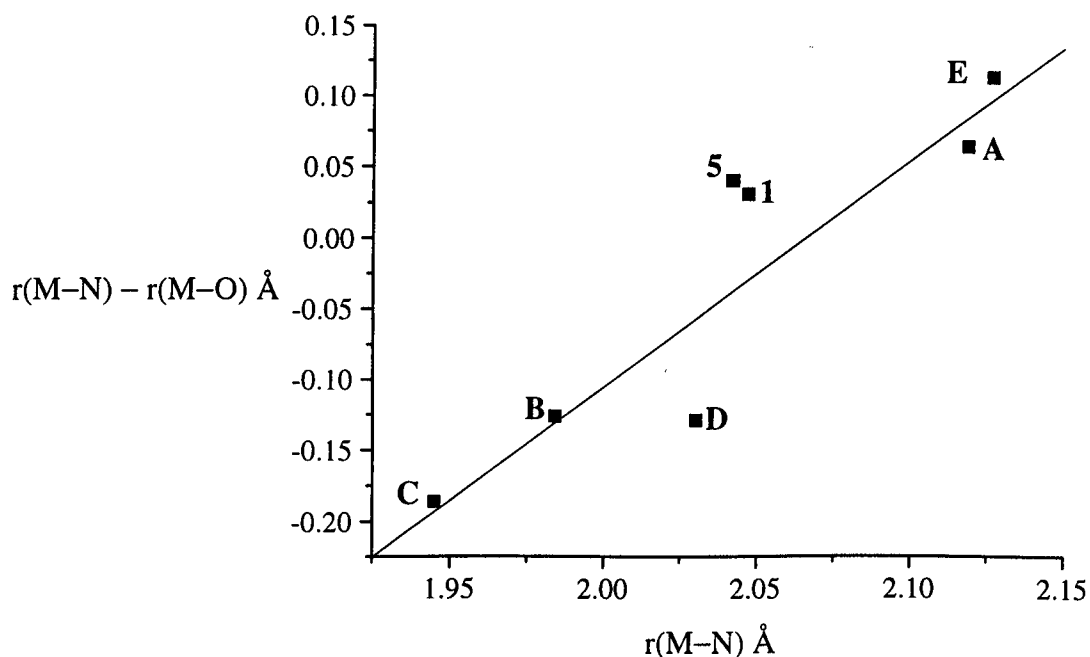


Figure 2.16 Plot of $(M-N) - (M-O)$ vs. $(M-N)$ distances for compounds that contain N,O-co-ordinated azocarbonyl ligands, adapted from ref. 5. See also Table 2.9.

According to Marabella *et al.* the substituent R attached to the co-ordinated nitrogen atom in Figure 2.15 directly affects the degree of M–N bonding, which in turn leads to a correlated variation in the M–O bonding. It was said that the azo ligand can be represented by one of three valence bond structures F, G and H (Figure 2.17). Structure F is the usual representation of the azo ligand, whereas G is the resonance form of F. Structure H represents the reduced hydrazido(2–) ligand. The charges on the nitrogen co-ordinated atom in structures G and H can be stabilised by the attached R group *via* multiple N–R bonding. Their theory said that strong multiple N–R bonding occurs at the expense of multiple M–N bonding.

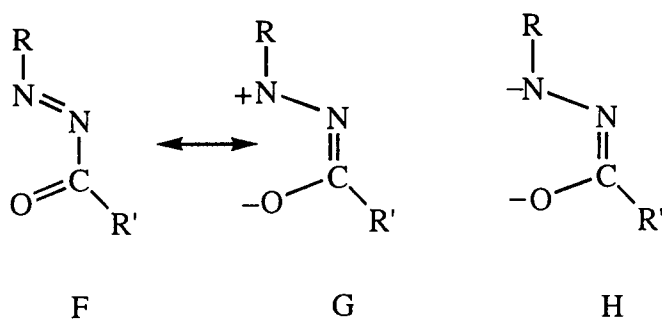
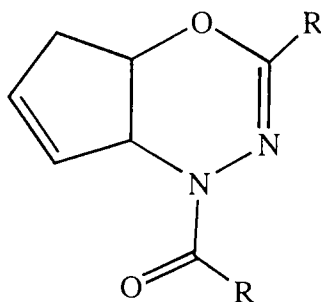


Figure 2.17 Valence bond representation of the azocarbonyl ligand.⁵

The substituent on the azodicarbonyl ligand also affects the electronic transitions of the metal azo complexes. As noted in Section 2.2.3 a change in the phosphine ligand affects the band maxima at *ca.* 300 nm in the UV/VIS spectra of Pt(PPh₃)₂(PhOCNNCOPh) **1** and Pt(PMe₃)₂(PhOCNNCOPh) **3** very little. However, on changing the azo ligand from azodibenzoyl (**1** and **3**) to azodiacetyl (**4**), we notice a shift of 15 nm to higher energy. This has also been noted by Campbell *et al.* in the related organic oxadiazine compound **I**.³¹



R = Ph (**Ia**)

R = Me (**Ib**)

Campbell *et al.* reported the C=O and C=N stretching frequencies as 1652 cm⁻¹ and 1635 cm⁻¹ respectively for **Ia**, and 1673 cm⁻¹ and 1660 cm⁻¹ respectively for **Ib**. A band maximum at *ca.* 290 nm ($\epsilon = 19800 \text{ dm}^3 \text{ mol}^{-1} \text{ cm}^{-1}$) is reported for **Ia** and was assigned as the electronic transition in the Ph-(O)C=N chromophore.³¹ They have noted that if R is an alkyl group in the R-(O)C=N chromophore then the band maximum shifts to around 240 nm. It would be tempting to make a direct comparison between the C=N electronic transition in the oxadiazines and the electronic transitions observed for the azodicarbonyl metallacycles investigated in this chapter. However, it should be realised that the metallacycles found in **1** and **5** are planar according to their crystal data, and the metal centre will also have a strong influence on any electronic transitions found in the azo ligand.

It is clear, however, that for the azodiacetyl complexes **1**, **3** and **4** the N=N double bond character is very weak, and this has been shown from the crystal structure of **1**.⁷ The UV/VIS spectra of **1**, **3-4** also provide evidence that the N=N double bond character is weak due to the absence of an electronic transition from the N=N bond. For instance the free azodibenzoyl ligand is reported to have a N=N transition at $\lambda_{\text{max}} = 474 \text{ nm}$,³² and azodicarboxylates were found in this study to contain band maxima at around 403 nm. In σ -bonded azo transition metal complexes, where the N=N double bond is thought to be retained, band maxima are reported to occur at around 400-500 nm. For instance, Fe(CO)₄L (L = cyclic azo) complexes have band maxima in the range of 430-480 nm and for W(CO)₅(azo) complexes their band maxima are reported to occur at around 391 nm.^{4,33} This tends to suggest that the azodiacetyl ligands are functioning less as azo groups due to the apparent lack of N=N double bond character, and the term

hydrazido, as originally used by Ittel and Ibers,⁷ would be a more accurate description of the ligand (Figure 2.18).

The azodicarboxylate complexes **2** and **5** appear to have a stronger N=N double bond compared to **1**, **3** and **4**, due to the presence of a band at around 460 nm which is associated with the N=N transition. Interestingly, the band at 330 nm, assigned for C=N transitions for oxadiazines,³¹ is much weaker for **2** and **5** compared to the azodiacyl complexes. Again it is tempting to draw parallels from this and suggest that the azodicarboxylate complexes retain more N=N double bond character than the azodiacyl complexes and that the C=N double bond character in **2** and **5** is weaker. Unfortunately, comparison between the C–N and N–N distances obtained from the crystal structures of Pt(PPh₃)₂(PhOCNNCOPh)⁷ **1** and Pt(PPh₃)₂(PrⁱO₂CNNCO₂Prⁱ) **5** proved inconclusive since the C–N and N–N distances are not statistically significant (Table 2.9).

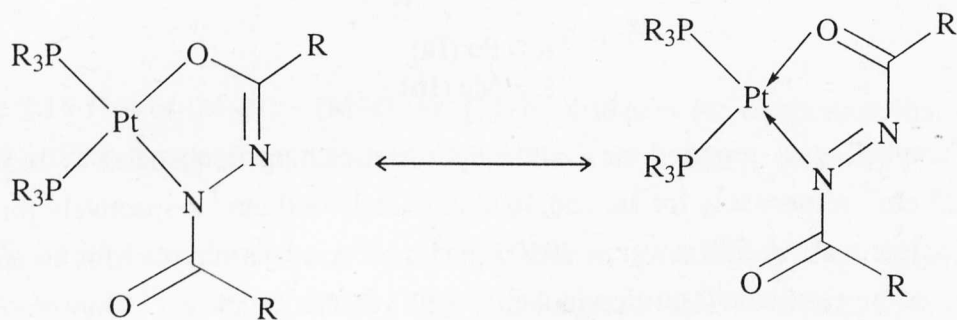


Figure 2.18 Representation of platinum(0) azodicarbonyl and platinum(II) hydrazido resonance forms.

Even though the azodicarboxylate complexes **2** and **5** might appear to have more N=N double character than the azodiacyl complexes **1**, **3-4**, both types of complex still lie to the right hand side of the resonance pair presented in Figure 2.18, with the azodiacyl complexes more so than the azodicarboxylate complexes.

2.3.3 The *trans*-influence of the metallacycle in 1-7

³¹P {¹H} NMR data of the azodiacyl complexes **1-7** have shown that the ¹J(PtP) coupling constant is strongly dependent on the atom *trans* to the phosphorus ligand in the metallacycle. This phenomenon is generally known as the “*trans*-influence”³⁴ of the ligand and is sometimes in parallel to the “*trans*-effect”.³⁵ In summary, the *trans*-effect of a ligand describes a kinetic effect and is a partial description of the transition state in a substitution reaction, whereas the *trans*-influence of a ligand is defined as the extent to which that ligand weakens the bond *trans* to it in the equilibrium state, *ie.* the ground state of the complex. It should also be noted that the *trans*-effect of a ligand may or may not be related to its *trans*-influence in the equilibrium state.

In a review by Appleton *et al.* the *trans*-influence was described as being affected by two major factors.³⁴ The first is the effect of a ligand L on the hybrid orbitals used by the metal in its bond to the *trans*-ligand A,^{36,37,38,39,40} and the second is the electronegativity of the ligand L. In an early model by Syrkin, it was described that the metal ion in a square planar complex uses $5d_{x^2-y^2}$, $6s$, $6p_x$ and $6p_y$ hybrid orbitals (Figure 2.14).⁴⁰ The $s + d$ hybrid orbital was said to be more available since the orbital energies are $5d \approx 6s < 6p$.⁴⁰ Therefore, if a ligand L forms a strong covalent L–M bond with the metal, the *trans*-ligand A will form a weaker A–M bond since both ligands L and A must share the same $s + d$ hybrid orbital if they are *trans* to each other.

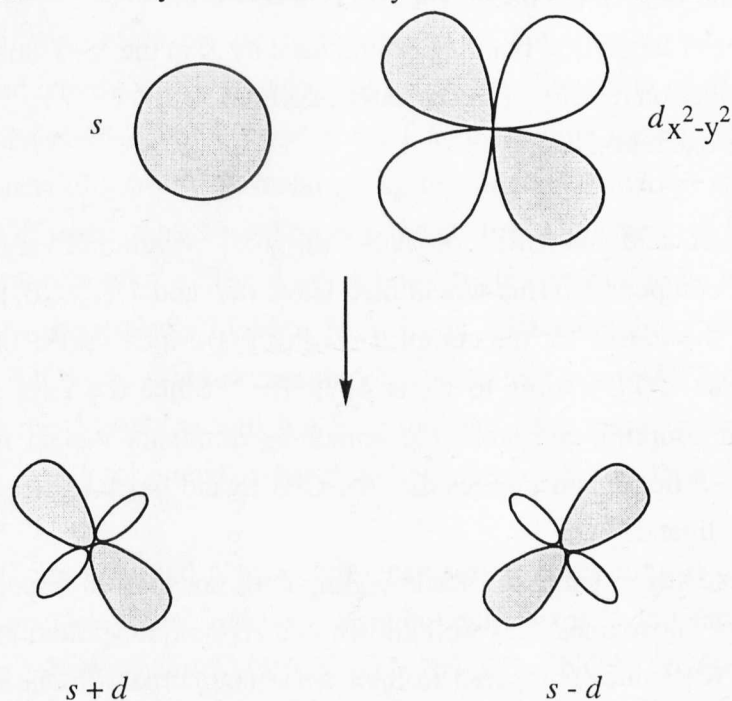


Figure 2.14 Sykin's $s \pm d$ hybrid orbitals.

Early molecular orbital analysis performed by Zumdahl and Drago on *cis*- $[\text{Pt}(\text{NH}_3)_2\text{L}_2]^{2+}$ ($\text{L} = \text{H}_2\text{O}, \text{NH}_3, \text{Cl}^-, \text{H}_2\text{S}, \text{PH}_3, \text{H}^-$ and CH_3^-)³⁸ showed that the *trans*-influence of L on the Pt–N bond increases in the following order; $\text{H}_2\text{O} < \text{NH}_3 < \text{Cl}^- < \text{H}_2\text{S} < \text{PH}_3 < \text{H}^- < \text{CH}_3^-$. The weakening of the Pt–N bond *trans* to L was said to be mainly due to Pt($6s$)–N and Pt($d_{x^2-y^2}$)–N interactions and not due to the decreased availability of Pt($6p_x, 6p_y$), in accordance with Syrkin's model.⁴⁰ More recent perturbation calculations by Shustorovich have also shown that d^8 square planar complexes use hybrid orbitals which have large contribution from the s and d_σ orbitals and relatively little from the p_σ orbitals.^{41,42}

Various experimental techniques have been employed to measure the *trans*-influence of a ligand, *e.g.* X-ray crystallography, infrared spectroscopy and NMR spectroscopy. The spin-spin coupling constant obtained from NMR experiments often gives a good indication of the s -component of the bond involved. The coupling constant $^1J(\text{XY})$, where atoms X and Y are covalently bonded and both have spin quantum

numbers $I = 1/2$, is thought to be dominated by the Fermi contact term.⁴³ This assumes that contributions to the coupling from interaction of the nuclear spin of the atom X, or Y, with the electronic orbital motion are negligible, and that the Fermi contact interaction at the nuclear spin and the s -electrons makes the dominant contribution. Equation 2.4 shows the approximate expression for the coupling constant ${}^1J(\text{PtP})$.⁴⁴

$${}^1J(\text{PtP}) \propto \gamma_{\text{Pt}} \gamma_{\text{P}} \alpha_{\text{Pt}}^2 \alpha_{\text{P}}^2 \left| \Psi_{\text{Pt}(6s)}(0) \right|^2 \left| \Psi_{\text{P}(3s)}(0) \right|^2 (\Delta E)^{-1}$$

γ_{X} = gyromagnetic ratio of the nucleus X.

α_{X}^2 = s -character of the hybrid bonding orbital used by X in the X–Y bond.

$\left| \Psi_{\text{Pt}(ns)}(0) \right|^2$ = electron density of the ns valence orbital.

$(\Delta E)^{-1}$ = average excitation energy. (2.4)

Pidcock *et al.* said that $(\Delta E)^{-1}$, α_{P}^2 and $\left| \Psi_{\text{P}(3s)}(0) \right|^2$ would not vary very much in a related series of compounds. This would then leave α_{Pt}^2 and $\left| \Psi_{\text{Pt}(6s)}(0) \right|^2$ as the factors which will vary the most.⁴⁴ In the complex *cis*-Pt(PEt₃)₂MeCl, ${}^1J(\text{PtP})$ *trans* to CH₃ is 1719 Hz, whereas ${}^1J(\text{PtP})$ *trans* to Cl is 4179 Hz.⁴⁵ Since the term $\left| \Psi_{\text{Pt}(6s)}(0) \right|^2$ is common to both coupling constants, the remaining dominant variant is α_{Pt}^2 which is related to the Pt–P bond, and implies that the CH₃ ligand has a higher *trans*-influence than the chloride ligand.

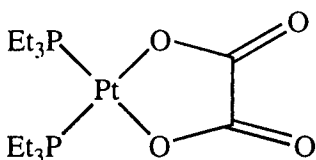
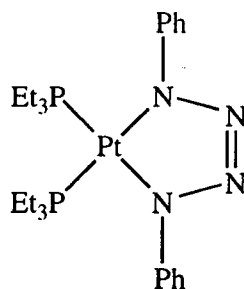
Pidcock also suggested that π -backbonding does not play an important part in the *trans*-influence of phosphines. It is well known that *cis*-bis(phosphine) Pt(II) complexes have higher ${}^1J(\text{PtP})$ values compared to their *trans* counterpart.⁴⁶ One explanation for this effect assumes that in *trans*-bis(phosphine) Pt(II) complexes, the two phosphine ligands are competing for electrons in the same d_{π} -orbital when π -backbonding, whereas in the *cis*-complex the two phosphine ligands are not competing for the same d_{π} -orbital.⁴⁷ Since π -backbonding is synergically linked with σ -bonding, any changes in π -backbonding will affect the σ -bond. Hence *trans*-complexes will have a weaker phosphorus-platinum bond compared to the *cis*-complexes, which is reflected in the ${}^1J(\text{PtP})$ coupling constants. Pidcock *et al.* threw doubts on this theory when they showed that ${}^1J(\text{PtP})_{\text{cis}}/{}^1J(\text{PtP})_{\text{trans}}$ for Pt(PBuⁿ₃)₂Cl₂ [Pt(II)] and Pt(PBuⁿ₃)₂Cl₄ [Pt(IV)] are 1.47 and 1.41 respectively. Pidcock *et al.* argued that π -backbonding should not be as dominant in Pt(IV), but the ${}^1J(\text{PtP})_{\text{cis}}/{}^1J(\text{PtP})_{\text{trans}}$ ratio for Pt(IV) is almost the same as Pt(II). This led to Pidcock *et al.* to conclude that σ -inductive effects are responsible for the *trans*-influence observed and not π -backbonding. In conclusion they said that phosphine has a higher *trans*-influence than chloride due to the phosphine ligand being a stronger σ -donor. However, Hartley responded that the similarity of the ${}^1J(\text{PtP})_{\text{cis}}/{}^1J(\text{PtP})_{\text{trans}}$ ratio could arise from not only a decrease in π -backbonding in the Pt(II) case on going from the *cis*- to *trans*-isomer but also a decrease in σ -bonding as

well.⁴⁶ Hence, the ratio of coupling constants of the *cis*- and *trans*-isomers would be very similar for both Pt(II) and Pt(IV) oxidation states. The decrease in σ -bonding in the Pt(IV) state on going from *cis* to *trans* should be similar to the decrease in π -backbonding and σ -bonding in the Pt(II) state. Hartley concluded that the oxidation state of the Pt atom does not necessarily indicate whether or not π -backbonding is present in the lower oxidation state of platinum phosphine complexes.

A more recent survey by Orpen and co-workers on numerous crystal structures of phosphine complexes has shown that metal π -backbonding remains an integral part of bonding interaction in metal phosphine complexes.^{48,49} They have shown that an increase in oxidation state of the metal results in the increase of the M–P metal phosphorus bond length, which is accompanied by the shortening of the P–A bond and an increase in the A–P–A bond angle in the PA₃ phosphine ligand. The shortening of the P–A bond resulting from the metal going to a higher oxidation state is consistent with a decrease of metal π -backbonding into the σ^* -orbital of the P–A bond and not the 3*d* orbitals on phosphorus.^{50,51} The A–P–A bond angle was said to be influenced by the population of the phosphine's LUMOs from metal π -backbonding.⁵² Population of the phosphine's LUMOs was said to drive the phosphine to a pyramidal structure, therefore the LUMOs of the phosphine will not be populated for complexes in high oxidation state due to the lack of metal π -backbonding, hence the A–P–A bond angle will increase.

Allen and Sze obtained a *trans*-influence series, combining results from a wide range of Pt(II) bis(phosphine) and bis(phosphite) complexes,⁵³ and showed that ¹J(PtP) decreases in the following series: ONO₂[−] < I[−], Br[−], Cl[−] < NCS[−], NCO[−], N₃[−], pyridine < NHEt₂ < NH₂Et < *p*-toluidine < NO₂[−] < AsEt₃ < CN[−] < P(OPh)₃ < PPh₃ < PMe₂Ph < PBuⁿ₃ < PEt₃ << Me[−] < Ph[−] < SiMe₂Ph. According to Allen and Sze, this order represents an increase in tendency for the ligands to concentrate Pt(6s) character into their bonds with Pt(II).

From the *trans*-influence series of Allen and Sze,⁵³ we can see that oxygen donors have a weaker *trans*-influence than nitrogen donors, *i.e.* a phosphine *trans* to oxygen will have a larger ¹J(PtP) value than a phosphine *trans* to nitrogen. A similar trend is observed if we examine the ¹J(PtP) value for the Pt(II) square planar complex *cis*-Pt(PEt₃)₂(C₂O₄)⁵⁴ and *cis*-Pt(PEt₃)₂(PhN=N=N–NPh).⁵⁵

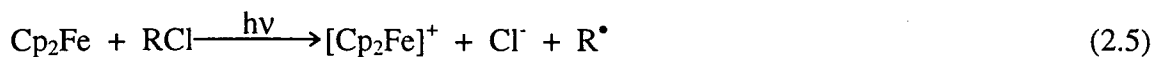
*cis*-Pt(PEt₃)₂(C₂O₄)*cis*-Pt(PEt₃)₂(PhN=N=N-NPh)

In *cis*-Pt(PEt₃)₂(C₂O₄) both phosphines are *trans* to the oxygen of the oxalate ligand and have a ¹J(PtP) value of 3522 Hz and in *cis*-Pt(PEt₃)₂(PhN=N=N-NPh) both phosphines are *trans* to nitrogen and have a ¹J(PtP) value of 3355 Hz, again demonstrating that nitrogen ligands have a higher *trans*-influence compared to oxygen ligands. We have assigned the phosphine ligands in complexes 1-7 on this basis.

The X-ray crystal structure of **5** also gives us an indication, but to a lesser extent, that the co-ordinated nitrogen atom in the metallacycle has a higher *trans*-influence than the co-ordinated oxygen atom. In Figure 2.13, the Pt-P1 [2.266(2) Å] bond *trans* to O1 in the metallacycle is slightly shortened compared to Pt-P2 [2.278(2) Å] bond *trans* to N1 but the difference is only 0.012 Å.

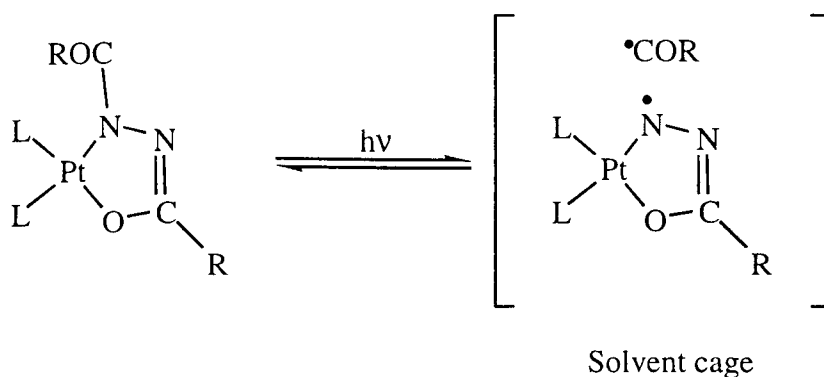
2.3.4 Photochemical reactions of azodicarbonyl metallacycles

Photolysis of complexes 1-5 in chlorinated solvents formed the corresponding *cis*-bis(phosphine) platinum dichloride. The photochemical process presumably occurs *via* a free radical mechanism, where the source of free radicals derives from the chlorinated solvent and/or the co-ordinated azodicarbonyl ligand. Evidence suggests that for complexes 1, 3 and 4, the source of free radicals is most likely from the chlorinated solvents since photolysis of complexes 1, 3 and 4 with trapping agents (ethene, diphenylacetylene) in benzene or THF did not yield any photoproducts. One possible mechanism could involve excitation of a complex-to-solvent charge transfer band to induce a photochemical reaction.⁵⁶ This is reported for several metallocene complexes where the appearance of a new complex-to-solvent charge transfer band was observed on dissolving the metallocene in halogenated solvent.^{57,58} For example, Traverso and Scandola have shown that Cp₂Fe undergoes photooxidation in chlorinated solvents RCl to yield [Cp₂Fe]⁺, Cl⁻ and the radical R[•] (Equation 2.5).⁵⁷

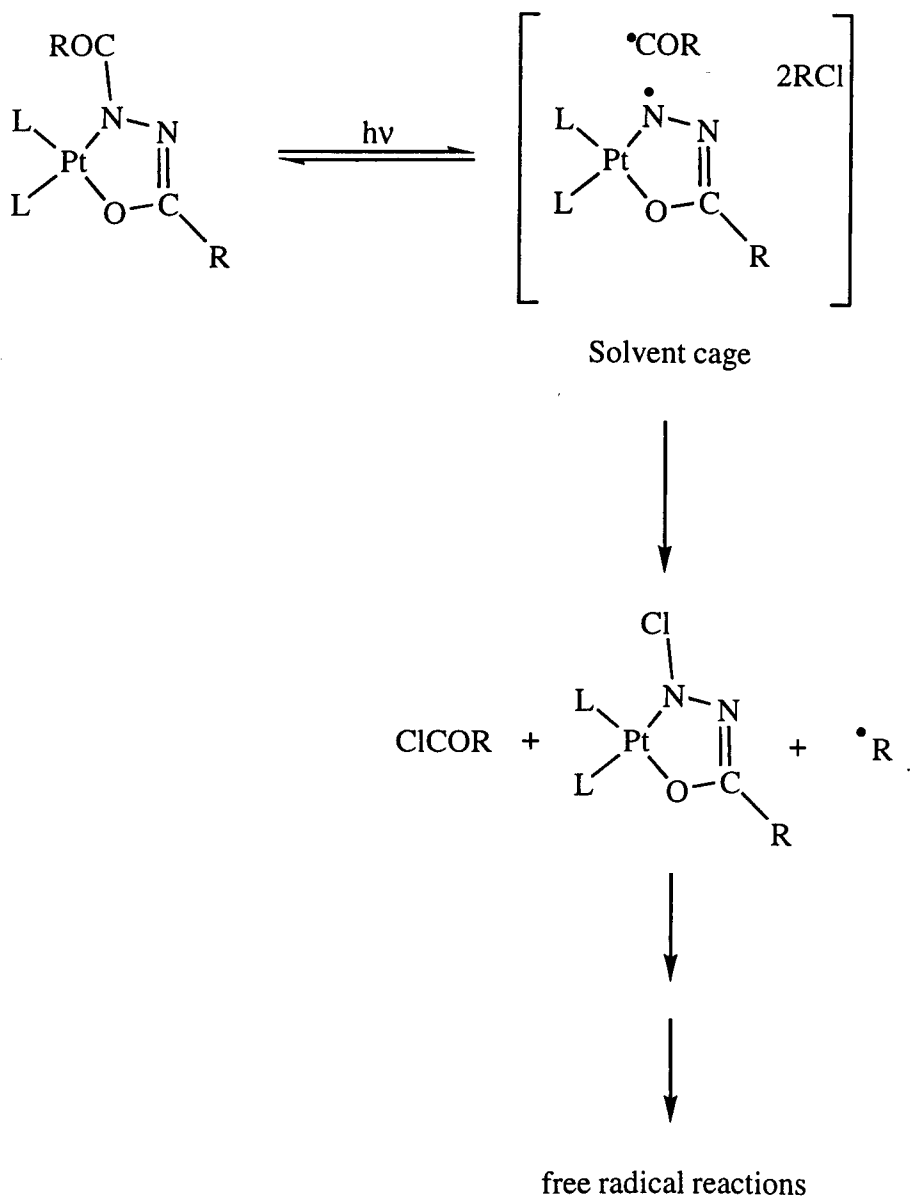


However, this mechanism seems unlikely to be responsible for the photochemical reactions observed since no significant difference can be observed in the UV/VIS

spectra of **1-5** whether the solvent employed was THF or CHCl_3 . An alternative mechanism which can create free radicals from the chlorinated solvents would involve homolytic bond cleavage of the azo ligand. In solvents such as THF, homolytic bond cleavage by photolysis of the azo ligand should lead to rapid reversible recombination due to the solvent cage effect (Scheme 2.2). However, in chlorinated solvents the newly cleaved bond in the azo ligand can react with a chlorine atom on the solvent molecule, thus forming the radical R^\bullet , which can initiate other free radical reactions (Scheme 2.3).



Scheme 2.2 Possible mechanism involving photoinduced homolytic bond cleavage of the azo ligand in $\text{PtL}_2(\text{ROCNNCOR})$ in THF.



Scheme 2.3 Possible mechanism for formation of free radicals involving photoinduced homolytic bond cleavage of the azo ligand in $\text{PtL}_2(\text{ROCNNCOR})$ in chlorinated solvents.

Complexes **2** and **5**, however, proved to be much more active compared to their azodiacyl counterpart. This would suggest that the azodiacyl ligand is more photo-resistant than the azodicarboxylate ligand. The most likely reason is that the azodicarboxylate ligand binds to platinum much more weakly than azodiacyl, as discussed in Section 2.3.1. The thermal reactivity of **2** and **5** with ethene and diphenylacetylene again demonstrates the lability of the azodicarboxylate ligand, since **1**, **3** and **4** show no similar thermal activities. However, possible mechanisms for the thermal/photochemical reactions of **2** and **5** remain unclear.

2.4 Conclusion

This chapter reports simple synthetic routes to complexes $\text{Pt}(\text{PR}^1_3)_2\text{-(R}^2\text{OCNNCOR}^2)$, containing the Pt–N–N–C–O metallacyclic unit. The structural evidence indicates that the metallacycle is a fully conjugated planar system. The role that the carbonyl group plays is an important factor in the co-ordination of this type of azo ligand, and it seems likely that if a carbonyl group is present next to the azo function, the metallacycle structure will always be preferred over other co-ordination modes. This should always apply unless the structure of the azo ligand is restricted to a *cis* only configuration, *i.e.* a cyclic azo compound. Here the carbonyl group would now find it harder to co-ordinate to the metal centre along with the nitrogen of the azo function due to steric constraints. The formation of a metallacycle complex with a cyclic azodicarbonyl complex would now appear to be improbable, and the co-ordination options now left would be either σ -bonding through the nitrogen atom(s) to form a σ -complex or π -bonding through the azo function to form an η^2 -azo complex.

The azodicarbonyl ligand is readily displaced photochemically in chlorinated solvents. The azodicarboxylate ligand of **2** and **5** has also been replaced photochemically and thermally in THF and benzene, but the azodiacyl complexes **1**, **3** and **4** proved photostable in these solvents.

2.5 References

- 1 S. N. Heaton, *D.Phil Thesis*, University of York, 1995.
- 2 H. Kisch and P. Holzmeier, *Adv. Organomet. Chem.*, 1992, **34**, 67.
- 3 (a) M. Herberhold and K. Leonhard, *Angew. Chem.*, 1976, **88**, 227; (b) M. Herberhold and K. Leonhard *Angew. Chem., Int. Ed. Engl.*, 1976, **15**, 230.
- 4 A. Albini and H. Kisch, *Top. Curr. Chem.*, 1976, **65**, 105.
- 5 C. P. Marabella, J. H. Enemark, W. E. Newton and J. W. McDonald, *Inorg. Chem.*, 1982, **21**, 623.
- 6 G. Avar, W. Rüssler and H. Kisch, *Z. Naturforsch., Teil B*, 1987, **42**, 50.
- 7 S. D. Ittel and J. A. Ibers, *Inorg. Chem.*, 1973, **12**, 2290.I
- 8 M. Green, R. B. L. Osborne and F. G. A. Stone, *J. Chem. Soc. (A)*, 1968, 3083.
- 9 S. Cenini, F. Porta, M. Pizzotti and C. Crotti, *J. Chem. Soc. Dalton Trans.*, 1985, 163.
- 10 M. Hidai and Y. Mizobe, *Chem. Rev.*, 1995, **95**, 1115.
- 11 J. Chatt, J. R. Dilworth and R. L. Richards, *Chem. Rev.*, 1978, **78**, 589.
- 12 H. I. Liu, A. Filipponi, N. Gavini, B. K. Burgess, B. Hedman, A. D. Cicco, C. R. Natoli, K. O. Hodgson, *J. Am. Chem. Soc.*, 1994, **116**, 2418 and reference therein.

- 13 J. Chatt, A. J. Pearman, R. L. Richards, *J. Chem. Soc., Dalton Trans.*, 1977, 1852.
- 14 J. E. Barclay, A. Hills, D. L. Hughes, G. J. Leigh, C. J. Macdonald, M. A. Bakar and H. Mohd.-Ali, *J. Chem. Soc., Dalton Trans.*, 1990, 2503.
- 15 J. R. Dilworth and A. S. Kasenally, *J. Organomet. Chem.*, 1973, **60**, 203.
- 16 (a) B. Longato and G. Trovó, *Inorg. Chem. Acta*, 1992, **192**, 13; (b) B. Longato, G. Trovó and G. Valle, *J. Chem. Soc. Dalton Trans.*, 1993, 669; (c) G. K. Anderson and G. Lumetta, *Inorg. Chem.*, 1987, **26**, 1291.
- 17 C. K. Johnson, *ORTEP, Report ORNL-5138*, Oak Ridge National Laboratory, TN, 1976.
- 18 (a) F. Hai-Fu, *SAPI91, Structure Analysis Programs with Intelligent Control*, Rigaku Corporation, Tokyo, Japan, 1993; (b) P. T. Beurskens, G. Admiraal, G. Beurskens, G. Bosman, W. P. Garcia-Granda, H. O. Gould, J. M. Smits, C. Smykalla, *The DIRDIF program system, Technical Report of the Crystallographic Laboratory*, University of Nijmegen, The Netherlands, 1992; (c) G. M. Sheldrick, *SHELXL 93, program for crystal structure refinement*, University of Gottingen, Germany.
- 19 G. K. Anderson, J. A. Davies and D. J. Schoeck, *Inorg. Chim. Acta*, 1983, **76**, L251.
- 20 R. S. Paonessa, A. L. Prignano and W. C. Trogler, *Organometallics*, 1985, **4**, 647.
- 21 P. S. Engel, *Chem. Rev.*, 1980, **80**, 99.
- 22 T. J. Kelly, *J. Am. Chem. Soc.*, 1962, **84**, 968.
- 23 K. N. Houk, Y.-M. Chang and P. S. Engel, *J. Am. Chem. Soc.*, 1975, **97**, 1824.
- 24 R. S. Dickson and J. A. Ibers, *J. Am. Chem. Soc.*, 1977, **99**, 2108.
- 25 A. Nakamura, T. Yoshida, M. Cowie, S. Otsuka and J. A. Ibers, *J. Am. Chem. Soc.*, 1977, **77**, 2108.
- 26 J. E. Huheey, E. A. Keiter and R. L. Keiter, *Inorganic Chemistry: Principles of Structure and Reactivity 4th Edition*, HarperCollins, New York, 1993.
- 27 M. W. Bishop, J. Chatt, J. R. Dilworth, M. B. Hursthouse, S. A. A. Jayaweera, A. Quick, *J. Chem. Soc. Dalton Trans.*, 1979, 914.
- 28 A. V. Butcher, J. Chatt, J. R. Dilworth, G. J. Leigh, M. B. Hursthouse, S. A. A. Jayaweera, A. Quick, *J. Chem. Soc. Dalton Trans.*, 1979, 921.
- 29 M. W. Bishop, J. Chatt, J. R. Dilworth, M. B. Hursthouse, M. Motevalli, *J. Chem. Soc. Dalton Trans.*, 1979, 914.
- 30 M. B. Hursthouse, S. A. A. Jayaweera, A. Quick, *J. Chem. Soc. Dalton Trans.*, 1979, 279.
- 31 J. A. Campbell, D. Mackay and T. D. Sauer, *Can. J. Chem.*, 1972, **50**, 371.
- 32 D. Mackay, U. F. Marx and W. A. Waters, *J. Chem. Soc.*, 1964, 4793.
- 33 C. C. Frazier, H. Kisch, *Inorg. Chem.*, 1978, **17**, 2736.

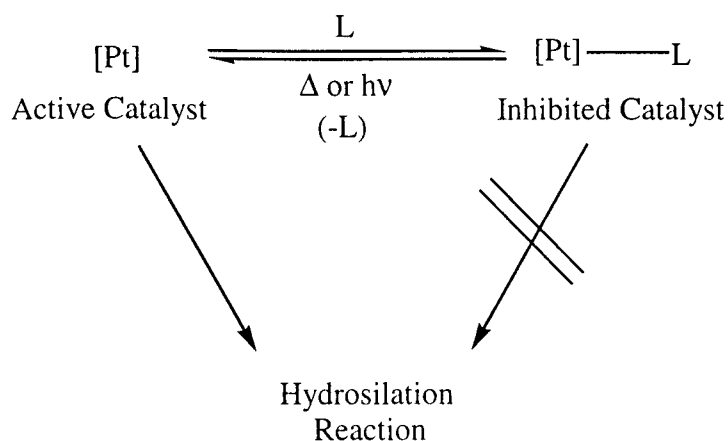
- 34 T. G. Appleton, H. C. Clark and L. E. Manzer, *Co-ord. Chem. Rev.*, 1973, **10**, 335.
- 35 F. Basolo, *Co-ord. Chem. Rev.*, 1996, **154**, 151.
- 36 R. Mason and A. D. C. Towl, *J. Chem. Soc. (A)*, 1970, 1601.
- 37 R. Mason, R. McWeeny and A. D. C. Towl, *Discuss. Faraday Soc.*, 1969, **47**, 20;
- 38 S. S. Zumdahl and R. S. Drago, *J. Am. Chem. Soc.*, 1968, **90**, 6669.
- 39 M. Randic, *J. Chem. Phys.*, 1962, **36**, 3278.
- 40 Y. K. Syrkin, *Izv. Akad. Nauk SSSR, Otd. Khim. Nauk*, 1948, 69.
- 41 E. Shustorovich, *J. Am. Chem. Soc.*, 1979, **101**, 792.
- 42 R. V. Parish, *Co-ord. Chem. Rev.*, 1982, **42**, 1.
- 43 J. A. Pope and D. P. Santry, *Mol. Phys.*, 1964, **8**, 1.
- 44 A. Pidcock, R. E. Richards and L. M. Venanzi, *J. Chem. Soc. (A)*, 1966, 1707.
- 45 F. H. Allen and A. Pidcock, *J. Chem. Soc. (A)*, 1968, 2700.
- 46 F. R. Hartley, *Chemistry of Platinum and Palladium*, Applied Science, London, 1973.
- 47 S. Ahrland and J. Chatt, *J. Chem. Soc.*, 1957, 1379.
- 48 A. G. Orpen and N. G. Connelly, *Organometallics*, 1990, **9**, 1206.
- 49 B. J. Dunne, R. B. Morris and A. G. Orpen, *J. Chem. Soc. Dalton Trans.*, 1991, 653.
- 50 S. -X. Xiao, W. C. Trogler, D. E. Ellis and Z. Berkovitch-Yellin, *J. Am. Chem. Soc.*, 1983, **105**, 7033.
- 51 D. S. Marynick, *J. Am. Chem. Soc.*, 1984, **106**, 4064.
- 52 B. M. Gimarc, *Molecular Structure and Bonding*, Academic Press, New York, 1979.
- 53 F. H. Allen and S. N. Sze, *J. Chem. Soc. (A)*, 1971, 2054.
- 54 R. S. Paonessa, A. L. Prignano and W. C. Trogler, *Organometallics*, 1985, **4**, 647.
- 55 S. W. Lee, G. A. Miller, C. F. Campana and W. C. Trogler, *Inorg. Chem.*, 1988, **27**, 1215.
- 56 G. L. Geoffroy and M. S. Wrighton, *Organometallic Photochemistry*, Academic Press, New York, 1979.
- 57 O. Traverso and F. Scandola, *Inorg. Chim. Acta*, 1970, **4**, 493.
- 58 P. Borrell and E. Henderson, *J. Chem. Soc., Dalton Trans.*, 1975, 432.

CHAPTER 3

AZO-INHIBITED HYDROSILATION CATALYSTS

3.1 INTRODUCTION

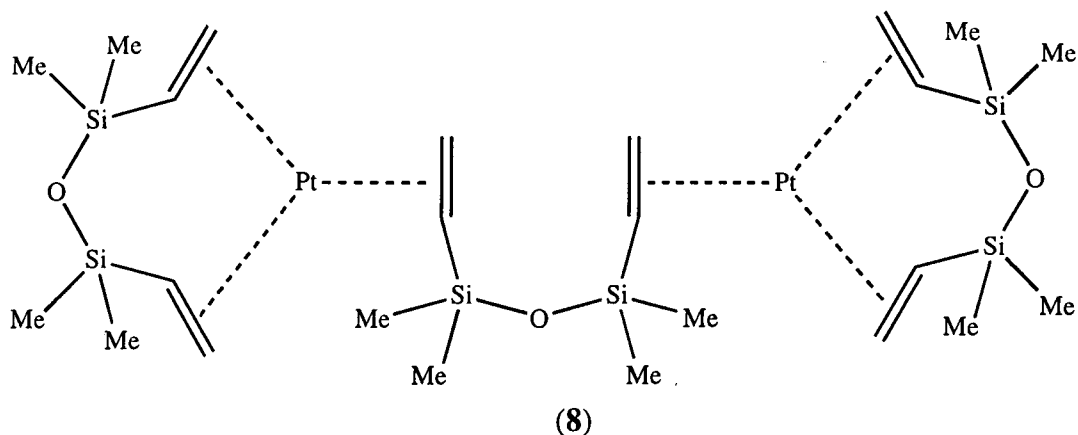
The hydrosilation reaction represents an important branch of chemistry in the silicone industry. Of the choice of transition metal catalysts, platinum catalysts are used the most often because they generally offer higher activity and larger catalytic turnovers compared to other transition metal catalysts.^{1,2,3} Due to the high activity of platinum catalysts, they are often inhibited to control hydrosilation. This is especially important when a pre-mixed composition of reactants and catalyst is required and initiation of hydrosilation is not desired until all the reactants are uniformly dispersed. For example, in the paper coating industry, a mixture of hydrosiloxane, vinylsiloxane and inhibited catalyst mixture is applied as a thin liquid film onto paper. The siloxane film solidifies, or cures, on *in situ* activation of the latent catalyst.⁴ The latent catalyst can then be re-activated thermally, and/or photochemically (Scheme 3.1). Industrially, inhibited catalysts are generally thermally activated. Photoactivated catalysts, however, would offer a less energy intensive pathway for initialising hydrosilation. No photoactivated hydrosilation catalysts have yet been found suitable for commercial applications.



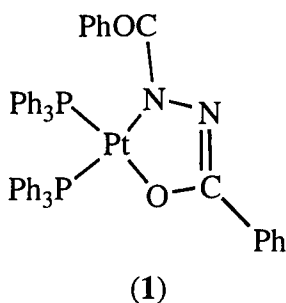
L = inhibitor

Scheme 3.1 Inhibition of platinum hydrosilation catalysts.

Heaton has previously reported that certain azo compounds can successfully inhibit the activity of Karstedt's catalyst, $[(\text{Pt}\{\eta^4\text{-(CH}_2\text{=CHSiMe}_2\text{)}_2\text{O}\})_2(\mu\text{-(CH}_2\text{=CHSiMe}_2\text{)}_2\text{O})]$ **8**.^{5,6,7}



Azo inhibitors were identified by Heaton as a potential method of photoactivating the hydrosilation reaction. It was found that only azo compounds with a carbonyl group adjacent to the azo function were effective as inhibitors of **8**. Unfortunately, characterisation of inhibited **8** with azodicarbonyl compounds revealed little structural features. ^1H NMR spectroscopy data of the inhibition product showed that the coordinated azodicarboxylate inhibitor, $\text{RO}_2\text{CNNCO}_2\text{R}$, contains equivalent R groups, which would initially suggest that the inhibitor is co-ordinating to platinum in an η^2 fashion *via* the azo's $\text{N}=\text{N}$ group. However, reported co-ordination behaviour of several complexes containing an azo ligand with a carbonyl group adjacent to the azo function suggested otherwise.⁸ In these azodicarbonyl complexes it was found that the azo ligand co-ordinates to the metal centre *via* the nitrogen of the azo function and the oxygen of the carbonyl group, thus forming a $\text{Pt}-\text{N}-\text{N}-\text{C}-\text{O}$ metallacycle, *e.g.* $\text{Pt}(\text{PPh}_3)_2(\text{PhOCNNCOPh})$ **1**.⁸ Based on these findings, Heaton proposed a polymeric structure for the inhibition product, whereby the azo ligand forms a $\text{Pt}-\text{N}-\text{N}-\text{C}-\text{O}$ metallacycle and acts as a bridging ligand, rendering all the R groups on the azo ligand equivalent (Figure 3.1).



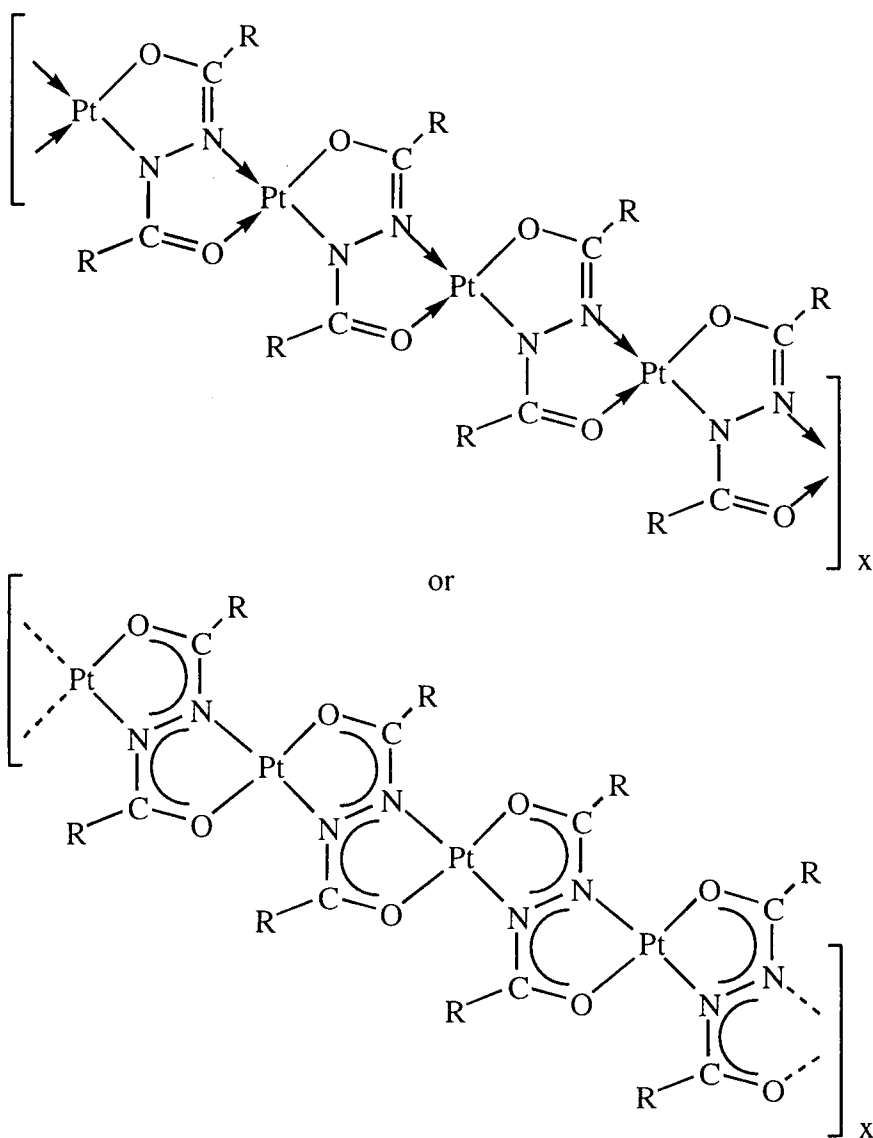


Figure 3.1 The top figure shows the proposed structure for azodicarbonyl inhibited **8**. The bottom figure shows possible delocalisation of electron density in the azo ligand (adapted from ref. 7).

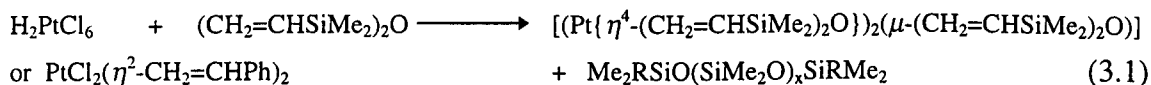
It was found that excess azodicarbonyl inhibitor is needed to prevent **8** from initiating hydrosilation. Activation of azo-inhibited **8** was reported to occur by heating or photolysis.⁵ In Heaton's previous investigation only the azo inhibitor $\text{Pr}^i\text{O}_2\text{C}(\text{N}=\text{N})\text{CO}_2\text{Pr}^i$ was examined in detail and no comparison between different azo inhibitors was made. Also work done on model platinum phosphine complexes $\text{Pt}(\text{PPh}_3)_2(\text{EtO}_2\text{C}(\text{N}=\text{N})\text{CO}_2\text{Et})$ **2** and $\text{Pt}(\text{PPh}_3)_2(\text{Pr}^i\text{O}_2\text{C}(\text{N}=\text{N})\text{CO}_2\text{Pr}^i)$ **5** has now shown them to be thermally and photochemically sensitive towards chlorinated solvents.⁹ This could have possible implications on the reported characterisation of azo-inhibited **8** which was carried out by Heaton in chlorinated solvent systems.⁷ In this chapter, further studies on azo-inhibited **8** are presented in non-chlorinated solvent systems, with the azo inhibitor

under investigation being ROCNNCOR (R = OEt, OPr¹ and OBu¹). The effect of changing the substituent R on the azo inhibitor will also be discussed.

3.2 RESULTS

3.2.1 Preparation of $[(Pt\{\eta^4-(CH_2=CHSiMe_2)_2O\})_2(\mu-(CH_2=CHSiMe_2)_2O)]$ **8**

The platinum divinylsiloxane compound **8** was prepared by the method reported by Lappert and co-workers, with minor modifications.¹⁰ Hexachloroplatinic acid, H_2PtCl_6 , and excess tetramethyldivinyldisiloxane, $(H_2C=CHSiMe_2)_2O$, were refluxed, with added water, under a nitrogen atmosphere. Alternatively, the complex $PtCl_2(\eta^2-CH_2=CHPh)_2$ suspended in toluene can be used in place of H_2PtCl_6 . A slightly yellow oil was obtained after the refluxed mixture was neutralised with $NaHCO_3$ (Equation 3.1). The crude product obtained displays NMR features corresponding to those reported for $[(Pt\{\eta^4-(CH_2=CH-SiMe_2)_2O\})_2(\mu-(CH_2=CHSiMe_2)_2O)]$ **8** (Table 3.1).⁶



Resonances were found to be present at *ca.* $\delta_{Si} -21$ in the $^{29}Si \{^1H\}$ NMR spectrum of **8** which is indicative of oligomeric siloxane materials, $Me_2RSiO(SiMe_2O)_xSiRMe_2$ [R = (CH=CH₂), CH₂CH₃, CH₂CH₂Cl; x = 0-14].⁵ The presence of oligomeric materials has also been reported by Lappert and co-workers from GC/MS analysis.¹⁰ The ^{29}Si NMR signals due to unreacted $(CH_2=CHSiMe_2)_2O$ were also detected at $\delta_{Si} -3.2$. The majority of the impurities found in **8** can be removed by flash chromatography. An unidentified impurity can be detected sometimes at $\delta_{Si} -4.2$.

A yield of 74 % for the synthesis of **8** was determined by its quantitative $^{29}Si \{^1H\}$ NMR spectrum using an inverse gated pulse sequence.

Complex **8** was found to be thermally, photochemically and aerobically unstable as an oil or in solution, tending to turn from yellow to dark brown in colour when left at room temperature. The change to a darker colour is normally indicative of colloidal platinum formation.^{11,12}

In the $^{29}Si \{^1H\}$ NMR spectrum of **8**, three resonances are present at δ 3.24, 2.41 and -0.55 . The signals at δ 3.24 and δ 2.41 are from the chelating $(CH_2=CHSiMe_2)_2O$ ligands and a broad signal at $\delta -0.55$ are from the bridging $(CH_2=CHSiMe_2)_2O$ ligand (Figure 3.2). The $^{195}Pt \{^1H\}$ NMR spectrum of **8** showed two singlets with a separation of 50 Hz between them. The signals observed in the $^{29}Si \{^1H\}$ NMR spectrum of **8** correspond to those reported by Lappert and co-workers, except that we did not observe the second signal for the bridging $(CH_2=CHSiMe_2)_2O$ ligand (Tables 3.1 and 3.2).

$^{29}\text{Si} \{^1\text{H}\}, \delta (J / \text{Hz})$	$^{195}\text{Pt} \{^1\text{H}\}, \delta$
3.24 [2Si, s, η^4 -(CH ₂ =CHSiMe ₂) ₂ O, $J(\text{PtSi}) = 42.9$]	-6143 ^a
2.41 [2Si, s, η^4 -(CH ₂ =CHSiMe ₂) ₂ O, $J(\text{PtSi}) = 42.9$]	
-0.55 [2Si, br., μ -(CH ₂ =CHSiMe ₂) ₂ O]	

Table 3.1 NMR data of **8** in C₆D₆ at 295 K. ^{29}Si observed at 59.63 MHz and ^{195}Pt observed at 85.28 MHz. *a* Signal contains two singlets with a separation of *ca.* 50 Hz.

$^{29}\text{Si} \{^1\text{H}\}, \delta (J / \text{Hz})$	$^{195}\text{Pt} \{^1\text{H}\}, \delta$
3.45 [2Si, s, η^4 -(CH ₂ =CHSiMe ₂) ₂ O, $J(\text{PtSi}) = 42.9$]	-6151 ^a
2.63 [2Si, s, η^4 -(CH ₂ =CHSiMe ₂) ₂ O, $J(\text{PtSi}) = 42.9$]	
0.18 [2Si, br., μ -(CH ₂ =CHSiMe ₂) ₂ O]	
0.17 [2Si, br., μ -(CH ₂ =CHSiMe ₂) ₂ O]	

Table 3.2 NMR data of **8** in [²H₈]toluene reported by Lappert and co-workers.⁵ *a* Signal contains two singlets with *ca.* 20 Hz separation.

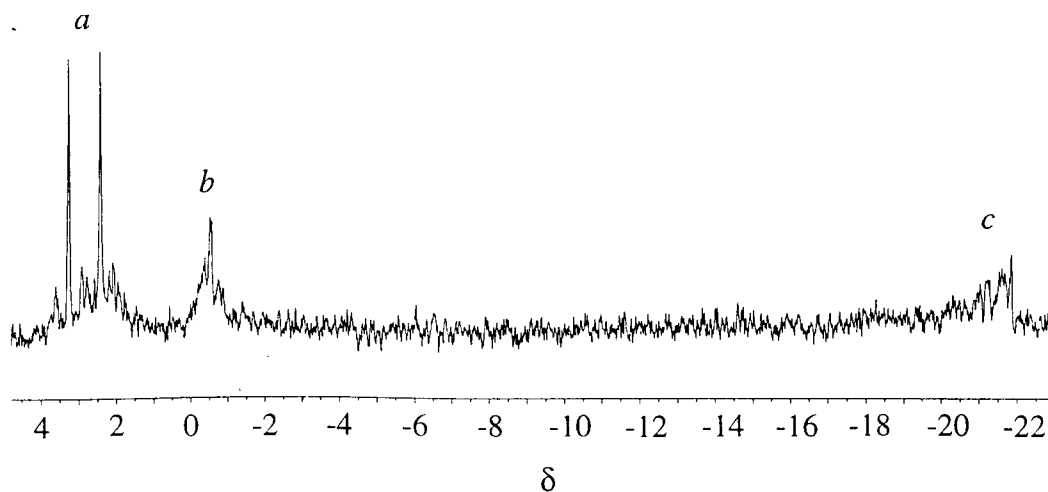


Figure 3.2 ^{29}Si (59.63 MHz) $\{^1\text{H}\}$ NMR spectrum of complex **8** in C₆D₆ at 295 K. *a* Chelating (CH₂=CHSiMe₂)₂O ligand. *b* Bridging (CH₂=CHSiMe₂)₂O ligand. *c* Oligomeric impurities.

The appearance of two ^{29}Si signals for the bridging ligand and two ^{29}Si signals for the two chelating ligands was, according to Lappert and co-workers, due to the conformation of the bridging ligand in **8**.⁶ In the crystal structure of **8**, it was found that

both the chelating ligands adopt the “chair” conformation, whereas the bridging ligand adopts a “V” conformation (Figure 3.3).

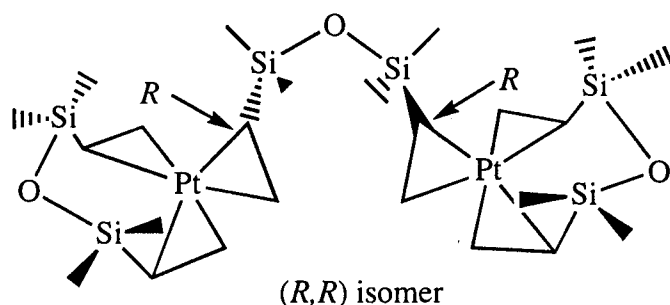


Figure 3.3 A drawing of **8** representing the crystal structure reported by Lappert and co-workers.⁵ Both chelating $(\text{CH}_2=\text{CHSiMe}_2)_2\text{O}$ ligands adopt the “chair” conformation.

Lappert and co-workers assumed that in solution both chelating ligands would adopt the “chair” conformation, as was the case in the crystal structure of **8**. The silicon atoms in the chelating $(\text{CH}_2=\text{CHSiMe}_2)_2\text{O}$ ligand are inequivalent if **8** is stereochemically rigid. However, it was suggested that rapid rotation occurs about the vinyl bond in the bridging $(\text{CH}_2=\text{CHSiMe}_2)_2\text{O}$ ligand at room temperature, hence the silicon atoms in the chelate ligand would now become equivalent. It was also suggested that the bridging $(\text{CH}_2=\text{CHSiMe}_2)_2\text{O}$ ligand can adopt either the “V” or the “chair” conformation. In the “V” conformation, the α -carbons on the two vinyl groups (α -carbon is next to silicon) are either (R,R) or (S,S) giving one isomer, (*rac*) (Figure 3.4). In the “chair” conformation, the α -carbons on the bridging ligand are either (R,S) or (S,R) giving another isomer, (*meso*). This then would leave us with two possible isomers $(R,R)/(S,S)$ (*rac*) or (R,S) (*meso*), which was suggested to be responsible for the four signals observed in the ^{29}Si $\{^1\text{H}\}$ -NMR spectrum and two signals in the ^{195}Pt $\{^1\text{H}\}$ NMR spectra of **8**.⁶

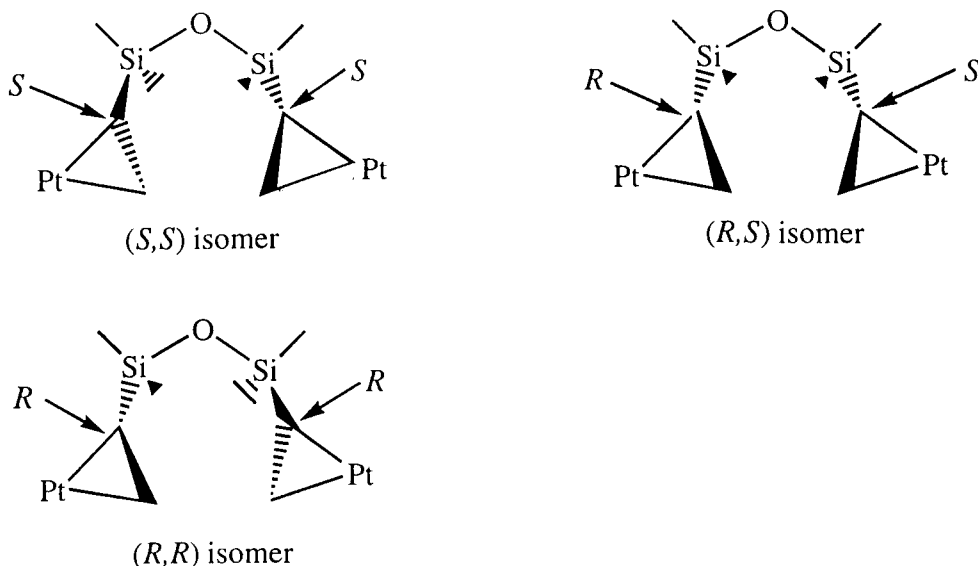


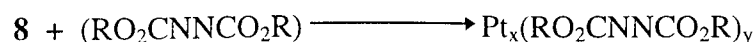
Figure 3.4 Possible conformation of the bridging $(\text{CH}_2=\text{CHSiMe}_2)_2\text{O}$ ligand in **8**. The (S,S) and (R,R) isomers adopt the “V” conformation, whereas the (R,S) isomer adopts the “chair” conformation. The two chelating $(\text{CH}_2=\text{CHSiMe}_2)_2\text{O}$ ligands are omitted for clarity.

3.2.2 Inhibition of $[(\text{Pt}\{\eta^4\text{-(CH}_2=\text{CH-SiMe}_2)_2\text{O}\})_2(\mu\text{-(CH}_2=\text{CHSiMe}_2)_2\text{O})]$ **8**

Heaton has previously shown that azodicarbonyl compounds can act successfully as inhibitors of **8**.⁷ His results from model hydrosilation systems have shown that azodicarbonyl-inhibited **8** does not initiate hydrosilation until it is thermally or photochemically activated. In this study, azodicarboxylates, $\text{RO}_2\text{CNNCO}_2\text{R}$ ($\text{R} = \text{Et}, \text{Pr}^i, \text{Bu}^t$), are studied further as inhibitors of **8**.

3.2.2a Characterisation of azodicarboxylate inhibited **8**

A two fold excess of azodicarboxylate compound was added to **8** in toluene, then purified by flash chromatography to remove excess vinylsiloxane and azo inhibitors, to yield a light brown solid (Equation 3.2).



¹H NMR spectra of **9** and **10** indicate the presence of only one set of resonances associated with the R group of the azodicarboxylate inhibitor (Figures 3.5-3.6 and Table 3.3). Compound **11** showed several unidentified features in the ¹H NMR spectrum

which were not found in either **9** and **10** (Figure 3.7). Table 3.4 summarises the ^1H NMR data for the free azo inhibitors, $\text{RO}_2\text{CNNCO}_2\text{R}$ ($\text{R} = \text{Et}, \text{Pr}^i, \text{Bu}^t$).

The ^1H ethyl resonances in **9** were broad at room temperature, but sharpen at elevated temperature (Figure 3.5). This is also observed for the ^1H isopropyl resonances in **10** (Figure 3.6). This is indicative of a fluxional exchange process. The ^{29}Si $\{^1\text{H}\}$ NMR spectra of **9-11** did not show any signals due to chelating or bridging $(\text{CH}_2=\text{CHSiMe}_2)_2\text{O}$ ligands, demonstrating that $\text{RO}_2\text{CNNCO}_2\text{R}$ displaces both the bridging and chelating divinylsiloxane ligand $(\text{CH}_2=\text{CHSiMe}_2)_2\text{O}$. Attempts to obtain ^{195}Pt $\{^1\text{H}\}$ spectra were unsuccessful.

^{29}Si $\{^1\text{H}\}$ NMR spectra of **8** in Figure 3.8 show that by increasing the concentration of $\text{EtO}_2\text{CNNCO}_2\text{Et}$ in an NMR sample of **8**, the intensity of the signals corresponding to the two chelating $(\text{CH}_2\text{CH}=\text{SiMe}_2)_2\text{O}$ ligands and the one bridging $(\text{CH}_2=\text{CHSiMe}_2)_2\text{O}$ ligand decreases and the intensity of the signal due to free $(\text{CH}_2=\text{CHSiMe}_2)_2\text{O}$ increases.

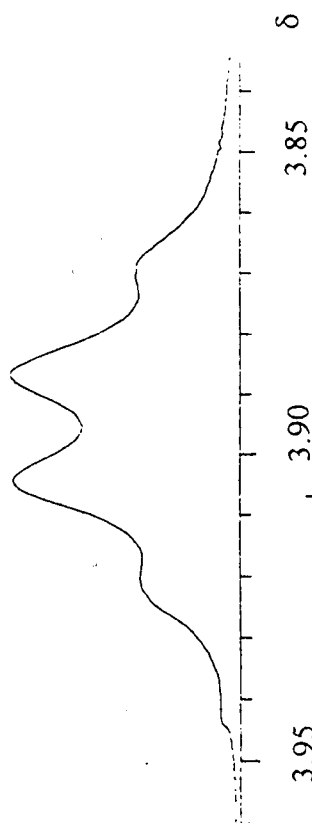
	R^a	$^1\text{H}, \delta$ (J / Hz)
9	Et	0.87 [3H, br. t, CH_3CH_2 , $J(\text{HH}) = 7.4$] 3.89 [2H, br. quart, CH_3CH_2 , $J(\text{HH}) = 7.4$]
10^b	Pr^i	0.97 [6H, br. d, $(\text{CH}_3)_2\text{CH}$, $J(\text{HH}) = 6.1$] 4.87 [1H, br. sept, $(\text{CH}_3)_2\text{CH}$, $J(\text{HH}) = 6.1$]
11	Bu^t	0.87 (br. t) 1.22 (br.) 1.33 (br.)

Table 3.3 ^1H (399.65 MHz) NMR data for **9-11** in C_6D_6 at 295 K. *a* R is the alkyl group on the azodicarboxylate ligand, $\text{RO}_2\text{CNNCO}_2\text{R}$. *b* Values reported by Heaton occur at δ 1.30 [d, $(\text{CH}_3)_2\text{CH}$, $J(\text{HH}) = 6.0$ Hz], δ 4.90 [sept, $(\text{CH}_3)_2\text{CH}$, $J(\text{HH}) = 6.0$ Hz] recorded in CDCl_3 at 293 K.⁷

	$^1\text{H}, \delta$ (J / Hz)
$\text{EtO}_2\text{CNNCO}_2\text{Et}$	0.85 [3H, t, CH_3CH_2 , $J(\text{HH}) = 7.0$] 3.92 [2H, quart, CH_3CH_2 , $J(\text{HH}) = 7.0$]
$\text{Pr}^i\text{O}_2\text{CNNCO}_2\text{Pr}^i$	1.01 [6H, d, $(\text{CH}_3)_2\text{CH}$, $J(\text{HH}) = 7.0$] 4.91 [1H, sept, $(\text{CH}_3)_2\text{CH}$, $J(\text{HH}) = 7.0$]
$\text{Bu}^t\text{O}_2\text{CNNCO}_2\text{Bu}^t$	1.23 (s)

Table 3.4 ^1H (399.65 MHz) NMR data for $\text{RO}_2\text{CNNCO}_2\text{R}$ ($\text{R} = \text{Et}, \text{Pr}^i, \text{Bu}^t$) in C_6D_6 at 295 K.

At room temperature



89

at 55 °C

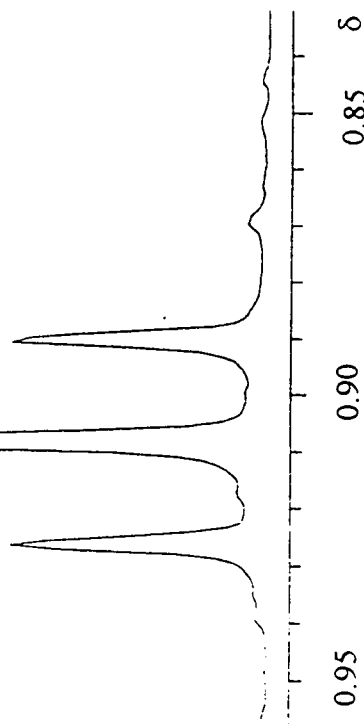
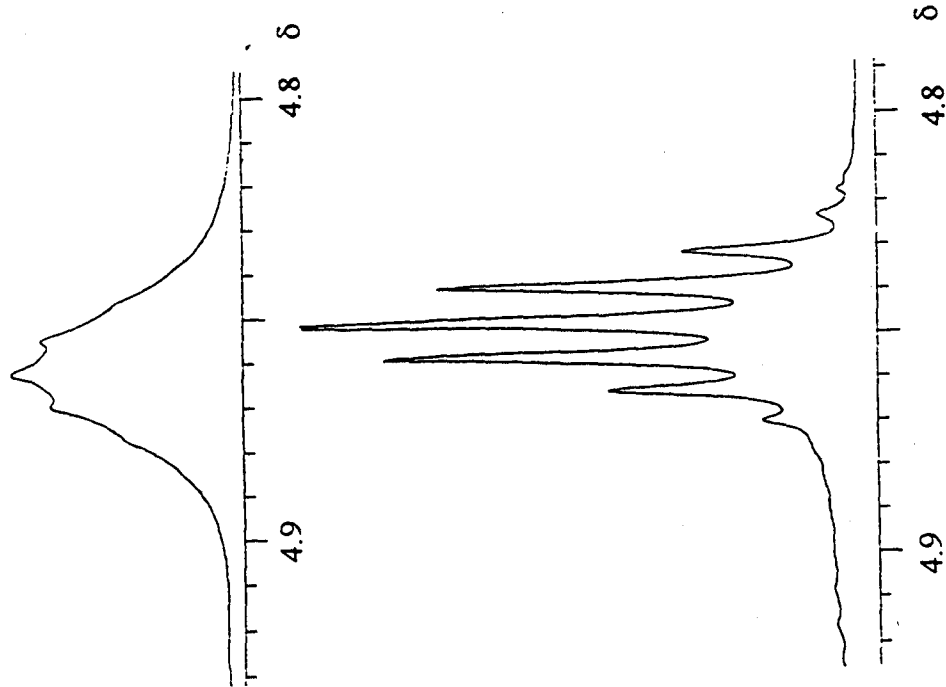


Figure 3.5 ^1H (399.65 MHz) NMR spectra of **9** in C_6D_6 .

At room temperature



at 55 °C

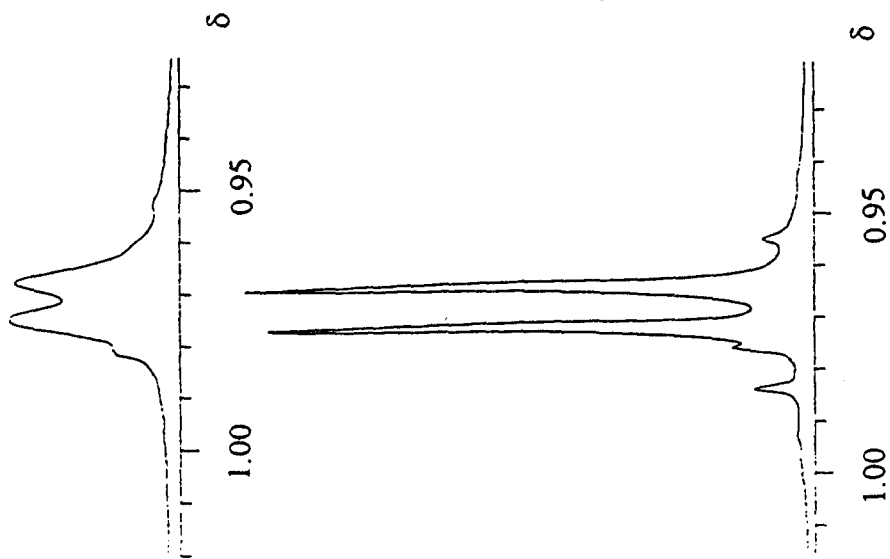


Figure 3.6 ^1H (399.65 MHz) NMR spectra of **10** in C_6D_6 .

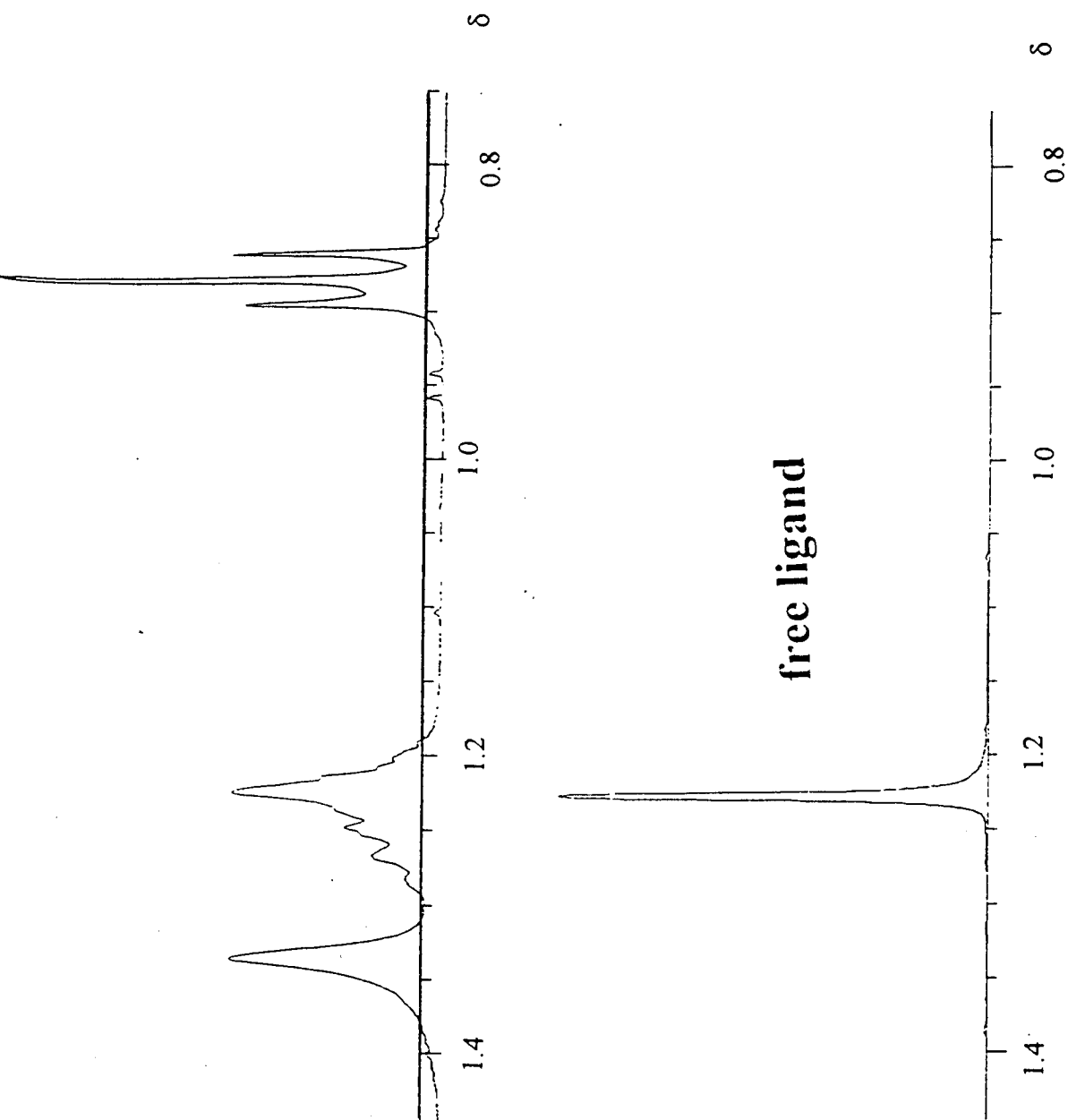


Figure 3.7 ^1H (399.65 MHz) NMR spectra of **11** in C_6D_6 .

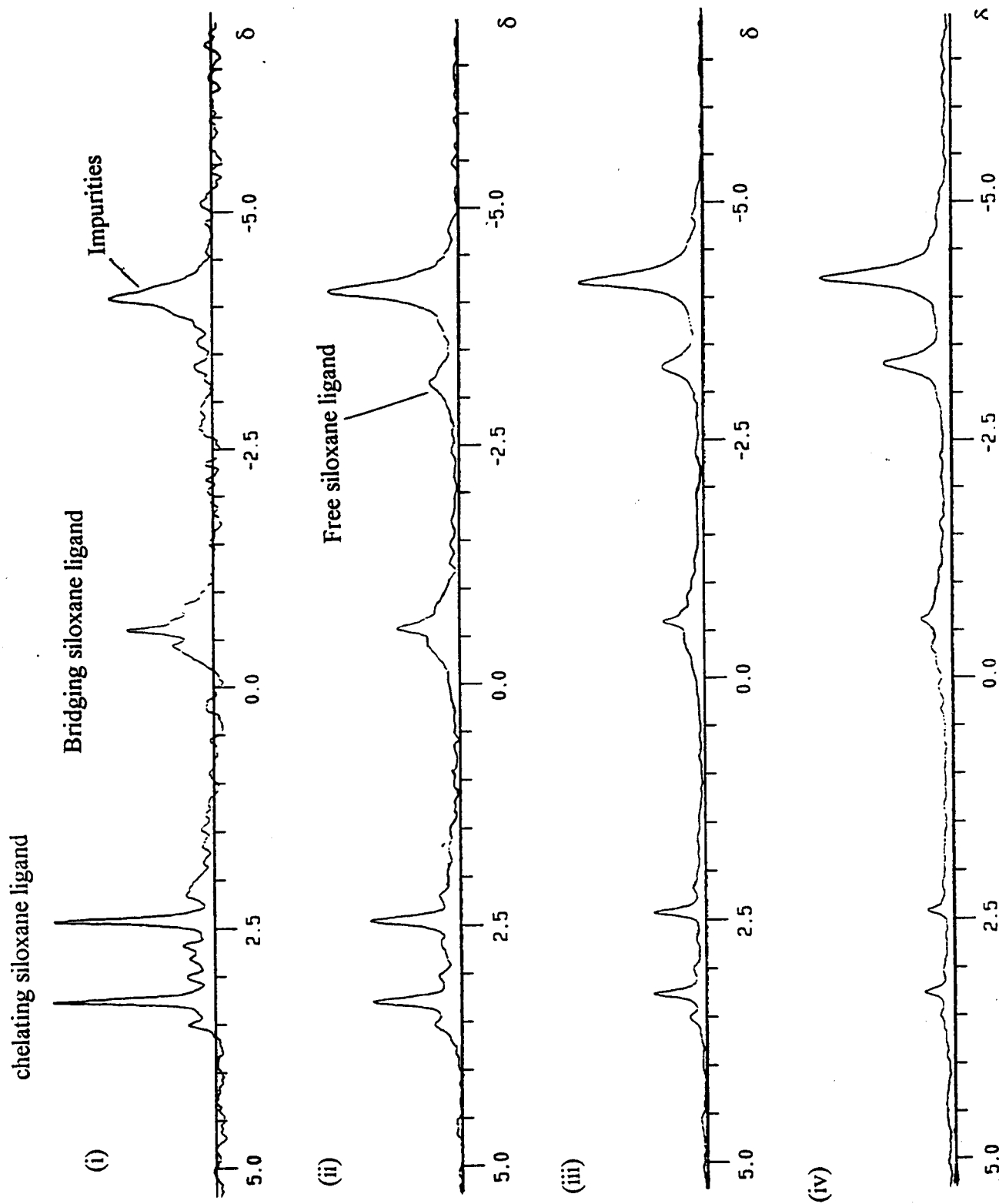


Figure 3.8 ^{29}Si (79.30 MHz) $\{^1\text{H}\}$ NMR spectra of **8** in C_6D_6 at 295 K with increasing concentration of $\text{EtO}_2\text{CNNCO}_2\text{Et}$. (i) 0 %. (ii) 30 %. (iii) 60 %. (iv) 90 %.

The UV/VIS spectra of **9** and **10** in THF show a shoulder band at *ca.* 312 nm (Figure 3.9). However, for **11** the shoulder in this region was very weak compared to **9** and **10**, a slight band probably exists at *ca.* 307 nm. The values of 312 nm for the shoulder band of **9** and **10** are slightly lower in energy than for the values reported by Heaton, *ca.* 305 nm, which was recorded in CH₂Cl₂.⁵ No such band exists for the uninhibited complex **8**. The UV/VIS spectra of the free azo inhibitor, RO₂CNNCO₂R (R = Et, Prⁱ and Bu^t) all show band maxima at *ca.* 403 nm.

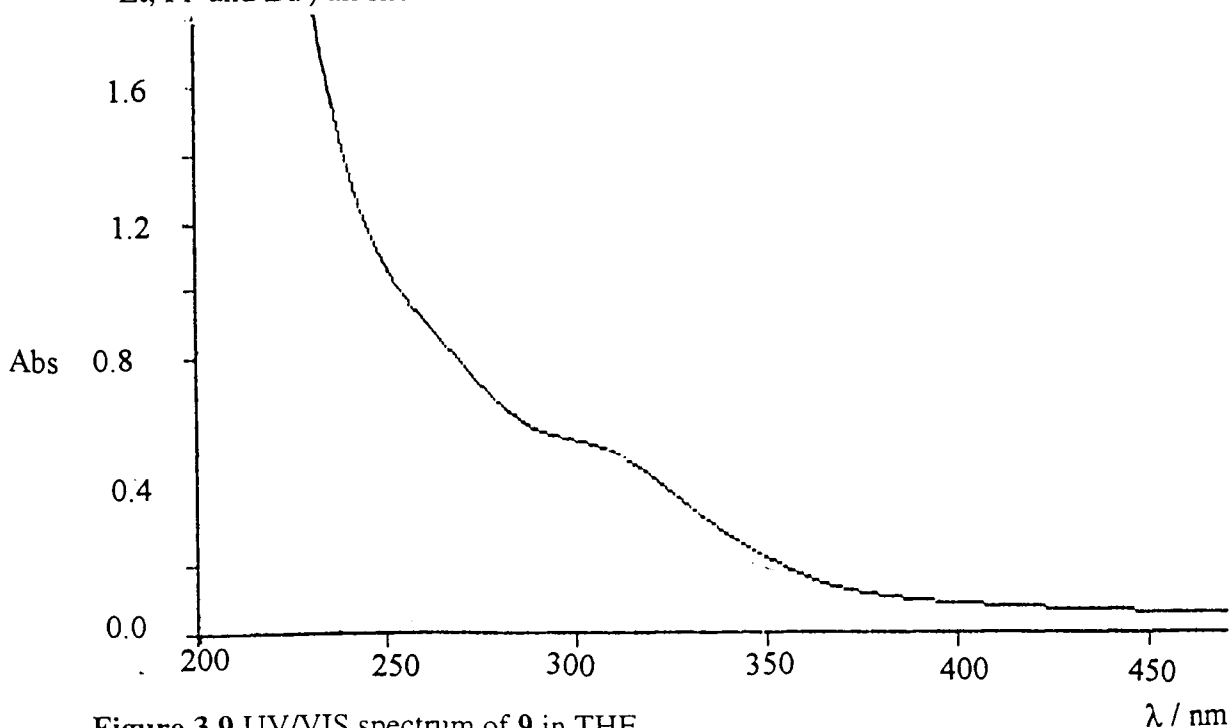


Figure 3.9 UV/VIS spectrum of **9** in THF.

IR spectra of compounds **9-11** were measured in THF, broad bands were detected for all three compounds at *ca.* 1750 cm⁻¹ and were assigned as a mixture of CO/CN stretches (Table 3.5 and Figures 3.10-3.12). Compound **11** contains an additional band at 1778 cm⁻¹, which roughly corresponds to that of the free azodicarboxylate inhibitor, Bu^tO₂CNNCO₂Bu^t.

	$\nu(\text{CO/CN}) / \text{cm}^{-1}$
9	1737
10	1734
11	1730, 1778
EtO ₂ CNNCO ₂ Et	1782 ^a
Pr ⁱ O ₂ CNNCO ₂ Pr ⁱ	1778 ^a
Bu ^t O ₂ CNNCO ₂ Bu ^t	1775 ^a

Table 3.5 IR data of $\nu(\text{CO/CN})$ stretches for **9-10**. ^a stretching frequencies reported for free azo inhibitor RO₂CNNCO₂R (R = Et, Prⁱ, Bu^t) are for $\nu(\text{CO})$ stretches only.

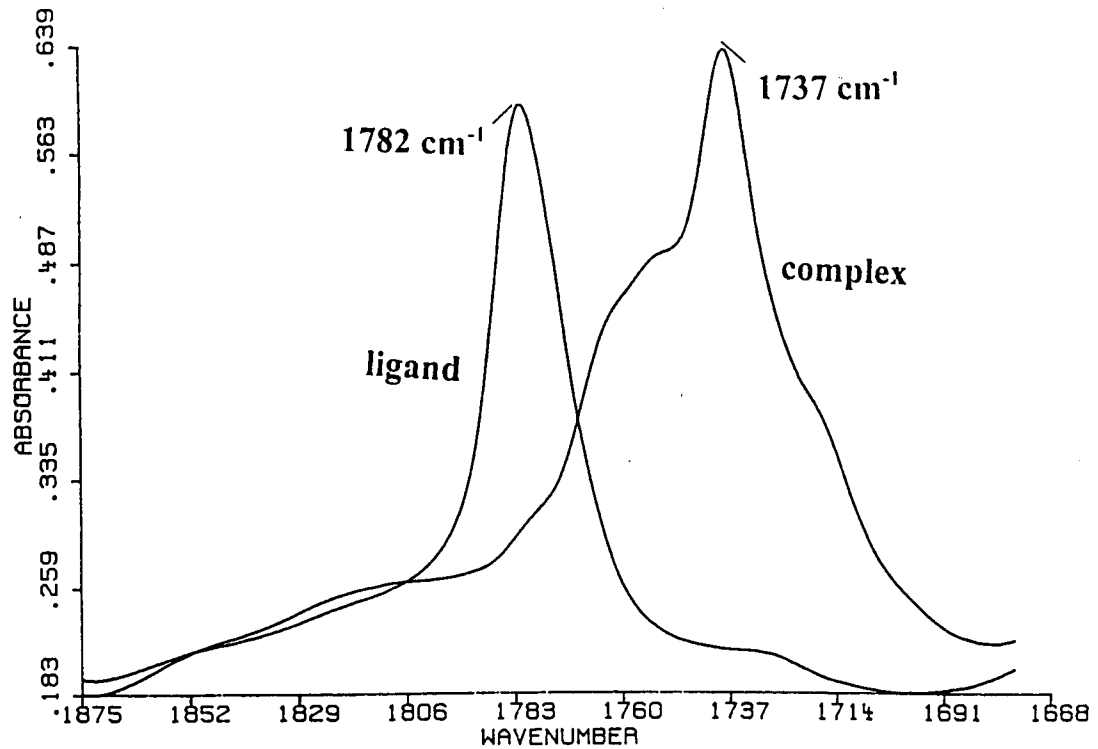


Figure 3.10 IR spectrum of 9 in THF. The spectrum of the free azo inhibitor EtO₂CNNCO₂Et is superimposed on top.

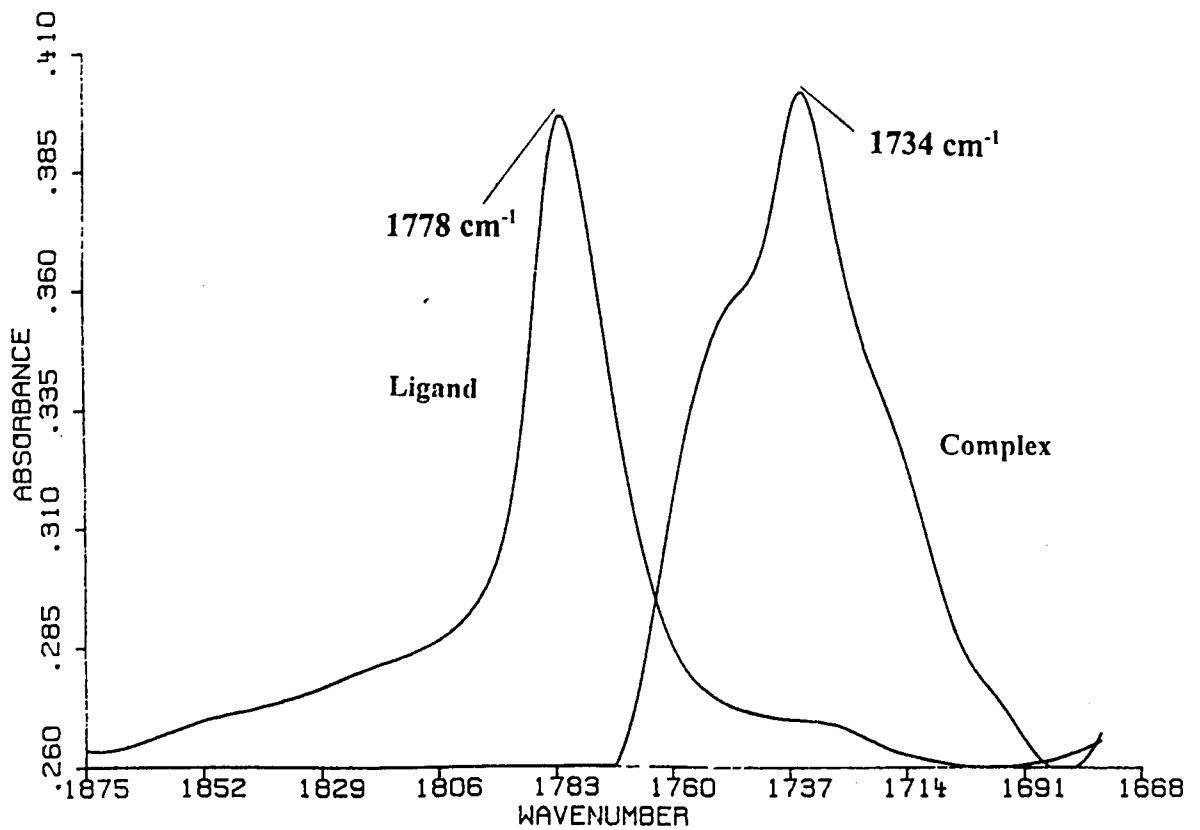


Figure 3.11 IR spectrum of 10 in THF. The spectrum of the free azo inhibitor PrⁱO₂CNNCO₂Prⁱ is superimposed on top.

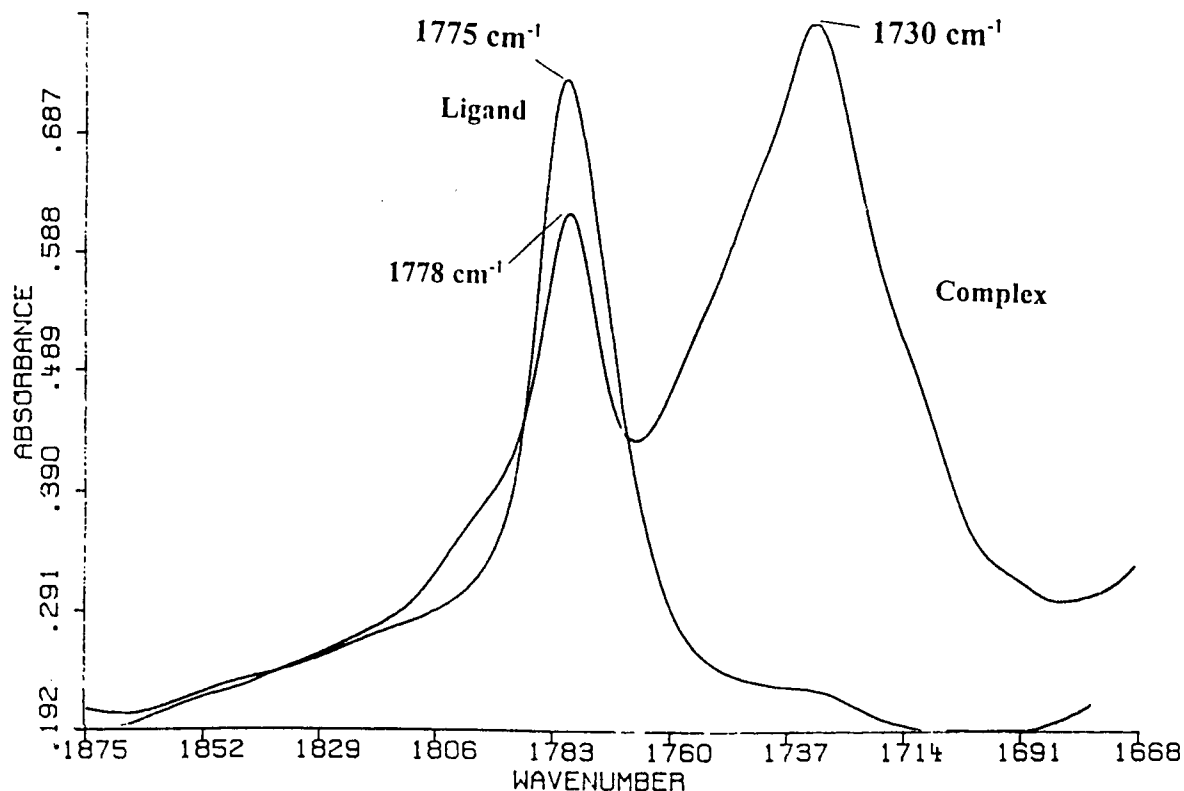


Figure 3.12 IR spectrum of **11** in THF. The spectrum of the free azo inhibitor $\text{Bu}^t\text{O}_2\text{CNNCO}_2\text{Bu}^t$ is superimposed on top.

3.2.2b Photolysis of compounds 9-11 in THF

Compounds **9-10** were dissolved in THF and photolysed with UV radiation and monitored by UV/VIS spectroscopy. The absorbance at 312 nm, the region of the shoulder in the spectra of **9-10**, was observed to decrease with increasing photolysis time (Table 3.6 and Figures 3.13-3.14)

Photolysis time	9 (%) ^a	10 (%) ^a	11 (%) ^a
0	100	100	100
1	88.2	84.0	94.3
2	80.6	68.4	88.4
3	72.0	60.9	80.3
4	67.0	58.1	75.7
5	61.9		72.5
6	58.9		70.2

Table 3.6 Data showing the percentage (%) of absorbance at 312 nm for **9-10** with increasing photolysis time. ^a Percentage of absorbance is related to absorbance before photolysis.

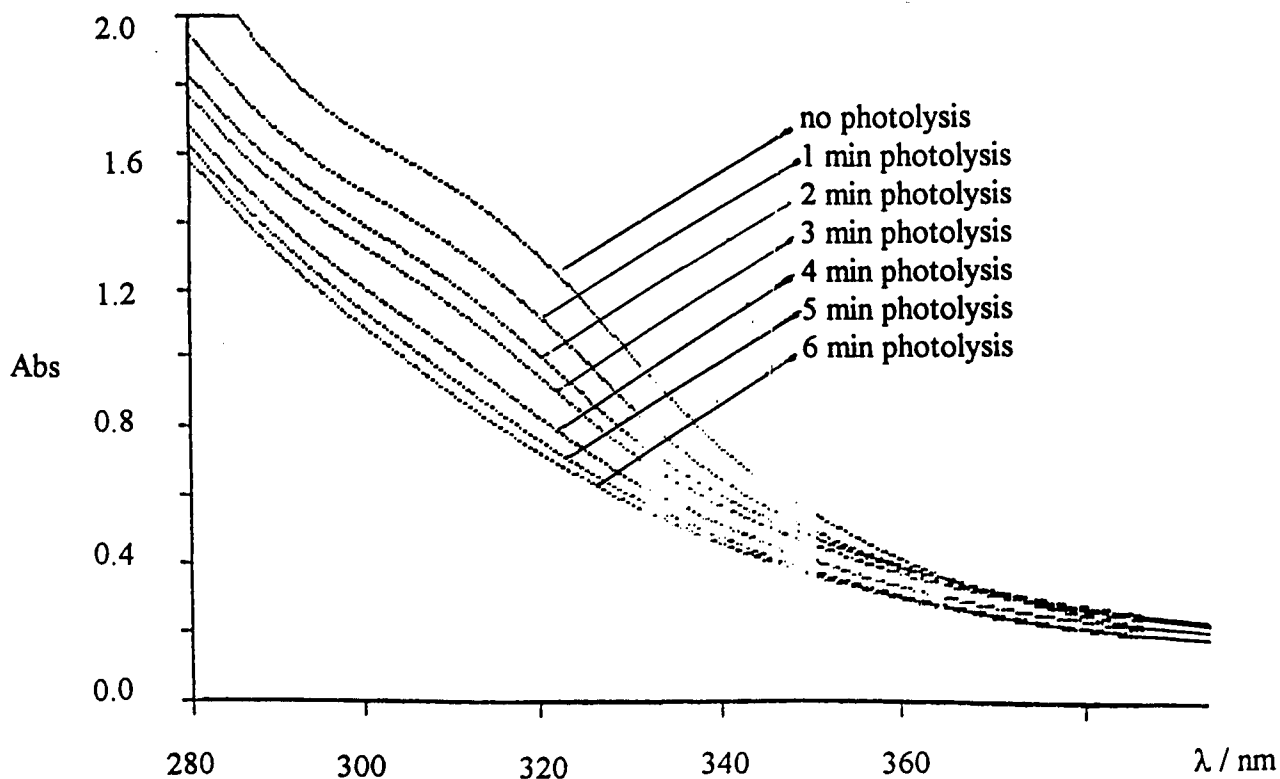


Figure 3.13 UV/VIS spectra of 9 after various photolysis times.

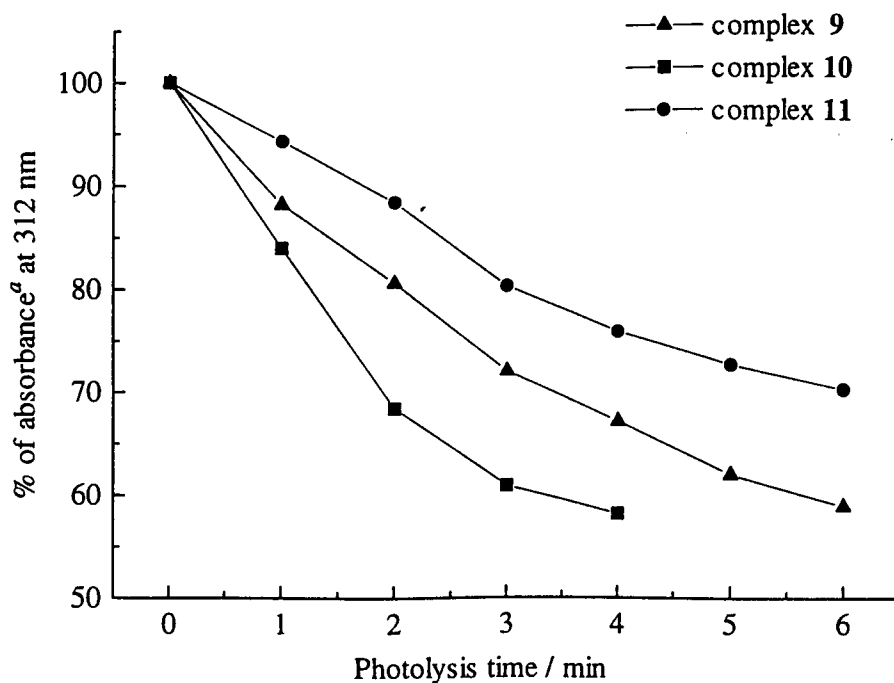


Figure 3.14 Plot showing the decrease in percentage of absorbance at 312 nm for compound 9-10 with increasing photolysis time. ^a Percentage of absorbance is related to the original absorbance value before photolysis.

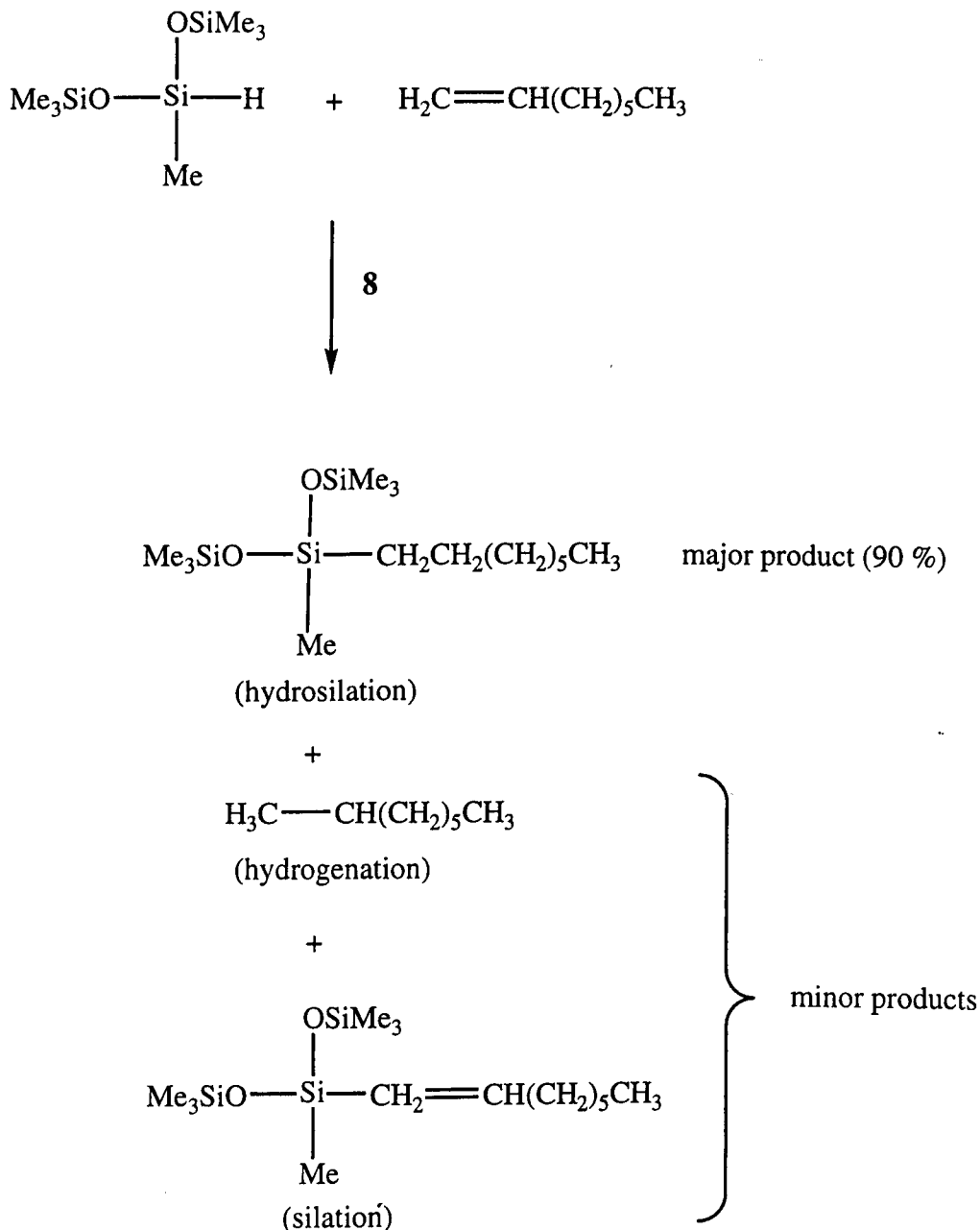
The plots for the decrease in absorbance at 312 nm show that **10** requires the least irradiation time to reach 60 % of its original value, this is then followed by **9** (Figure 3.14). However, **11** did not follow the same trend as **9** and **10**, as its absorbance value at 312 nm tended towards a higher percentage of its original value from the others. This could be due to the difficulty in observing a prominent band for **11** near the 312 nm region, so a fair comparison of **11** with **9** and **10** might not be valid.

3.2.3 Hydrosilation using azo-inhibited **8**

3.2.3a Model hydrosilation system

The model hydrosilation system employed consisted of an equal molar amount of 1-octene and 1,1,1,3,5,5,5-heptamethyltrisiloxane. Addition of **8** to the model hydrosilation system causes instantaneous reaction between the silane and the alkene. A ratio of $1:1 \times 10^{-5}$ of Si-H to Pt was used in the model hydrosilation system. GC analysis showed that the major product formed was due to hydrosilation (*ca.* 90 %) and the minor products were from hydrogenation and silation (Scheme 3.2).

Heaton reported that addition of mercury to a mixture of siloxane and alkene containing the azodicarbonyl inhibited **8** did not inhibit hydrosilation upon thermal activation.⁷ This result indicated that the species formed on thermal activation gave a homogeneous hydrosilation catalyst.^{13,14} However, Lewis and co-workers have reported that **8** itself forms platinum colloids during hydrosilation and that it is affected by the presence of mercury.¹⁵



Scheme 3.2 Reaction of 1-octene with 1,1,1,3,5,5,5-heptamethyltrisiloxane catalysed by complex **8**.

3.2.3b Photoactivation of azo-inhibited **8** in a model hydrosilation system

Complex **8** was inhibited with a 40 fold excess of the azo compound $\text{RO}_2\text{CNNCO}_2\text{R}$ ($\text{R} = \text{Et}, \text{Pr}^i, \text{Bu}^t$) in 1-octene to form the azo-inhibited species **9a** ($\text{R} = \text{Et}$), **10a** ($\text{R} = \text{Pr}^i$) and **11a** ($\text{R} = \text{Bu}^t$). Addition of 1,1,1,3,5,5,5-heptamethyltrisiloxane did not initiate the hydrosilation reaction, as shown by the GC analysis of the reaction mixture. However, compounds **9-10**, purified by flash chromatography to remove excess azo, did initiate hydrosilation between 1-octene and 1,1,1,3,5,5,5-heptamethyltrisiloxane. This observation is in agreement with Heaton's previous investigation of

azo-inhibited **8**. Heaton found that up to 40 fold excess of azo to Pt was required to prevent hydrosilation.⁷

Figure 3.15 shows the experimental set-up for the model hydrosilation studied using inhibited catalysts **9a**, **10a** and **11a**. Two identical samples containing the reaction mixture of alkene, silane and the inhibited catalyst **9a**, **10a** or **11a** were photolysed; one of the samples was shielded from light to observe thermal effects. Photolysis time of the samples varied from one to five minutes. At the end of photolysis the samples were analysed by GC to monitor for signs of hydrosilation over time.

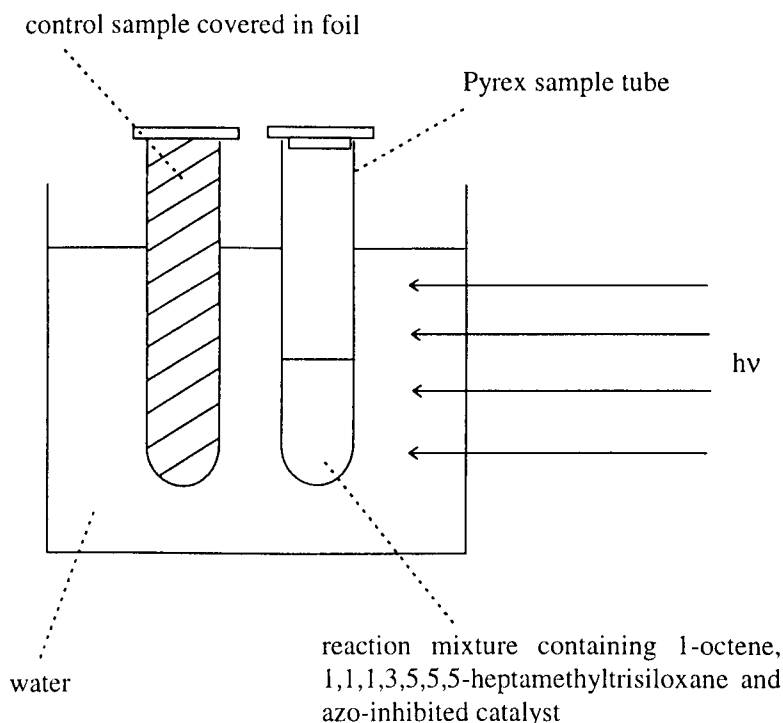


Figure 3.15 Photolysis set-up for the photoactivation of inhibited catalysts **9a-11a** in a model hydrosilation system.

It was found that the model hydrosilation system using the inhibited catalyst **9a** and **10a** required the longest photolysis time before hydrosilation was initiated, whereas for **11a** hydrosilation began only after 1 min of photolysis (Tables 3.7-3.13 and Figures 3.16 and 3.17).

Time / min ^a	Hydrosilation Product / %
0.0	2
11.0	3
29.8	3
42.5	3
65.3	4

Table 3.7 Percentage of hydrosilation product formed after 2 min photolysis on the model hydrosilation system with azo-inhibited catalyst **9a**. Amount of hydrosilation product generated from the control sample is 4 %. *a* Time starts at the end of photolysis.

Time / min ^a	Hydrosilation product / %
0.0	13
12.7	16
23.0	26
36.0	45
50.0	69
78.3	76
89.0	78
98.5	81

Table 3.8 Percentage of hydrosilation product formed after 5 min photolysis on the model hydrosilation system with azo-inhibited catalyst **9a**. Amount of hydrosilation product generated from control sample is 4 %. *a* Time starts at the end of photolysis.

Time / min	Hydrosilation product / %
0.0	2
8.9	5
18.7	5
27.5	5
36.5	8
45.6	3
55.0	4

Table 3.9 Percentage of hydrosilation product formed after 2 min photolysis on the model hydrosilation system with azo-inhibited catalyst **10a**. Amount of hydrosilation product generated from control sample is 2 %. *a* Time starts at the end of photolysis.

Time / min	Hydrosilation product / %
0.0	8
10.3	58
32.2	80
52.0	90

Table 3.10 Percentage of hydrosilation product formed after 5 min photolysis on the model hydrosilation system with azo-inhibited catalyst **10a**. Amount of hydrosilation product generated from controlled sample is 2 %.

Time / min	Hydrosilation product / %
0.0	5
8.6	12
17.8	16
37.8	34
50.7	51
68.2	67
90.0	71

Table 3.11 Percentage of hydrosilation product formed after 1 min photolysis on the model hydrosilation system with azo-inhibited catalyst **11a**. Amount of hydrosilation product generated from control sample is 4 %.

Time / min	Hydrosilation product / %
0.0	12
9.5	60
19.0	82
20.3	86
44.3	90

Table 3.12 Percentage of hydrosilation product formed after 2 min photolysis on the model hydrosilation system with azo-inhibited catalyst **11a**. Amount of hydrosilation product generated from control sample is 10 %.

Time / min	Hydrosilation product / %
0.0	20.0
9.0	84.4
18.4	90.8
36.5	91.1

Table 3.13 Percentage of hydrosilation product formed after 5 min photolysis on the model hydrosilation system with azo-inhibited catalyst **11a**. Amount of hydrosilation product from control sample is 15 %.

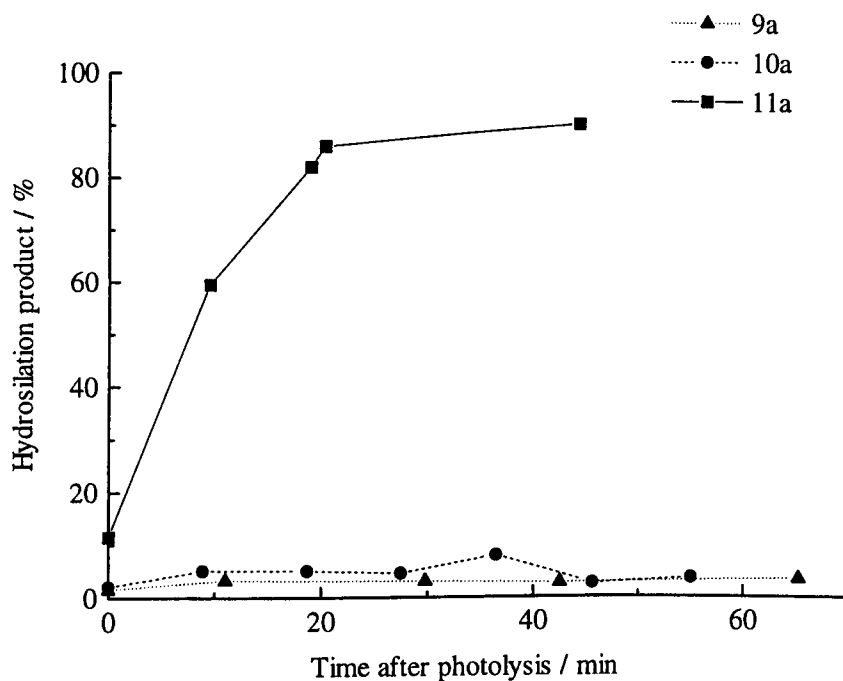


Figure 3.16 Plots of amount of hydrosilation product formed with respect to time after 2 min photolysis on the model hydrosilation system using the inhibited catalysts **9a**, **10a** or **11a**. Amount of hydrosilation product generated from the control sample; **9a** (4 %), **10a** (2 %), **11a** (10 %).

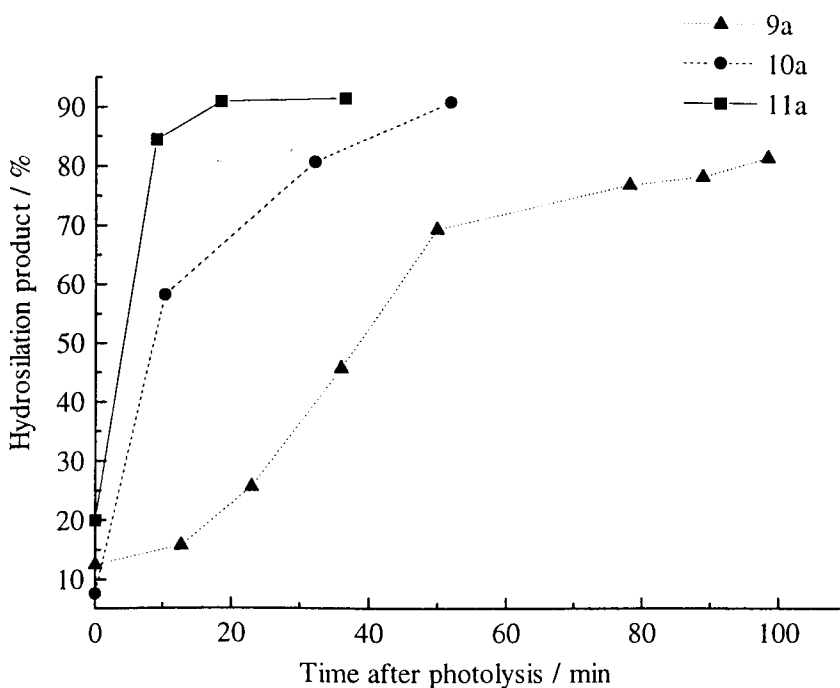


Figure 3.17 Plots of amount of hydrosilation product formed with respect to time after 5 min photolysis on the model hydrosilation system using the inhibited catalysts **9a**, **10a** or **11a**. Amount of hydrosilation product generated from the control sample; **9a** (4 %), **10a** (2 %), **11a** (10 %).

Figure 3.18 shows that as the photolysis time for activating azo-inhibited **8** increases, so does the rate of hydrosilation between 1-octene and 1,1,1,3,5,5,5-heptamethyl-trisiloxane. For systems using **9a** and **10a** as catalyst there is relatively little variation in the amount of hydrosilation product formed from the control sample (2-4 %), whereas for systems using **11a** as catalysts the amount of hydrosilation product formed is comparatively higher and was found to increase with increasing photolysis time.

This indicates that **11a** is thermally and photochemically more labile compared to **9a** and **10a**, which suggests that azo inhibitor $\text{Bu}^t\text{O}_2\text{CNNCO}_2\text{Bu}^t$ in **11a** is a weaker inhibitor compared to $\text{EtO}_2\text{CNNCO}_2\text{Et}$ (**9a**) and $\text{Pr}^i\text{O}_2\text{CNNCO}_2\text{Pr}^i$ (**10a**). From Figure 3.15, it appears that $\text{EtO}_2\text{CNNCO}_2\text{Et}$ is the most effective, and $\text{Bu}^t\text{O}_2\text{CNNCO}_2\text{Bu}^t$ is the least effective azo inhibitor.

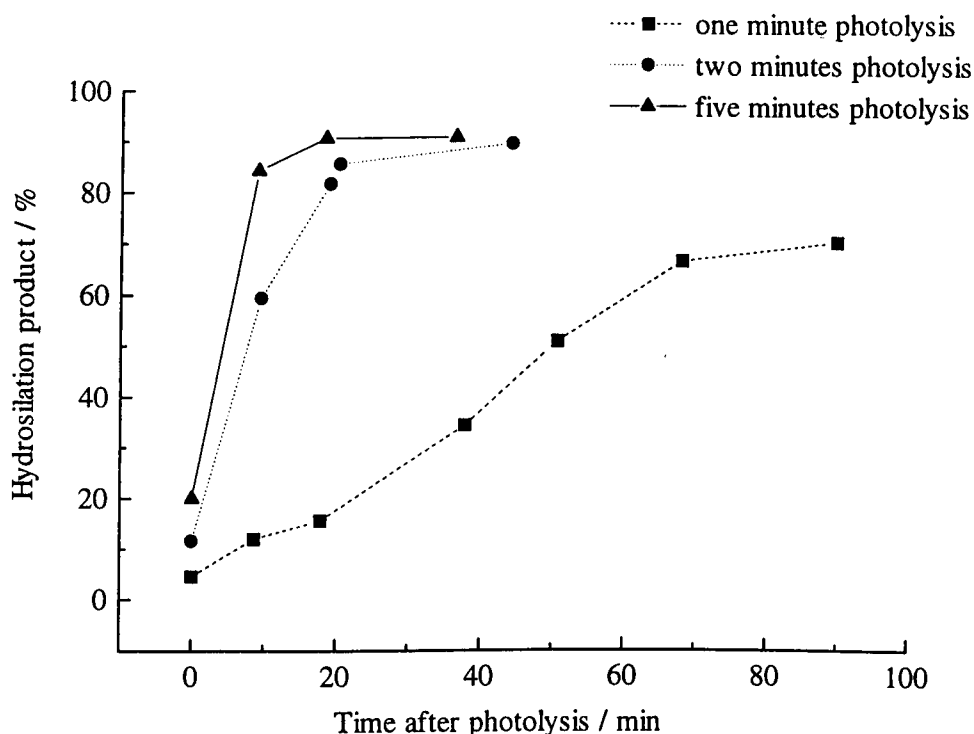
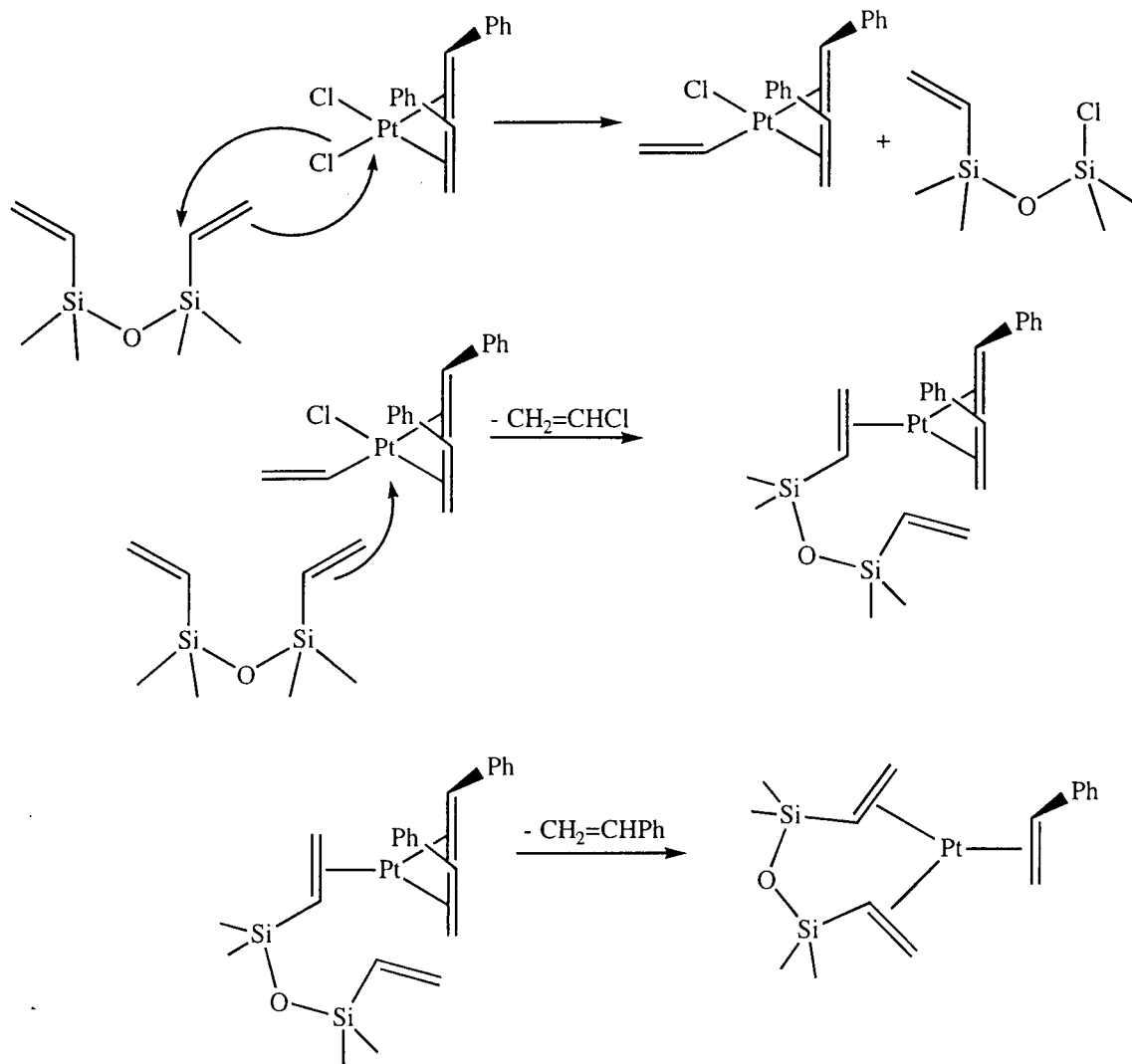


Figure 3.18 Plots of amount of hydrosilation product formed with respect to time after various photolysis time on the model hydrosilation system with inhibited catalyst **11a**. Amount of hydrosilation product generated from controlled samples; after 1 min photolysis (4 %), after 2 min photolysis (10 %) and after 5 min photolysis (15 %).

3.3 DISCUSSIONS

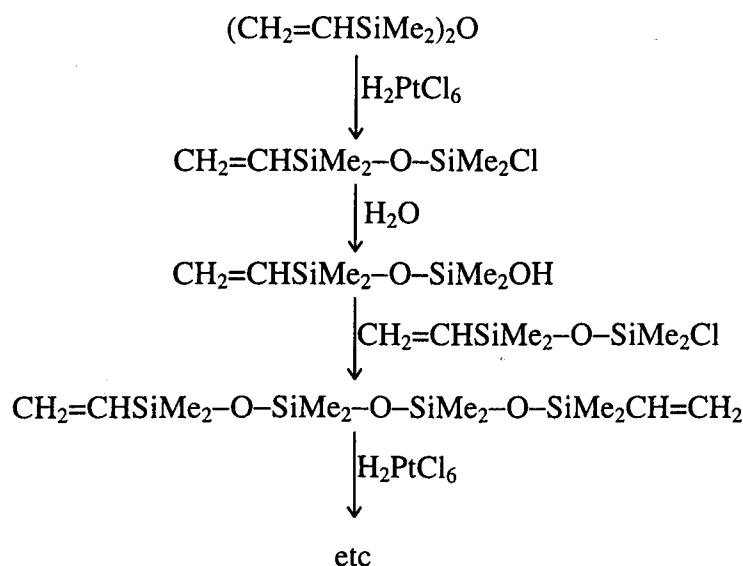
3.3.1 Preparation of $[(Pt\{\eta^4-(CH_2=CHSiMe_2)_2O\})_2(\mu-(CH_2=CHSiMe_2)_2O)]$ **8**

The reaction between H_2PtCl_6 or $PtCl_2(\eta^2-CH_2=CHPh)_2$ with $(CH_2=CHSiMe_2)_2O$ produces the highly active Karstedt's catalyst.⁵ The active component of Karstedt's catalyst has been shown to be the tris-tetramethyldivinylsiloxane platinum(0) complex $[(Pt\{\eta^4-(CH_2=CHSiMe_2)_2O\})_2(\mu-(CH_2=CHSiMe_2)_2O)]$ **8**.⁶ The reduction of H_2PtCl_6 , a Pt(IV) species, to complex **8**, a Pt(0) species, by $(CH_2=CHSiMe_2)_2O$ was examined by Lappert using a Pt(II) model.¹⁶ It was reported that $PtCl_2(\eta^2-CH_2=CHPh)_2$ was reduced by $(CH_2=CHSiMe_2)_2O$ to form $Pt[\eta^4-(CH_2=CHSiMe_2)_2O](\eta^2\text{-styrene})$. The vinyl group in $(CH_2=CHSiMe_2)_2O$ was thought to undergo substitution with a chloride ligand on $PtCl_2(\eta^2-CH_2=CHPh)_2$ to form chlorosilane, leading to the reduction of Pt(II) to Pt(0) (Scheme 3.3). A similar process is believed to occur between H_2PtCl_6 and $(CH_2=CHSiMe_2)_2O$.¹⁶



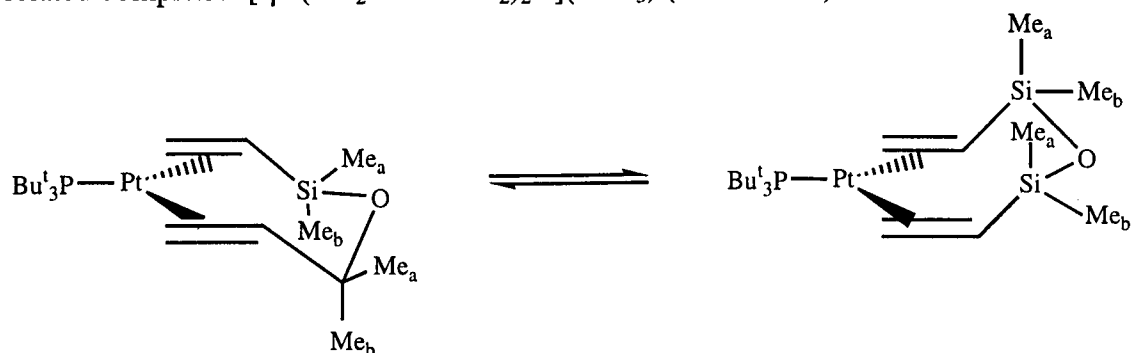
Scheme 3.3 Proposed mechanism for the reduction of Pt(II), $\text{PtCl}_2(\eta^2\text{-CH}_2\text{=CHPh})_2$, to Pt(0), $\text{Pt}[\eta^4\text{-(CH}_2\text{=CH-SiMe}_2)_2\text{O}](\eta^2\text{-styrene})$.¹⁶

The oligomeric siloxane impurities $\text{Me}_2\text{RSiO}(\text{SiMe}_2\text{O})_x\text{SiRMe}_2$ [$\text{R} = (\text{CH}=\text{CH}_2)$, CH_2CH_3 , $\text{CH}_2\text{CH}_2\text{Cl}$; $x = 0\text{-}14$] are believed to be formed from the chlorosilanes produced on reduction of H_2PtCl_6 by $(\text{CH}_2\text{=CHSiMe}_2)_2\text{O}$.¹⁷ The chlorosilanes formed are believed to react with water present in the system to form silanols. The silanols in turn couple with any chlorosilane to form the siloxane oligomer (Scheme 3.4).



Scheme 3.4 Formation of oligomeric siloxane impurity from the preparation of **8** (adapted from ref. 5).

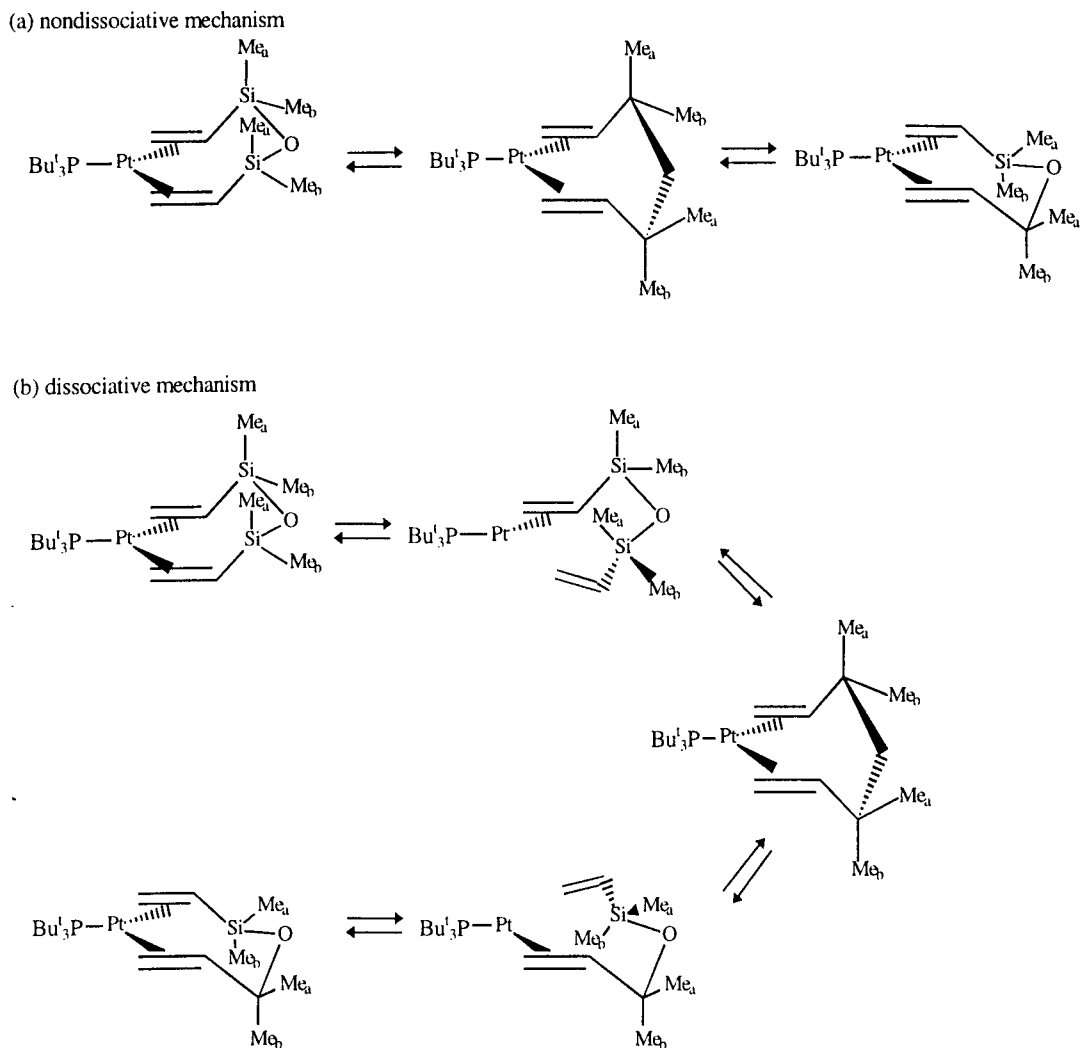
As discussed in Section 3.2.1, the $(\text{CH}_2=\text{CHSiMe}_2)_2\text{O}$ ligands in the crystal structure of complex **8** were found by Lappert and co-workers to adopt the “chair” conformation for both the chelating ligands, whilst the bridging ligand adopts a “V” shape conformation.⁶ It was briefly mentioned by Lappert that NMR spectra of complex **8** exhibited fluxional behaviour in solution, but unfortunately no further details were given.⁶ The chelate ligands of **8** in solution were assumed to adopt the same type of conformation as in the solid state, *ie.* the “chair” conformation. One possible fluxional process would involve a “flipping” motion of the chelating $(\text{CH}_2=\text{CHSiMe}_2)_2\text{O}$ chair conformer, which was observed with NMR spectroscopy by Bassindale *et al.* for the related complex $\text{Pt}[\eta^2-(\text{CH}_2=\text{CHSiMe}_2)_2\text{O}](\text{PBU}^t_3)$ (Scheme 3.5).¹⁸



Scheme 3.5 Fluxional process of $\text{Pt}[\eta^2-(\text{CH}_2=\text{CHSiMe}_2)_2\text{O}](\text{PBU}^t_3)$.¹⁸

Two possible mechanisms were suggested to be responsible for the “flipping” motion in the chelate ligand of $\text{Pt}[\eta^2-(\text{CH}_2=\text{CHSiMe}_2)_2\text{O}](\text{PBU}^t_3)$. The first involves a stepwise, nondissociative rotation about the alkene C=C axis and the second involves a stepwise

dissociation-reassociation mechanism (Scheme 3.6). Both mechanisms would maintain Pt–C and P–C coupling despite the fact that the second mechanism is dissociative. This is because bonding is always maintained on at least one end of the chelate ligand.¹⁹



Scheme 3.6 Proposed mechanism for the “flipping” motion of the chelate ligand in $\text{Pt}[\eta^2\text{-(CH}_2\text{=CHSiMe}_2\text{)}_2\text{O}](\text{PBu}_3)$. (a) nondissociative mechanism. (b) dissociative mechanism.

3.3.2 Inhibition of $[(\text{Pt}\{\eta^4\text{-(CH}_2\text{=CHSiMe}_2\text{)}_2\text{O}\})_2(\mu\text{-(CH}_2\text{=CHSiMe}_2\text{)}_2\text{O})]$ **8**

Present work on the catalytic inhibition of **8** with azodicarbonyl compounds supports the finding reported previously by Heaton that the azodicarbonyl inhibitor appears to displace completely both the bridging and chelating $(\text{CH}_2\text{=CHSiMe}_2)_2\text{O}$ ligands in **8**.⁵ This is unlike other inhibitors of **8**, whereby only the bridging $(\text{CH}_2\text{=CHSiMe}_2)_2\text{O}$ ligand was found to be displaced. For example, investigations on fumarates and maleates, known inhibitors of **8**, have shown that the bridging

divinylsiloxane ligand in **8** is replaced by the inhibitor ligands whilst the chelating divinylsiloxane ligand is retained.^{5,20,21}

Further examples of the lability of the bridging $(\text{CH}_2=\text{CHSiMe}_2)_2\text{O}$ ligand in **8** are reported by Lappert and co-workers.²² They have shown that the bridging $(\text{CH}_2=\text{CHSiMe}_2)_2\text{O}$ ligand can be displaced by a variety of alkene ligands. For instance, treatment of **8** with maleic anhydride, styrene and excess $(\text{CH}_2=\text{CHSiMe}_2)_2\text{O}$ ligands yields $\text{Pt}[\eta^4-(\text{CH}_2=\text{CHSiMe}_2)_2\text{O}][\eta^2-\text{CHC}(\text{O})\text{OC}(\text{O})\text{CH}]$,⁵ $\text{Pt}[\eta^4-(\text{CH}_2=\text{CHSiMe}_2)_2\text{O}](\eta^2\text{-styrene})$,¹⁶ and $\text{Pt}[\eta^4-(\text{CH}_2=\text{CHSiMe}_2)_2\text{O}][\eta^2-(\text{CH}_2=\text{CHSiMe}_2)\text{-OSiMe}_2\text{CH}=\text{CH}_2]$,¹⁶ respectively (Figure 3.19).

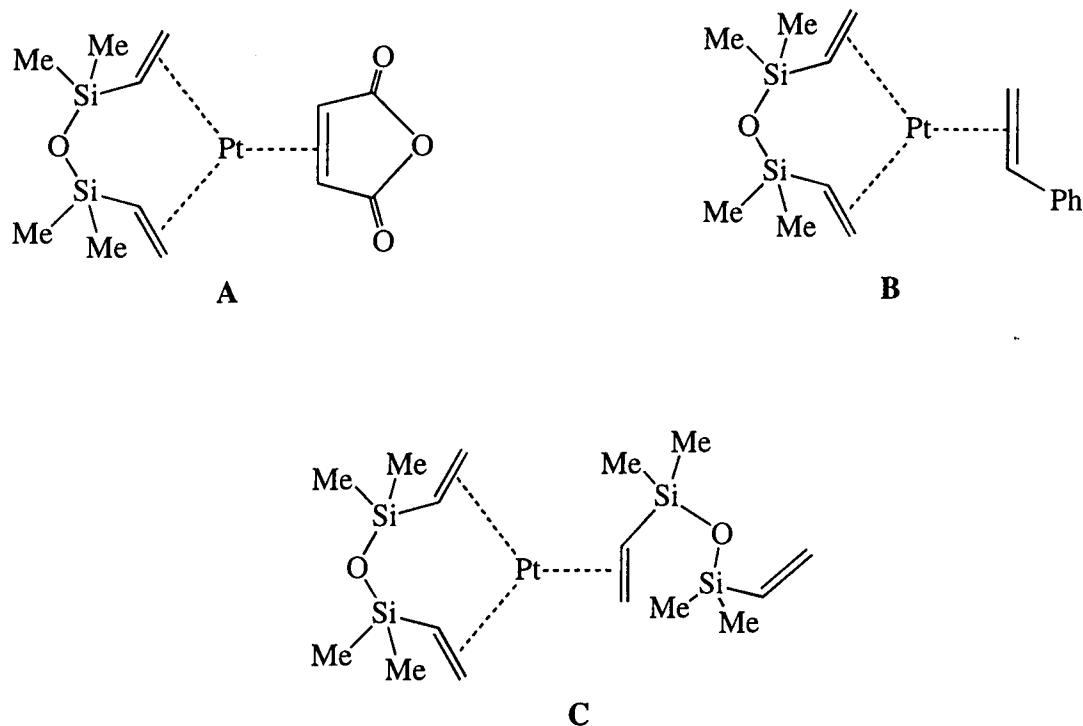


Figure 3.19 A- $\text{Pt}[\eta^4-(\text{CH}_2=\text{CHSiMe}_2)_2\text{O}][\eta^2-\text{CHC}(\text{O})\text{OC}(\text{O})\text{CH}]$, B- $\text{Pt}[\eta^4-(\text{CH}_2=\text{CHSiMe}_2)_2\text{O}](\eta^2\text{-styrene})$ and C- $\text{Pt}[\eta^4-(\text{CH}_2=\text{CHSiMe}_2)_2\text{O}][\eta^2-(\text{CH}_2=\text{CHSiMe}_2)\text{OSiMe}_2\text{CH}=\text{CH}_2]$.

Stoichiometric amounts of phosphines have also been found to displace the bridging $(\text{CH}_2=\text{CHSiMe}_2)_2\text{O}$ ligand in **8** successfully. For example, monodentate phosphine PR_3 ($\text{R} = \text{C}_6\text{H}_4\text{Me}$, Cy) reacts with **8** to form $\text{Pt}[\eta^2-(\text{CH}_2=\text{CHSiMe}_2)_2\text{O}](\text{PR}_3)$.²² Surprisingly, reaction of the bis(phosphine) ligand dppe with **8** resulted in the formation of the binuclear species $\{\text{Pt}[\eta^2-(\text{CH}_2=\text{CHSiMe}_2)_2\text{O}]\}_2(\mu\text{-dppe})$ (Figure 3.20) where the dppe ligand now acts as a bridging ligand instead of chelating as usual.

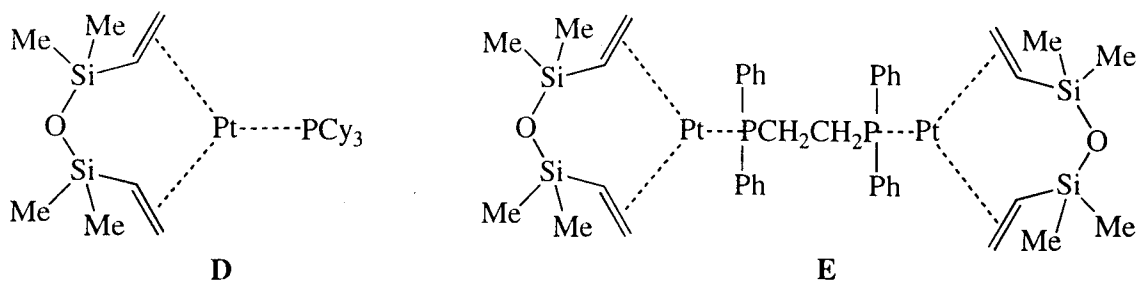


Figure 3.20 D-Pt[η^2 -(CH₂=CHSiMe₂)₂O](PR₃). E-Pt[η^2 -(CH₂=CHSiMe₂)₂O](μ -dppe).

The fact that azodicarbonyl inhibitors displace both the bridging and chelating ligands suggests that azodicarbonyl inhibitors bind more strongly to the platinum centre than the ligands/inhibitors mentioned previously. Supporting evidence from model studies on Pt(PR₃)₂(R'OCNNCOR') (R = Ph, Me; R' = Ph, Me, OEt, OPrⁱ) complexes have shown that the azodicarbonyl ligand forms a Pt–N–N–C–O metallacycle.^{8,23,24} The formation of the more rigid Pt–N–N–C–O metallacycle structure would be favoured over the bridging and chelating structure adopted by the flexible (CH₂=CHSiMe₂)₂O ligand in **8**. The absence of a band maximum at $\lambda \approx 400$ nm in the UV/VIS spectra for **9-11** also indicates a lack of N=N double bond character in the azo inhibitor of **9-11**, which is again a feature of the Pt–N–N–C–O metallacycle.⁹ Transition metal azo complexes with an intact N=N double bond normally have a band maximum at *ca.* 400 nm, *e.g.* for Fe(CO)₄L (L = cyclic azo) the band maximum is observed at around 430–480 nm.²⁵ However, there is still no definitive proof as to whether or not the azodicarbonyl inhibitors in **9-11** adopt the same binding mode as the azo ligands in Pt(PR₃)₂(ROCNNCOR). It is clear, nevertheless, that the carbonyl group on the azo inhibitor plays an important role in binding to the platinum centre in **9-11**, since azo compounds without carbonyl groups adjacent to the azo function were found to be ineffective as inhibitors of **8**.⁵

3.3.3 Effectiveness of EtO₂CNNCO₂Et, PrⁱO₂CNNCO₂Prⁱ and Bu^tO₂CNNCO₂Bu^t as inhibitors of **8**

Heaton found that an excess of azo inhibitor relative to platinum in **8** was required to prevent hydrosilation and that increasing the amount of azo-inhibitors also increases the photolysis time required to initiate hydrosilation.⁵ Hydrosilation was therefore believed to occur only when all the azo inhibitors in the system are destroyed, forming CO₂, N₂ and a radical pair.²⁶

In our present studies, the photoactivation of azo-inhibited **8**, *ie.* **9a**, **10a** and **11a**, in a model hydrosilation system revealed that after 5 min photolysis, the rate of hydrosilation was found to increase with the inhibited catalyst **9a** < **10a** < **11a** (Figure 3.17). Photolysis times of 1–2 minutes on model hydrosilation systems containing

inhibited catalysts **9a** and **10a** did not successfully initiate hydrosilation (Figure 3.15). This indicates that the azo inhibitor $\text{RO}_2\text{CNNCO}_2\text{R}$ binds to platinum with decreasing strength as the substituent R increases in size. The IR spectrum of complex **11** shows the presence of the free azo inhibitor, $\text{Bu}^t\text{O}_2\text{CNNCO}_2\text{Bu}^t$, whereas for complexes **9** and **10**, no free azo inhibitor was detected. This again indicates that the bulky $\text{Bu}^t\text{O}_2\text{CNNCO}_2\text{Bu}^t$ azo inhibitor binds to platinum most weakly. Similar properties are also present in the model complexes of $\text{Pt}(\text{PPh}_3)_2(\text{RO}_2\text{CNNCO}_2\text{R})$ [$\text{R} = \text{Et}$ (**2**), Pr^i (**5**)].⁹ It was found that photolysis of $\text{Pt}(\text{PPh}_3)_2(\text{Pr}^i\text{O}_2\text{CNNCO}_2\text{Pr}^i)$ **5** in a chlorinated solvent yielded *cis*- $\text{Pt}(\text{PPh}_3)_2\text{Cl}_2$ at a faster rate than photolysis of $\text{Pt}(\text{PPh}_3)_2(\text{EtO}_2\text{CNNCO}_2\text{Et})$ **2**, suggesting that azodicarbonyl ligands with smaller R groups bind to platinum stronger.

We must also stress that after photoactivation of azo-inhibited catalysts **9a-11a**, which resulted in hydrosilation in our model system, the reaction mixture still appears to contain some free azo inhibitors since their distinctive yellow colour persists after up to 5 minutes of photolysis. This is contrary to the findings of Heaton who reported that thermolysis or photolysis of complex **8** in chloroform with azo inhibitors 1,1'-(azodicarbonyl)dipiperidine, diethylazodicarboxylate or diisopropylazodicarboxylate initiated hydrosilation only after a loss of yellow colouration, which indicates that all the azo inhibitors are destroyed prior to hydrosilation.⁷ It was suggested that photolysis of **8** with azo inhibitors results in the destruction of both co-ordinated and free azo inhibitors, and as the co-ordinated azo inhibitor is destroyed it is immediately replaced by free azo. The fact that the yellow colouration of free azo persists in our hydrosilation system suggests a different process is operative. One explanation is that platinum colloids are formed during photolysis and are responsible for catalysing hydrosilation and are unaffected by the azo's inhibiting effect. However, Heaton reported that addition of mercury to the reaction did not impede hydrosilation, indicating the active catalyst is homogeneous, and not colloidal in nature.^{7,13,14} At present, it is not clear whether or not the absence of chlorinated solvents in our system plays a major role in the observed differences with Heaton's results.

3.4 CONCLUSIONS

In our present studies on azodicarboxylate-inhibited **8**, *ie.* **9a**, **10a** and **11a**, we have shown that the size of substituent R on the azodicarboxylate inhibitor $\text{RO}_2\text{CNNCO}_2\text{R}$ can influence the effectiveness of inhibition to **8**, and thus effectiveness of binding to platinum. The effect observed was steric in origin only, though electronic alteration to the azo inhibitor is also expected to have a marked influence. For instance, the azodiacyl ligand proved to be both thermally and photochemically more robust in the platinum phosphine complex $\text{Pt}(\text{PPh}_3)_2(\text{ROCNNCOR})$ when compared to the azodicarboxylate ligand in $\text{Pt}(\text{PPh}_3)_2(\text{RO}_2\text{CNNCO}_2\text{R})$.⁹ However, the binding mode of

the azodicarbonyl inhibitors in **9**, **10** and **11** has not been proved unambiguously but it is likely that they adopt the same Pt–N–N–C–O metallacyclic structure found in Pt(PPh₃)₂(ROCNNCOR) (R = Me, Ph, OEt, OPrⁱ).^{8,23,9}

3.5 REFERENCES

- 1 B. Marciniec and J. Gulinski, *J. Organomet. Chem.*, 1993, **446**, 15.
- 2 B. Marciniec, *Comprehensive Handbook on Hydrosilation*, Pergamon, Oxford, 1992.
- 3 I. Ojima, *The Chemistry of Organic Silicon Compounds*, Wiley, 1989, **25**, 1479.
- 4 M. D. Fey and J. E. Wilson, *Handbook of Pressure Sensitive Adhesive Technology*, Silicone Release Coatings, **18**, 384.
- 5 B. D. Karstedt, U.S. Patent 3,775,452, 1973.
- 6 P. B. Hitchcock, M. F. Lappert and N. J. Warhurst, *Angew. Chem. Int. Ed. Engl.*, 1991, **30**, 438.
- 7 S. N. Heaton, *D.Phil Thesis*, University of York, 1995.
- 8 S. D. Ittel and J. A. Ibers, *J. Am. Chem. Soc.*, 1972, **94**, 2290.
- 9 D. Chan, L. Cronin, S. B. Duckett, P. Hupfield and R. N. Perutz, *New J. Chem.*, 1998, 511.
- 10 G. Chandra, P. Y. Lo, P. B. Hitchcock and M. F. Lappert, *Organometallics*, 1987, **6**, 191.
- 11 L. N. Lewis, *J. Am. Chem. Soc.*, 1990, **112**, 5998.
- 12 L. N. Lewis, J. R. Uriarte and N. Lewis, *J. Mol. Cat.*, 1991, **127**, 67.
- 13 G. M. Whitesides, M. Hackett, R. L. Brainard, J. P. M. Lavalleye, A. F. Sowinski, A. N. Izumi, S. S. Moore, D. W. Brown, E. M. Staudt, *Organometallics*, 1985, **4**, 1819.
- 14 D. R. Anton, R. H. Crabtree, *Organometallics*, 1983, **2**, 855.
- 15 L. N. Lewis and N. Lewis, *J. Am. Chem. Soc.*, 1986, **108**, 7228.
- 16 M. F. Lappert and F. P. E. Scott, *J. Organomet. Chem.*, 1995, **502**, 163.
- 17 N. J. W. Warhurst, *D.Phil Thesis*, University of Sussex, 1990.
- 18 A. R. Bassindale, S. S. D. Brown and P. Lo, *Organometallics*, 1994, **13**, 738.
- 19 J. P. Jesson and E. L. Muetteries, *Dynamic Nuclear Magnetic Resonance Spectroscopy*, eds. L. M. Jackman and F. A. Cotton, Academic Press, New York, 1975, 279.
- 20 S. S. D. Brown, R. G. Taylor and P. K. Y. Lo, D.E. Patent 4,204,305 1992.
- 21 P. K. Y. Lo, U.S. Patent 4,774,111 (1987).
- 22 P. B. Hitchcock, M. F. Lappert, C. MacBeath, F. P. E. Scott and N. J. W. Warhurst, *J. Organomet. Chem.*, 1997, **534**, 139.

- 23 S. Cenini, F. Porta, M. Pizzotti and C. Crotti, *J. Chem. Soc. Dalton Trans.*, 1985, 163.
- 24 C. P. Marabella, J. H. Enemark, W. E. Newton and J. W. McDonald, *Inorg. Chem.*, 1982, **21**, 623.
- 25 A. Albin and H. Kisch, *Top. Curr. Chem.*, 1976, **65**, 105.
- 26 P. S. Engel, *Chem. Rev.*, 1980, **80**, 99.

CHAPTER 4

PLATINUM CARBOXYLATE COMPLEXES

4.1 INTRODUCTION

It has been reported by Trogler and co-workers¹ that photolysis of the oxalate complex, $\text{Pt}(\text{PEt}_3)_2(\text{C}_2\text{O}_4)$, results in the irreversible formation of two molecules of carbon dioxide and the reactive 14-electron fragment, $\text{Pt}(\text{PEt}_3)_2$. Although the $\text{Pt}(\text{PEt}_3)_2$ metal fragment was not observed directly, it was trapped with either ethene or diphenylacetylene to form $\text{Pt}(\text{PEt}_3)_2(\eta^2\text{-CH}_2=\text{CH}_2)$ or $\text{Pt}(\text{PEt}_3)_2(\eta^2\text{-PhC}\equiv\text{CPh})$ respectively.¹ Also, the metal fragment formed on photolysis of $\text{Pt}(\text{PEt}_3)_2(\text{C}_2\text{O}_4)$ proved to be an effective hydrosilation catalyst and reacts with HSiEt_3 to yield *cis*- $\text{Pt}(\text{PEt}_3)_2(\text{H})(\text{SiEt}_3)$.^{1,2} Anderson and co-workers reported that photolysis of the $\text{Pt}(\text{dppe})(\text{C}_2\text{O}_4)$ analogue also yields a similar 14-electron fragment.³

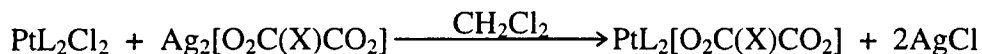
Malonates and phthalates are dicarboxylate compounds with a carbon bridge between the two carboxylate groups, and in some ways resemble oxalates. Like the oxalate ligand, malonate and phthalate ligands can act as chelates in transition metal complexes to form six- and seven-membered rings, co-ordinating to the metal *via* the oxygen atom on the carboxylate group, *e.g.* $\text{Pt}(\text{dppe})(\text{O}_2\text{CCH}_2\text{CO}_2)$ and $\text{Pt}(\text{PPh}_3)_2[\text{O}_2\text{C}(\text{C}_6\text{H}_4)\text{CO}_2]$.⁴ If the malonate and phthalate ligands are proved to be as photosensitive as the oxalate ligand, there is the potential to alter the carbon backbone which connects the carboxylate groups which would allow us to change the properties of the ligand. For example, attaching a long carbon chain would allow the ligand to be more soluble in hydrocarbon solvents. Also, addition of chromophores to the backbone should make the photosensitivity of the ligand tunable.

In this chapter, platinum(II) malonate and phthalate complexes, $\text{Pt}(\text{dppe})(\text{O}_2\text{CCH}_2\text{CO}_2)$ **12**, $\text{Pt}(\text{PMe}_3)_2[\text{O}_2\text{C}(1,2\text{-C}_6\text{H}_4)\text{CO}_2]$ **13** and $\text{Pt}(\text{COD})(\text{O}_2\text{CCH}_2\text{CO}_2)$ **14** are prepared and characterised. The ability of malonate and phthalate to act as photosensitive ligands in complexes **12-14** will be discussed.

4.2 RESULTS

4.2.1 Preparation of platinum(II) carboxylate complexes

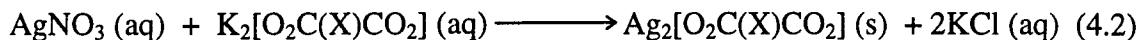
The platinum(II) malonate and phthalate complexes, $\text{PtL}_2[\text{O}_2\text{C}(\text{X})\text{CO}_2]$ [$\text{L}_2 = \text{dppe}$, $\text{X} = \text{CH}_2$ (**12**); $\text{L} = \text{PMe}_3$, $\text{X} = 1,2\text{-C}_6\text{H}_4$ (**13**); $\text{L}_2 = \text{COD}$, $\text{X} = \text{CH}_2$ (**14**)], were prepared using the procedure described by Anderson and co-workers for the synthesis of **12**.⁴ This involved the reaction of *cis*-platinum(II) dichloride, *cis*- PtL_2Cl_2 ($\text{L}_2 = \text{dppe}$, COD ; $\text{L} = \text{PMe}_3$), with an excess of the silver carboxylate salt, $\text{Ag}_2[\text{O}_2\text{C}(\text{X})\text{CO}_2]$, suspended in CH_2Cl_2 (Equation 4.1). The silver carboxylate salt was easily prepared from precipitation by dissolving $\text{K}_2[\text{O}_2\text{C}(\text{X})\text{CO}_2]$ and AgNO_3 in water (Equation 4.2).⁵



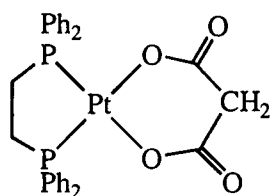
$\text{L}_2 = \text{dppe}$, $\text{X} = \text{CH}_2$ (12)

$\text{L} = \text{PMe}_3$, $\text{X} = 1,2\text{-C}_6\text{H}_4$ (13)

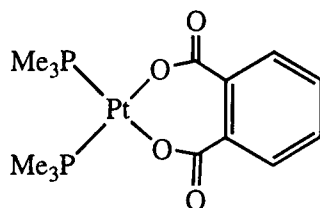
$\text{L}_2 = \text{COD}$, $\text{X} = \text{CH}_2$ (14) (4.1)



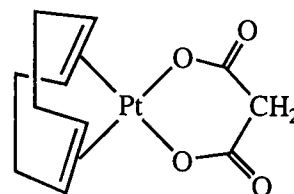
All synthetic procedures were carried out in the absence of light to prevent possible photo-degradation of the product. The resultant platinum(II) carboxylate complexes $\text{Pt}(\text{dppe})(\text{O}_2\text{CCH}_2\text{CO}_2)$ **12**, $\text{Pt}(\text{PMe}_3)_2[\text{O}_2\text{C}(1,2\text{-C}_6\text{H}_4)\text{CO}_2]$ **13** and $\text{Pt}(\text{COD})(\text{O}_2\text{C-CH}_2\text{CO}_2)$ **14** were obtained as white powders, in moderate to high yields (60-80 %). All of the platinum(II) carboxylate complexes were found to be sparingly soluble in acetonitrile and chlorinated solvents and were insoluble in THF or benzene. Attempts to prepare $\text{Pt}(\text{dppe})[\text{O}_2\text{C}(1,2\text{-C}_6\text{H}_4)\text{CO}_2]$ using the above procedure yielded a black/brown solution which is indicative of metallic platinum formation.⁶



(12)



(13)



(14)

4.2.2 NMR Characterisation of platinum(II) carboxylate complexes

The $^{31}\text{P} \{^1\text{H}\}$ NMR spectrum of **12** in CD_3CN displays a singlet resonance at δ 32.7, with ^{195}Pt satellites [$^1J(\text{PtP}) = 3665$ Hz], indicating that both the phosphorus nuclei are equivalent. This is in fairly good agreement with the values reported by Anderson and co-workers for the same compound [$\delta_{\text{P}} 29.1$, $^1J(\text{PtP}) = 3665$ in CDCl_3].⁴ In the ^1H NMR spectrum of **12** we can observe a singlet resonance at δ 3.34 which is assigned to the methylene group on the malonate ligand. The doublet at δ 2.58 and the multiplets at δ 7.60-8.00 are assigned to the $-\text{CH}_2\text{CH}_2-$ and Ph groups respectively, which are found on the dppe ligand (Figure 4.1). In the $^{13}\text{C} \{^1\text{H}\}$ NMR spectrum of **12** the signal for the carboxylate carbon atoms can be found at δ 174.0 (Figure 4.2).

Complex **13** contains a singlet phosphorus resonance at δ -27.4 in its $^{31}\text{P} \{^1\text{H}\}$ NMR spectrum which is accompanied by ^{195}Pt satellites [$^1J(\text{PtP}) = 3564$ Hz] (Table 4.1). The ^1H NMR spectrum of **13** shows a symmetrical set of multiplets in the aromatic region, δ 7.35-7.50, which is indicative of a AA'BB' spin system⁷ and is assigned to the

protons on the phenylene backbone of the phthalate ligand (Figures 4.3 and 4.4). A doublet resonance with ^{195}Pt satellites at δ 1.51 is assigned to the methyl protons on the PMe_3 ligand. On closer inspection of the resonance at δ 1.51 we find that it is a filled in doublet, belonging to an $[\text{A}_n\text{X}]_2$ pattern.⁸ This is typically found for mutually *cis*-phosphine complexes where $^2J(\text{PP}')$ is large and the two phosphines are chemically equivalent.⁹ According to theoretical calculations,¹⁰ a 1:2:1 triplet will be observed when $|J(\text{AX}) - J(\text{AX}')|^2 < 2J(\text{XX}')\Delta(\nu/2)$, where $\Delta(\nu/2)$ is the resolving power of the spectrometer. A 1:1 doublet will be observed when $|J(\text{AX}) - J(\text{AX}')|^2 > 4J(\text{XX}')\Delta(\nu/2)$. Intermediate coupling is said to give filled in doublets, when neither of the two previous conditions are meant. In the previous case of complex **12**, the ^1H NMR spectrum only showed a doublet resonance for CH_2 in dppe, which indicates that $^2J(\text{PP}')$ is small (0-15 Hz).^{11,12}

The ^{13}C $\{^1\text{H}\}$ NMR spectrum of **13** also shows the methyl carbons on the PMe_3 giving rise to the multiplets observed at δ 14.6, which is described as an AX_2 spin system⁹ (Table 4.3 and Figure 4.5). For the ^{13}C $\{^1\text{H}\}$ spectrum of **12**, only a doublet resonance for CH_2 in dppe was observed (Table 4.3). This indicates that $^2J(\text{PP}')$ is very small and that $^3J(\text{P}'\text{C})$ is less than the resolving power of the spectrometer.⁹

A summary of NMR data for complexes **12-14** can be found in Tables 4.1-4.3.

Compound	δ (J / Hz)
Pt(dppe)(O ₂ CCH ₂ CO ₂) 12 ^a	2.58 [4H, d, $\underline{\text{CH}}_2$, $J(\text{PH}) = 17.3$] 3.34 (2H, s, $\underline{\text{CH}}_2$) 7.00-8.00 (10H, m, Ph)
Pt(PMe ₃) ₂ [O ₂ C(1,2-C ₆ H ₄)CO ₂] 13 ^a	1.51 [18H, d ^b , $\underline{\text{CH}}_3$, $J(\text{PH}) = 11.7$, $J(\text{PtH}) = 36.2$] 7.35-7.50 (4H, m, Ph)
Pt(COD)(O ₂ CCH ₂ CO ₂) 14 ^c	2.30, 2.73 [8H, br. m, CH_2CH_2 (COD)] 3.37 (2H, s, $\underline{\text{CH}}_2$) 5.39 [4H, br. s, $\underline{\text{CH}}=\underline{\text{CH}}$ (COD), $J(\text{PtH}) = 66.5$]

Table 4.1 ^1H (300.13 MHz, 295 K) NMR spectroscopic data of complexes **12-14**. Couplings to Pt refer to satellites from ^{195}Pt . *a* In CD_3CN . *b* filled in doublet. *c* In CD_2Cl_2 .

Compound	δ (J / Hz)
Pt(dppe)(O ₂ CCH ₂ CO ₂) 12	32.7 [s, $J(\text{PtP}) = 3665$]
Pt(PMe ₃) ₂ [O ₂ C(1,2-C ₆ H ₄)CO ₂] 13	-27.4 [s, $J(\text{PtP}) = 3564$]

Table 4.2 ³¹P {¹H} (121.49 MHz, 295 K) NMR spectroscopic data of complexes **12** and **13** in CD₃CN. Couplings to Pt refer to satellites from ¹⁹⁵Pt.

Compound	δ (J / Hz)
Pt(dppe)(O ₂ CCH ₂ CO ₂) 12	27.5 [d, P $\underline{\text{C}}\text{H}_2$, $J(\text{PC}) = 51$] 51.1 (s, $\underline{\text{C}}\text{H}_2$) 126.4-133.7 (Ph) 174.0 (s, $\underline{\text{C}}\text{O}$)
Pt(PMe ₃) ₂ [O ₂ C(1,2-C ₆ H ₄)CO ₂] 13	14.6 (m, P $\underline{\text{C}}\text{H}_3$) 127.4-139.2 (Ph) 175.3 (s, $\underline{\text{C}}\text{O}$)

Table 4.3 ¹³C {¹H} (75.47 MHz, 295 K) NMR spectroscopic data for complexes **12** and **13** in CD₂Cl₂.

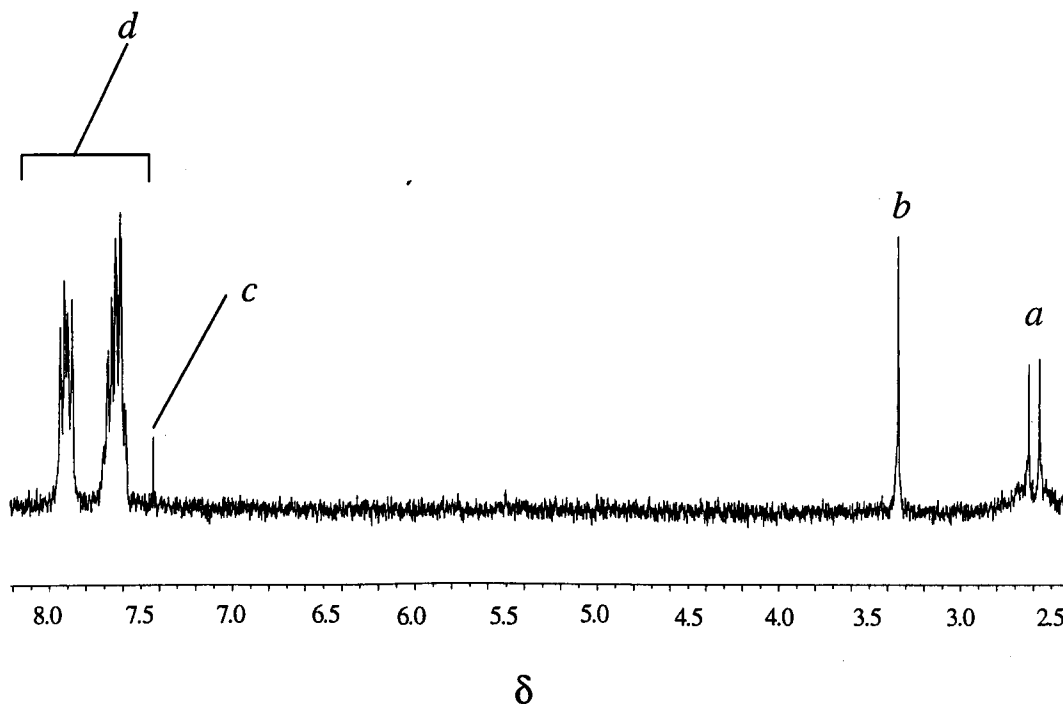


Figure 4.1 ¹H (300.13 MHz, 295 K) NMR spectrum of **12** in CD₃CN. *a* $\underline{\text{C}}\text{H}_2$ (dppe). *b* $\underline{\text{C}}\text{H}_2$ (malonate). *c* CHCl₃. *d* Ph (dppe).

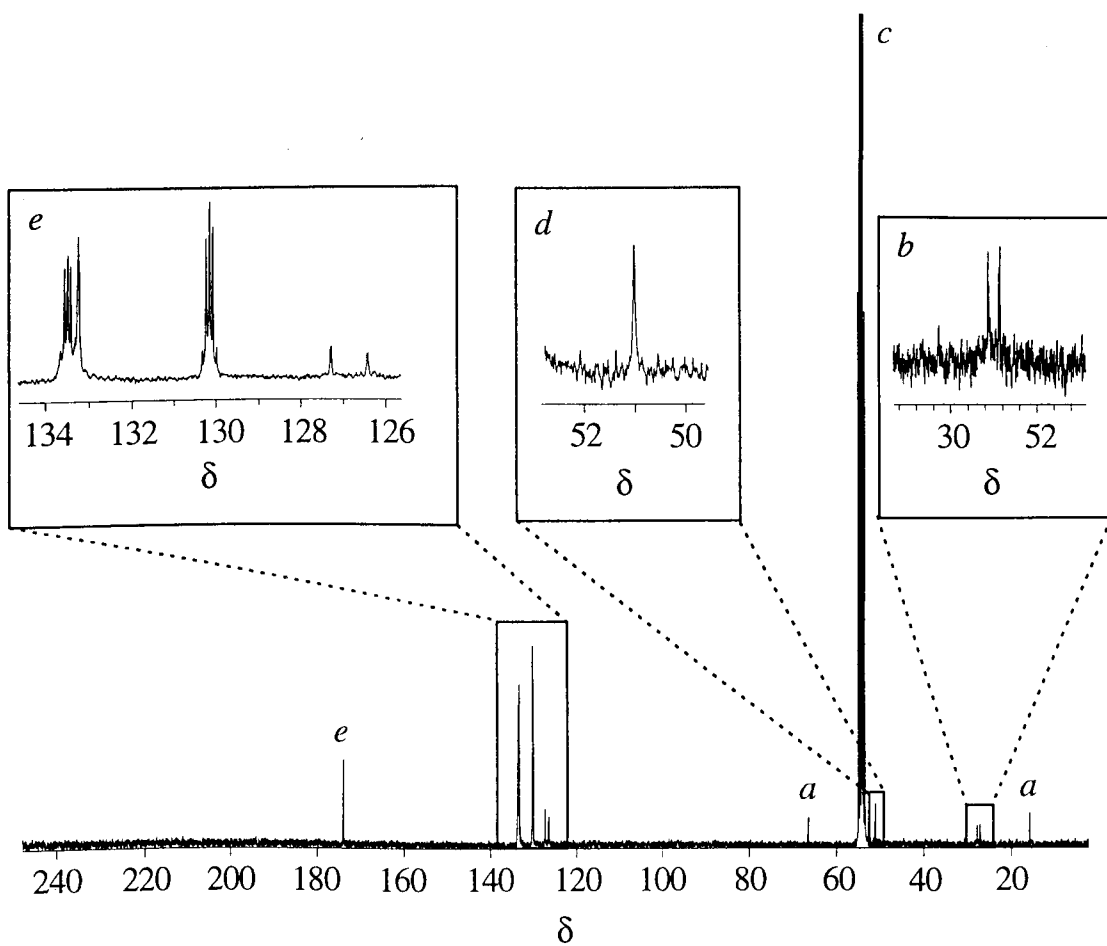


Figure 4.2 ^{13}C $\{^1\text{H}\}$ (75.47 MHz, 295 K) NMR spectrum of **12** in CD_2Cl_2 . *a* ether. *b* PCH_2 . *c* CD_2Cl_2 . *d* $\text{O}_2\text{CCH}_2\text{CO}_2$. *e* Ph, *f* $\text{O}_2\text{CCH}_2\text{CO}_2$.

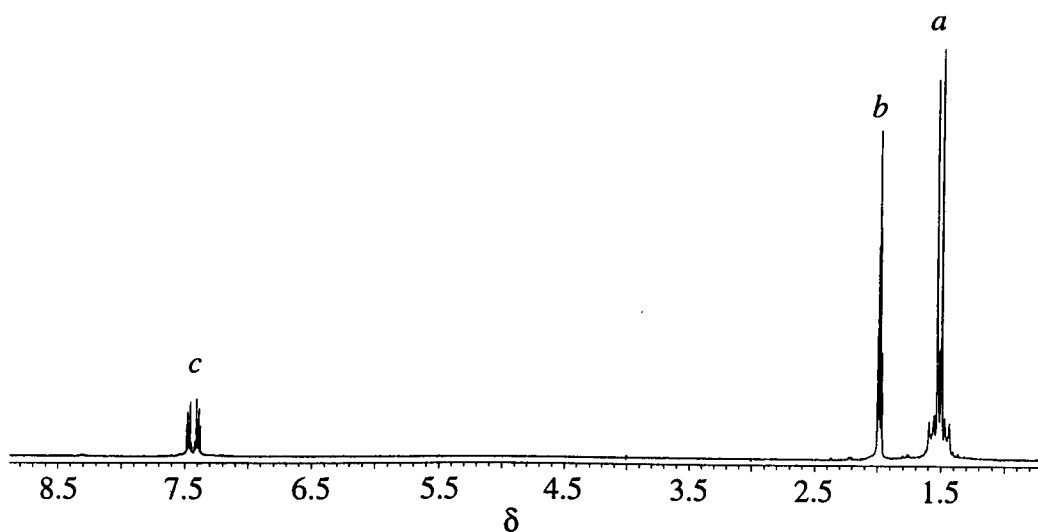


Figure 4.3 ^1H (300.13 MHz, 295 K) NMR spectrum of **13** in CD_3CN . *a.* PCH_3 with ^{195}Pt satellites. *b.* acetonitrile. *c.* $\text{O}_2\text{C}(1,2\text{-C}_6\text{H}_4)\text{CO}_2$.

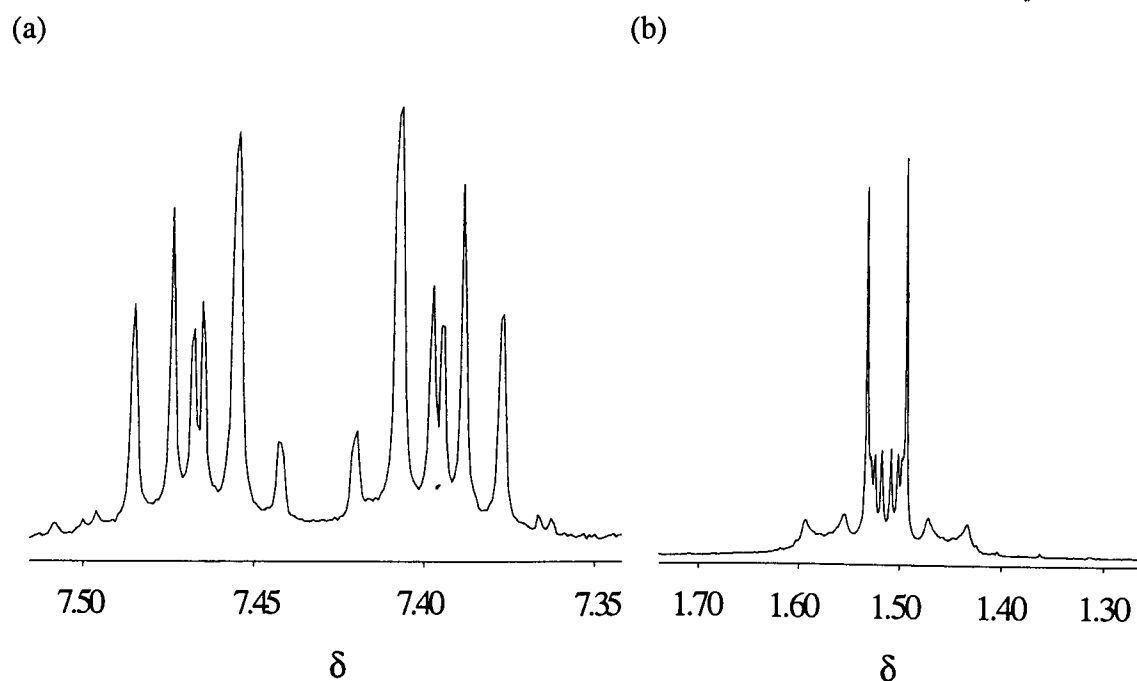


Figure 4.4 ^1H (300.13 MHz, 295 K) NMR spectrum of **13** in CD_3CN , showing the expanded regions of (a) $\text{O}_2\text{C}(1,2\text{-C}_6\text{H}_4)\text{CO}_2$ and (b) PCH_3 with ^{195}Pt satellites.

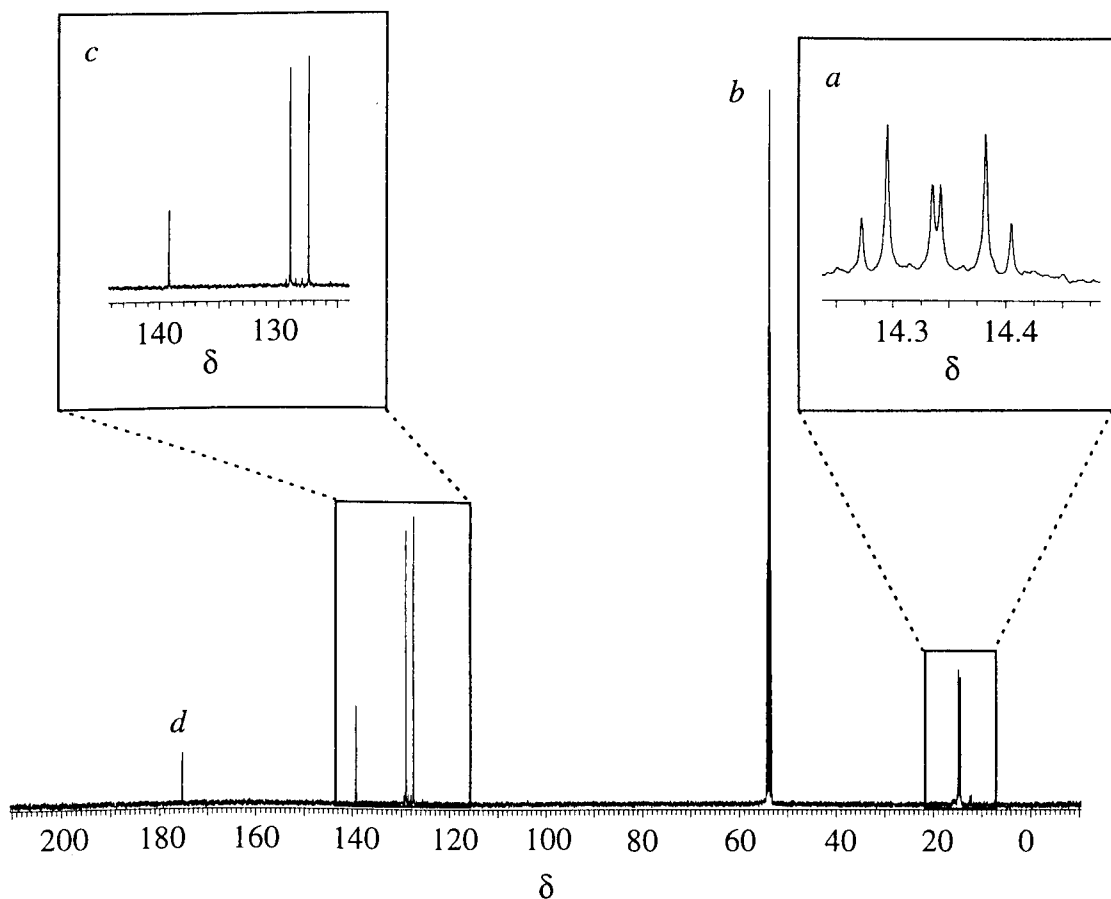


Figure 4.5 ^{13}C $\{^1\text{H}\}$ (75.47 MHz, 295 K) NMR spectrum of **13** in CD_2Cl_2 . *a* PCH_3 . *b* CD_2Cl_2 . *c* $\text{O}_2\text{C}(1,2\text{-C}_6\text{H}_4)\text{CO}_2$. *d* $\text{O}_2\text{C}(1,2\text{-C}_6\text{H}_4)\text{CO}_2$.

4.2.3 IR characterisation of platinum(II) carboxylate complexes

The IR spectra of **12** and **14** show C=O stretching bands at *ca.* 1650 cm^{-1} ; they are broad in appearance and their shapes suggest that they are composites of several overlapping bands (Table 4.4 and Figure 4.6). The weaker C–O stretching bands are located at *ca.* 1350 cm^{-1} . The C=O and C–O stretching bands of complexes **12** and **14** are slightly lower in energy than those of platinum(II) bis(phosphine) oxalate complexes, *e.g.* for $\text{Pt}(\text{PMe}_3)_2(\text{C}_2\text{O}_4)$,¹ $\nu(\text{C}=\text{O})$ is 1703 cm^{-1} and $\nu(\text{C}-\text{O})$ is 1363 cm^{-1} .

Compound	$\nu(\text{C}=\text{O}) / \text{cm}^{-1}$	$\nu(\text{C}-\text{O}) / \text{cm}^{-1}$
Pt(dppe)(O ₂ CCH ₂ CO ₂) 12 ^a	1649 1650 ^b	1354 1357 ^b
Pt(COD) ₂ (O ₂ CCH ₂ CO ₂) 14 ^c	1675	1340
Pt(PMe ₃) ₂ (C ₂ O ₄) ^d	1703	1363
Pt(PPh ₃) ₂ (C ₂ O ₄) ^e	1710	1350
Pt(dppe)(C ₂ O ₄) ^f	1705	1356
Pt(PPh ₃) ₂ [O ₂ C(1,2-C ₆ H ₄)CO ₂] ^g	1690	-
Pt(PPh ₃) ₂ (O ₂ CCH ₂ CO ₂) ^g	1770	-
Pt(dppm)(O ₂ CCH ₂ CO ₂) ^b	1640	1357

Table 4.4 IR spectroscopic data for platinum(II) carboxylate complexes. *a* In KBr pellet *b* From ref. 4, in KBr pellet. *c* In CH₂Cl₂. *d* From ref. 1, in CH₂Cl₂. *e* From ref. 13, in nujol. *f* From ref. 3, in KBr pellet. *g* From ref. 14, in KBr pellet.

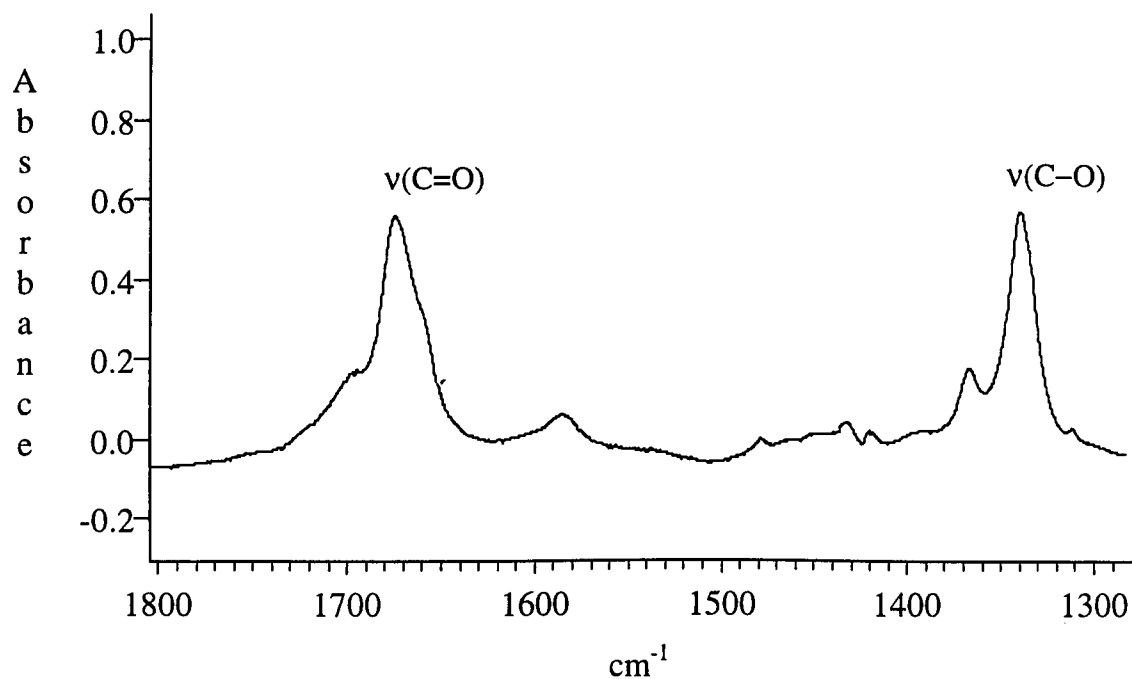


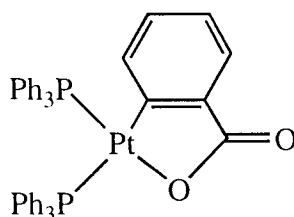
Figure 4.6 IR spectrum for complex **14** in CH₂Cl₂ showing the $\nu(\text{C}=\text{O})$ and $\nu(\text{C}-\text{O})$ stretching bands of the malonate ligand.

4.2.4 Photolysis of platinum(II) dicarboxylate complexes

Photolysis of complex **12** in CD₃CN in the presence of either diphenylacetylene or ethene (1 atm) resulted in the appearance of an unidentified singlet phosphorus resonance, assigned as product **A4**, at δ_p 47.6 [$J(\text{PtP}) = 3625$ Hz]. Despite prolonged photolysis, up to 4 days, conversion of **12** to the unidentified product **A4** remained very low. The singlet phosphorus resonance of product **A4** does not correspond to the formation of either Pt(dppe)(η^2 -CH₂=CH₂) [δ_p 53.5, $J(\text{PtP}) = 3278$ Hz] or Pt(dppe)(η^2 -PhC≡CPh) [δ_p 48.7, $J(\text{PtP}) = 3125$ Hz].³ This suggests that the 14-electron fragment Pt(dppe) was not formed on photolysis of **12**.

Complex **13** was similarly photolysed in CD₃CN in the presence of either diphenylacetylene or ethene with the expectation of detecting the formation of the Pt(PMe₃)₂ metal fragment. Like with complex **12**, formation of Pt(PMe₃)₂(η^2 -CH₂=CH₂)¹⁵ and Pt(PMe₃)₂(η^2 -PhC≡CPh)¹⁵ was not detected. However, prolonged photolysis did yield a small amount of product **B4**, which displays two doublet resonances in the ³¹P {¹H} NMR spectrum, both with ¹⁹⁵Pt satellites, at δ_p -11.2 [$J(\text{PtP}) = 1849$ Hz] and δ_p -29.7 [$J(\text{PtP}) = 3712$ Hz], with $J(\text{PP}) = 19$ Hz. A second product **C4** was also detected and has a singlet resonance at δ_p -28.2 with ¹⁹⁵Pt satellites [$J(\text{PtP}) = 3960$ Hz]. Hence, the ³¹P NMR data indicate that **B4** contains two mutually *cis* phosphine ligands which are inequivalent and **C4** contains a single phosphorus environment. The presence of products **B4** and **C4** is also confirmed by ¹H NMR spectroscopy. The methyl groups on the two inequivalent phosphines of **B4** can be seen as two doublet resonances at δ_H 1.78 [$^2J(\text{PH}) = 11.2$ Hz] and δ_H 1.86 [$^2J(\text{PH}) = 11.0$ Hz], with overlapping ¹⁹⁵Pt satellites which were not clearly defined. The methyl groups on the phosphines of **C4** can be located at δ_H 1.62 as a doublet [$^2J(\text{PH}) = 9.8$ Hz] with ¹⁹⁵Pt satellites which are obscured by the methyl signals of unreacted **13**.

Product **B4** is likely to have a similar structure to the compound formed on photolysis of Pt(PPh₃)₂[O₂C(1,2-C₆H₄)CO₂].¹⁴ It has been reported that thermolysis or photolysis of Pt(PPh₃)₂[O₂C(1,2-C₆H₄)CO₂] resulted in the loss of one molecule of carbon dioxide from the phthalate ligand, yielding the five-membered Pt-O-C-C-C metallacycle Pt(PPh₃)₂[O₂C(1,2-C₆H₄)] [δ_p 15.5, $J(\text{PtP}^O) = 4128$ Hz; δ_p 27.8, $J(\text{PtP}^C) = 1977$ Hz; $J(\text{PP}) = 15$ Hz].¹⁴



From reference 14.

From the data in the $^{31}\text{P} \{^1\text{H}\}$ NMR spectrum of **B4**, we envisage that **B4** contains the same Pt–O–C–C–C metallacycle. The doublet resonance at $\delta_{\text{P}} -11.2$ has a $J(\text{PtP})$ value of 1849 Hz which is consistent with a phosphorus atom *trans* to an aryl ligand and the doublet resonance at $\delta_{\text{P}} -29.7$ has a $J(\text{PtP})$ value of 3712 Hz which is consistent with a phosphorus *trans* to an oxygen ligand.¹⁴ The identity of **C4** remains unclear.

Photolysis of **12-14** in chlorinated solvents resulted in the formation of the corresponding platinum(II) dichloride complexes, *ie.* $\text{Pt}(\text{dppe})\text{Cl}_2$, *cis*- $\text{Pt}(\text{PMe}_3)_2\text{Cl}_2$ and $\text{Pt}(\text{COD})\text{Cl}_2$.

4.3 DISCUSSIONS

4.3.1 Preparation of platinum(II) carboxylate complexes

Platinum(II) carboxylate complexes were easily prepared from the reaction between platinum(II) chloride and a silver carboxylate salt, the driving force of this reaction being the formation of the highly insoluble silver chloride compound. An alternative method for preparing these type of complexes uses the platinum(0) bis(phosphine) dioxygen complex, $\text{PtP}_2(\eta^2\text{-O}_2)$ (P = phosphine), and the dicarboxylic acid, $\text{X}(\text{CO}_2\text{H})_2$ (X = carbon backbone), which yields the corresponding platinum(II) bis(phosphine) dicarboxylate complex and hydrogen peroxide.¹⁴

4.3.2 Reactivity of platinum(II) carboxylate complexes

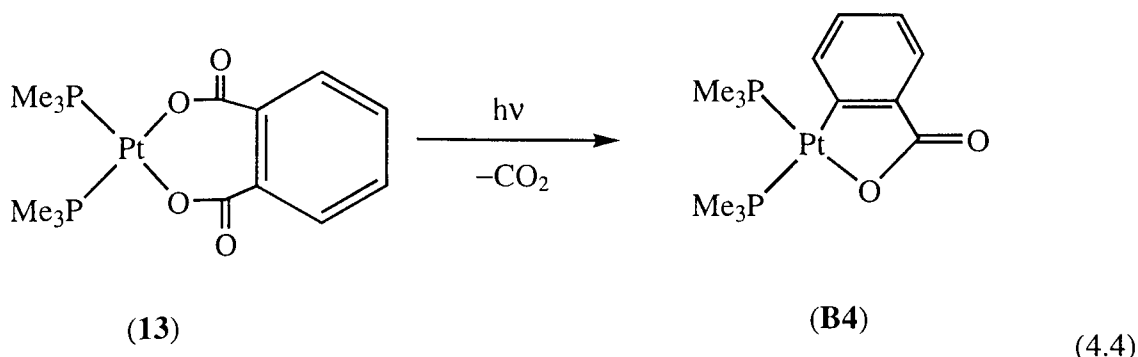
Platinum(II) malonate and phthalate complexes of the type $\text{PtL}_2(\text{O}_2\text{CXCO}_2)$ (L = PMe_3 , $\text{L}_2 = \text{dppe}$, X = carbon backbone) were found to display different photochemical properties to their platinum(II) oxalate analogues, *e.g.* $\text{Pt}(\text{PEt}_3)_2(\text{C}_2\text{O}_4)$.¹ Our observations indicate that platinum(II) malonate and phthalate complexes do not yield the PtL_2 14-electron metal fragment upon photolysis. This is almost certainly due to the presence of the carbon backbone which connects the two carboxylate groups attached to the metal.

The photochemical formation of $\text{Pt}(\text{PEt}_3)_2$ from $\text{Pt}(\text{PEt}_3)_2(\text{C}_2\text{O}_4)$ is believed to occur *via* transfer of two electrons from the platinum centre to the oxalate ligand, either simultaneously or in rapid succession.¹ The oxalate dianion thus formed irreversibly fragments to two molecules of carbon dioxide, leaving behind the $\text{Pt}(\text{PEt}_3)_2$ metal moiety (Equation 4.3)

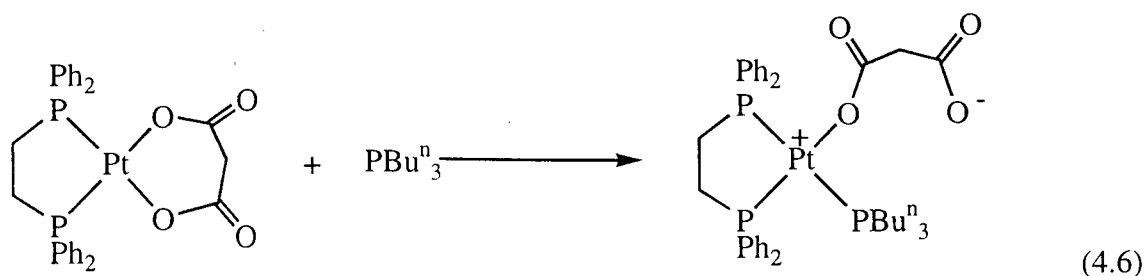
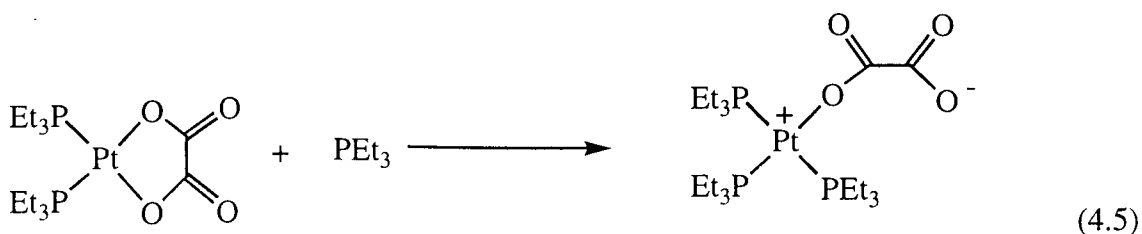


This mechanism is unlikely to occur for platinum(II) malonate and phthalate complexes because of the presence of the carbon backbone connecting the two carboxylate groups, so that formation of two molecules of carbon dioxide is now unfavourable.

Based on our NMR data, and those reported by Scherer *et al.*,¹⁴ we believe that **B4**, formed on photolysis of **13**, contains a five-membered Pt–C–C–O metallacyclic structure (Equation 4.4).

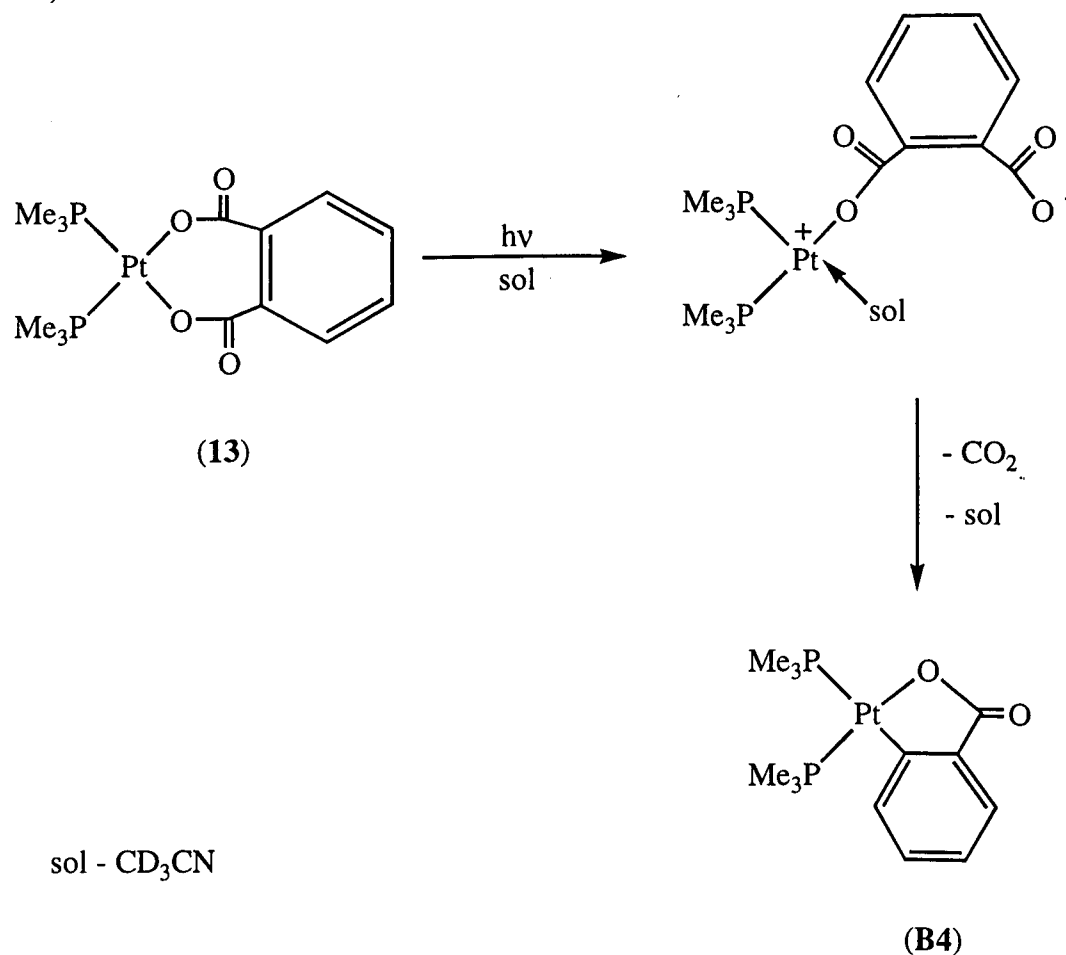


Possible mechanisms for this photoprocess could be better understood by examining the reactivity of complexes with chelating dicarboxylate ligands. It has been reported that one end of the dicarboxylate ligand in platinum(II) oxalate and malonate complexes can be displaced in the presence of phosphine to yield non-chelating platinum(II) oxalate and malonate complexes (Equations 4.5 and 4.6).^{1,4}



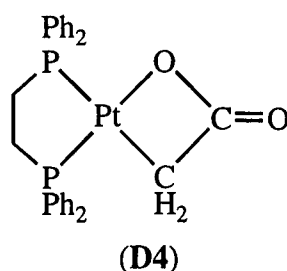
Anderson and co-workers reported that the co-ordinated malonate ligand is more labile than the oxalate ligand, and suggested that this could be due to the greater ionic character present in the Pt–O bond in the malonate complexes and that five-membered chelate rings, or metallacycles, *e.g.* oxalate complexes, are thermodynamically more stable than six-membered chelate rings, *e.g.* malonate complexes.⁴ It therefore seems

likely that the phthalate ligand in **13** also possess these properties. Hence, one possible mechanism for the formation of **B4** from photolysis **13** would initially involve the displacement of one carboxylate group by a solvent molecule (CD_3CN). Further photolysis would yield a molecule of carbon dioxide from the dangling end of the phthalate ligand and the formation of a stable five-membered metallacycle (Scheme 4.1).



Scheme 4.1 Possible mechanism for the formation of **B4** on photolysis of **13** in CD_3CN .

It would be plausible that **12** should also eject one molecule of carbon dioxide to form a metallacycle which is similar to the process suggested for the formation of **B4** from **13**, but this was not observed. One reason could be that ejection of a molecule of carbon dioxide on photolysis of **12** would yield a strained four-membered metallacycle, **D4**, which is expected to be unfavourable.



The photo-products **A4**, formed from photolysis of **12**, and **C4**, the second product formed from photolysis of **13**, both contain equivalent phosphorus atoms as shown by their ^{31}P { ^1H } NMR spectra. The possibility of **A4** and **C4** being platinum(II) carbonate complexes, $\text{PtL}_2(\text{CO}_3)$ (L = phosphine) was ruled out since the ^{31}P chemical shifts and $J(\text{PtP})$ values did not correspond to the values quoted in literature.^{3,16} The identities of photo-products **A4** and **C4** remain unclear.

4.4 CONCLUSIONS

In this chapter, the photochemistry of platinum(II) malonate and phthalate complexes were found to be different from those of platinum(II) oxalate complexes.^{1,2,3} Formation of the 14-electron platinum bis(phosphine) fragment was not observed on photolysis of the platinum(II) malonate and phthalate complexes prepared. This was thought to be due to the presence of the carbon backbone which connects the two carboxylate groups. A mechanism for the photochemical formation of a five-membered metallacycle **B4** formed from the photolysis of the seven-membered metallacycle **13** is proposed which involves the unhinging of the chelating phthalate ligand initially to form a monodentate phthalate complex. This was largely based on reports by Anderson and co-workers who suggested that the chelating malonate ligand is more labile than the oxalate ligand, and is easily converted to a monodentate ligand by displacement with an incoming phosphine ligand.⁴

The low solubilities and photo-sensitivities of the platinum(II) malonate and phthalate complexes described in this chapter indicate that malonate and phthalate ligands are ultimately poor ligands to use for initiating photochemical processes.

4.5 REFERENCES

- 1 R. S. Paonessa, A. L. Prignano and W. C. Trogler, *Organometallics*, 1985, **4**, 647.
- 2 A. L. Prignano and W. C. Trogler, *J. Am. Chem. Soc.*, 1987, **109**, 3586.
- 3 G. K. Anderson, G. J. Lumetta and J. W. Siria, *J. Organomet. Chem.*, 1992, **434**, 253.
- 4 G. K. Anderson and G. J. Lumetta, *Inorg. Chem.*, 1987, **26**, 1291.
- 5 A. K. Galway, P. J. Herley and M. A. Mohamed, *J. Chem. Soc., Faraday Trans. 1*, 1988, **84**, 729.
- 6 P. B. Hitchcock, M. F. Lappert and N. J. Warhurst, *Angew. Chem. Int. Ed. Engl.*, 1991, **30**, 438.
- 7 H. Günther, *NMR Spectroscopy: Basic Principles, Concepts and Applications in Chemistry*, 2nd Ed., Wiley, Chichester, 1995.

- 8 J. A. Rahn, L. Baltusis and J. H. Nelson, *Inorg. Chem.*, 1990, **29**, 750.
- 9 D. A. Redfield, L. W. Cary and J. H. Nelson, *Inorg. Chem.*, 1975, **14**, 50.
- 10 R. K. Harris, *Can. J. Chem.*, 1964, **42**, 2275.
- 11 J. G. Verkade, *Coord. Chem. Rev.*, 1973, **9**, 1.
- 12 F. B. Oglivie, J. M. Jenkins and J. G. Verkade, *J. Am. Chem. Soc.*, 1970, **92**, 1916.
- 13 A. W. Addison, R. D. Gillard, P. S. Sheridan and L. R. H. Sheridan, *J. Chem. Soc., Dalton Trans.*, 1974, 709.
- 14 O. J. Scherer, K. Hussong and G. Wolmershäuser, *J. Organomet. Chem.*, 1985, **289**, 215.
- 15 D. L. Packett, A. Syed and W. C. Trogler, *Organometallics*, 1988, **7**, 159.
- 16 T. K. Miyamoto, Y. Suzuki and H. Ichida, *Bull. Chem. Soc. Jpn.*, 1992, **65**, 3386.

CHAPTER 5

PLATINUM SILYL HYDRIDE COMPLEXES

5.1 INTRODUCTION

5.1.1 Transition Metal Silyl Hydride complexes

There is tremendous interest in the chemistry of silyl and silyl hydride transition metal complexes.¹ This is because they play an important role in industry, representing key species in catalytic processes, namely hydrosilation and, of more recent interest, competitive dehydrogenative silation.^{2,3}

Originally proposed by Chalk and Harrod⁴, the initial stage of the transition metal catalysed hydrosilation reaction involves the formation of a metal silyl hydride. Harrod's work on transition metal catalysed polysilane formation also involves the formation of a metal silyl hydride.⁵ Platinum silyl hydride complexes are therefore of special interest since platinum is the metal of choice for hydrosilation catalysts.^{6,7}

5.1.2 Dynamic Processes in Platinum Metal Silyl Hydride Complexes

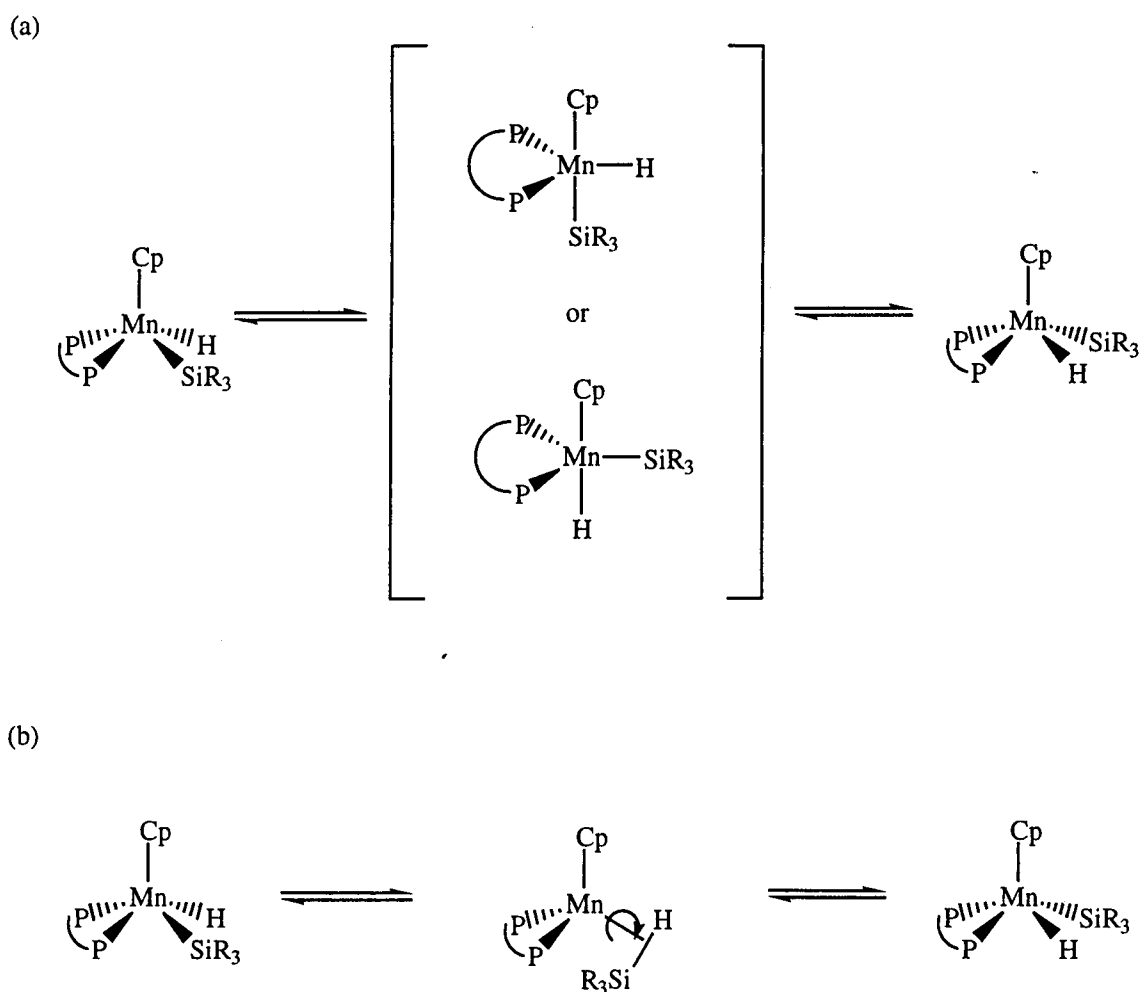
Complexes of the type *cis*-Pt(PR'₃)₂(H)(SiR₃) exhibit two forms of dynamic exchange in solution: (a) mutual phosphine exchange, where the PR'₃ positions interchange intramolecularly whilst retaining phosphorus-proton spin correlation (this can also be viewed as the interchange of position between the silyl and hydride ligand). (b) reversible reductive elimination, oxidative addition of the silane.⁸ An example of the mutual phosphine exchange process in a platinum silyl hydride complex was noted by Pidcock *et al.* for *cis*-Pt(PPh₃)₂(H)(SiPh₃) from the variable temperature ¹H NMR spectra.⁹ The corresponding ³¹P {¹H} NMR spectra revealed behaviour indicative of phosphine dissociation rather than reversible addition-elimination of the silane ligand.

Clark and Hampden-Smith later found that the analogous compound *cis*-Pt(PCy₃)₂(H)(SiPh₃)^{10,11} undergoes both intramolecular phosphine interchange and reversible addition-elimination of silane. Clark and Hampden-Smith argued that the absence of the reversible addition-elimination equilibrium of the silane ligand in the PPh₃ analogue was due to the lack of inter-ligand repulsion found in the PCy₃ analogue. They have also proposed that a platinum species with η²-silane is the intermediate responsible for the intramolecular phosphine exchange. The η²-bound silane ligand in this intermediate facilitates scrambling of the phosphines by rotation about the Si-H bond.

Silane exchange has also been observed for [CpPt(SiMe₂OSiMe₃)₂H]⁷ and [(dppe)Pt(SiMe₃)₂]¹² with the disilane HSiMe₂OSiMe₂H to form the corresponding chelating disilyl complex.

Similar mutual phosphine exchange processes have been seen for other transition metal silyl hydride complexes. For example, Sun *et al.* found that the manganese

complex $\text{CpMn}(\text{P}_2)(\text{H})(\text{SiPh}_n\text{H}_{3-n})$ [$\text{P}_2 = \text{dmpe, dmpp, dmpm}$] undergoes positional exchange of the silyl and hydride ligand, which also corresponds to mutual phosphine exchange.¹³ This complex was described as having a four-legged piano stool geometry⁸ with the silyl and hydride ligand lying *cis* to each other. Two possible mechanisms were suggested to account for this exchange process. The first mechanism involves an η^2 -silane intermediate, which is similar to the intermediate proposed by Clark and Hampden-Smith for the mutual phosphine exchange process in *cis*- $\text{Pt}(\text{PCy}_3)_2(\text{H})(\text{SiPCy}_3)$.¹⁰ The second, and according to Sun *et al.* the more likely mechanism, involves the pseudorotation of the four ligands. This involves forming a trigonal bipyramidal intermediate with the cyclopentadienyl ring in the axial position and the chelating phosphine ligand in the equatorial plane. The silyl and the hydride ligand can be located in either of the remaining axial positions (Scheme 5.1).



Scheme 5.1 Proposed mechanisms for phosphine exchange in $\text{CpMn}(\text{P}_2)(\text{H})(\text{SiR}_3)$ ($\text{R} = \text{Ph}$ or H ; $\text{P}_2 = \text{dmpe, dmpp, dmpm}$). (a) Involves the formation of a trigonal bipyramidal complex. (b) Involves the formation of an η^2 -silane complex.

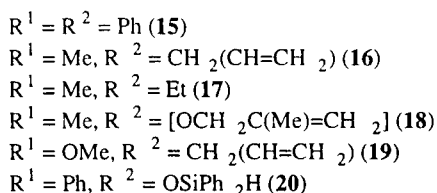
In this chapter the platinum silyl hydride system, *cis*-Pt(PCy₃)₂(H)(SiR₃), studied originally by Clark and Hampden-Smith, is examined in more detail. Thermodynamic and activation parameters are obtained for silyl and phosphine exchange in *cis*-Pt(PCy₃)₂(H)(SiPh₃) **15**, *cis*-Pt(PCy₃)₂(H)(SiMe₂CH₂CH=CH₂) **16** and *cis*-Pt(PCy₃)₂(H)(SiMe₂Et) **17**. In addition, ¹H and ³¹P {¹H} NMR data are obtained for *cis*-Pt(PCy₃)₂(H)[SiMe₂OCH₂C(Me)=CH₂] **18**, *cis*-Pt(PCy₃)₂(H)[Si(OMe)CH₂CH=CH₂] **19** and *cis*-Pt(PCy₃)₂(H)(SiPh₂OSiPh₂H) **20**. The thermal and photochemical reactions of these complexes are also investigated.

5.2 RESULTS

5.2.1 Preparation of *cis*-Pt(PCy₃)₂(H)(SiR₃) complexes

The 14-electron Pt(PCy₃)₂ complex was reacted with various silanes to form the Si-H oxidative addition product *cis*-Pt(PCy₃)₂(H)(SiR¹₂R²) {R¹ = R² = Ph (**15**); R¹ = Me, R² = (CH₂CH=CH₂) (**16**); R¹ = Me, R² = Et (**17**); R¹ = Me, R² = [OCH₂C(Me)=CH₂] (**18**); R¹ = OMe, R² = (CH₂CH=CH₂) (**19**)}. The complexes *cis*-Pt(PCy₃)₂(H)(SiPh₃) **15** and *cis*-Pt(PCy₃)₂(H)(SiMe₂CH₂CH=CH₂) **16** were synthesised by reaction of Pt(PCy₃)₂ with the corresponding silane in pentane or hexane at 0 °C. These reactions yielded the products as white solids in moderate yields (40-50 %) (Scheme 5.2). Complexes **17-19** were characterised in solution by ¹H and ³¹P {¹H} NMR spectroscopy; attempts to isolate them yielded only oily residues [Table 5.1 (a) and (b)].

Pt(PCy₃)₂ was also reacted with the disilanes, HSiPh₂OSiPh₂H and HSiMe₂C₆H₄SiMe₂H. The reaction of Pt(PCy₃)₂ with HSiPh₂OSiPh₂H formed the complex *cis*-Pt(PCy₃)₂(H)(SiPh₂OSiPh₂H) **20**. The reaction of Pt(PCy₃)₂ with HSiMe₂C₆H₄SiMe₂H at -77 °C formed an as yet unidentified species **A5**. When the reaction was carried out at room temperature a further, as yet unknown, compound **B5** was formed alongside **A5**.



Scheme 5.2 Preparation of *cis*-Pt(PCy₃)₂(H)(SiR¹₂R²).

5.2.2 ^1H and ^{31}P $\{^1\text{H}\}$ NMR characterisation of *cis*-Pt(PCy₃)₂(H)(SiR₃)

Complexes **15-20** all yield a hydride resonance at around $\delta -3.5$ in their ^1H NMR spectra. All the complexes studied undergo temperature dependent dynamic behaviour as first described by Clark and Hampden-Smith.¹⁰ The limiting low temperature ^1H NMR spectra of complexes **15-20** contain hydride resonances with doublet of doublets multiplicity and ^{195}Pt satellites (Figure 5.1). The limiting low temperature ^{31}P $\{^1\text{H}\}$ NMR spectra for complexes **15-20** contain two doublet resonances with ^{195}Pt satellites at *ca.* δ 40 (Figure 5.2). Both ^1H and ^{31}P $\{^1\text{H}\}$ NMR data of **15-20** confirm that they are monohydride species with two mutually *cis* phosphine ligands of the form *cis*-Pt(PCy₃)₂(H)(SiR₃). Note that the coupling constants $J(\text{PtP})$ differ quite substantially, the lower platinum-phosphorus coupling constant is indicative of the phosphorus atom *trans* to silicon due to the higher *trans*-influence compared to the hydride ligand¹⁴ (see Section 2.3.1 for a brief discussion of the *trans*-influence of a ligand). NMR data for complexes **15-20** are summarised in Tables 5.1 (a) and (b).

On addition to the platinum centre, all the proton resonances of the silyl group are shifted to lower field relative to the proton resonances of the corresponding free silane. This is demonstrated in Figure 5.1 where the allyl proton resonances of the silyl ligand in *cis*-Pt(PCy₃)₂(H)(SiMe₂CH₂CH=CH₂) **16** are shifted to lower field when compared to the free silane ligand HSiMe₂CH₂CH=CH₂. Also of interest are the two methyl groups and the methylene group adjacent to the silicon atom in complex **16**. Both groups are sufficiently close to the platinum centre to show coupling. The methyl resonance is a doublet at δ 0.83 due to weak coupling to the *trans* phosphorus atom; it also possesses ^{195}Pt satellites [$^4J(\text{PH})_{\text{trans}} = 1.6$ Hz, $^3J(\text{PtH}) = 26.7$ Hz]. The methylene resonance is a doublet at δ 2.41, which arises from coupling to the vinyl CH group and possesses ^{195}Pt satellites [$^3J(\text{HH}) = 8.3$, $^3J(\text{PtH}) = 30.8$]. The complexes *cis*-Pt(PCy₃)₂(H)(SiMe₂Et) **17**, *cis*-Pt(PCy₃)₂(H)(SiMe₂OCH₂CH=CH₂) **18** and *cis*-Pt(PCy₃)₂(H)[Si(OMe)₂CH₂-CH=CH₂] **19** also contain methyl groups on the silicon atom whose proton resonances show couplings to ^{195}Pt . The species formed in the reaction of Pt(PCy₃)₂ with the disilanes HSiPh₂OSiPh₂H and HMe₂Si(C₆H₄)SiMe₂H are discussed in Section 5.2.8.

	$^1\text{H}, \delta (J / \text{Hz})$
15^a	-3.95 [1H, dd, Pt <u>H</u> , $^2J(\text{PH})_{\text{trans}} = 141.8$, $^2J(\text{PH})_{\text{cis}} = 23.3$, $J(\text{PtH}) = 784.2$] 1.12-2.50 (22H, m, PC ₆ <u>H</u> ₁₁) 7.20-8.40 (10H, m, PC ₆ <u>H</u> ₅)
16^a	-3.46 [1H, dd, Pt <u>H</u> , $^2J(\text{PH})_{\text{trans}} = 144.1$, $^2J(\text{PH})_{\text{cis}} = 26.1$, $J(\text{PtH}) = 853.3$] 1.05 [6H, d, Si <u>CH</u> ₃ , $^4J(\text{PH}) = 1.6$, $^3J(\text{PtH}) = 26.5$] 1.10-2.30 (22H, m, PC ₆ <u>H</u> ₁₁) 2.41 [2H, d, Si <u>CH</u> ₂ CH=CH ₂ , $^3J(\text{HH}) = 8.3$, $^3J(\text{PtH}) = 30.8$] 5.16, 5.25 (2H, m, SiCH ₂ CH= <u>CH</u> ₂) 6.52 (1H, m, SiCH ₂ <u>CH</u> =CH ₂)
17^a	-3.54 [1H, dd, Pt <u>H</u> , $^2J(\text{PH})_{\text{trans}} = 144.0$, $^2J(\text{PH})_{\text{cis}} = 25.8$, $J(\text{PtH}) = 858.3$] 0.85 [6H, d, Si <u>CH</u> ₃ , $^4J(\text{PH}) = 1.6$, $^3J(\text{PtH}) = 26.7$] 1.10-2.40 [27H, m, PC ₆ <u>H</u> ₁₁ , Si <u>CH</u> ₂ <u>CH</u> ₃]
18^b	-4.15 [1H, dd, Pt <u>H</u> , $^2J(\text{PH})_{\text{trans}} = 140.5$, $^2J(\text{PH})_{\text{cis}} = 27.7$, $J(\text{PtH}) = 888.5$] 1.16 [6H, s, Si <u>CH</u> ₃ , $^3J(\text{PtH}) = 29.9$] 1.20-2.40 [25H, m, PC ₆ <u>H</u> ₁₁ , C(<u>CH</u> ₃)=CH ₂] 4.52 (2H, br., SiO <u>CH</u> ₂) 5.24, 5.51 [2H, br., C(CH ₃)= <u>CH</u> ₂]
19^c	-4.00 [1H, dd, Pt <u>H</u> , $^2J(\text{PH})_{\text{trans}} = 141.8$, $^2J(\text{PH})_{\text{cis}} = 28.0$, $J(\text{PtH}) = 863.4$] 0.80-2.77 (22H, m, PC ₆ <u>H</u> ₁₁) 2.40 [2H, d, Si <u>CH</u> ₂ CH=CH ₂ , $^3J(\text{HH}) = 8.9$] 3.84 [6H, s, Si(O <u>CH</u> ₃)] 5.13-5.30 (2H, m, SiCH ₂ CH= <u>CH</u> ₂) 6.50 (1H, m, SiCH ₂ <u>CH</u> =CH ₂)
20^c	-4.00 [1H, dd, Pt <u>H</u> , $^2J(\text{PH})_{\text{trans}} = 140.7$, $^2J(\text{PH})_{\text{cis}} = 27.2$, $J(\text{PtH}) = 851.4$] 0.71-2.79 (22H, m, PC ₆ <u>H</u> ₁₁) 6.06 [1H, s, Si <u>H</u> , $J(\text{SiH}) = 213.0$] 7.04-7.15 (20H, m, SiC ₆ <u>H</u> ₅)

Table 5.1a ^1H NMR spectroscopic data of complexes **15-20**. *a* In [$^2\text{H}_8$]toluene at 250 K, ^1H (500.13 MHz). *b* In [$^2\text{H}_8$]toluene at 240 K, ^1H (500.13 MHz). *c* In C_6D_6 at 295 K, ^1H (200.13 MHz).

	$^{31}\text{P} \{^1\text{H}\}, \delta (J / \text{Hz})$
15^a	37.3 [d, P ^H , $J(\text{PP}) = 13, J(\text{PtP}) = 2642$] 41.1 [d, P ^{Si} , $J(\text{PP}) = 13, J(\text{PtP}) = 1560$]
16^a	41.6 [d, P ^H , $J(\text{PP}) = 12, J(\text{PtP}) = 2677$] 42.8 [d, P ^{Si} , $J(\text{PP}) = 12, J(\text{PtP}) = 1420$]
17^a	42.2 [d, P ^H , $J(\text{PP}) = 12, J(\text{PtP}) = 2704$] 43.1 [d, P ^{Si} , $J(\text{PP}) = 12, J(\text{PtP}) = 1387$]
18^b	41.9 [d, P ^H , $J(\text{PP}) = 13, J(\text{PtP}) = 2658$] 42.0 [br., P ^{Si} , $J(\text{PtP}) = 1369$]
19^c	41.9 [d, P ^H , $J(\text{PP}) = 14, J(\text{PtP}) = 2638$] 42.4 [br. d, P ^{Si} , $J(\text{PtP}) = 1408$]
20^c	43.1 [d, P ^{Si} , $J(\text{PP}) = 15, J(\text{PtP}) = 1428$] 43.4 [d, P ^H , $J(\text{PP}) = 15, J(\text{PtP}) = 2612$]

Table 5.1b $^{31}\text{P} \{^1\text{H}\}$ NMR spectroscopic data of complexes **15-20**. P^H indicates phosphorus is *trans* to hydride and P^{Si} indicates phosphorus is *trans* to silicon. *a* In $[\text{}^2\text{H}_8]\text{toluene}$ at 250 K, ^{31}P (202.46 MHz). *b* In $[\text{}^2\text{H}_8]\text{toluene}$ at 240 K, ^{31}P (202.46 MHz). *c* In C_6D_6 at 295K, ^{31}P (81.02 MHz).

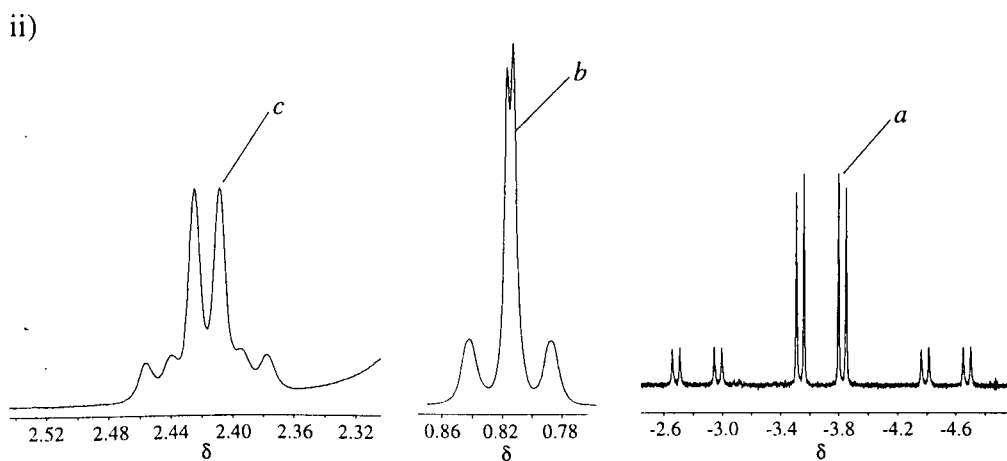
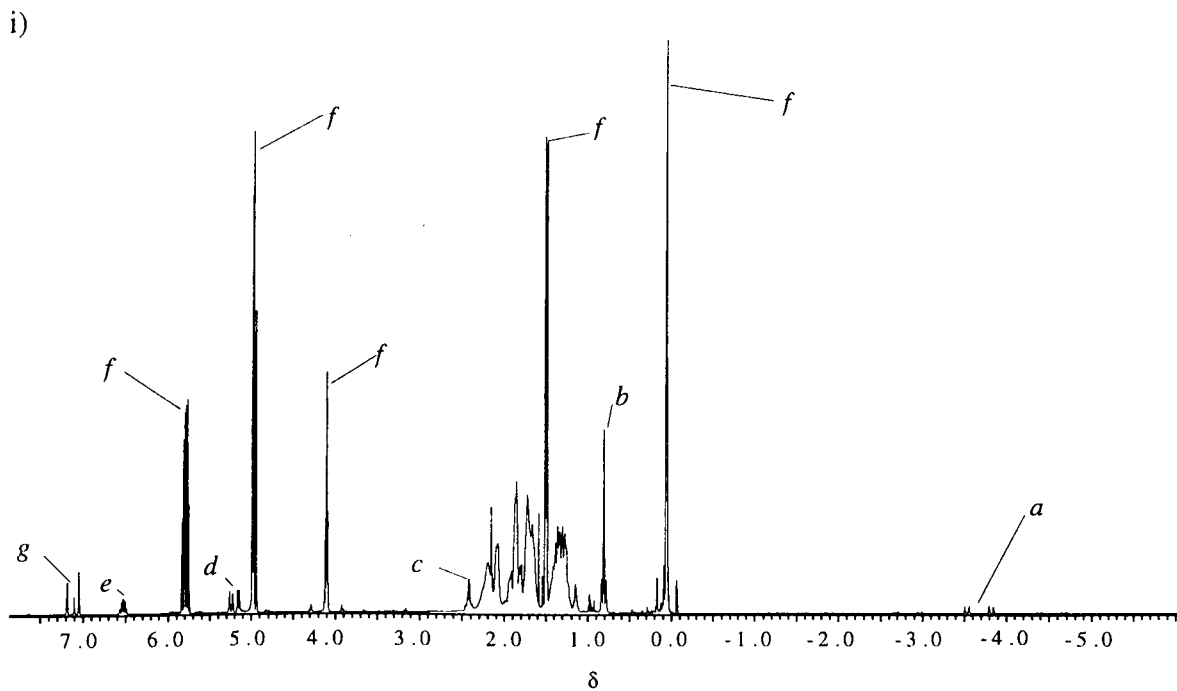


Figure 5.1 ^1H (500.13 MHz, 250 K) NMR spectrum of *cis*-Pt(PCy₃)₂(H)-(SiMe₂CH₂CH=CH₂) **16** in [²H₈]toluene with excess free silane. (i) Complete spectrum. (ii) Expansion of ¹⁹⁵Pt coupled resonances. *a* Pt-H. *b* SiMe₂. *c* CH₂CH=CH₂. *d* CH₂CH=CH₂. *e* CH₂CH=CH₂. *f* Free silane. *g* Toluene.

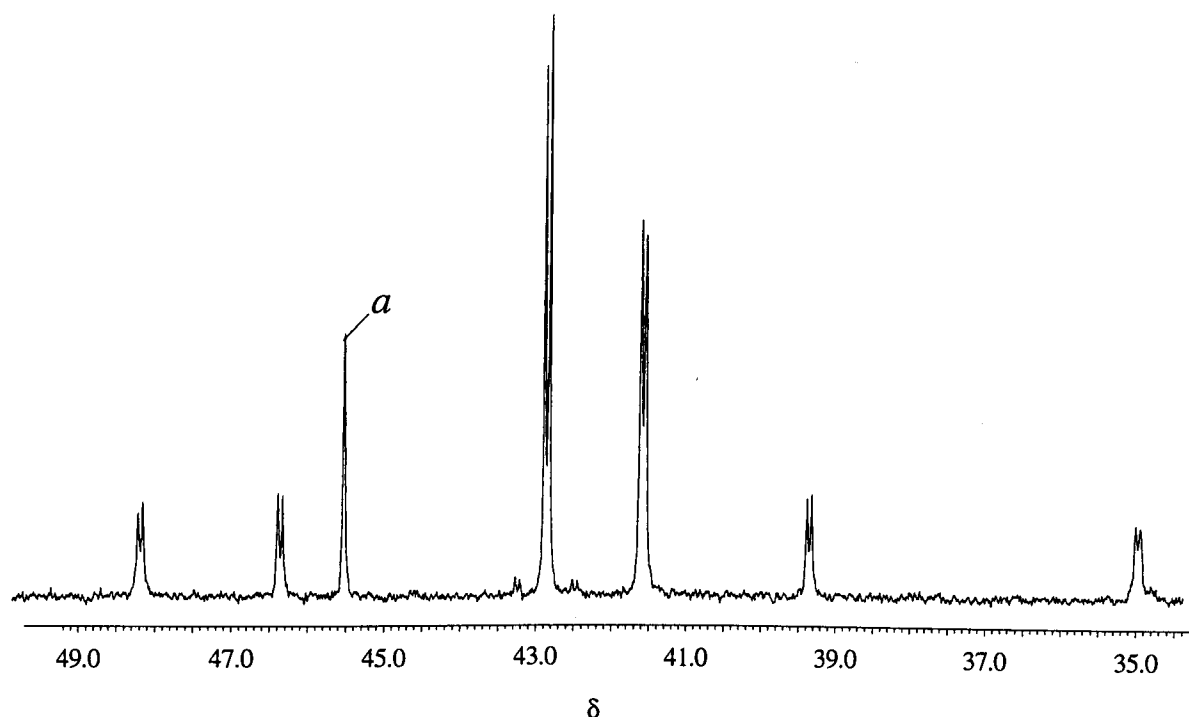


Figure 5.2 ^{31}P $\{^1\text{H}\}$ (202.46 MHz) NMR spectrum of *cis*-Pt(PCy₃)₂(H)-(SiMe₂CH₂CH=CH₂) **16** in [²H₈]toluene (250 K). *a* Phosphine oxide.

5.2.3 Fluxional behaviour of *cis*-Pt(PCy₃)₂(H)(SiR₃)

Complexes **15-20** all show signs of fluxional behaviour; for **16-18** these dynamic processes are slowed down to give low-temperature limiting spectra at *ca.* 250 K. In complexes **19** and **20**, where there are oxygen based substituents attached to the silicon, the low temperature limit is reached at around room temperature. This indicates that electron withdrawing groups are able to reduce the rate of exchange. These features are illustrated by comparing the spectra in Figures 5.3 and 5.4. The hydride spectra shown in Figure 5.4 were recorded at 300 K on a 500 MHz spectrometer and show that the hydride resonances of complexes **16** and **17** are substantially distorted whereas the hydride resonances of **15** and **18** are affected to a much smaller extent.

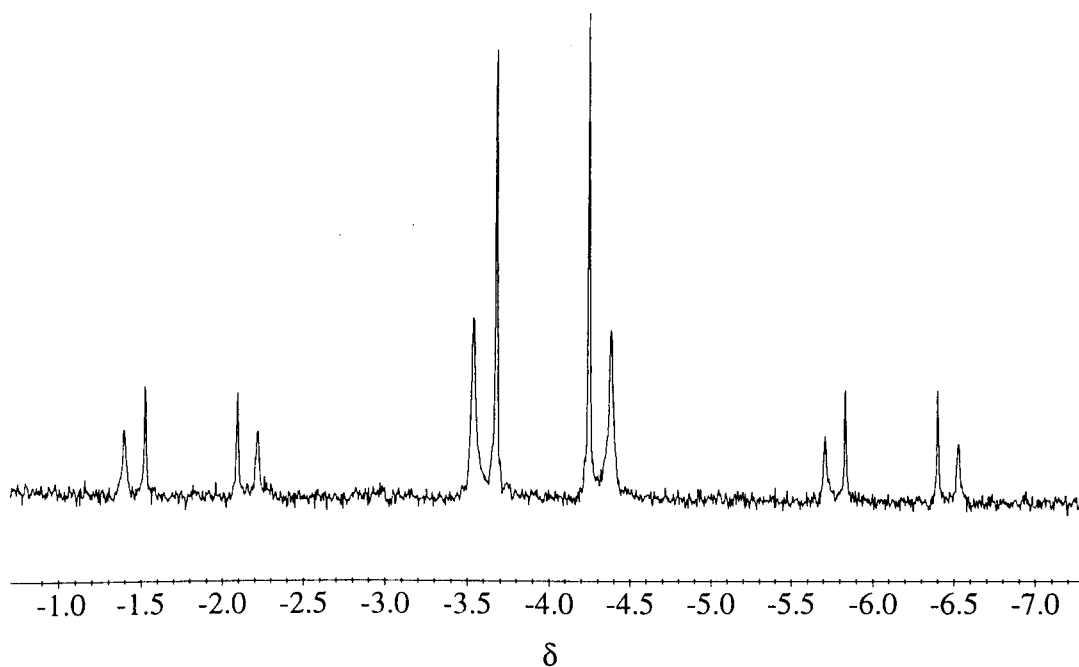


Figure 5.3 ^1H (200.13 MHz) NMR spectrum of *cis*-Pt(PCy₃)₂(H)[Si(OMe)₂-CH₂CH=CH₂] **19** in C₆D₆ (295 K) showing the hydride region only.

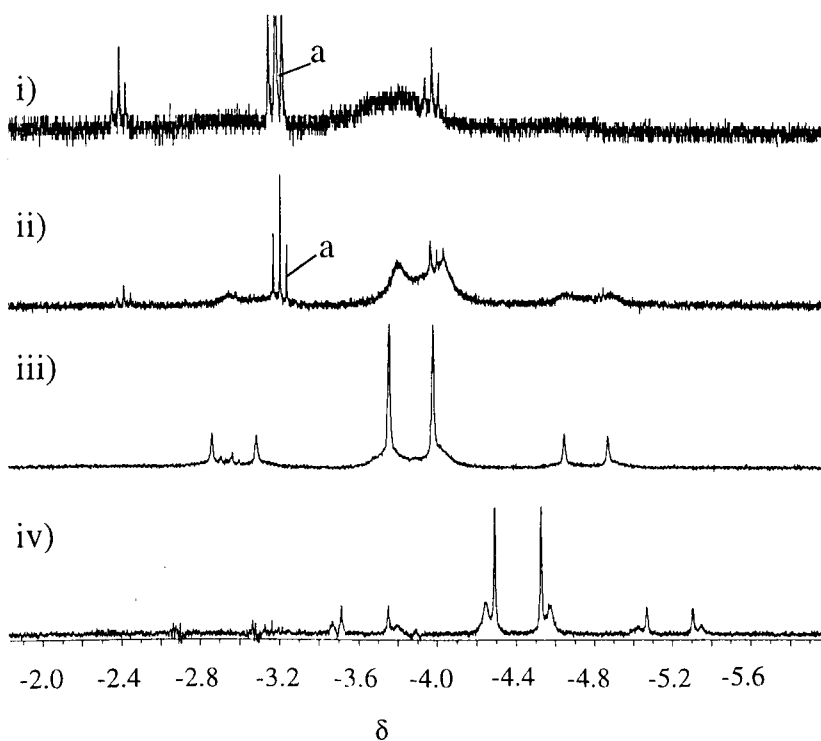


Figure 5.4 ^1H (500.13 MHz) NMR spectra of *cis*-Pt(PCy₃)₂(H)(SiR₃) in [²H₈]toluene (300 K) showing the hydride region only. (i) *cis*-Pt(PCy₃)₂(H)(SiMe₂Et) **17**. (ii) *cis*-Pt(PCy₃)₂(H)(SiMe₂CH₂CH=CH₂) **16**. (iii) *cis*-Pt(PCy₃)₂(H)[SiMe₂OCH₂C(Me)=CH₂] **18**. (iv) *cis*-Pt(PCy₃)₂(H)(SiPh₃) **15**. *a trans*-Pt(PCy₃)₂(H)₂.

From Figure 5.4, complex **17** appears to have the highest rate of exchange at room temperature when compared to complexes **15**, **16** and **18**. In complex **17** the hydride resonance is almost indistinguishable from the baseline at 300 K [Figure 5.4 (i)]. It appears that π -acceptors and electronegative groups stabilise the complexes, since only **16** and **17** appear to be undergoing fast exchange processes at 300 K and both complexes only contain alkyl groups adjacent to the silicon atom. Complexes **15** and **18** appear to have a comparatively slow rate of exchange at 300 K and both complexes have π -acceptors or electronegative groups adjacent to the silicon atom.

NMR samples of **15**, **16**, **17** and **18** prepared *in situ*, all contain hydride resonances as normal, undistorted doublet of doublets at 250 K. On warming these samples the hydride resonances begin to show signs of dynamic behaviour. The hydride resonance of complex **16** at 250 K has the expected doublet of doublets fine structure. On warming, the outer lines of this pattern gradually decrease in intensity whilst the inner lines remain sharp with constant separation $\{|^2J(\text{PH})_{\text{trans}}| - |^2J(\text{PH})_{\text{cis}}|\}$. This situation holds until 285 K at which point the outer lines of the doublet of doublets are no longer visible. Further warming of the complex results in the broadening of the inner lines until eventual thermal decomposition of complex **16** to *trans*-Pt(PCy₃)₂(H)₂ occurs (Figure 5.5a). Figure 5.5b shows the corresponding ³¹P {¹H} NMR spectra of **16** over the temperature range 250-300 K. On warming the sample from 250 K to 300 K the two doublet resonances initially collapse into two broad singlets, and then coalesce. Despite some decomposition to *trans*-Pt(PCy₃)₂(H)₂ at around 290 K, identical spectra were reproduced upon subsequent cooling.

The *cis*-platinum silyl hydride complexes, **15-20**, all eventually decompose in solution to *trans*-Pt(PCy₃)₂(H)₂ as indicated by the appearance of a new hydride resonance [δ_{H} (500.15 MHz, 300 K) -3.08, t, $^2J(\text{PH})_{\text{cis}} = 17.2$ Hz, $J(\text{PtH}) = 793.1$ Hz; δ_{P} (202.46 MHz, 300 K) 52.4, s, $J(\text{PtP}) = 2887$ Hz]. The rate of conversion of the *cis*-platinum silyl hydride complex to the *trans*-platinum dihydride complex depends critically on the R groups adjacent to silicon, and on the concentration of free silane. As can be seen from Figure 5.4 both **16** and **17** show signs of decomposition to *trans*-Pt(PCy₃)₂(H)₂ while **15** and **18** are essentially intact.

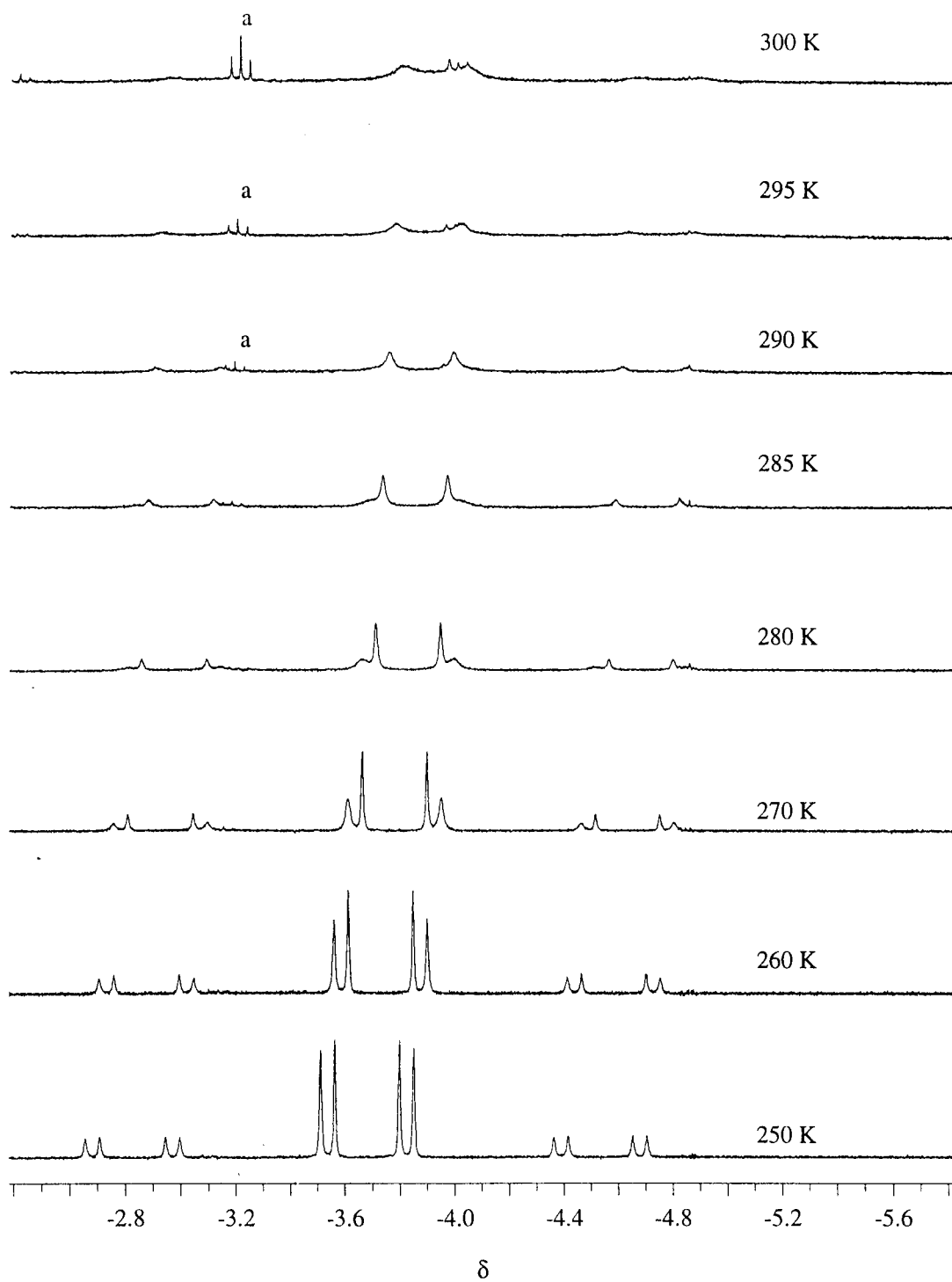


Figure 5.5 (a) Variable temperature ^1H (500.13 MHz) NMR spectra of *cis*- $\text{Pt}(\text{PCy}_3)_2(\text{H})(\text{SiMe}_2\text{CH}_2\text{CH}=\text{CH}_2)$ **16** in $[\text{}^2\text{H}_8]\text{toluene}$ showing the hydride region. *a* *trans*- $\text{Pt}(\text{PCy}_3)_2(\text{H})_2$.

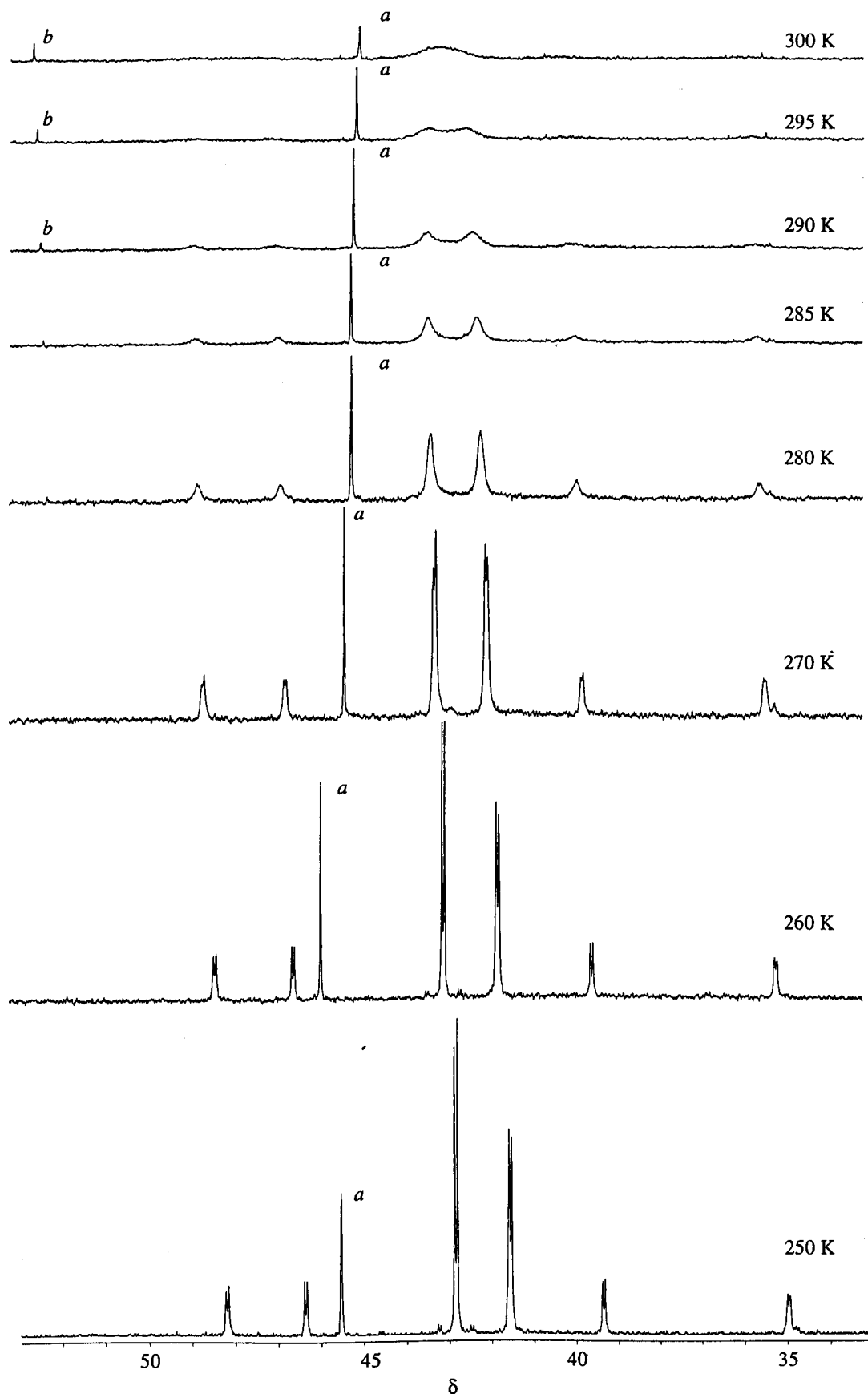
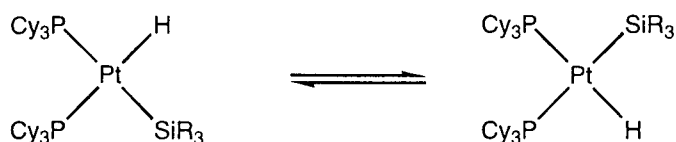


Figure 5.5 (b) Low temperature ^{31}P $\{^1\text{H}\}$ (202.46 MHz) NMR spectra of $\text{cis-Pt}(\text{PCy}_3)_2(\text{H})(\text{SiMe}_2\text{CH}_2\text{CH}=\text{CH}_2)$ 16 in $[\text{}^2\text{H}_8]\text{toluene}$. *a* Phosphine oxide. *b* $\text{trans-Pt}(\text{PCy}_3)_2(\text{H})_2$.

5.2.3a Mutual Exchange of Phosphine Ligands in *cis*-Pt(PCy₃)₂(H)(SiR₃)

The invariant lines observed for the monohydride resonance in the temperature dependent ¹H NMR spectra [Figure 5.5 (a)] are characteristic of an intramolecular process¹⁵ where the phosphine ligands undergo mutual exchange whilst retaining P–H spin correlation (Scheme 5.2). Figure 5.6 shows the phosphorus spin states associated with the transitions of the hydride resonance depends on the signs of the *cis* and *trans* proton-phosphorus coupling constants.



Scheme 5.2 Mutual exchange of phosphine in *cis*-Pt(PCy₃)₂(H)(SiR₃).

a)	Phosphorus nucleus 1	α	β	α	β
	Phosphorus nucleus 2	β	β	α	α
b)	Phosphorus nucleus 1	β	α	β	α
	Phosphorus nucleus 2	β	β	α	α

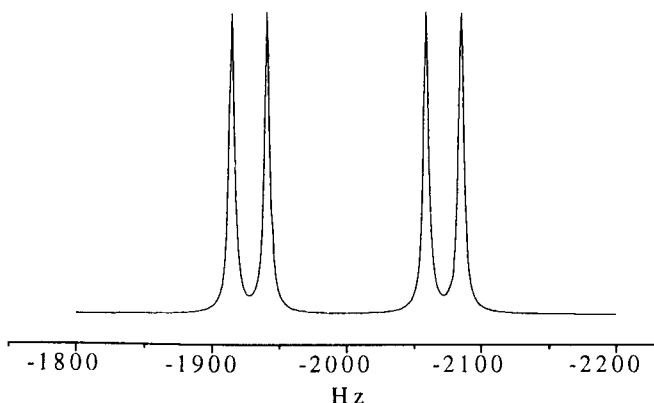


Figure 5.6 Calculated ¹H NMR spectrum of *cis*-Pt(PCy₃)₂(H)(SiR₃) showing possible labelling of phosphorus spin states for the doublet of doublets hydride transitions using DNMR-SIM, simulated at 500.13 MHz. ¹⁹⁵Pt satellites are not displayed. a) ²J(PH)_{trans} and ²J(PH)_{cis} are of opposite sign, b) ²J(PH)_{trans} and ²J(PH)_{cis} are of the same sign.

The mutual phosphine exchange process of *cis*-Pt(PCy₃)₂(H)(SiR₃) in solution was simulated using the dynamic NMR spectra simulation programme DNMR-SIM,¹⁶ see Section 5.2.6. In Figure 5.7 the result of simulating the mutual phosphine exchange is illustrated. Figure 5.7 (a) shows the effect of increasing the rate of mutual phosphine exchange when both ²J(PH)_{trans} and ²J(PH)_{cis} are of the opposite signs while Figure 5.7 (b) corresponds to the situation where ²J(PH)_{trans} and ²J(PH)_{cis} are of the same sign. Initially, the outer lines of the doublet of doublets of the simulated hydride resonance

decreased in intensity as was observed in the real temperature dependent NMR spectra. As the rate of mutual phosphine exchange was increased the outer lines not only decreased in intensity but broaden until they are no longer observed. Further increase in the rate of mutual phosphine exchange resulted in the appearance of a new resonance in the centre of the hydride signal. The inner lines remained sharp and invariant at all times with a separation of $\{|^2J(\text{PH})_{\text{trans}}| - |^2J(\text{PH})_{\text{cis}}|\}$.

When $^2J(\text{PH})_{\text{trans}}$ and $^2J(\text{PH})_{\text{cis}}$ are of the same sign, the inner lines of the simulated doublet of doublets hydride resonance collapsed and reformed in the centre as the rate of mutual phosphine exchange was increased. The outer lines remained invariant throughout. Note the separation between the two invariant lines in this case is $\{|^2J(\text{PH})_{\text{trans}}| + |^2J(\text{PH})_{\text{cis}}|\}$. This situation does not therefore match the experimental data.

Notice that the invariant lines of the hydride transitions are associated with the phosphorus spin states $\alpha\alpha$ and $\beta\beta$ and that the collapsing lines are the proton transitions associated with the $\alpha\beta$ and $\beta\alpha$ phosphorus spin states which are permuted by interchange of the phosphorus atoms (Figure 5.6).⁹

At the higher mutual phosphine exchange rate limit both phosphorus atoms will appear to be equivalent and a triplet hydride resonance will be observed. If $^2J(\text{PH})_{\text{trans}}$ and $^2J(\text{PH})_{\text{cis}}$ are of the same sign, the observed $^2J(\text{PH})$ will have a value of $\{|^2J(\text{PH})_{\text{trans}}| + |^2J(\text{PH})_{\text{cis}}|\}/2$. If $^2J(\text{PH})_{\text{trans}}$ and $^2J(\text{PH})_{\text{cis}}$ are of opposite sign, the observed $^2J(\text{PH})$ will have a value of $\{|^2J(\text{PH})_{\text{trans}}| - |^2J(\text{PH})_{\text{cis}}|\}/2$.

As Figure 5.7 clearly demonstrates, the collapse of the outer lines rather than the inner lines indicates that $^2J(\text{PH})_{\text{trans}}$ and $^2J(\text{PH})_{\text{cis}}$ are of opposite sign as was the case for *cis*-Pt(PPh₃)₂(H)(SiPh₃).⁹ Since we only observe the collapse of the outer lines of the hydride resonance in the variable temperature ¹H NMR spectra for **15-18**, $^2J(\text{PH})_{\text{trans}}$ and $^2J(\text{PH})_{\text{cis}}$ must be of opposite sign.

Comparing the real and simulated hydride NMR spectra, Figures 5.5 (a) and 5.7 (a) respectively, we find that the simulated spectra of the phosphine interchange process at a slow rate agree well with the experimental hydride spectra of *cis*-Pt(PCy₃)₂(H)-(SiMe₂CH₂CH=CH₂) **16** at low temperatures. However, as the temperature is increased, the inner lines of the doublet of doublets resonance of **16** do not remain sharp and invariant, but instead, they begin to broaden. This is also true in the cases of complexes **15**, **17** and **18**. The appearance of a new central line is not observed at higher temperatures as is predicted in the simulated spectra for high rates of mutual phosphine exchange. This is because of a second dynamic exchange, involving the addition-elimination of the free silane.¹⁰ This clearly demonstrates that mutual phosphine exchange is not the sole dynamic process occurring in *cis*-Pt(PCy₃)₂(H)(SiR₃) in solution at higher temperatures. However, it is clear that mutual phosphine exchange is the dominant process at lower temperatures.

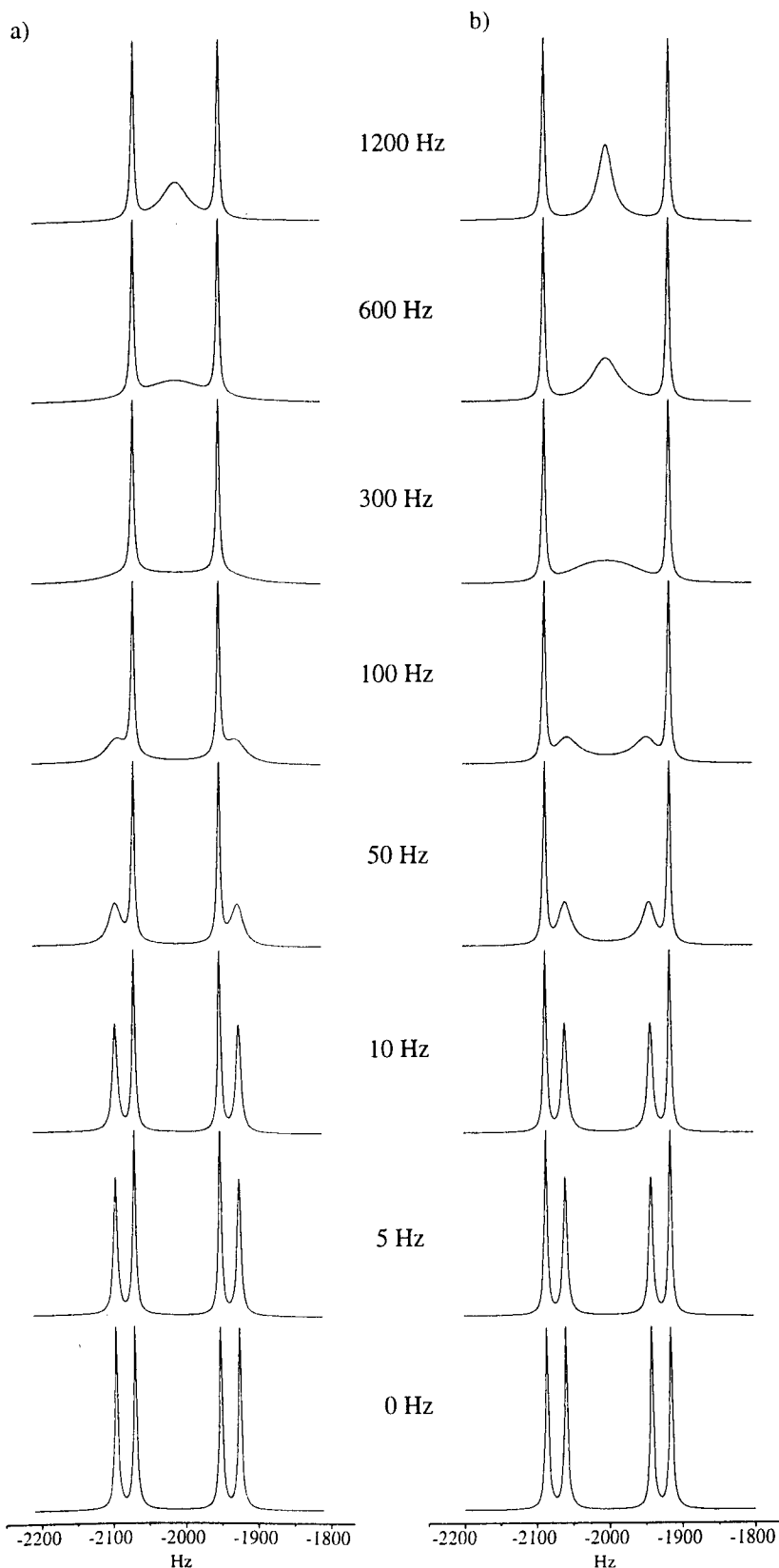
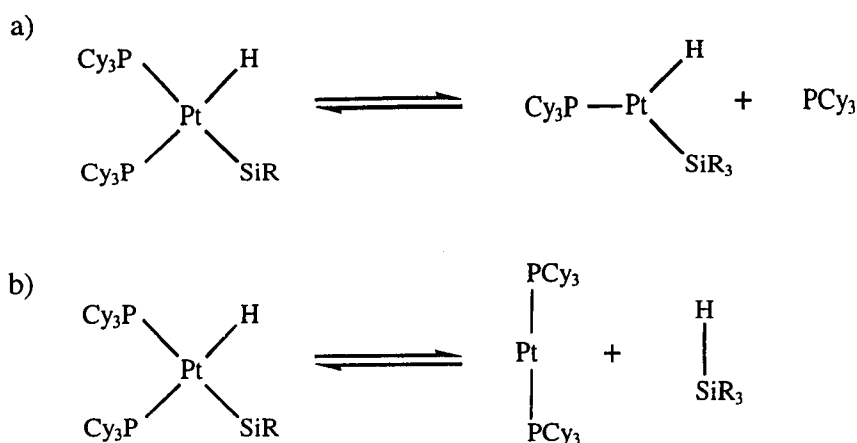


Figure 5.7 Calculated ^1H hydride NMR spectra of $\text{cis-Pt}(\text{PCy}_3)_2(\text{H})(\text{SiR}_3)$ showing the effects of altering the rate of the phosphine interchange process using DNMR-SIM, simulated at 500.13 MHz. ^{195}Pt satellites are not simulated. (a) $^2J(\text{PH})_{\text{trans}}$ and $^2J(\text{PH})_{\text{cis}}$ are of opposite sign. (b) $^2J(\text{PH})_{\text{trans}}$ and $^2J(\text{PH})_{\text{cis}}$ are of the same sign.

5.2.3b Reversible dissociation of silane from *cis*-Pt(PCy₃)₂(H)(SiR₃)

As well as the mutual phosphine interchange process (Scheme 5.2), complexes **15-18** exhibit another type of dynamic exchange process in solution in our studies. This is evident from the broadening of the hydride resonances upon warming the solutions of *cis*-Pt(PCy₃)₂(H)(SiR₃) from low temperature. As mentioned previously the hydride resonances coalesced into a very broad band on warming, accompanied by decomposition to *trans*-Pt(PCy₃)₂(H)₂ [Figure 5.5 (a)]. Two possible dynamic processes could account for the broadening of the hydride resonance: (a) reversible dissociation of phosphine from *cis*-Pt(PCy₃)₂(H)(SiR₃) and (b) reversible dissociation of silane from *cis*-Pt(PCy₃)₂(H)(SiR₃) (Scheme 5.3).



Scheme 5.3 Possible processes responsible for the broadening of the hydride resonance at elevated temperature in *cis*-Pt(PCy₃)₂(H)(SiR₃). (a) reversible phosphine dissociation. (b) reversible silane dissociation.

Both processes (a) and (b) in Scheme 5.3 involve the disruption of the spin-spin coupling between the phosphorus atoms and the hydride through bond scission. Both these processes are said to be non-mutual exchange processes. As originally noted by Clark and Hampden-Smith, the non-mutual exchange process observed was that of the reversible silane dissociation mechanism.¹⁰ We observed several pieces of evidence to support this. For example, upon dissolving the complex *cis*-Pt(PCy₃)₂(H)(SiMe₂CH₂CH=CH₂) **16** in C₆D₆ at room temperature, detectable traces of free silane and Pt(PCy₃)₂ were observed by ¹H and ³¹P {¹H} NMR spectroscopy, although no free phosphine was detected. Similarly, GC analysis of a benzene solution of **16** at room temperature produced a peak at the same retention time as that of HSiMe₂CH₂CH=CH₂. When an NMR sample of **16** was prepared at low temperature in [²H₈]toluene and ³¹P {¹H} NMR spectra were subsequently measured at 250 K only signals due to **16** were observed. However, on warming the sample to 290 K a signal

corresponding to $\text{Pt}(\text{PCy}_3)_2$ was detected (Figure 5.8). Similarly, the ^1H NMR spectrum of complex **15** at 315 K shows free silane but not at 280 K (Figure 5.9).

These observations support silane exchange over phosphine exchange, since trace amounts of the free phosphine PCy_3 should be detectable if free phosphine exchange was significant at elevated temperatures.

Further support for the silane dissociation process was found in a spin saturation transfer NMR experiment.¹⁷ The intensity of the Si–H resonance from the free silane in the ^1H NMR spectrum decreased markedly upon irradiation (or saturation) of the hydride resonance in the complex. By irradiating the hydride resonance the spin population of the α and β states of the hydride ligand are equalised. If the silyl and the hydride ligands are in rapid exchange with the free silane, the spin saturated hydride will be converted to a free silane ligand. Since α and β spin states in the newly formed free silane have equal population, they will not contribute to the Si–H resonance of the free silane. Hence, we observe an overall decrease in intensity of the Si–H resonance upon irradiation of the hydride resonance (Figure 5.10).

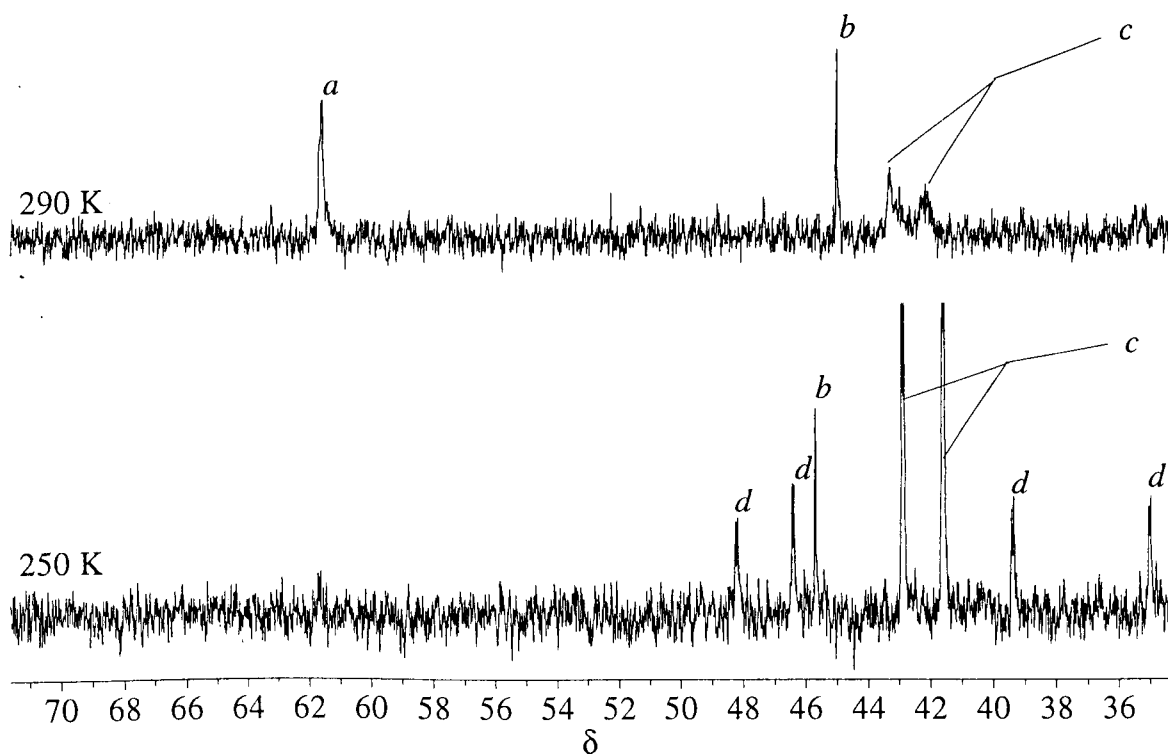


Figure 5.8 Quantitative ^{31}P $\{^1\text{H}\}$ (202.46 MHz) NMR spectra of *cis*- $\text{Pt}(\text{PCy}_3)_2(\text{H})(\text{SiMe}_2\text{CH}_2\text{CH}=\text{CH}_2)$ **16** showing dissociation to $\text{Pt}(\text{PCy}_3)_2$ (top figure) at elevated temperatures. *a* $\text{Pt}(\text{PCy}_3)_2$. *b* Phosphine oxide. *c* Complex **16**. *d* ^{195}Pt satellites from complex **16** at low temperature (bottom figure).

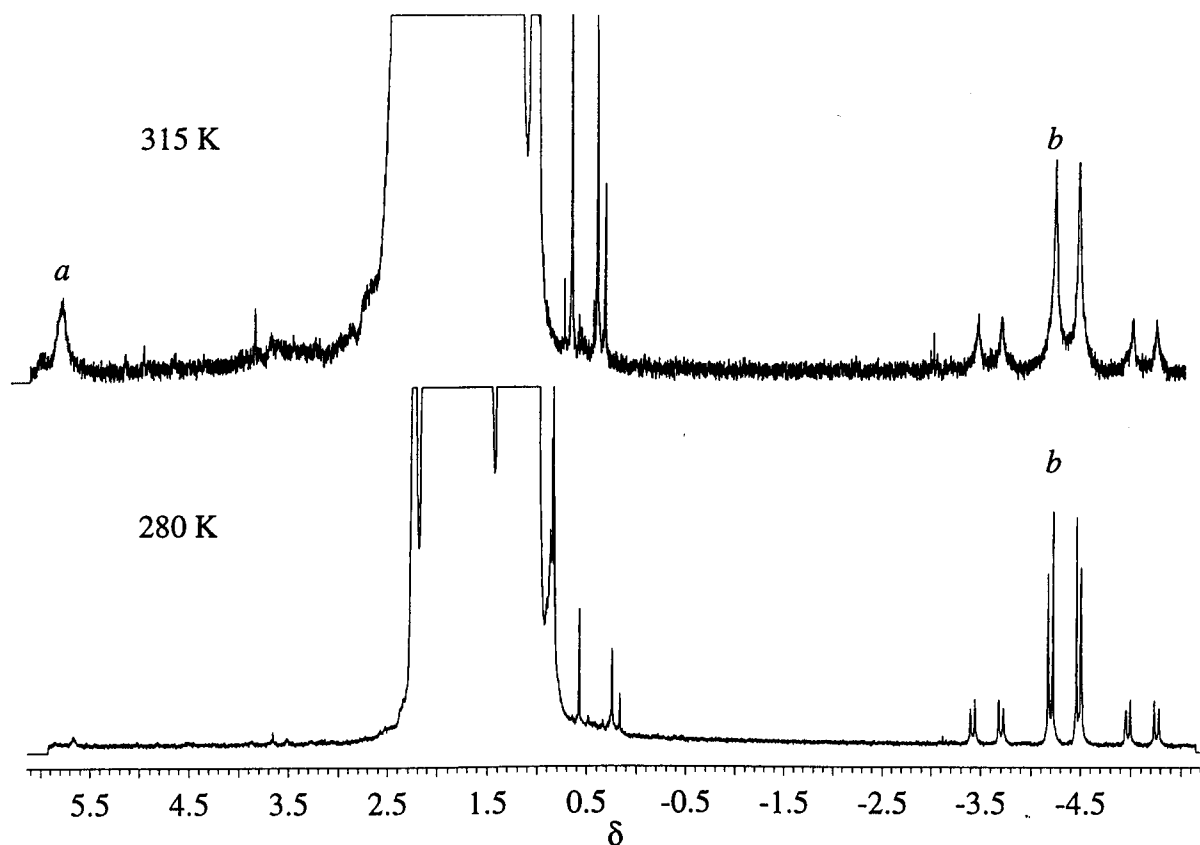


Figure 5.9 ^1H NMR (500.13 MHz) spectra of *cis*-Pt(PCy₃)₂(H)(SiPh₃) **15** in C₆D₆, showing dissociation of HSiPh₃ at elevated temperatures. *a* Si-H from HSiPh₃. *b* Pt-H from complex **15** with ^{195}Pt satellites.

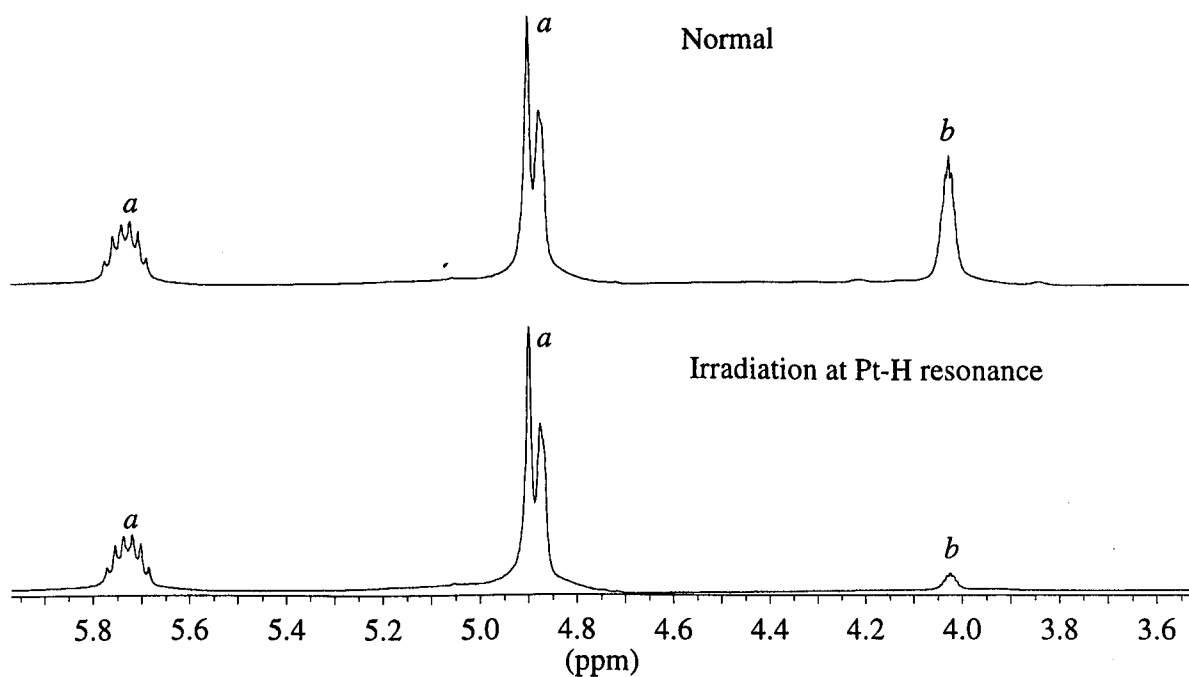
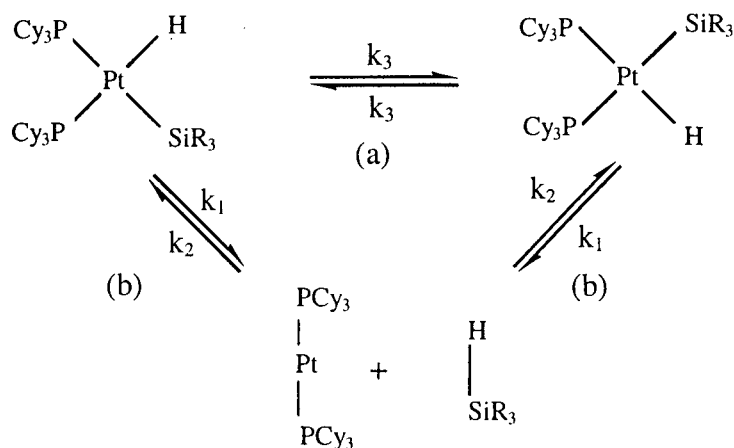


Figure 5.10 ^1H (500.13 MHz) NMR spectra of *cis*-Pt(PCy₃)₂(H)(SiMe₂CH₂CH=CH₂) **16** with excess free silane. The top spectrum shows the normal free silane resonances. The bottom spectrum shows that there is a decrease in intensity in the Si-H resonance when the Pt-H hydride resonance of **16** is irradiated. *a* CH=CH₂, *b* Si-H.

It is clear, therefore, that at least two dynamic exchange processes are occurring in solution at high temperatures for *cis*-Pt(PCy₃)₂(H)(SiR₃). These involve both mutual phosphine exchange and reversible silane dissociation (Scheme 5.4).

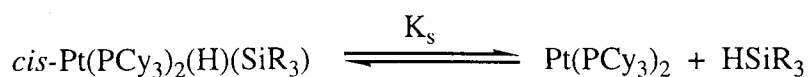


Scheme 5.4 Dynamic exchange processes of *cis*-Pt(PCy₃)₂(H)(SiR₃) in solution at high temperatures: (a) mutual phosphine exchange and (b) free silane exchange.

When both exchange processes (a) and (b) in Scheme 5.4 were calculated in a NMR simulation programme, the dynamic ¹H NMR spectra obtained matched those observed experimentally. From these calculations, the rate constants *k*₁, *k*₂ and *k*₃ in Scheme 5.4 were obtained for a range of temperatures. Using these rate constants, activation parameters Δ*H*[‡], Δ*S*[‡], and Δ*G*[‡] can be calculated for the processes (a) and (b) in Scheme 5.4. These processes are discussed in section 5.2.5.

5.2.4 Thermodynamic parameters for the free silane exchange process in *cis*-Pt(PCy₃)₂(H)(SiR₃)

As mentioned previously in section 5.2.3b, the silane ligand dissociates reversibly from the complex *cis*-Pt(PCy₃)₂(H)(SiR₃) in solution at high temperatures [Scheme 5.4 (b)]. Since the relative concentrations of *cis*-Pt(PCy₃)₂(H)(SiR₃), HSiR₃ and Pt(PCy₃)₂ can be measured using quantitative ¹H and ³¹P {¹H} NMR spectroscopy, the equilibrium constant *K*_S for these steps can be obtained (Equation 5.1).



$$K_S = \frac{[\text{Pt}(\text{PCy}_3)_2][\text{HSiR}_3]}{[cis\text{-Pt}(\text{PCy}_3)_2(\text{H})(\text{SiR}_3)]} \quad (5.1)$$

^{31}P $\{^1\text{H}\}$ NMR spectra were recorded using an inverse gated pulse sequence, with a delay period of at least ten times the acquisition time.¹⁸ The inverse gated pulse sequence suppresses the build up of the Nuclear Overhauser effect,¹⁹ whilst still decoupling ^1H , and thus provides a quantitative measurement of ^{31}P intensities. The ^1H NMR resonance of the Si–H group on the free silane was found to have a long relaxation time of up to 8 seconds at room temperature. A 60 seconds delay between acquisition was therefore used to allow for reliable integration analysis of the proton spectrum.

Once K_S is established for a range of temperatures, ΔH° and ΔS° for the dissociation of *cis*-Pt(PCy₃)₂(H)(SiR₃) can be obtained by applying the van't Hoff isochore (Equation 5.2, R = gas constant). Since ΔH° is only weakly temperature dependent, we should observe an almost linear relationship when plotting $\ln(K_S)$ against T^{-1} .

$$\ln(K_S) = \frac{\Delta S^\circ}{R} - \frac{\Delta H^\circ}{RT} \quad (5.2)$$

5.2.4a Standard enthalpy and entropy of reaction for the dissociation of *cis*-Pt(PCy₃)₂(H)(SiPh₃) **15** to Pt(PCy₃)₂ and HSiPh₃

A sample of **15** was prepared in [$^2\text{H}_8$]toluene and kept in ice prior to recording the corresponding NMR spectra. Quantitative ^1H and ^{31}P $\{^1\text{H}\}$ NMR spectra were recorded initially at 290 K and subsequently at +5 degree intervals to 310 K. Table 5.2 shows the calculated equilibrium constants of dissociation (or free silane exchange) of *cis*-Pt(PCy₃)₂(H)(SiPh₃) **15** from 290 K to 310 K. The relative concentrations of **15**, [HSiPh₃] and [Pt(PCy₃)₂] were obtained from the integrals of the hydride resonance of **15**, the Si–H resonance of HSiPh₃ in the ^1H NMR spectra and the integrals of the phosphorus resonance of **15** and Pt(PCy₃)₂. Figure 5.11 shows the van't Hoff plot of $\ln(K_S)$ against T^{-1} as a straight line. The thermodynamic parameters for the dissociation of **15** were determined as $\Delta H^\circ = 74 \pm 10 \text{ kJ mol}^{-1}$ and $\Delta S^\circ = 243 \pm 35 \text{ J K}^{-1} \text{ mol}^{-1}$.

Temp. / K	K_S	$\ln(K_S)$	$T^{-1} / 10^{-3} \text{ K}^{-1}$
290	0.189	-1.66	3.45
295	0.276	-1.28	3.39
300	0.531	-0.63	3.33
305	0.821	-0.20	3.28
310	1.330	0.28	3.23

Table 5.2 The effect of temperature on the equilibrium constant K_S for *cis*-Pt(PCy₃)₂(H)(SiPh₃) **15** in [²H₈]toluene.

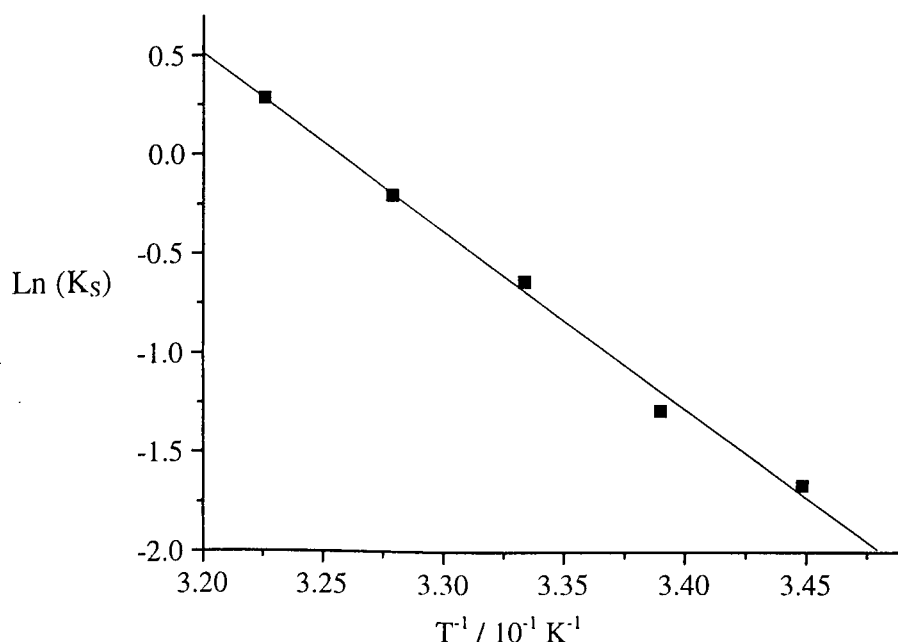


Figure 5.11 Plot of $\ln(K_S)$ against T^{-1} for the dissociation of *cis*-Pt(PCy₃)₂(H)(SiPh₃) **15** in [²H₈]toluene. The squares are the experimental points, the line shows the calculated line of best fit.

5.2.4b Standard enthalpy and entropy of reaction for the dissociation of *cis*-Pt(PCy₃)₂(H)(SiMe₂CH₂CH=CH₂) **16** to Pt(PCy₃)₂ and HSiMe₂CH₂CH=CH₂

An NMR sample of *cis*-Pt(PCy₃)₂(H)(SiMe₂CH₂CH=CH₂) **16** was prepared in [²H₈]toluene and stored in liquid nitrogen prior to running the appropriate NMR spectra. This precaution was required to prevent excessive decomposition to *trans*-Pt(PCy₃)₂(H)₂ which occurs at room temperature during sample preparation. Equilibrium constants of

dissociation were obtained as for **15** (Table 5.3, Figure 5.12) yielding $\Delta H^\circ = 45 \pm 8 \text{ kJ mol}^{-1}$ and $\Delta S^\circ = 155 \pm 30 \text{ J K}^{-1} \text{ mol}^{-1}$.

Temp. / K	K_S	$\ln(K_S)$	$T^{-1} / 10^{-3} \text{ K}^{-1}$
265	0.180	-1.71	3.77
270	0.267	-1.32	3.70
275	0.354	-1.04	3.64
280	0.584	-0.53	3.57
285	0.725	-0.32	3.51

Table 5.3 The effect of temperature on the dissociation equilibrium constant K_S for *cis*-Pt(PCy₃)₂(H)(SiMe₂CH₂CH=CH₂) **16** in [²H₈]toluene.

5.2.4c Standard enthalpy and entropy of reaction for the dissociation of *cis*-Pt(PCy₃)₂(H)(SiMe₂Et) **17** to Pt(PCy₃)₂ and HSiMe₂Et.

An NMR sample of *cis*-Pt(PCy₃)₂(H)(SiMe₂Et) **17** was prepared by adding a slight excess of the silane HSiMe₂Et to a [²H₈]toluene solution of Pt(PCy₃)₂ where the SiH:Pt ratio was 1.06:1.00. Again to prevent thermal decomposition to the *trans* platinum dihydride the NMR sample was prepared at low temperature and kept frozen in liquid nitrogen prior to data collection. Equilibrium constants for dissociation were obtained, as for **15** and **16** (Table 5.4, Figure 5.12), yielding $\Delta H^\circ = 27 \pm 2 \text{ kJ mol}^{-1}$ and $\Delta S^\circ = 94 \pm 7 \text{ J K}^{-1} \text{ mol}^{-1}$.

The standard enthalpies (ΔH°) and standard entropies (ΔS°) of the dissociation of complexes **15-17** are summarised in Table 5.5. The combined van't Hoff plots of complexes **15-17** are in Figure 5.12.

Temp. / K	K_S	$\ln(K_S)$	$T^{-1} / 10^{-3} \text{ K}^{-1}$
250	0.218	-1.52	4.00
255	0.284	-1.26	3.92
260	0.368	-1.00	3.85
265	0.455	-0.79	3.77
270	0.562	-0.58	3.70

Table 5.4 The effect of temperature on the equilibrium constant of dissociation K_S for *cis*-Pt(PCy₃)₂(H)(SiMe₂Et) **17** in [²H₈]toluene.

	$\Delta H^\circ / \text{kJ mol}^{-1}$	$\Delta S^\circ / \text{J K}^{-1} \text{ mol}^{-1}$	$\Delta G^\circ_{300} / \text{kJ mol}^{-1}$
<i>cis</i> -Pt(PCy ₃) ₂ (H)(SiPh ₃) 15	74 ± 10	243 ± 35	2
<i>cis</i> -Pt(PCy ₃) ₂ (H)(SiMe ₂ CH ₂ CH=CH ₂) 16	45 ± 8	155 ± 30	-2
<i>cis</i> -Pt(PCy ₃) ₂ (H)(SiMe ₂ Et) 17	27 ± 2	94 ± 7	-2

Table 5.5 Summary of thermodynamic parameters of the dissociation of *cis*-Pt(PCy₃)₂(H)(SiR₃) in [²H₈]toluene (error bars as 95 % probability on least squares fit).

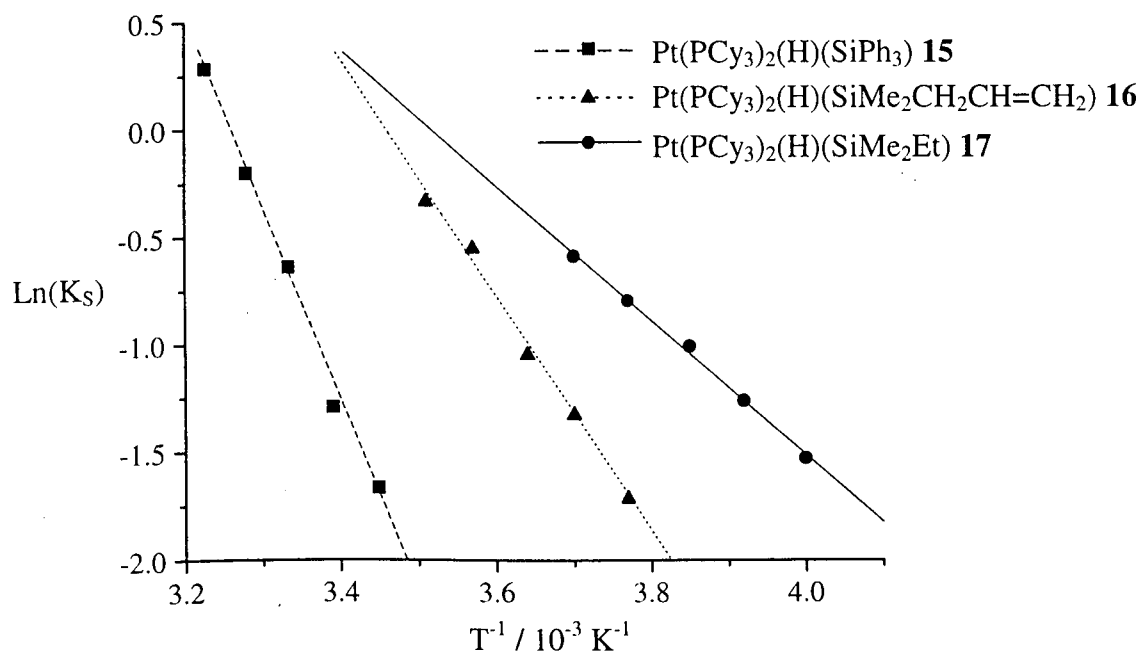


Figure 5.12 Linear plots of $\ln(K_S)$ against T^{-1} for the dissociation of *cis*-Pt(PCy₃)₂(H)(SiR₃) in [²H₈]toluene.

5.2.5 Activation parameters for the dynamic processes of *cis*-Pt(PCy₃)₂(H)(SiR₃) in solution

Using the programme DNMR-SIM, dynamic NMR spectra were calculated for the complex *cis*-Pt(PCy₃)₂(H)(SiR₃). The two dynamic exchange processes simulated were the reversible silane dissociation process (k_1 and k_2) and the mutual phosphine exchange process (k_3) (Scheme 5.4). The DNMR-SIM programme allows for the input of the forward rate constant between each different chemical configurations. Hence the rate of exchange for the two dynamic processes observed in *cis*-Pt(PCy₃)₂(H)(SiR₃) in solution can be extracted from the calculated spectra using DNMR-SIM. Since k_1 , k_2 and k_3 values are a function of temperature, the activation parameters of these dynamic processes, ΔH^\ddagger , ΔS^\ddagger and ΔG^\ddagger_{300} can be calculated using the Eyring equation (Equation 5.3, h = Planck constant, k = Boltzmann constant and R = gas constant).

$$\ln\left(\frac{k}{T}\right) = \ln\left(\frac{k}{h}\right) + \frac{\Delta S^\ddagger}{R} - \frac{\Delta H^\ddagger}{RT} \quad (5.3)$$

5.2.6 DNMR-SIM¹⁶

The programme DNMR-SIM¹⁶ allows for the simulation of dynamic NMR spectra for a system with a maximum total of five different magnetically equivalent groups. The programme consists of four main areas: (a) Main Parameters, (b) Configurations, (c) Rate Constants, (d) Populations for systems which contain non mutual exchange processes or Exchange Vectors for systems which contain purely mutual exchange processes.

5.2.6a Main Parameters

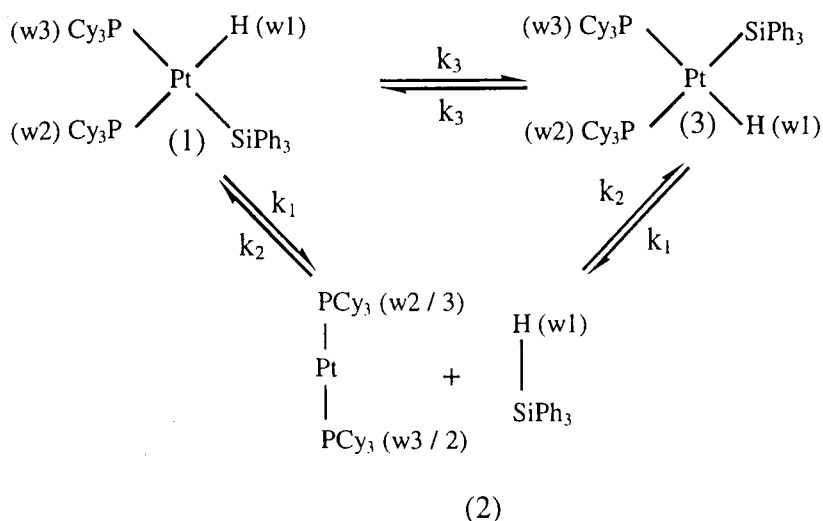
In this section, the first parameter which the programme requires is the maximum number of magnetically equivalent nuclei in the system. For the platinum silyl hydride system, *cis*-Pt(PCy₃)₂(H)(SiR₃), we are only concerned with the hydride ligand which is coupled to the two magnetically inequivalent phosphorus atoms. Couplings to ¹⁹⁵Pt and ²⁹Si are ignored to simplify the situation, so we only examine the dynamic behaviour of the doublet of doublets hydride resonance, and not the ¹⁹⁵Pt satellites. The maximum number of magnetically equivalent nuclei in this case was three.

The next parameter is the number of different chemical configurations in the system. In our proposed mechanism in Scheme 5.4, we have three different chemical configurations. That is two configurations for the silyl and hydride ligand exchange, or phosphine mutual exchange and one configuration for silane dissociation.

The number of data points and the output range of the simulated spectrum are required next. In all our simulations, the number of data points used was 4720 and the range of the simulated spectrum corresponds to 1500 Hz at 500.13 MHz. The programme then asks if the system is undergoing pure mutual exchange. Although we have mutual phosphine exchange present in our system, silane dissociation, which is not a mutual exchange process, is also present. The width at half height is set corresponding to the line width obtained for the hydride spectrum at low temperature at which point there are no fluxional processes apparent.

5.2.6b Configuration

In this section we need to enter the necessary NMR data for each of the three chemical configurations. This is illustrated in Scheme 5.5 and Table 5.6 for *cis*-Pt(PCy₃)₂(H)(SiPh₃) **15**. In configuration 1, (w1), (w2) and (w3) represent the hydride, *trans* and *cis* phosphine ligands in Pt(PCy₃)₂(H)(SiPh₃) **15**, respectively. In configuration 2, (w1) represents the SiH in the free silane, (w2) and (w3) represent the two phosphine ligands in Pt(PCy₃)₂. In configuration 3, (w1), (w2) and (w3) represent the hydride, *cis* and *trans* phosphine ligands in Pt(PCy₃)₂(H)(SiPh₃) (**15**), respectively.



Scheme 5.5 Proposed dynamic exchange processes of *cis*-Pt(PCy₃)₂(H)(SiPh₃). (1), (2) and (3) are the three chemical configurations used in DNMR-SIM. The labels (w1), (w2) and (w3) refer to the labelling system used in DNMR-SIM, see also Table 5.6.

Configuration 1	(w1)	(w2)	(w3)
Chemical Shift (Hz)	-1975.5	-12000.0	-12769.3
$J(w1, \text{Hz})$		141.8	-23.3
$J(w2, \text{Hz})$			13.0

Configuration 2	(w1)	(w2)	(w3)
Chemical Shift (Hz)	2750.7	-15000.0	-15000.0
$J(w1, \text{Hz})$		0.000	0.0
$J(w2, \text{Hz})$			0.0

Configuration 3	(w1)	(w2)	(w3)
Chemical Shift (Hz)	-1975.5	-12769.3	-12000.0
$J(w1, \text{Hz})$		-23.3	141.8
$J(w2, \text{Hz})$			13.0

Table 5.6 Data entries for the chemical configurations in DNMR-SIM. Data shown are for *cis*-Pt(PCy₃)₂(H)(SiPh₃) **15**. See Scheme 5.5 for the labelling of (w1), (w2) and (w3).

5.2.6c Rate Constants

In this section, the estimated forward rate constants between all the specified chemical configurations are entered into the programme. Configuration 1 to configuration 2 is the dissociation of silane (k_1), configuration 1 to configuration 3 is the mutual phosphine exchange (k_3) and configuration 2 to configuration 3 is the addition of silane to Pt(PCy₃)₂ (k_2) (Table 5.7 and Scheme 5.5). Note, k_1 and k_2 are related to the equilibrium constant for silane dissociation, K_S , calculated in Section 5.2.4.

	Configuration 2	Configuration 3
Configuration 1	k_1	k_3
Configuration 2		k_2

Table 5.7 Data entries for the forward rate constant between each chemical configurations in DNMR-SIM. k_1 = silane dissociation. k_2 = silane addition. k_3 = mutual phosphine exchange.

5.2.6d Population Levels

The population levels of all three different chemical configurations are specified in this section. Since configurations 1 and 3 are the same, they will have the same population. The population of 2, at a specific temperature, was calculated from the thermodynamic data obtained in Section 5.2.4.

5.2.6e Comparison between simulated and observed spectra.

The output of the simulated spectra from DNMR-SIM were compared against the observed spectra graphically using the spreadsheet package Origin.²⁰ Rate constants k_1 , k_2 and k_3 are adjusted in order to obtain the best fit between the simulated spectrum and the observed spectrum. This procedure was repeated for all the observed dynamic ^1H NMR spectra of complexes **15-17**.

5.2.7 Simulation of dynamic NMR spectra

5.2.7a Simulations of the dynamic NMR spectra of *cis*-Pt(PCy₃)₂(H)(SiPh₃) **15**

^1H NMR spectra of complex **15** were obtained from 285 K to 315 K in [$^2\text{H}_8$]toluene. The hydride spectra for complex **15** were then calculated using DNMR-SIM with the aim to match the observed spectra by varying the rate constants k_1 , k_2 and k_3 as described in Section 5.2.6. Figure 5.13 shows the results obtained from the dynamic NMR spectra simulation programme DNMR-SIM. Rate constants were calculated as for a first-order process since different concentrations of silane did not affect the line shape of the hydride resonance in the dynamic ^1H NMR spectra.

The rate constants k_1 were calculated between the temperature range of 280 K to 315 K (Table 5.8). The Eyring plot of $\ln(k_1 / T)$ against T^{-1} yielded a straight line (Figure 5.14) with activation parameters $\Delta H^\ddagger_{k_1} = 106 \pm 5 \text{ kJ mol}^{-1}$, $\Delta S^\ddagger_{k_1} = 123 \pm 15 \text{ J mol}^{-1} \text{ K}^{-1}$ and $\Delta G^\ddagger_{300(k_1)} = 70 \text{ kJ mol}^{-1}$.

The rate constants k_2 were calculated for the temperature range of 300 K to 315 K (Table 5.9). The Eyring plot of $\ln(k_2 / T)$ against T^{-1} yielded a straight line (Figure 5.15) with activation parameters $\Delta H^\ddagger_{k_2} = 32 \pm 4 \text{ kJ mol}^{-1}$, $\Delta S^\ddagger_{k_2} = -121 \pm 14 \text{ J mol}^{-1} \text{ K}^{-1}$ and $\Delta G^\ddagger_{300(k_2)} = 68 \text{ kJ mol}^{-1}$.

The rate constants k_3 were calculated for the temperature range 300 K to 315 K (Table 5.10). The Eyring plot of $\ln(k_3 / T)$ against T^{-1} yielded a straight line (Figure 5.16) with activation parameters $\Delta H^\ddagger_{k_3} = 73 \pm 3 \text{ kJ mol}^{-1}$, $\Delta S^\ddagger_{k_3} = 29 \pm 9 \text{ J mol}^{-1} \text{ K}^{-1}$ and $\Delta G^\ddagger_{300(k_3)} = 64 \text{ kJ mol}^{-1}$. All error bars represent 95 % probability for a least squares fit.

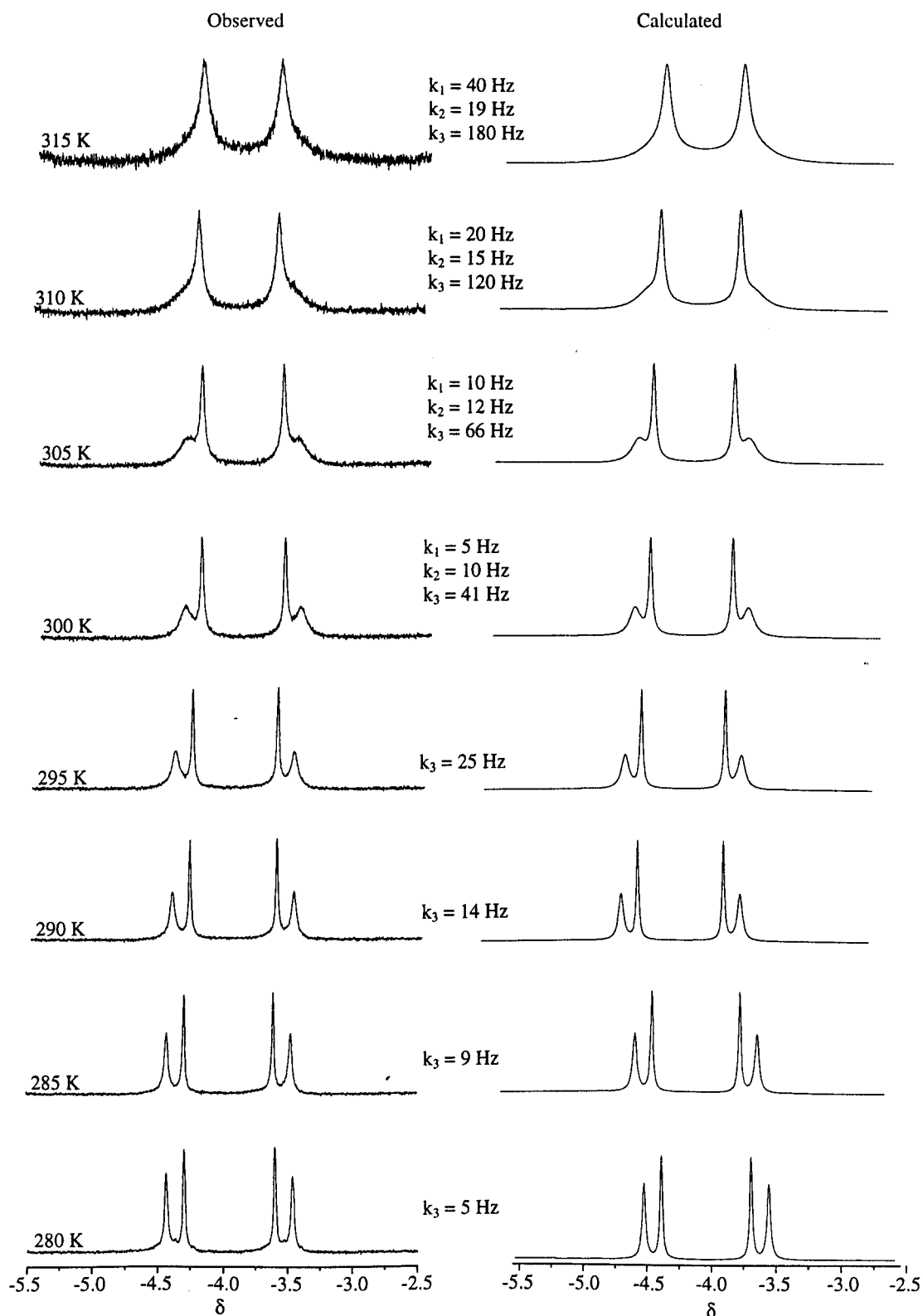


Figure 5.13 Observed and calculated 500.13 MHz ^1H hydride NMR spectra of *cis*- $\text{Pt}(\text{PCy}_3)_2(\text{H})(\text{SiPh}_3)$ **15** as a function of temperature. k_1 = silane dissociation, k_2 = silane addition and k_3 = mutual phosphine exchange.

Temp. / K	k_1 / s^{-1}	$\ln(k_1 / T)$	$T^{-1} / 10^{-3} \text{ K}^{-1}$
300	5	-4.09	3.33
305	10	-3.42	3.28
310	20	-2.74	3.23
315	40	-2.06	3.17

Table 5.8 The effect of temperature on the rate of silane dissociation, k_1 , for *cis*-Pt(PCy₃)₂(H)(SiPh₃) **15** in [²H₈]toluene.

Temp. / K	k_2 / s^{-1}	$\ln(k_2 / T)$	$T^{-1} / 10^{-3} \text{ K}^{-1}$
300	10	-3.40	3.33
305	12	-3.24	3.28
310	15	-3.03	3.23
315	19	-2.81	3.17

Table 5.9 The effect of temperature on the rate of silane addition, k_2 , for *cis*-Pt(PCy₃)₂(H)(SiPh₃) **15** in [²H₈]toluene.

Temp. / K	k_3 / s^{-1}	$\ln(k_3 / T)$	$T^{-1} / 10^{-3} \text{ K}^{-1}$
280	5	-4.13	3.57
285	9	-3.46	3.51
290	14	-3.03	3.45
295	25	-2.46	3.39
300	41	-1.99	3.33
305	66	-1.53	3.28
310	120	-0.95	3.23
315	180	-0.56	3.17

Table 5.10 The effect of temperature on the rate of mutual phosphine exchange, k_3 , for *cis*-Pt(PCy₃)₂(H)(SiPh₃) **15** in [²H₈]toluene.

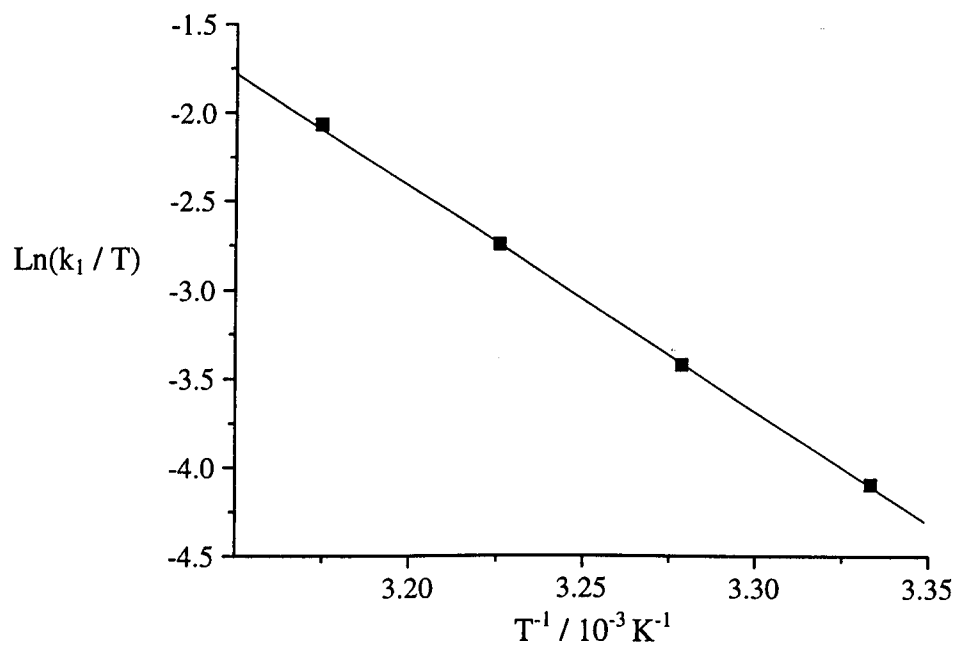


Figure 5.14 Eyring plot showing the temperature dependence of the rate of silane dissociation, k_1 , for *cis*-Pt(PCy₃)₂(H)(SiPh₃) **15** in [²H₈]toluene.

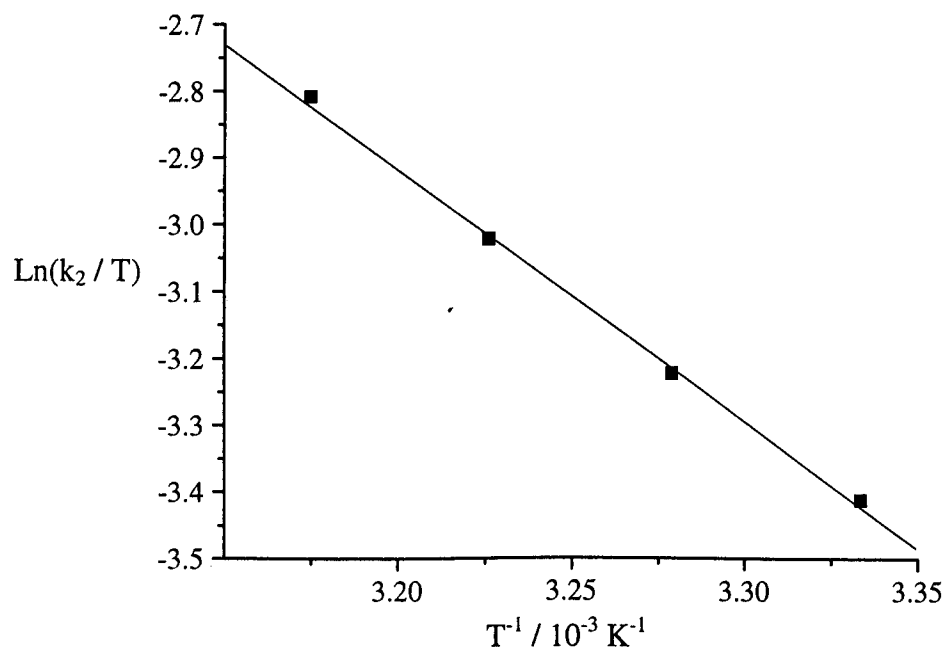


Figure 5.15 Eyring plot showing the temperature dependence of the rate silane addition, k_2 , for *cis*-Pt(PCy₃)₂(H)(SiPh₃) **15** in [²H₈]toluene.

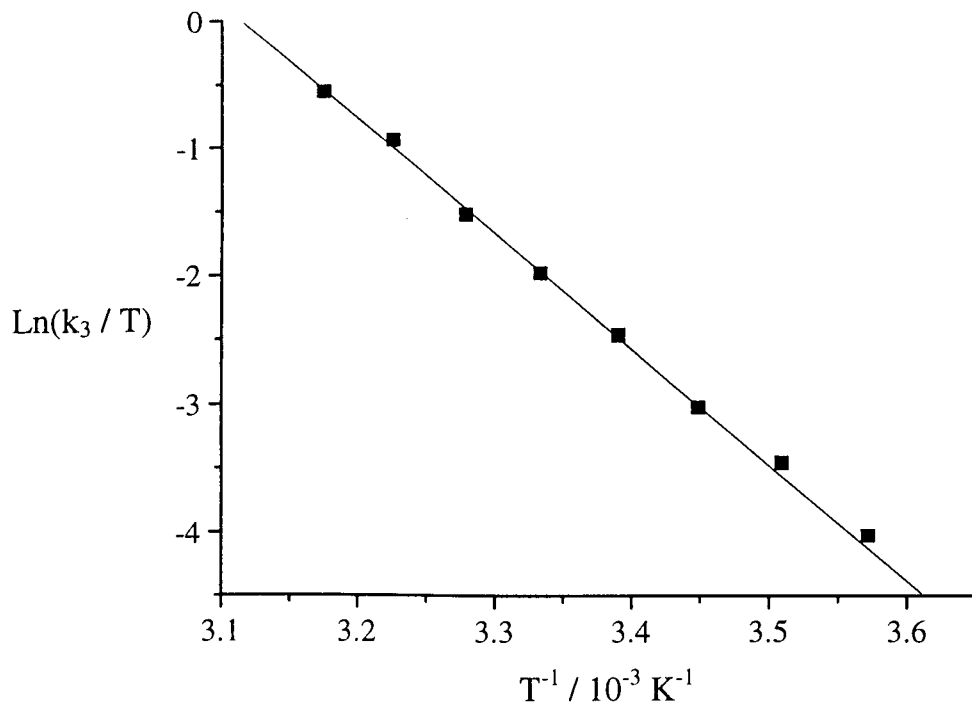


Figure 5.16 Eyring plot showing the temperature dependence of the rate of silane addition, k_3 , for *cis*-Pt(PCy₃)₂(H)(SiPh₃) **15** in [²H₈]toluene.

5.2.7b Simulations of the dynamic NMR spectra of *cis*-Pt(PCy₃)₂(H)-(SiMe₂CH₂CH=CH₂) **16**

¹H NMR spectra of **16** were recorded for temperatures from 255 K to 300 K in [²H₈]toluene. The rate constants k_1 , k_2 and k_3 were calculated as for **15** using DNMR-SIM.

The activation parameters for silane dissociation, k_1 (Table 5.11), were calculated as $\Delta H^\ddagger_{k_1} = 99 \pm 9 \text{ kJ mol}^{-1}$, $\Delta S^\ddagger_{k_1} = 124 \pm 32 \text{ J mol}^{-1} \text{ K}^{-1}$ and $\Delta G^\ddagger_{300(k_1)} = 61 \text{ kJ mol}^{-1}$.

The activation parameters for silane addition, k_2 (Table 5.12), were calculated as $\Delta H^\ddagger_{k_2} = 50 \pm 5 \text{ kJ mol}^{-1}$, $\Delta S^\ddagger_{k_2} = -42 \pm 16 \text{ J mol}^{-1} \text{ K}^{-1}$ and $\Delta G^\ddagger_{300(k_2)} = 63 \text{ kJ mol}^{-1}$.

The activation parameters for mutual phosphine exchange, k_3 (Table 5.13), were calculated as $\Delta H^\ddagger_{k_3} = 69 \pm 2 \text{ kJ mol}^{-1}$, $\Delta S^\ddagger_{k_3} = 40 \pm 7 \text{ J mol}^{-1} \text{ K}^{-1}$ and $\Delta G^\ddagger_{300(k_3)} = 58 \text{ kJ mol}^{-1}$.

Temp. / K	k_1 / s^{-1}	$\ln(k_1 / T)$	$T^{-1} / 10^{-3} \text{ K}^{-1}$
280	7	-3.68	3.57
285	15	-2.94	3.51
290	30	-2.27	3.45
295	70	-1.44	3.39
300	120	-0.92	3.33

Table 5.11 The effect of temperature on the rate of silane dissociation, k_1 , for *cis*-Pt(PCy₃)₂(H)(SiMe₂CH₂CH=CH₂) **16** in [²H₈]toluene.

Temp. / K	k_2 / s^{-1}	$\ln(k_2 / T)$	$T^{-1} / 10^{-3} \text{ K}^{-1}$
280	13	-3.07	3.57
285	20	-2.66	3.51
290	29	-2.30	3.45
295	40	-2.00	3.39
300	62	-1.58	3.33

Table 5.12 The effect of temperature on the rate of silane addition, k_2 , for *cis*-Pt(PCy₃)₂(H)(SiMe₂CH₂CH=CH₂) **16** in [²H₈]toluene.

Temp. / K	k_3 / s^{-1}	$\ln(k_3 / T)$	$T^{-1} / 10^{-3} \text{ K}^{-1}$
255	3	-4.44	3.92
260	6	-3.77	3.85
265	10	-3.27	3.77
270	20	-2.60	3.70
275	33	-2.12	3.64
280	58	-1.57	3.57
285	100	-1.05	3.51
290	200	-0.37	3.45
295	300	0.02	3.39
300	490	0.49	3.33

Table 5.13 The effect of temperature on the rate of mutual phosphine exchange, k_3 , for *cis*-Pt(PCy₃)₂(H)(SiMe₂CH₂CH=CH₂) **16** in [²H₈]toluene.

5.2.7c Simulations of the dynamic NMR spectra of *cis*-Pt(PCy₃)₂(H)(SiMe₂Et) **17**

¹H NMR spectra of **17** were recorded for temperatures ranging from 240 K to 300 K in [²H₈]toluene. The rate constants k_1 , k_2 and k_3 were calculated as for **15** and **16** using DNMR-SIM. Figure 5.17 shows the observed and the calculated variable temperature ³¹P {¹H} NMR spectra of **17**. The calculated spectra in Figure 5.19 were simulated using DNMR-SIM. The rate constants k_1 , k_2 and k_3 , obtained from the ¹H NMR spectra of **17**, were used without change for the simulation of the ³¹P {¹H} NMR spectra.

The activation parameters for silane dissociation, k_1 (Table 5.14), were calculated as $\Delta H^\ddagger_{k_1} = 100 \pm 11 \text{ kJ mol}^{-1}$, $\Delta S^\ddagger_{k_1} = 142 \pm 38 \text{ J mol}^{-1} \text{ K}^{-1}$ and $\Delta G^\ddagger_{300(k_1)} = 57 \text{ kJ mol}^{-1}$.

The activation parameters for silane addition, k_2 (Table 5.15), were calculated as $\Delta H^\ddagger_{k_2} = 74 \pm 11 \text{ kJ mol}^{-1}$, $\Delta S^\ddagger_{k_2} = 49 \pm 39 \text{ J mol}^{-1} \text{ K}^{-1}$ and $\Delta G^\ddagger_{300(k_2)} = 59 \text{ kJ mol}^{-1}$.

The activation parameters for mutual phosphine exchange, k_3 (Table 5.16), were calculated as $\Delta H^\ddagger_{k_3} = 66 \pm 2 \text{ kJ mol}^{-1}$, $\Delta S^\ddagger_{k_3} = 33 \pm 7 \text{ J mol}^{-1} \text{ K}^{-1}$ and $\Delta G^\ddagger_{300(k_3)} = 56 \text{ kJ mol}^{-1}$.

Summaries of the activation parameters of **15-17** can be found in Tables 5.17-5.19 and Figures 5.18-5.20.

Temp. / K	k_1 / s^{-1}	$\ln(k_1 / T)$	$T^{-1} / 10^{-3} \text{ K}^{-1}$
270	6	-3.81	3.70
278	25	-2.41	3.60
280	38	-2.00	3.57
283	57	-1.60	3.53
288	110	-0.96	3.47
290	140	-0.73	3.45

Table 5.14 The effect of temperature on the rate of free silane exchange, k_1 , for *cis*-Pt(PCy₃)₂(H)(SiMe₂Et) **17** in [²H₈]toluene.

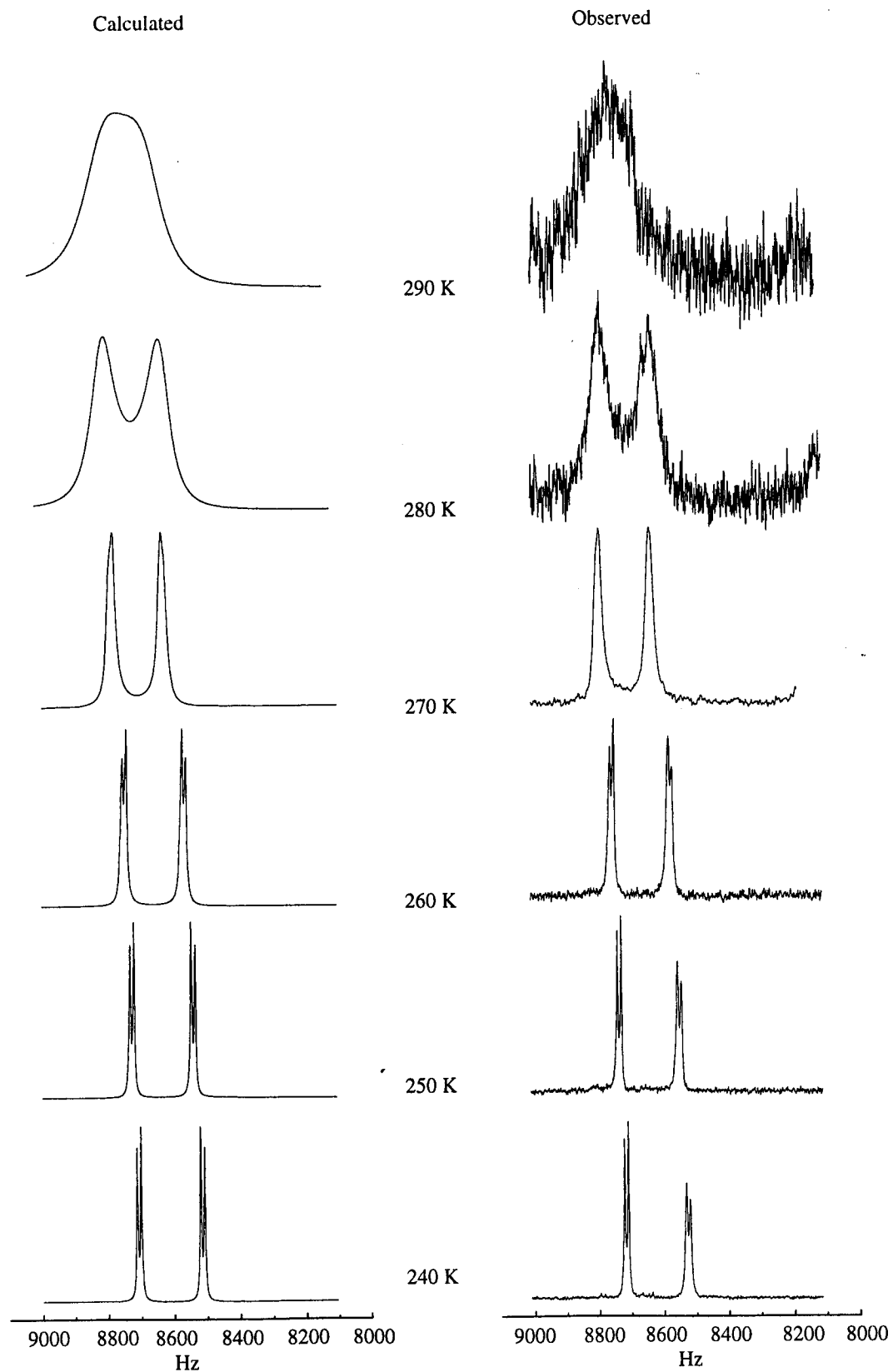


Figure 5.17 Selected calculated and observed 202.46 MHz ^{31}P $\{^1\text{H}\}$ NMR spectra of *cis*-Pt(PCy₃)₂(H)(SiMe₂CH₂CH=CH₂) **17** as a function of temperature.

Temp. / K	k_2 / s^{-1}	$\ln (k_2 / T)$	$T^{-1} / 10^{-3} \text{ K}^{-1}$
270	11	-3.20	3.70
278	31	-2.19	3.60
280	44	-1.85	3.57
283	58	-1.59	3.53
288	92	-1.14	3.47
290	108	-0.98	3.45

Table 5.15 The effect of temperature on the rate of silane addition, k_2 , for *cis*-Pt(PCy₃)₂(H)(SiMe₂Et) **17** in [²H₈]toluene.

Temp. / K	k_3 / s^{-1}	$\ln (k_3 / T)$	$T^{-1} / 10^{-3} \text{ K}^{-1}$
240	1	-5.48	4.17
250	4	-4.24	4.00
260	14	-2.92	3.85
270	43	-1.84	3.70
273	53	-1.64	3.66
278	105	-0.97	3.60
280	140	-0.69	3.57
283	190	-0.40	3.53
288	300	0.04	3.47
290	380	0.27	3.45

Table 5.16 The effect of temperature on the rate of mutual phosphine exchange, k_3 , for *cis*-Pt(PCy₃)₂(H)(SiMe₂Et) **17** in [²H₈]toluene.

	$\Delta H^\ddagger_{k_1} /$ kJ mol^{-1}	$\Delta S^\ddagger_{k_1} /$ $\text{J K}^{-1} \text{mol}^{-1}$	$\Delta G^\ddagger_{300(k_1)} /$ kJ mol^{-1}
<i>cis</i> -Pt(PCy ₃) ₂ (H)(SiPh ₃) 15	106 ± 5	123 ± 15	70
<i>cis</i> -Pt(PCy ₃) ₂ (H)(SiMe ₂ CH ₂ CH=CH ₂) 16	99 ± 9	124 ± 32	61
<i>cis</i> -Pt(PCy ₃) ₂ (H)(SiMe ₂ Et) 17	100 ± 11	142 ± 38	57

Table 5.17 Activation parameters for silane dissociation, k_1 , in *cis*-Pt(PCy₃)₂(H)(SiPh₃) **15**, *cis*-Pt(PCy₃)₂(H)(SiMe₂CH₂CH=CH₂) **16** and *cis*-Pt(PCy₃)₂(H)(SiMe₂Et) **17** in [²H₈]toluene. (Error bars quoted as 95 % probability on least squares fit).

	$\Delta H^\ddagger_{k_2} /$ kJ mol^{-1}	$\Delta S^\ddagger_{k_2} /$ $\text{J K}^{-1} \text{mol}^{-1}$	$\Delta G^\ddagger_{300(k_2)} /$ kJ mol^{-1}
<i>cis</i> -Pt(PCy ₃) ₂ (H)(SiPh ₃) 15	32 ± 12	-121 ± 14	68
<i>cis</i> -Pt(PCy ₃) ₂ (H)(SiMe ₂ CH ₂ CH=CH ₂) 16	50 ± 5	-42 ± 16	63
<i>cis</i> -Pt(PCy ₃) ₂ (H)(SiMe ₂ Et) 17	74 ± 11	49 ± 39	59

Table 5.18 Activation parameters for silane addition, k_2 , in *cis*-Pt(PCy₃)₂(H)(SiPh₃) **15**, *cis*-Pt(PCy₃)₂(H)(SiMe₂CH₂CH=CH₂) **16** and *cis*-Pt(PCy₃)₂(H)(SiMe₂Et) **17** in [²H₈]toluene (Error bars quoted as 95 % probability on least squares fit).

	$\Delta H^\ddagger_{k_3} /$ kJ mol^{-1}	$\Delta S^\ddagger_{k_3} /$ $\text{J K}^{-1} \text{mol}^{-1}$	$\Delta G^\ddagger_{300(k_3)} /$ kJ mol^{-1}
<i>cis</i> -Pt(PCy ₃) ₂ (H)(SiPh ₃) 15	73 ± 3	29 ± 9	64
<i>cis</i> -Pt(PCy ₃) ₂ (H)(SiMe ₂ CH ₂ CH=CH ₂) 16	69 ± 2	40 ± 7	58
<i>cis</i> -Pt(PCy ₃) ₂ (H)(SiMe ₂ Et) 17	66 ± 2	33 ± 7	56

Table 5.19 Activation parameters for mutual phosphine exchange, k_3 , in *cis*-Pt(PCy₃)₂(H)(SiPh₃) **15**, *cis*-Pt(PCy₃)₂(H)(SiMe₂CH₂CH=CH₂) **16** and *cis*-Pt(PCy₃)₂(H)(SiMe₂Et) **17** in [²H₈]toluene (Error bars quoted as 95 % probability on least squares fit).

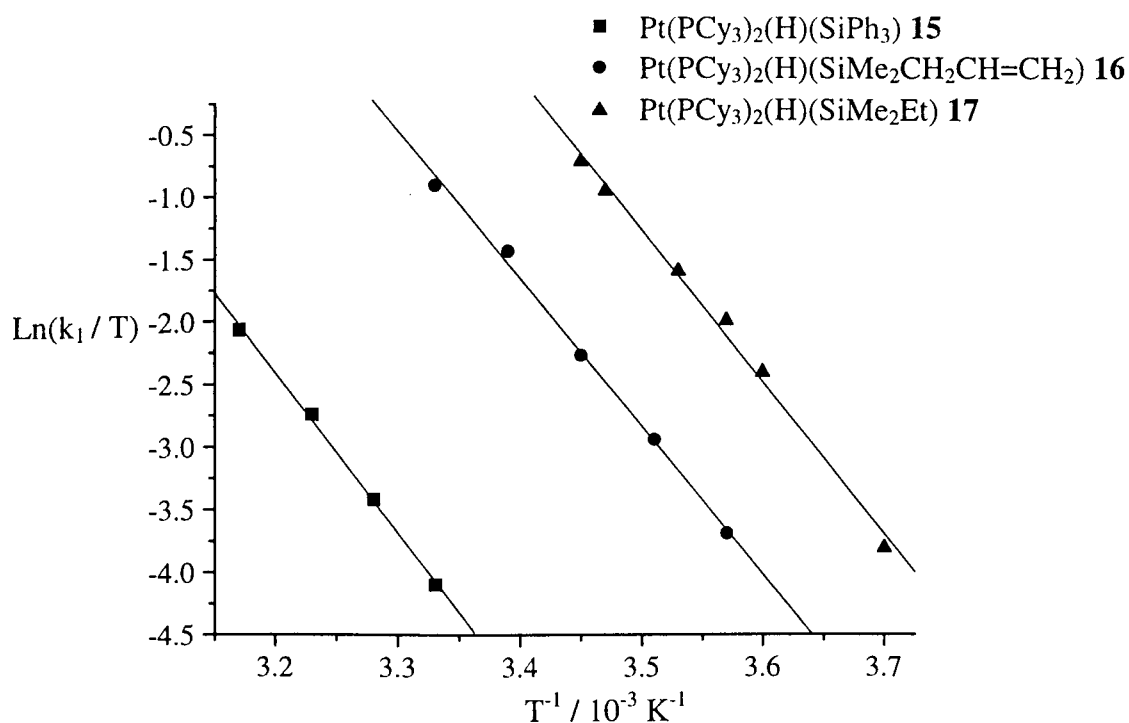


Figure 5.18 Eyring plots showing the temperature dependence of the rate of silane dissociation, k_1 , of *cis*-Pt(PCy₃)₂(H)(SiR₃) in [²H₈]toluene.

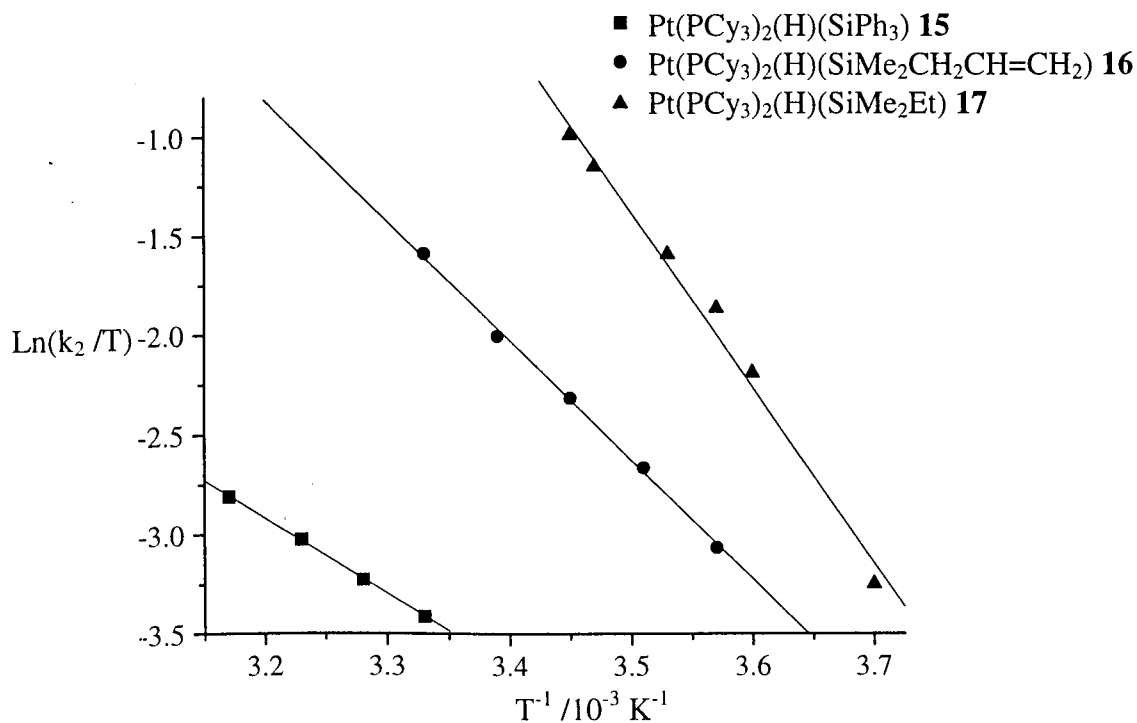


Figure 5.19 Eyring plots showing the temperature dependence of the rate of silane addition, k_2 , of *cis*-Pt(PCy₃)₂(H)(SiR₃) in [²H₈]toluene.

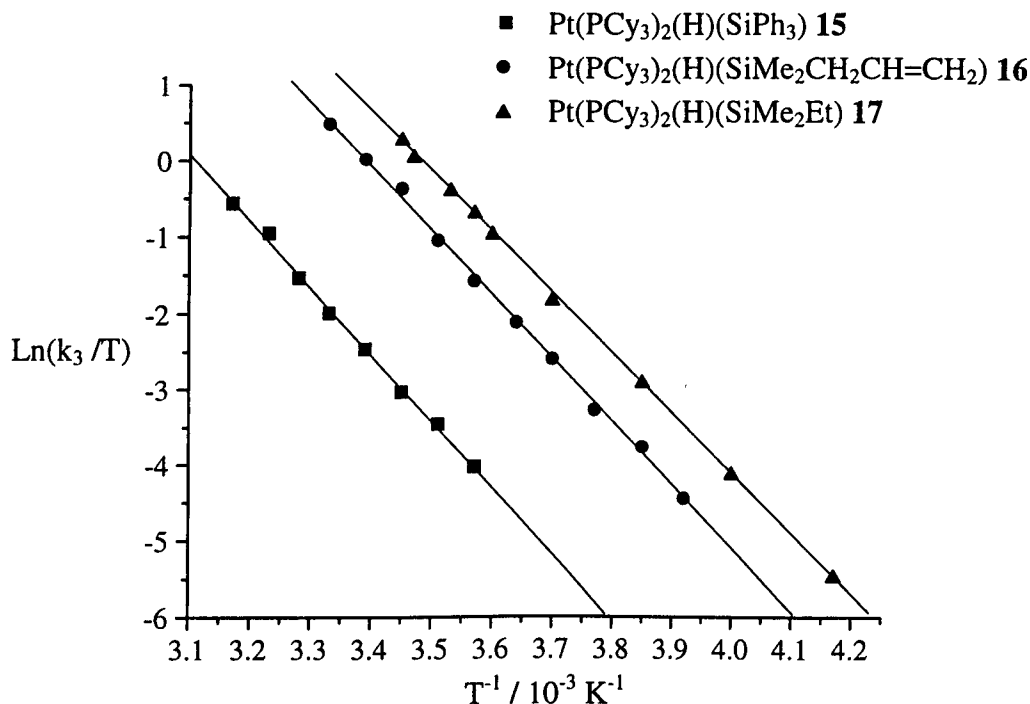


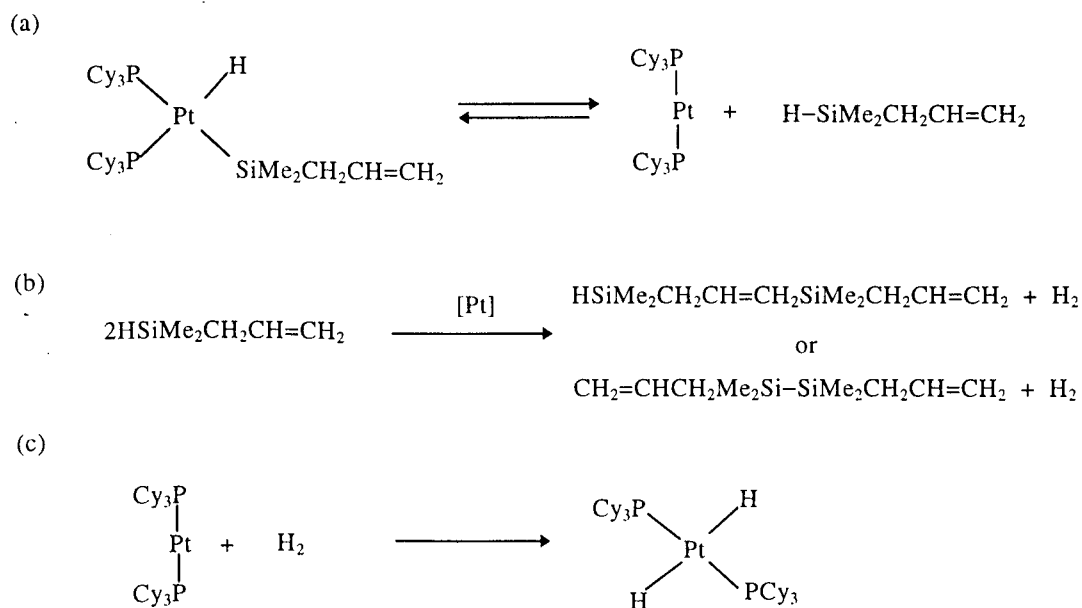
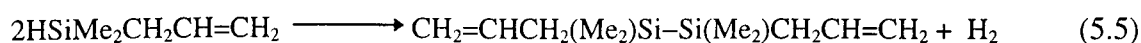
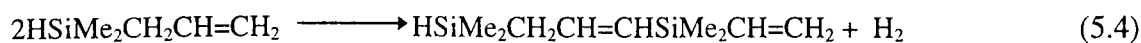
Figure 5.20 Eyring plots showing the temperature dependence of the rate of mutual phosphine exchange, k_3 , of *cis*-Pt(PCy₃)₂(H)(SiR₃) in [²H₈]toluene.

5.2.8 Thermal reactions of *cis*-Pt(PCy₃)₂(H)(SiR₃)

As mentioned previously, the complex *cis*-Pt(PCy₃)₂(H)(SiR₃) degrades thermally in solution to form *trans*-Pt(PCy₃)₂(H)₂. The *trans*-platinum dihydride complex itself does not react with the tertiary silanes used in this investigation at room temperature. Interestingly, Ebsworth has reported that *trans*-Pt(PCy₃)₂(H)₂ reacts with SiH₄ or SiClH₃ to give the corresponding *trans*-platinum silyl hydride complex.²¹ The identification of the organosilane thermal decomposition product would allow us to determine the most plausible mechanism for this thermal degradation process.

The complex *cis*-Pt(PCy₃)₂(H)(SiMe₂CH₂CH=CH₂) **16** was used to identify the organosilane products formed on thermal decomposition to *trans*-Pt(PCy₃)₂(H)₂. Complex **16** was dissolved in C₆D₆ under an argon atmosphere and then immediately analysed by GC. A peak is observed from the chromatograph corresponding to the presence of the silane HSiMe₂CH₂CH=CH₂. The free silane peak gradually disappeared over 30 minutes and three new peaks were eventually formed with retention times of 7.2 minutes, 19.0 minutes and 33.9 minutes (for GC conditions see experimental section 6.5). The long retention time observed for the final peak at 33.9 minutes would suggest that oligomeric silanes are being produced. GC-MS analysis of the three peaks did not, however, reveal clearly the type of organosilane products formed on thermal

decomposition of **16**. Nevertheless, the GC-MS of the organosilane with a retention time of 19.0 minutes did show a mass peak at $m/z = 198$ which could correspond to the dehydrogenative silation³ or dehydrosilyl coupling⁵ of two allyldimethylsilane molecules (Equation 5.4 and 5.5). In either case, molecular hydrogen is formed and can react with $\text{Pt}(\text{PCy}_3)_2$ to form $\text{trans-Pt}(\text{PCy}_3)_2(\text{H})_2$, the thermal decomposition product of **16** (Scheme 5.6). We have also found that addition of hydrogen (1 atm) to an NMR sample **16** in C_6D_6 at room temperature yielded $\text{trans-Pt}(\text{PCy}_3)_2(\text{H})_2$ and signals due to dissolved H_2 were not detected in the ^1H NMR spectrum. This indicates that H_2 reacts readily with **16** to form $\text{trans-Pt}(\text{PCy}_3)_2(\text{H})_2$.



Scheme 5.6 Possible processes responsible for the thermal decomposition of *cis*- $\text{Pt}(\text{PCy}_3)_2(\text{H})(\text{SiMe}_2\text{CH}_2\text{CH}=\text{CH}_2)$ **16** to *trans*- $\text{Pt}(\text{PCy}_3)_2(\text{H})_2$.

5.2.9 Photochemical reactions of *cis*-Pt(PCy₃)₂(H)(SiR₃)

Clark *et al.* found that the complex *cis*-Pt(PCy₃)₂(H)(SiPh₃) **15** undergoes quantitative *cis*-*trans* isomerisation when irradiated by a weak UV source to yield *trans*-Pt(PCy₃)₂(H)(SiPh₃) **21**. However, no characterisation was reported for this complex.¹¹ In our studies we have found that the complexes *cis*-Pt(PCy₃)₂(H)(SiMe₂CH₂CH=CH₂) **16** and *cis*-Pt(PCy₃)₂(H)(SiMe₂Et) **17** can also undergo *cis*-*trans* isomerisation when photolysed with UV light at 250 K to form *trans*-Pt(PCy₃)₂(H)(SiMe₂CH₂CH=CH₂) **22** and *trans*-Pt(PCy₃)₂(H)(SiMe₂Et) **23** respectively. For comparison, the *cis*-*trans* photo isomerisation of **15** was also studied. This isomerisation process proceeded at room temperature but thermal decomposition to *trans*-Pt(PCy₃)₂(H)₂ was also observed.

Figure 5.21 (i) shows the ¹H NMR spectrum of **16** after 4 hours photolysis at -78 °C. Here the new triplet resonance of the *trans* isomer **22** was observed at δ -2.64 [²J(PH) = 18.1 Hz, J(PtH) = 561.3 Hz]. On warming the sample to 300 K [Figure 5.24 (ii)] complex **16** thermally decomposes to *trans*-Pt(PCy₃)₂(H)₂. In contrast the *trans* isomer **22** was thermally stable at this temperature. Table 5.20 summarises some selected NMR data for *trans*-Pt(PCy₃)₂(H)(SiPh₃) **21**, *trans*-Pt(PCy₃)₂(H)(SiMe₂CH₂CH=CH₂) **22** and *trans*-Pt(PCy₃)₂(H)(SiMe₂Et) **23** as formed by photolysis of the corresponding *cis*-isomer.

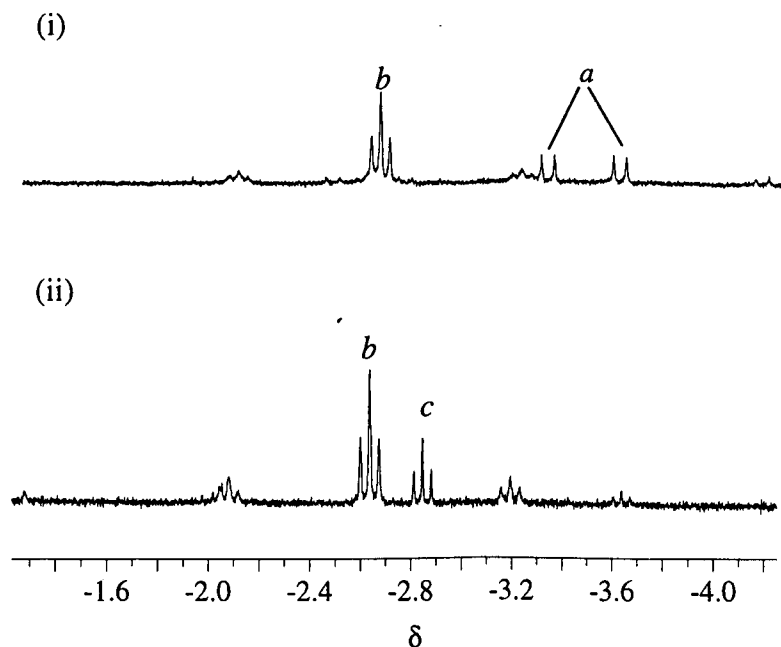


Figure 5.21 ¹H NMR spectrum (500.13 Mhz) of *cis*-(PCy₃)₂(H)(SiMe₂CH₂CH=CH₂) **16** in [²H₈]toluene after 4 hours photolysis at -78 °C. Only the hydride regions are shown. (i) at 250 K. (ii) at 300 K. *a* Complex **16**. *b* *trans*-Pt(PCy₃)₂(H)-(SiMe₂CH₂CH=CH₂) **22**. *c* *trans*-Pt(PCy₃)₂(H)₂.

	^1H , δ (J / Hz)	^{31}P { ^1H }, δ (J / Hz)
21^a	-3.00 [t, Pt- <u>H</u> , $^2J(\text{PH}) = 16.6$, $J(\text{PtH}) = 584.2$]	37.5 [s, $J(\text{PtP}) = 2656$]
22^a	-2.64 [t, Pt- <u>H</u> , $^2J(\text{PH}) = 18.1$, $J(\text{PtH}) = 561.3$]	43.5 [s, $J(\text{PtP}) = 2747$]
23^b	-2.85 [t, Pt- <u>H</u> , $^2J(\text{PH}) = 18.5$, $J(\text{PtH}) = 552.1$]	43.4 [s, $J(\text{PtP}) = 2772$]

Table 5.20 Selected ^1H (500.13 MHz) and ^{31}P { ^1H } (202.46 MHz) NMR data of complexes **21-23**. *a* in [$^2\text{H}_8$]toluene at 250 K. *b* in C_6D_6 at 300 K.

5.2.9a Photolysis of *trans*-Pt(PCy₃)₂(H)₂ with HSiR₃

As mentioned previously, the complex *trans*-Pt(PCy₃)₂(H)₂ does not appear to react thermally with the tertiary silanes studied. However, low temperature photolysis of *trans*-Pt(PCy₃)₂(H)₂ with HSiPh₃ yielded *trans*-Pt(PCy₃)₂(H)(SiPh₃) **21**. Complete conversion was not achieved possibly due to insufficient photolysis time (Figure 5.22).

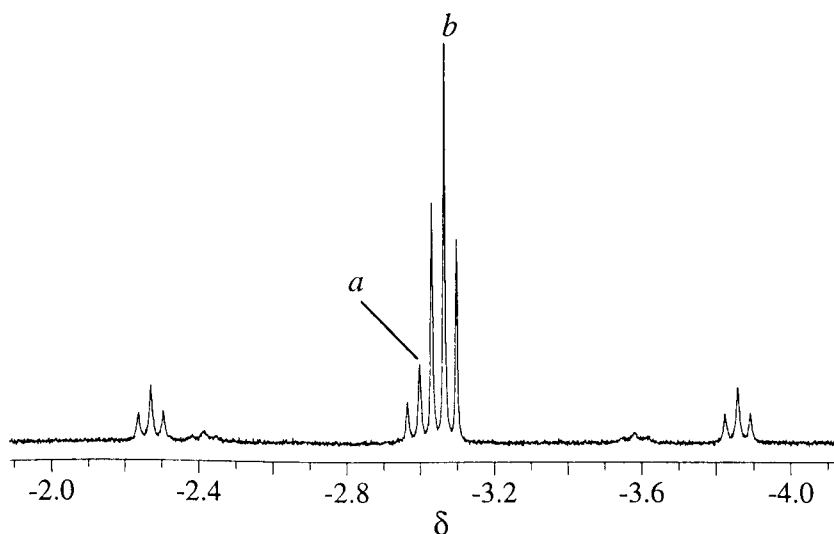


Figure 5.22 ^1H (500.13 MHz) NMR spectrum of *trans*-Pt(PCy₃)₂(H)₂ with HSiPh₃ in [$^2\text{H}_8$]toluene after 3 hours photolysis at -77°C . Only the hydride region is shown. *a* *trans*-Pt(PCy₃)₂(H)(SiPh₃). *b* *trans*-Pt(PCy₃)₂(H)₂.

Photolysis of an NMR sample of *trans*-Pt(PCy₃)₂(H)₂ with HSiMe₂Et in C_6D_6 at room temperature formed *trans*-Pt(PCy₃)₂(H)(SiMe₂Et) **23** in very low yield (Figure 5.23). The *cis*-platinum silyl hydride **17** was detected when an NMR sample of *trans*-Pt(PCy₃)₂(H)₂ and HSiMe₂Et in [$^2\text{H}_8$]toluene are photolysed *in situ* in the NMR spectrometer at 250 K (Figure 5.24).

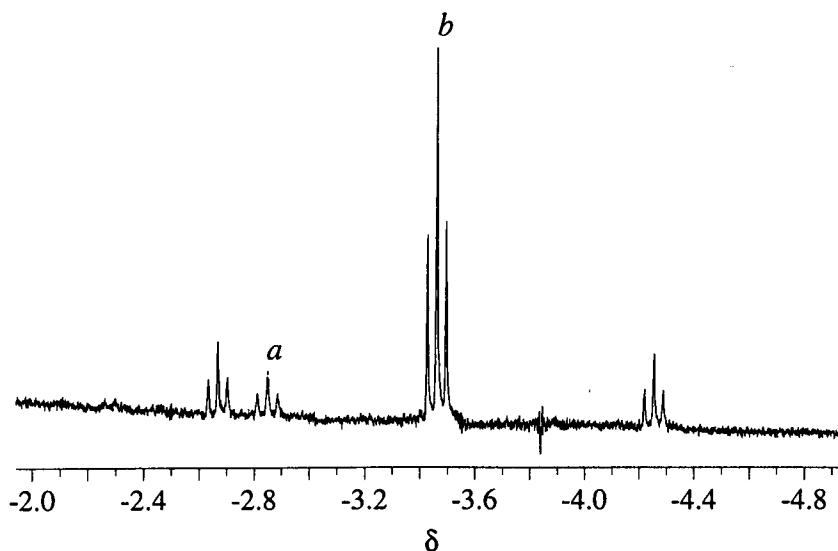


Figure 5.23 ^1H (500.13 MHz, 300 K) NMR spectrum of *trans*-Pt(PCy₃)₂(H)₂ with excess HSiMe₂Et in C₆D₆ after 1 day photolysis at room temperature (only the hydride region is shown). *a* *trans*-Pt(PCy₃)₂(H)(SiMe₂Et) **23**. *b* *trans*-Pt(PCy₃)₂(H)₂.

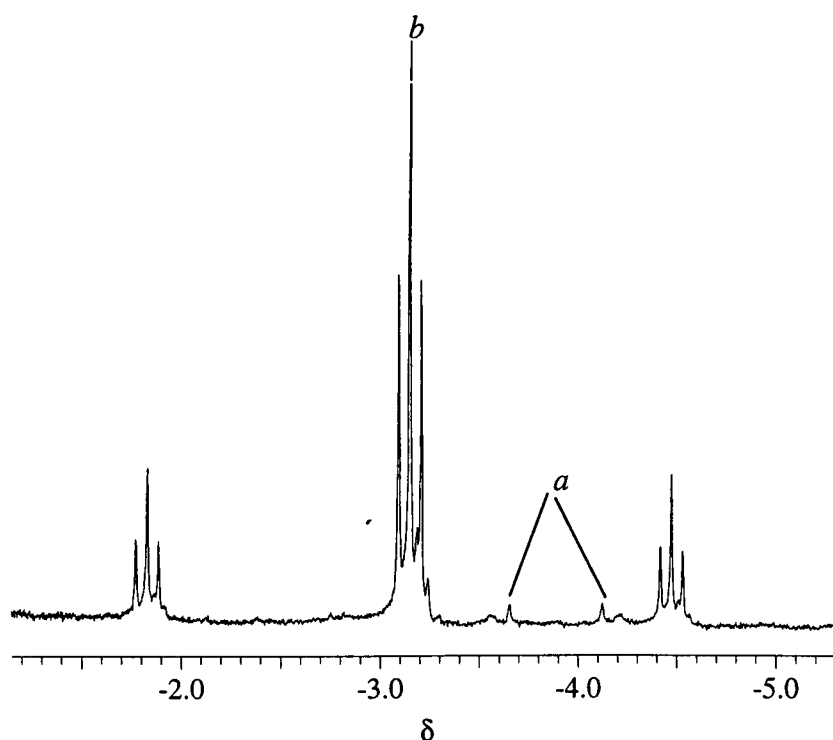


Figure 5.24 ^1H (300.13 MHz, 250 K) NMR spectrum of *trans*-Pt(PCy₃)₂(H)₂ with excess HSiMe₂Et in [²H₈]toluene after 1 hour *in-situ* photolysis (only the hydride region is shown). *a* *cis*-Pt(PCy₃)₂(H)(SiMe₂Et) **17**. *b* *trans*-Pt(PCy₃)₂(H)₂.

The initial appearance of *cis*-Pt(PCy₃)₂(H)(SiMe₂Et) **17** from the photolysis of *trans*-Pt(PCy₃)₂(H)₂ indicates that **17** is the complex formed in the first instance when *trans*-Pt(PCy₃)₂(H)₂ is photolysed with HSiMe₂Et. The *cis*-platinum silyl hydride **17** then proceeds to isomerise to the *trans*-isomer **23** on further UV irradiation.

5.2.10 Reaction of Pt(PCy₃)₂ with disilanes

Eaborn *et al.* have previously reported that reaction of Pt(PPh₃)₂(C₂H₄) with (HPh₂Si)₂O or HMe₂Si(C₆H₄)SiMe₂H at 45 °C yields the metallacyclic complexes Pt(PPh₃)₂(SiPh₂OSiPh₂) or Pt(PPh₃)₂[SiMe₂(C₆H₄)SiMe₂].²² Their evidence for this product was based upon elemental analysis (C, H) and the absence of $\nu(\text{Pt-H})$ at *ca.* 2100 cm⁻¹ in the IR spectrum.

In our studies, similar reactions between Pt(PCy₃)₂ and the disilanes (HPh₂Si)₂O and HMe₂Si(C₆H₄)SiMe₂H was carried out. NMR data of the product formed between Pt(PCy₃)₂ and (HPh₂Si)₂O show a doublet of doublets hydride resonance with ¹⁹⁵Pt satellites in the ¹H NMR spectrum and two inequivalent doublet resonances, again with ¹⁹⁵Pt satellites, in the ³¹P {¹H} NMR spectrum. The ¹H NMR spectrum also shows a singlet resonance at δ 6.06 which is close to the Si-H resonance of the free disilane. These features indicate that only one of the two Si-H bonds on the disilane has been oxidatively added to the platinum metal centre to form *cis*-Pt(PCy₃)₂(H)(SiPh₂OSiPh₂H) **20**. The four-membered cyclic disilyl complex Pt(PCy₃)₂(SiPh₂OSiPh₂) was not observed even when excess Pt(PCy₃)₂ was reacted with (HPh₂Si)₂O at ambient temperatures.

The reaction of Pt(PCy₃)₂ with 1,2-bis(dimethylsilyl)benzene, HMe₂Si(C₆H₄)SiMe₂H, did not result in the formation of the *cis* oxidative addition product as was observed with (HPh₂Si)₂O. Instead, two platinum phosphine complexes were formed when the reaction was carried out at room temperature, as evident from the corresponding ³¹P {¹H} NMR spectrum. Here we observed two singlet resonances both with ¹⁹⁵Pt satellites. One broad resonance was located at δ_{P} 56.1 [$J(\text{PtP}) = 1531$ Hz] **A5** and the other was a singlet resonance at δ_{P} 33.5 [$J(\text{PtP}) = 1437$ Hz] **B5**. In the ¹H NMR spectrum a broad hydride resonance was observed at δ_{H} -1.89 [$J(\text{PtH}) = 675.2$ Hz] and the methyl resonance of a co-ordinated disilane was observed at δ_{H} 0.94 possessing ¹⁹⁵Pt satellites [$J(\text{PtH}) = 28.3$ Hz]. Reaction of Pt(PCy₃)₂ with HMe₂Si(C₆H₄)SiMe₂H at -78 °C only yielded the product with a broad phosphorus resonance at δ_{P} 56.1 and the ¹H resonances at δ_{H} -1.89 and δ_{H} 0.94. The ratio of the methyl and hydride resonances was 6:1. From these data, we can infer that the complex formed at low temperature is **A5** and that it is a hydride species with the disilyl ligand attached to the platinum centre. Also, the ¹H NMR spectrum of **A5** with ¹⁹⁵Pt selectively decoupled at δ -5700 (see below) removes ¹⁹⁵Pt coupling to both the hydride and methyl resonances.

Complex **A5** decomposes thermally to *trans*-Pt(PCy₃)₂(H)₂ at room temperature, in a similar fashion to the *cis*-platinum silyl hydride complexes **15-20**. However, **A5** does not appear to form **B5** at room temperature. On cooling an NMR sample of **A5** to 200 K, the broad hydride resonance at δ_{H} -1.89 sharpens to a doublet resonance with a coupling constant of 8.3 Hz (Figure 5.25) and the broad phosphorus resonance sharpens

to a singlet resonance. Low temperature $^{195}\text{Pt} \{^1\text{H}\}$ NMR spectroscopy of **A5** shows one doublet resonance at $\delta_{\text{Pt}} -5700$ with a coupling to phosphorus of about 1540 Hz. The ^{195}Pt NMR spectrum of **A5** with ^1H coupled shows a broad doublet of triplets where the doublet coupling corresponds to $J(\text{PtP})$ and the triplet coupling corresponds to $J(\text{PtH})$ (Figure 5.26). The triplet multiplicity of the ^1H -coupled ^{195}Pt NMR spectrum indicates that there are two equivalent hydride ligands attached directly to platinum (The value of $J(\text{PtH})$ agrees with that derived from the ^1H spectrum). It is also clear from the low temperature $^{195}\text{Pt} \{^1\text{H}\}$ NMR spectrum of **A5** that only one phosphorus atom is attached to the platinum centre. The doublet coupling observed for the hydride at low temperature is also consistent with coupling to one single phosphorus atom.

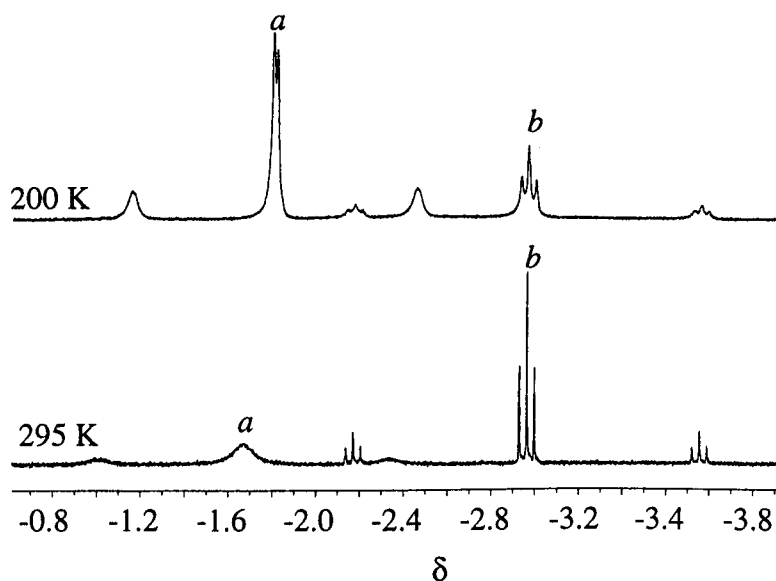


Figure 5.25 ^1H (500.13 MHz) NMR spectra of complex **A5** in $[\text{}^2\text{H}_8]\text{toluene}$ (only the hydride region is shown). *a* unknown complex **A5**. *b* $\text{trans-Pt}(\text{PCy}_3)_2(\text{H})_2$.

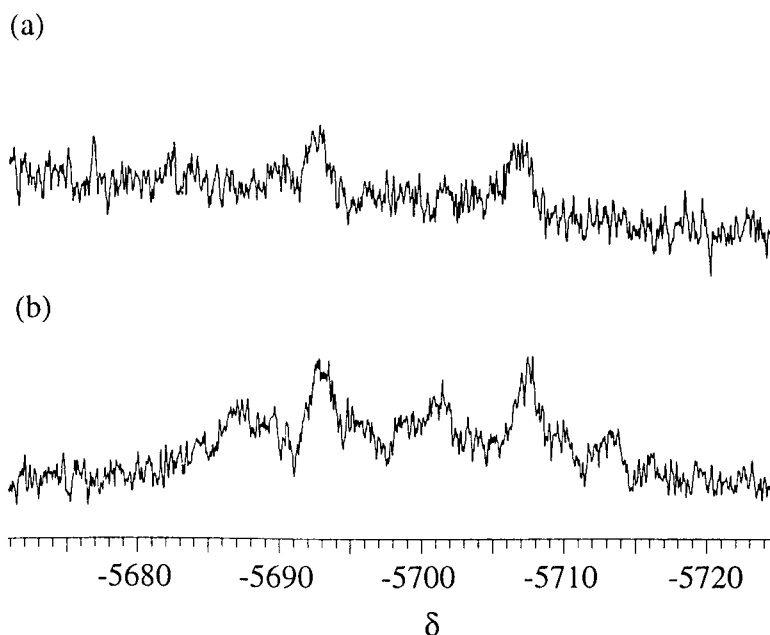


Figure 5.26 (a) ^{195}Pt $\{^1\text{H}\}$ (107.52 MHz, 200 K) NMR spectrum of **A5**. (b) ^{195}Pt (107.52 MHz, 200 K) NMR spectrum of **A5**.

5.3 DISCUSSIONS

5.3.1 Preparation of Platinum Silyl Hydride Complexes

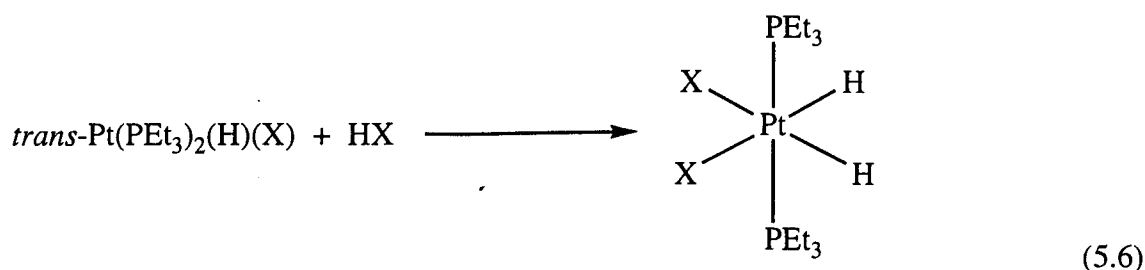
The reaction of $\text{Pt}(\text{PCy}_3)_2$ with the silane HSiR_3 has provided a convenient method of preparing the complex $\text{cis-Pt}(\text{PCy}_3)_2(\text{H})(\text{SiR}_3)$ in this investigation. Other methods of preparation of silyl complexes using platinum(0) compounds such as $\text{Pt}(\text{PPh}_3)_4$ or $\text{Pt}(\text{PPh}_3)_2(\text{C}_2\text{H}_4)$ with HSiR_3 have been employed in the past.^{23,24} Early attempts at forming Pt–Si bonds by reaction of a platinum halide with LiSiR_3 ²⁵ or $\text{Hg}(\text{SiMe}_3)_2$ have also been made.²⁶

Ebsworth *et al.* have successfully reacted $\text{trans-Pt}(\text{PCy}_3)_2(\text{H})_2$ with a series of primary or secondary silanes, SiH_2R_2 ($\text{R} = \text{H}, \text{Cl}$ or SiH_3) to form the corresponding $\text{trans-Pt}(\text{PCy}_3)_2(\text{H})(\text{SiH}_2\text{R})$ or $\text{trans-Pt}(\text{PCy}_3)_2(\text{H})(\text{SiHR}_2)$ complexes.²¹ They observed a six-co-ordinate trihydride platinum species of the type $\text{trans-Pt}(\text{PCy}_3)_2(\text{H})_3(\text{SiH}_2\text{R})$ by ^{31}P $\{^1\text{H}\}$ NMR spectroscopy at -80°C when $\text{trans-Pt}(\text{PCy}_3)_2(\text{H})_2$ was reacted with SiH_3R . On warming to room temperature the trihydride platinum species decomposed to $\text{trans-Pt}(\text{PCy}_3)_2(\text{H})(\text{SiH}_2\text{R})$. They reported that $\text{trans-Pt}(\text{PCy}_3)_2(\text{H})(\text{SiH}_2\text{R})$ has a relatively high field chemical shift for the hydride resonance, with $^1J(\text{PtH})$ and $\nu(\text{Pt-H})$ values that were quite low. This suggested that the strong *trans*-influence of the silyl ligand is comparable to that of the hydride ligand.

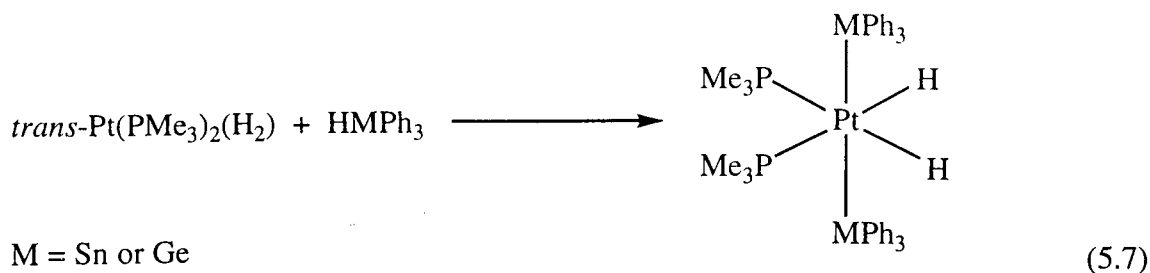
In our studies, the IR bands of $\nu(\text{Pt-H})$ for $\text{cis-Pt}(\text{PCy}_3)_2(\text{H})(\text{SiPh}_3)$ **15** and $\text{cis-Pt}(\text{PCy}_3)_2(\text{H})(\text{SiMe}_2\text{CH}_2\text{CH}=\text{CH}_2)$ **16** are at 2078 cm^{-1} and 2085 cm^{-1} respectively. It

has been reported that the IR band for $\nu(\text{Pt-H})$ is at 1872 cm^{-1} for *trans*- $\text{Pt}(\text{PCy}_3)_2(\text{H})(\text{SiH}_2\text{Cl})$.²¹ It is clear therefore that the $\nu(\text{Pt-H})$ IR bands for the *cis*-silyl hydride platinum complexes are much higher than those seen for the *trans*-silyl hydride complexes. The much higher value for the $\nu(\text{Pt-H})$ bands is clearly due to the absence of the high *trans*-influence of a silyl ligand. The high *trans*-influence of the silyl ligand is also demonstrated in the corresponding $J(\text{PtP})$ values, since Pt-P coupling constants give a good indication of how much *s*-character is present in the bond.^{14,27} As we can see from Table 5.1 (b), Pt-P bonds *trans* to silyl ligands have a much smaller $J(\text{PtP})$ value than Pt-P bonds *trans* to hydride. The $J(\text{PtP})$ value of the phosphorus atom *trans* to the silyl ligand is over 1000 Hz smaller in magnitude compared to the phosphorus atom *trans* to the hydride ligand.

It is possible, because of steric factors, that the tertiary silanes we used in this study have restricted access to the metal centre of *trans*- $\text{Pt}(\text{PCy}_3)_2(\text{H})_2$, due to the bulky PCy_3 ligands (cone angle²⁸ 179°). As a result, interaction of the Si-H bond with the metal centre may be less favoured, while for sterically undemanding silanes, *e.g.* SiH_4 , oxidative addition to the *trans*-platinum dihydride should be possible and a six-coordinate platinum(IV) species $\text{Pt}(\text{PCy}_3)_2(\text{H})_3(\text{SiH}_3)$ is accessible. The six-coordinate trihydride species can undergo facile reductive elimination of molecular dihydrogen to yield *trans*- $\text{Pt}(\text{PCy}_3)_2(\text{H})(\text{SiH}_3)$.²¹ Six-coordinate platinum dihydride complexes containing smaller phosphine ligands have been isolated when hydrogen halides add to *trans*- $\text{Pt}(\text{PEt}_3)_2(\text{H})(\text{X})$ ($\text{X} = \text{Cl}, \text{Br}, \text{I}$).²⁹ Here, the products generally assume a *trans, cis, cis*- $\text{PtL}_2\text{H}_2\text{X}_2$ structure (Equation 5.6).

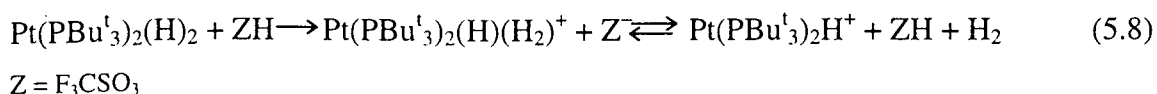


Trogler and co-workers have also isolated several six-coordinate platinum(IV) dihydride species by reacting $\text{Pt}(\text{PMe}_3)_2(\text{H})_2$ with HMPH_3 ($\text{M} = \text{Sn}$ or Ge) to give *cis, cis, trans*- $\text{Pt}(\text{PMe}_3)_2(\text{H})_2(\text{MPH}_3)_2$ (Equation 5.7) which have been identified from their NMR spectra. Reaction of HSiPh_3 with $\text{Pt}(\text{PMe}_3)_2\text{H}_2$ only yielded *cis*- $\text{Pt}(\text{PMe}_3)_2(\text{H})(\text{SiPh}_3)$.³⁰



Trogler reported that the six-co-ordinate platinum(IV) *cis, cis, trans*-Pt(PMe₃)₂(H)₂(MPh₃)₂ complexes are stable as solids but decompose in solution to the four-co-ordinate platinum(II) compounds, Pt(PMe₃)₂(MPh₃)₂ (M = Sn or Ge). Unfortunately, the geometry of the four-co-ordinate platinum (II) complex was not reported. The small size and good donor properties of the PMe₃ ligand³¹ accounted for the stabilisation of the six-co-ordinated platinum(IV) dihydride species, which was not possible for the PCy₃ analogue.

Recently, Gusev and co-workers reported the first d⁸ Pt(II) dihydrogen complex, [Pt(PBu₃)₂(H)(H₂)]⁺ in their study of the bulky dihydride complex *trans*-Pt(PBu₃)₂(H)₂ (Equation 5.8).³²



The dihydrogen complex [Pt(PBu₃)₂(H)(H₂)]⁺ was reported to undergo facile intermolecular H₂ exchange. The activation parameters for H₂ dissociation from [Pt(PBu₃)₂(H)(H₂)]⁺ was found to be, ΔH[‡] = 46 ± 2 kJ mol⁻¹ and ΔS[‡] = 8 ± 6 J K⁻¹ mol⁻¹.

5.3.2 Dynamic Exchange in *cis*-Pt(PCy₃)₂(H)(SiR₃)

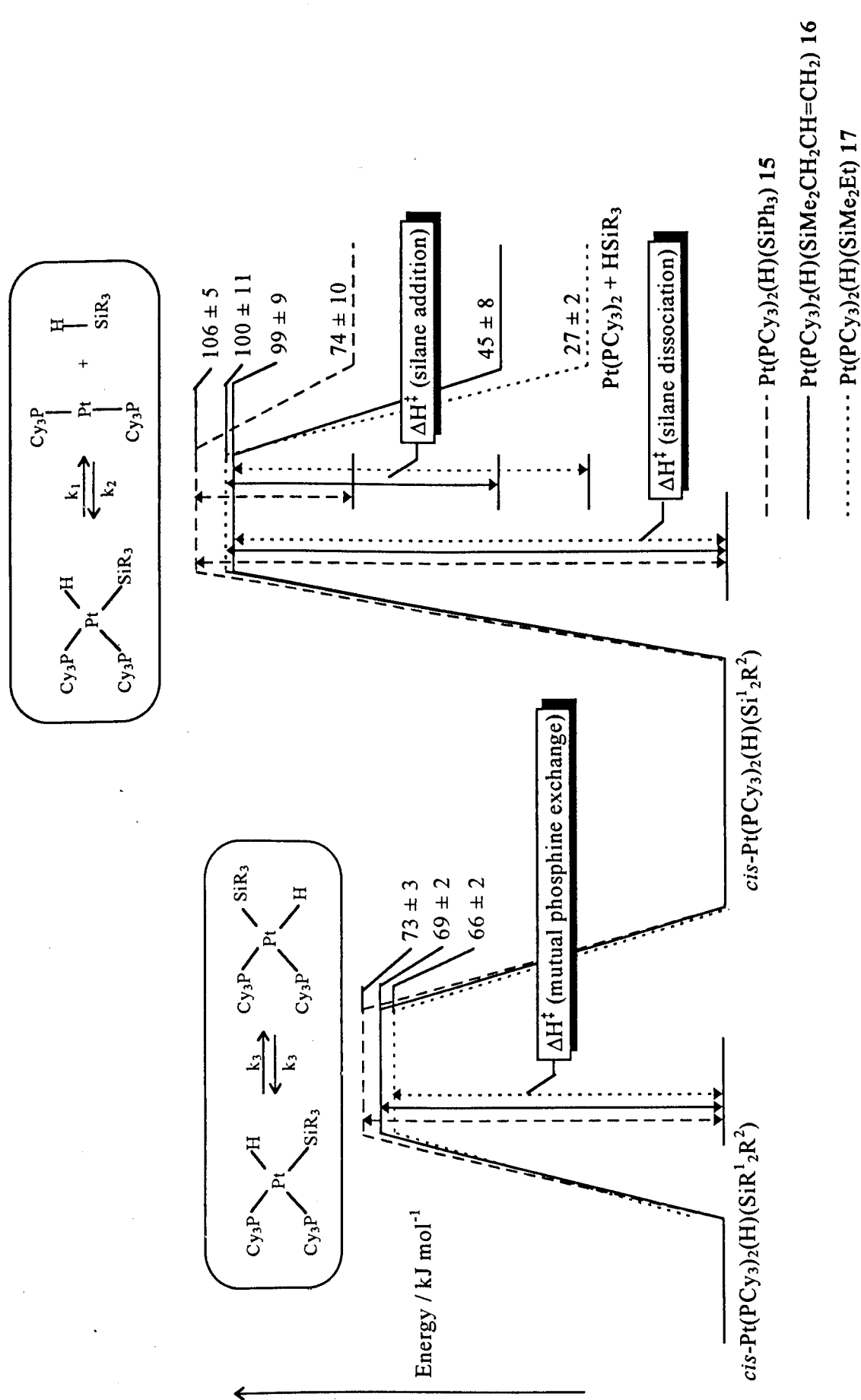
The thermodynamic parameters obtained for the dissociation of silane (Table 5.5), K_S, show that out of complexes **15-17**, complex **15** is the most thermodynamically stable on the basis of enthalpy with ΔH° = 74 ± 10 kJ mol⁻¹. This is followed by **16** (ΔH° = 45 ± 8 kJ mol⁻¹) and **17** (ΔH° = 27 ± 2 kJ mol⁻¹). This result was as expected, since good π-acceptor groups, such as SiPh₃ in complex **15**, normally stabilise the Si-H oxidative addition product.³³ This is mainly due to strong metal to ligand π-backbonding into the Si-H σ*-orbital which leads to the cleavage of the Si-H bond and the formation of a strong M-Si bond (see Section 1.3.2). Metal to ligand backbonding is not expected to be as strong in complexes **16** and **17**, hence the Pt-Si bond is expected to be comparatively weaker. Complex **15** was also found to be entropically more favoured to dissociate HSiPh₃, possibly due to the release of steric strain upon dissociation of HSiPh₃, the largest silane released on elimination in these studies. As a

result of the enthalpic and entropic factors working in opposite directions, the values of ΔG°_{300} for complexes **15**, **16** and **17** turn out to be the same.

The second exchange process in *cis*-Pt(PCy₃)₂(H)(SiR₃) is mutual phosphine exchange, which involves the positional change of the silyl and the hydride ligand. From the dynamic NMR data of complexes **15**, **16**, and **17**, we found that mutual phosphine exchange (k_3) is dominant at low temperatures in the range of 250 K to 270 K. Silane elimination and addition, k_1 and k_2 respectively, were only observed at higher temperatures. Scheme 5.7 summarises the activation parameters obtained for **15-17**.

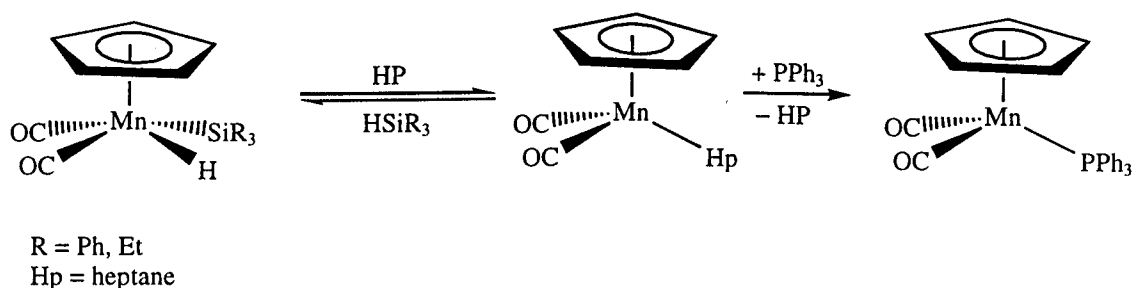
From the relative energy diagram in Scheme 5.7 the activation barrier for mutual phosphine exchange is very similar for **15-17**, all three complexes possessing a $\Delta H^\ddagger_{k_3}$ value of approximately 70 kJ mol⁻¹. However, small but significant differences can be found; **17** appears to have the smallest barrier of activation for mutual phosphine exchange, and this is followed by **16** and **15** (Table 5.19). The most obvious explanation would be due to the size of the substituents on the silicon atom, since large substituents such as phenyl rings would offer the most resistance to any form of rearrangement, compared to smaller methyl or ethyl groups.

In the elimination of silane from Pt(PCy₃)₂(H)(SiR₃), **15-17**, it was found that all three complexes possess a $\Delta H^\ddagger_{k_1}$ value of approximately 100 kJ mol⁻¹. ΔS^\ddagger values for silane elimination indicate that **17** has the most dissociative transition state, whilst **15** and **16** are virtually the same. As a result, the free energy barrier to silane dissociation follows the order **17** < **16** < **15**.



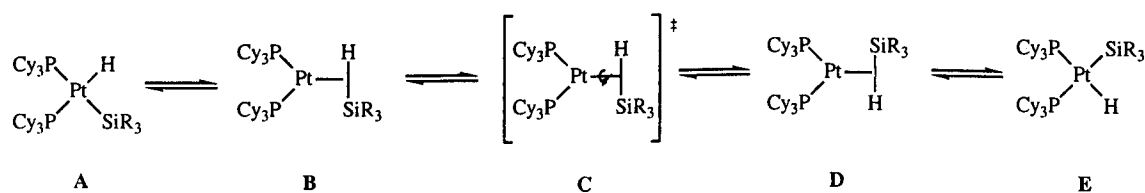
Scheme 5.7 Energy diagram showing the activation enthalpies of mutual phosphine exchange and silane dissociation/addition. All energy levels are relative to $cis\text{-Pt}(\text{PCy}_3)_2(\text{H})(\text{SiR}^1_2\text{R}^2)$.

Significant variation can be seen in the activation barrier of re-addition of silane to $\text{Pt}(\text{PCy}_3)_2$. We found that $\Delta H^\ddagger_{k_2}$ is smallest for HSiPh_3 and largest for HSiMe_2Et (Table 5.18). Parallels can be drawn from the reported ΔH^\ddagger values of dissociation of HSiR_3 from $\text{CpMn}(\text{CO})_2(\text{H})(\text{SiR}_3)$ (Scheme 5.8).^{34,35} The ΔH^\ddagger of dissociation of silane was found to be lower for HSiEt_3 ($\Delta H^\ddagger = 115 \pm 3 \text{ kJ mol}^{-1}$)³⁴ than HSiPh_3 ($\Delta H^\ddagger = 122 \pm 1 \text{ kJ mol}^{-1}$).³⁵



Scheme 5.8 Silane elimination from $\text{CpMn}(\text{CO})_2(\text{H})(\text{SiR}_3)$, adapted from ref. 34.

The intermediate involved in the mutual phosphine exchange process is most likely to be an η^2 -silane complex, as suggested originally by Clark and Hampden-Smith.¹⁰ Thus, rotation about the Si–H bond in the η^2 -silane intermediate would explain the phosphine exchange observed in the variable temperature NMR spectra (Scheme 5.9).



Scheme 5.9 Mutual phosphine exchange with an η^2 -silane intermediate as the suggested activated complex.

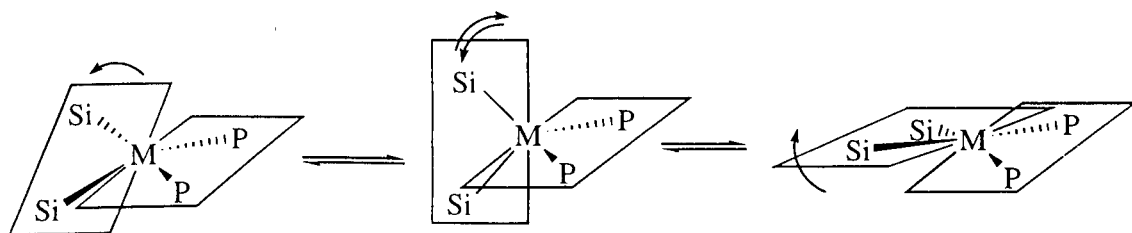
It is important to note that rate constants measured by dynamic NMR methods are rarely the same as those for the actual chemical exchange processes considered.³⁶ For the phosphine exchange process shown in Scheme 5.9, the transition state C is equally likely to proceed to either structure D or go back to structure B, since B and D have the same energy. If the process goes from A to E, only half the exchange process will be visible to NMR. Therefore the actual exchange rate is twice the observed rate, *ie.* $k_{\text{act}} = 2k_3$. Taking this into account, the actual activation parameters for phosphine exchange are summarised in Table 5.21. Compared to the activation parameters obtained for the

observed rate in Table 5.19, there are no substantial differences between ΔH^\ddagger and ΔG^\ddagger , but ΔS^\ddagger is slightly higher.

	$\Delta H^\ddagger_{k_{act}} /$ kJ mol ⁻¹	$\Delta S^\ddagger_{k_{act}} /$ J K ⁻¹ mol ⁻¹	$\Delta G^\ddagger_{300(k_{act})}$ / kJ mol ⁻¹
<i>cis</i> -Pt(PCy ₃) ₂ (H)(SiPh ₃) 15	73 ± 3	35 ± 9	62
<i>cis</i> -Pt(PCy ₃) ₂ (H)(SiMe ₂ CH ₂ CH=CH ₂) 16	70 ± 2	45 ± 7	56
<i>cis</i> -Pt(PCy ₃) ₂ (H)(SiMe ₂ Et) 17	66 ± 2	39 ± 6	55

Table 5.21 Activation parameters for actual mutual phosphine exchange in *cis*-Pt(PCy₃)₂(H)(SiPh₃) **15**, *cis*-Pt(PCy₃)₂(H)(SiMe₂CH₂CH=CH₂) **16** and *cis*-Pt(PCy₃)₂(H)(SiMe₂Et) **17** in [²H₈]toluene (Error bars quoted as 95 % probability on least squares fit).

Tsuji has recently reported a similar type of mutual phosphine exchange process in *cis*-bis(silyl)bis(phosphine)platinum and *cis*-bis(stannyl)bis(phosphine)palladium complexes.³⁷ They reported that the spin-spin couplings between P, Si and Pt are retained during the fluxional process observed in their system, similar to our own findings in this investigation where the spin-spin coupling between H, P and Pt are retained during the mutual phosphine exchange process. The mechanism of exchange was attributed to a unimolecular twist-rotation process, occurring *via* a pseudotetrahedral transition state (Scheme 5.10). Activation parameters for *cis*-Pt(PMe₂Ph)₂(SiPh₂Me)₂ and *cis*-Pt(PMe₂Ph)₂(SiMe₂F)₂ were reported to be $\Delta H^\ddagger = 57 \pm 2$ kJ mol⁻¹, $\Delta S^\ddagger = 17 \pm 9$ J K⁻¹ mol⁻¹ and $\Delta H^\ddagger = 34 \pm 1$ kJ mol⁻¹, $\Delta S^\ddagger = -60 \pm 6$ J K⁻¹ mol⁻¹, respectively. One unusual feature of these complexes is that they are already non-planar at platinum in the ground state with a dihedral angle of 38°.



Scheme 5.10 Proposed mechanism for mutual exchange of phosphine ligands in *cis*-bis(silyl)bis(phosphine) platinum complex, adapted from ref. 37.

Oxidative addition of silane is commonly believed to occur initially *via* interaction between the metal and the hydrogen of the approaching Si-H bond, and is

then followed by the silicon atom. Figure 5.27 illustrates a similar type of interaction for C–H oxidative addition.³⁸

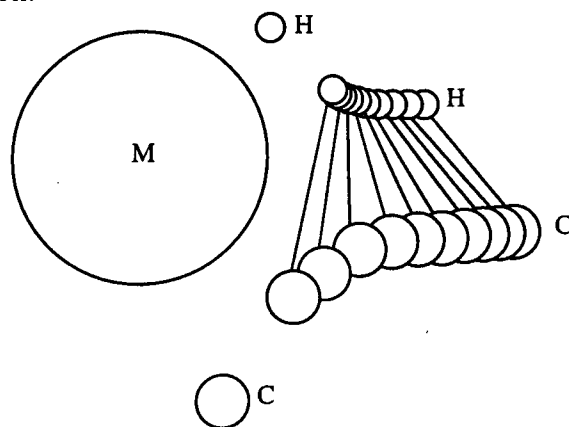


Figure 5.27 A kinetic pathway for the reaction $M + C-H \longrightarrow C-M-H$ as deduced from a series of structures of agostic complexes (adapted from ref. 38).

Ab initio calculations by Sakaki on the oxidative addition of SiH_4 to $Pt(PH_3)_2$ have also shown that the transition state of the reaction involves SiH_4 approach platinum with the H atom in the lead (Figure 5.28).^{39,40} It was also suggested that the initial interaction between the silane and $Pt(PH_3)_2$ results in a precursor complex, which can be considered as a van der Waals complex (Figure 5.29). However, according to Sakaki the stabilisation energy gained from the formation of such a complex is very small, *ca.* 6 kJ mol^{-1} .⁴⁰

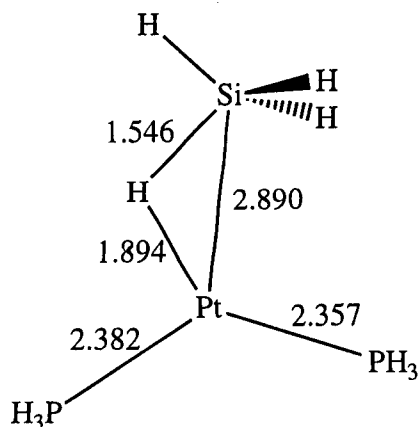


Figure 5.28 Optimised structure of transition state of Si–H oxidative addition to $Pt(PH_3)_2$, bond lengths in Å.^{39,40}

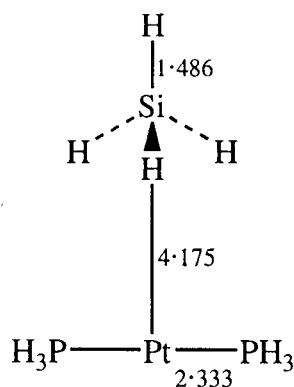
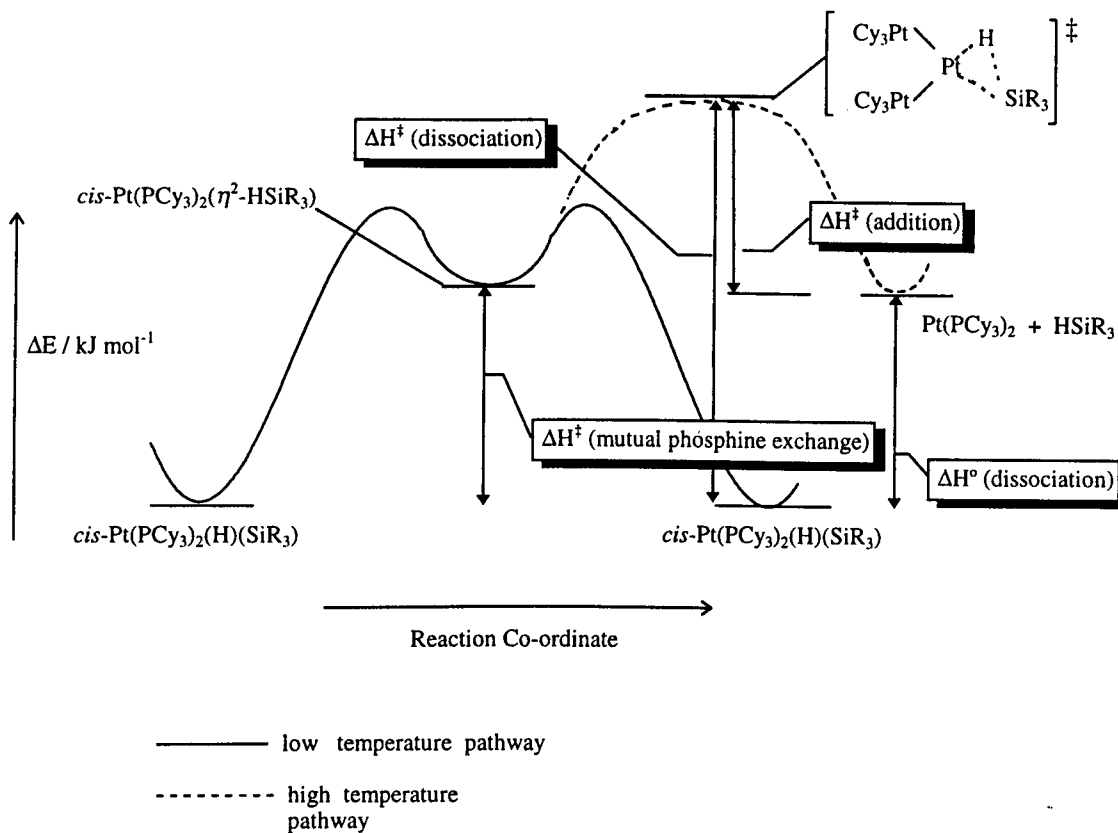


Figure 5.29 Optimised structure of precursor complex $\text{Pt}(\text{PH}_3)_2(\text{SiH}_4)$, bond lengths in Å.^{39,40}

In the transition state calculated by Sakaki for Si–H oxidative addition to $\text{Pt}(\text{PH}_3)_2$ (Figure 5.28), the Si–H bond has only lengthened slightly compared to free SiH_4 , and the Pt–H and Pt–Si distances are still relatively long compared to that of the final product.^{39,40} This indicates that the transition state is reached near the beginning of the oxidative addition pathway, and hence the barrier for silane addition should be small. Interestingly, it was also demonstrated that the transition state for C–H oxidative addition to $\text{Pt}(\text{PH}_3)_2$ is reached relatively late in the oxidative addition pathway. The reason for the difference in the activation barrier for C–H and Si–H oxidative addition can be explained by the bond strengths involved and has been discussed in Section 1.3.1.

In relation to the addition/elimination of silane to $\text{Pt}(\text{PCy}_3)_2$, it seems plausible to suggest that the activated intermediate involved is similar to the structure in Figure 5.28. In this investigation, the enthalpy of activation for silane addition, $\Delta H^\ddagger_{k_2}$, is significantly smaller than the enthalpy of activation for silane elimination, $\Delta H^\ddagger_{k_1}$. These findings support the argument that Si–H addition is reached early on in the oxidative addition pathway. Addition of HSiPh_3 to the $\text{Pt}(\text{PCy}_3)_2$ moiety was found to be the most entropically disfavoured; the negative value for the entropy of activation indicates a associative transition state.

It is plausible that silane dissociation at higher temperatures goes *via* an η^2 -silane intermediate as proposed in Scheme 5.9 for mutual phosphine exchange, since the energy difference between the activated complex for silane addition/dissociation and mutual phosphine exchange is *ca.* 30 kJ mol⁻¹ for **15-17**. Scheme 5.11 presents two possible reaction profiles for *cis*- $\text{Pt}(\text{PCy}_3)_2(\text{H})(\text{SiR}_3)$. At low temperature only mutual phosphine exchange is dominant, and occurs *via* an η^2 -silane intermediate. At higher temperatures it is presumed that the barrier from the η^2 -silane intermediate to the next intermediate, responsible for silane addition/dissociation, is overcome and both processes can occur.

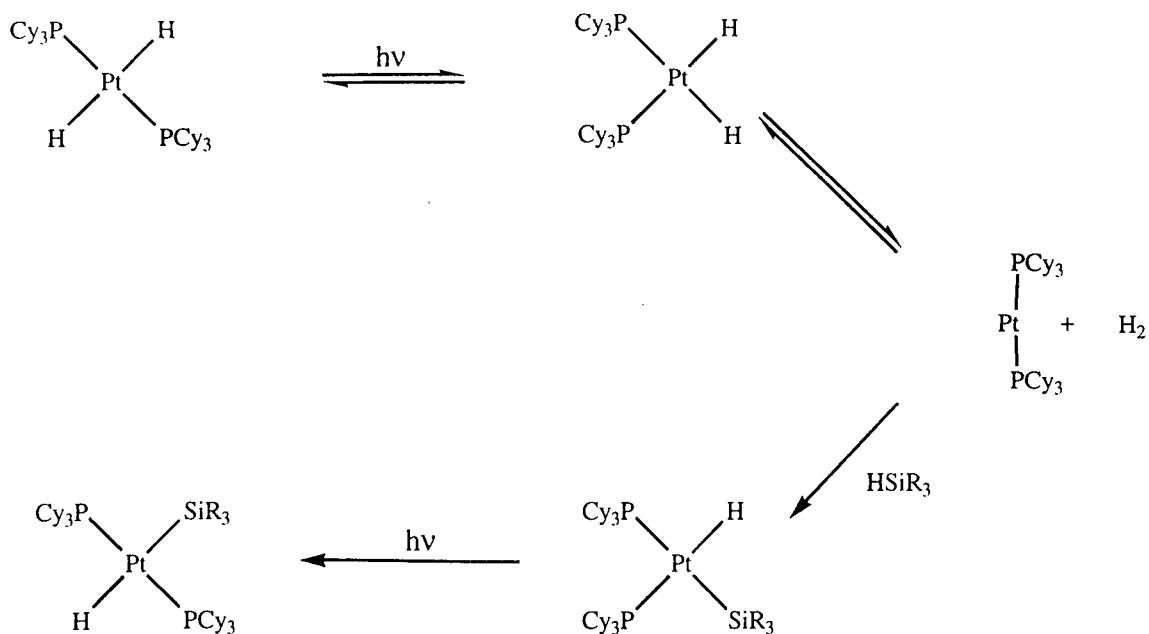


Scheme 5.11 Possible reaction profiles for the high and low temperature dynamic processes of *cis*-Pt(PCy₃)₂(H)(SiR₃).

It is important to note that we are only considering the dominant processes exhibited in the dynamic NMR data. One other possible process which was not observed was phosphine dissociation from *cis*-Pt(PCy₃)₂(H)(SiR₃) (Scheme 5.3). This could be because phosphine dissociation occurs on a much slower timescale than that accessible to NMR spectroscopy. However, no PCy₃ was detected in the temperature range studied.

5.3.3 Photochemistry of *trans*-Pt(PCy₃)₂(H)₂ and *cis*-Pt(PCy₃)₂(H)(SiR₃)

Photolysis of *trans*-Pt(PCy₃)₂(H)₂ in the presence of silane was found to yield a small amount of the oxidative addition product *trans*-Pt(PCy₃)₂(H)(SiR₃). It was revealed by low temperature photolysis that the initial product formed was *cis*-Pt(PCy₃)₂(H)(SiR₃). One probable mechanism for this process would involve the isomerisation of *trans*-Pt(PCy₃)₂(H)₂ to the unstable *cis*-dihydride complex which can lose molecular hydrogen leaving the 14-electron bis(phosphine) complex Pt(PCy₃)₂. Pt(PCy₃)₂ can then react with the excess silane present to form the *cis*-silyl hydride oxidative addition product; further photolysis would then isomerise the *cis*-silyl hydride complex to the *trans*-isomer (Scheme 5.12).

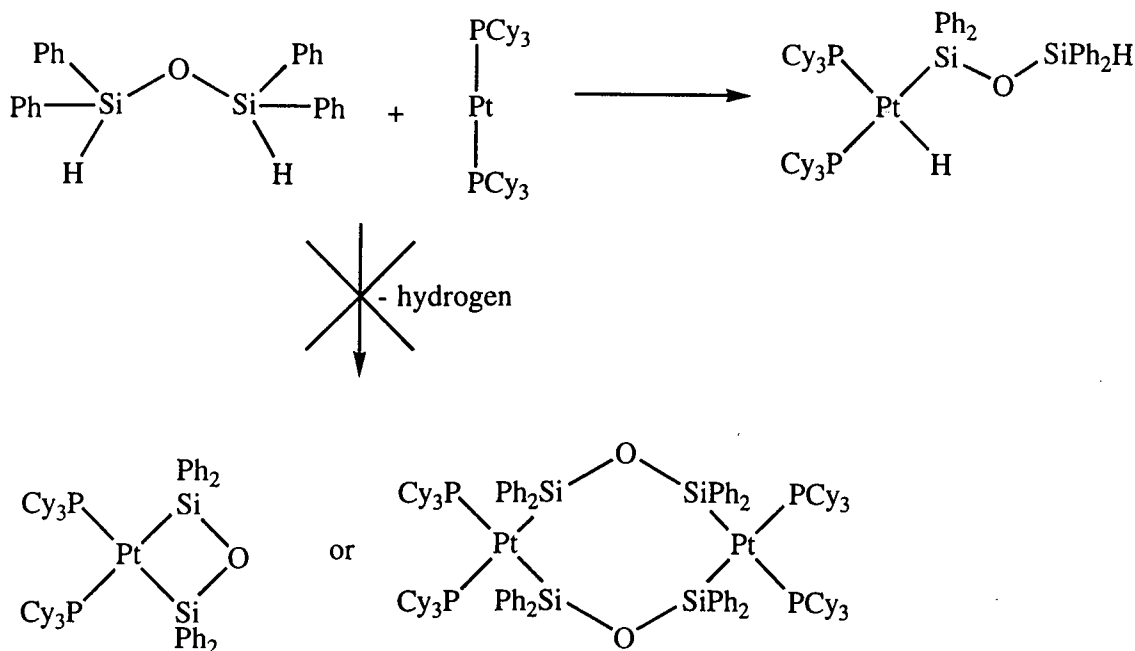


Scheme 5.12 Probable photochemical routes to $trans\text{-Pt}(\text{PCy}_3)_2(\text{H})(\text{SiR}_3)_2$.

However, even after long photolysis time, the conversion of $trans\text{-Pt}(\text{PCy}_3)_2(\text{H})_2$ to $trans\text{-Pt}(\text{PCy}_3)_2(\text{H})(\text{SiR}_3)$ is very low at room temperature. One possible explanation for this is that addition of H_2 occurs at a much faster rate than that of silane. This is supported by the fact that H_2 reacts rapidly with $cis\text{-Pt}(\text{PCy}_3)_2(\text{H})(\text{SiR}_3)$ to form $trans\text{-Pt}(\text{PCy}_3)_2(\text{H})_2$.

5.3.4 Reactions of $\text{Pt}(\text{PCy}_3)_2$ with disilanes

The reaction of $(\text{SiPh}_2\text{H})_2\text{O}$ with $\text{Pt}(\text{PCy}_3)_2$ yielded the complex $cis\text{-Pt}(\text{PCy}_3)_2(\text{H})(\text{SiPh}_2\text{OSiPh}_2\text{H})$ **20**. It was found that reaction of the disilane $(\text{SiPh}_2\text{H})_2\text{O}$ with excess $\text{Pt}(\text{PCy}_3)_2$ did not yield a dimeric Pt complex, where the disilane is acting as a bridging ligand, or a platinum cyclic silyl complex (Scheme 5.13).



Scheme 5.13

The absence of a cyclic silyl complex or a dimeric complex as illustrated in Scheme 5.13 is probably due to the flexibility of the Si–O–Si linkage and the repulsion between the PCy₃ ligand and the unattached HSiPh₂ group. For instance, Eaborn has reported the formation of Pt(PPh₃)₂(SiPh₂OSiPh₂), using the less sterically demanding PPh₃ ligand.²² It was envisaged that the use of a more rigid disilane, HSiMe₂(C₆H₄)SiMe₂H, would lead to the participation of both silyl groups in co-ordinating to the metal centre, forming a chelate structure. Reaction of excess HSiMe₂(C₆H₄)SiMe₂H with Pt(PCy₃)₂ was found to form two separate species **A5** and **B5** at room temperature and only **A5** at low temperature (*ca.* 250 K). As mentioned previously, Eaborn reported a similar reaction with Pt(PPh₃)₂(CH₂=CH₂) and HSiMe₂(C₆H₄)SiMe₂H to yield the chelating disilyl complex *cis*-Pt(PPh₃)₂[SiMe₂(C₆H₄)SiMe₂].²² The NMR data of **A5** revealed that this species contains one phosphine ligand, the disilyl ligand SiMe₂(C₆H₄)SiMe₂ and a hydride resonance (Section 5.2.8). At low temperatures, **A5** exhibits a chemical shift of $\delta -5700$ in the ¹⁹⁵Pt {¹H} NMR spectrum, which is coupled to one phosphorus nucleus. Tanaka and co-workers have previously reported that the ¹⁹⁵Pt NMR signals of Pt(II) bis(phosphine) disilyl complexes are usually found in the region of $\delta -3800$ to $\delta -5240$ and that of Pt(IV) silyl complexes are located at *ca.* $\delta -6000$.⁴¹ This suggests that **A5** could be a Pt(IV) species since it lies outside the reported upper limits for Pt(II) complexes. For comparison, *cis*-Pt(PCy₃)₂(H)(SiPh₃) has a chemical shift of $\delta_{\text{Pt}} -5205$. Proton coupled ¹⁹⁵Pt NMR spectrum of **A5** shows that Pt is coupled to two equivalent hydride ligands, providing further evidence that **A5** is a Pt(IV) complex. Hence **A5** would probably be a Pt(IV) disilyl dihydride complex (Figure 5.30).

Compound **B5**, the species which was formed at room temperature when $\text{Pt}(\text{PCy}_3)_2$ was reacted with $\text{HSiMe}_2(\text{C}_6\text{H}_4)\text{SiMe}_2\text{H}$, was first suspected to be similar to the one reported by Eaborn for the analogous PPh_3 complex. This would then suggest that **A5** is an intermediate on the way to **B5**. However, compound **A5** does not appear to convert to **B5** at room temperature, but instead **A5** decomposes slowly to *trans*- $\text{Pt}(\text{PCy}_3)_2(\text{H})_2$, see Section 5.2.8. The identity of **B5** remains unclear.

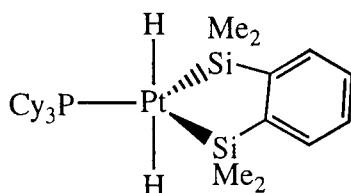
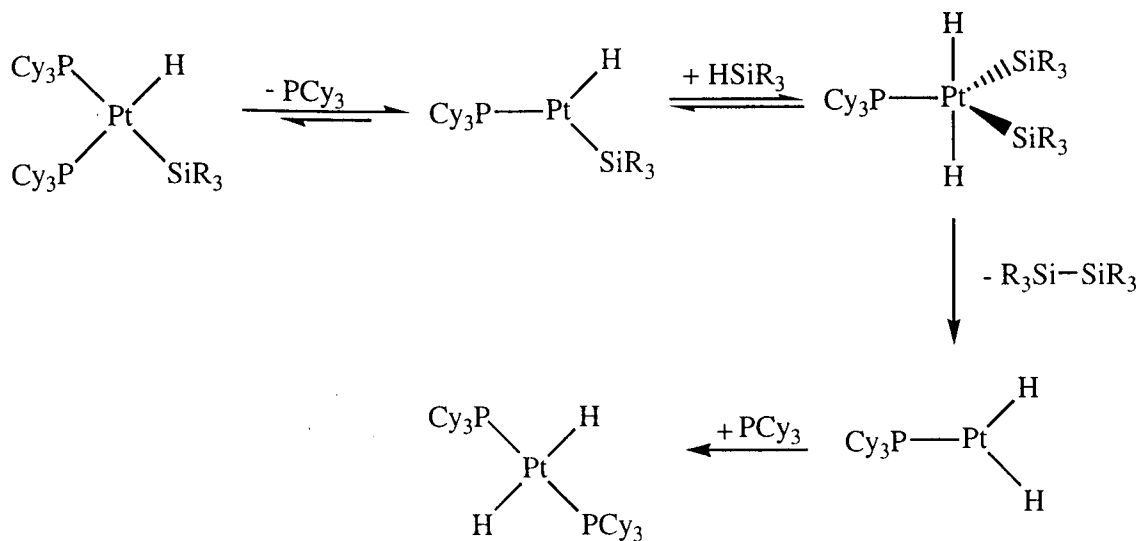


Figure 5.30 Possible structure for complex **A5**.

Analogues of the proposed structure for **A5** could also be involved in the thermal degradation of *cis*- $\text{Pt}(\text{PCy}_3)_2(\text{H})(\text{SiR}_3)$ to *trans*- $\text{Pt}(\text{PCy}_3)_2(\text{H})_2$. Scheme 5.14 outlines a possible mechanism for conversion of *cis*- $\text{Pt}(\text{PCy}_3)_2(\text{H})(\text{SiR}_3)$ to *trans*- $\text{Pt}(\text{PCy}_3)_2(\text{H})_2$ involving a Pt(IV) disilyl dihydride species above room temperature. The proposed trigonal bipyramidal structure in Scheme 5.14 reductively eliminates disilane, forming a silicon-silicon bond.



Scheme 5.14 Proposed mechanism for the thermal degradation of $\text{Pt}(\text{PCy}_3)_2(\text{H})(\text{SiR}_3)$ to *trans*- $\text{Pt}(\text{PCy}_3)_2(\text{H})_2$.

The proposed trigonal bipyramidal Pt(IV) bis(silyl) dihydride in Scheme 5.14 has both hydrides in the axial positions, which is probably the least sterically demanding position with respect to the PCy_3 and silyl ligands.

5.4 CONCLUSIONS

In this chapter we have demonstrated that *cis*-Pt(PCy₃)₂(H)(SiR₃) complexes undergo mutual phosphine exchange and silane dissociation near room temperature and only mutual phosphine exchange at lower temperatures. The substituent R on the silyl group plays an important part in determining the strength of the Pt–Si interaction. General observations indicated that strong electron withdrawing or π -accepting R groups help to stabilise the Si–H oxidation product to platinum. Thermodynamic data obtained for **15–17** further demonstrated this fact with *cis*-Pt(PCy₃)₂(H)(SiPh₃) **15** having the highest ΔH° of silane dissociation and the alkyl substituted silyl ligands in **16** and **17** have significantly smaller values of ΔH° . Due to the bulk of the PCy₃ ligands, **15** was also found to be the most entropically favoured to eliminate silane with **17** being the least favoured. This in turn gave very similar ΔG°_{300} values of 2, –2, and –2 kJ mol^{–1} for **15**, **16** and **17**, respectively, an example of enthalpy-entropy compensation.

The activation barrier for dissociation of silane is greatest for **15** by a fairly substantial margin. However, the reverse situation was found for the activation barrier of addition of HSiPh₃ to Pt(PCy₃)₂ which is much smaller compared to those for HSiMe₂CH₂CH=CH₂ and HSiMe₂Et. It was also found that silane elimination from **15–17** resulted in an entropically similar transition state, whilst the transition state for silane addition is entropically unfavourable for HSiPh₃. ΔG^\ddagger_{300} values for both silane addition and elimination were found to be marginally more favourable for HSiMe₂Et, possibly due to its small size. The activation parameter for mutual phosphine exchange was found to be similar for **15–17**, but again **15** was revealed to possess the largest enthalpy of activation for this process. Again the complex containing the smallest silane HSiMe₂Et has the lowest ΔG^\ddagger_{300} value.

An η^2 -silane complex is proposed to be responsible for the mutual silane exchange observed in *cis*-Pt(PCy₃)₂(H)(SiR₃) and it is implicated in the reaction profile for silane elimination from *cis*-Pt(PCy₃)₂(H)(SiR₃). The involvement of a pseudotetrahedral intermediate, proposed by Tsuji for the phosphine exchange process in *cis*-bis(silyl)bis(phosphine)platinum complex,³⁷ instead of an η^2 -silane intermediate could also account for this exchange. However, this seems unlikely in our case since the existence of a pseudotetrahedral complex should allow relatively easy *cis-trans* isomerisation which was not observed without photolysis.

Slow thermal decomposition of *cis*-Pt(PCy₃)₂(H)(SiR₃) to *trans*-Pt(PCy₃)₂(H)₂ was observed. Involvement of a Pt(IV) complex containing two silyl and two hydride ligands is possible. Formation of a Pt(IV) species was also suggested to be observed for the reaction between Pt(PCy₃)₂ and the disilane, HSiMe₂(C₆H₄)SiMe₂H. *Trans*-Pt(PCy₃)₂(H)(SiR₃) was found to be thermally stable and can be easily obtained by photolysis of the corresponding *cis* compound. *Trans*-Pt(PCy₃)₂H₂ was found to be

thermally unreactive towards the tertiary silanes used in this investigation; photochemical reactions of the *trans* dihydride complex with silanes also proved to be difficult.

5.5 REFERENCES

- 1 T. D. Tilley, *The Chemistry of Organic Silicon Compounds*, eds. S. Patai, Z. Rappoport, Wiley, New York, 1989, 1415.
- 2 M. Brookhart and B. E. Grant, *J. Am. Chem. Soc.*, 1995, **115**, 2151 and references therein.
- 3 M. L. Christ, B. Chaudret and S. Sabo-Etienne, *Organometallics*, 1995, **14**, 1082.
- 4 A. J. Chalk and J. F. Harrod, *J. Am. Chem. Soc.*, 1965, **87**, 16.
- 5 (a) C. Aitken, J. F. Harrod, E. Samuel, *J. Organomet. Chem.*, 1985, **279**, C11; (b) C. Aitken, J. F. Harrod, E. Samuel, *J. Am. Chem. Soc.*, 1986, **108**, 405; (c) J. F. Harrod, Y. Mu, E. Samuel, *Polyhedron*, 1991, **10**, 1239.
- 6 M. Green, J. A. K. Howard, J. Proud, J. L. Spencer and F. G. A. Stone, *J. Chem. Soc. Chem. Commun.*, 1976, 671.
- 7 L. D. Boardman, *Organometallics*, 1992, **11**, 4149.
- 8 U. Schubert, *Adv. Organomet. Chem.*, 1991, **30**, 151.
- 9 H. Azizian, K. R. Dixon, C. Eaborn, A. Pidcock, N. M. Shuaib and J. Vinaixa, *J. Chem. Soc., Chem. Comm.*, 1982, 1020.
- 10 H. C. Clark and M. J. Hampden-Smith, *Coord. Chem. Rev.*, 1987, **79**, 229.
- 11 H. C. Clark, G. Ferguson, M. J. Hampden-Smith, H. Ruegger and B. L. Ruhl, *Can. J. Chem.*, 1988, **66**, 3120.
- 12 C. J. Müller and U. Schubert, *J. Organomet. Chem.*, 1991, **418**, C4.
- 13 J. Sun, R. S. Lu, R. Bau and G. K. Yang, *Organometallics*, 1994, **13**, 1317.
- 14 T. G. Appleton, H. C. Clark and L. E. Manzer, *Coord. Chem. Rev.*, 1973, **10**, 335.
- 15 J. P. Jesson and E. L. Muetteries, *Dynamic Nuclear Magnetic Resonance Spectroscopy*, eds. L. M. Jackman and F. A. Cotton, Academic Press, New York, 1975, 279.
- 16 G. Hägele and R. Fuhler, *DNMR - SIM, Simulation for Dynamic NMR Spectra V1.00*, Heinrich-Heine University of Düsseldorf, Germany, 1994.
- 17 J. W. Faller, *The Determination of Organic Structures by Physical Methods*, eds. F. C. Nachod and J. J. Zukerman, Academic, New York, 1973, **5**, Chapter 2.
- 18 S. Braun, H. -O. Kalinowski and S. Berger, *100 and More Basic NMR Experiments - A Practical Course*, VCH, Cambridge, 1996, 99.

- 19 (a) R. K. Harris, *Nuclear Magnetic Resonance Spectroscopy*, Longman, Harlow, 1986, 108; (b) W. Kemp, *NMR in Chemistry: A Multinuclear Introduction*, Macmillan, London, 1986, 88.
- 20 *Microcal Origin Ver. 3.54*, Micro Software Inc., Northampton, USA, 1994.
- 21 E. A. Ebsworth, V. M. Marganian and F. J. S. Reed, *J. Chem. Soc., Dalton Trans.*, 1978, 1167.
- 22 C. Eaborn, T. N. Metham and A. Pidcock, *J. Organomet. Chem.*, 1973, **63**, 107.
- 23 J. Chatt, P. C. Eaborn and P. N. Kapoor, *J. Chem. Soc. (A)*, 1970, 881.
- 24 L. A. Latif, C. Eaborn, A. P. Pidcock and N. S. Weng, *J. Organomet. Chem.*, 1994, **474**, 217.
- 25 R. J. Cross and F. Glockling, *J. Chem. Soc.*, 1965, 5422.
- 26 (a) F. Glockling and A. K. Hooten, *J. Chem. Soc. (A)*, 1967, 1066; (b) A. F. Clemmit and F. Glockling, *Ibid.*, 1971, 1164.
- 27 F. R. Hartley, *Chemistry of Platinum and Palladium*, Applied Science, London, 1973.
- 28 C. A. Tolman, *J. Am. Chem. Soc.*, 1970, **92**, 2959.
- 29 D. W. Anderson, E. A. V. Ebsworth and D. W. H. Rankin, *J. Chem. Soc., Dalton Trans.*, 1973, 854.
- 30 D. L. Packett, A. Syed and W. C. Trogler, *Organometallics*, 1998, **7**, 159.
- 31 C. A. Tolman, *Chem. Rev.*, 1977, **77**, 313.
- 32 D. G. Gusev, J. U. Notheis, J. R. Rambo, B. E. Hauger, O. Eisenstein and K. G. Caulton, *J. Am. Chem. Soc.*, 1994, **116**, 7409.
- 33 J. Y. Corey and J. Braddock-Wiking, *Chem. Rev.*, 1999, **99**, 175.
- 34 D. M. Hester, J. Sun, A. W. Harper and G. K. Yang, *J. Am. Chem. Soc.*, 1992, **114**, 5234.
- 35 A. J. Hart-Davis and W. A. G. Graham, *J. Am. Chem. Soc.*, 1971, **93**, 4388.
- 36 M. L. H. Green, L. -L. Wong and A. Sella, *Organometallics*, 1992, **11**, 2660.
- 37 Y. Tsuji, K. Nishiyama, S. Hori, M. Ebihara and T. Kawamura, *Organometallics*, 1998, **17**, 507.
- 38 R. H. Crabtree, E. M. Holt, M. E. Lavin and S. M. Morehouse, *Inorg. Chem.*, 1985, **24**, 1986.
- 39 S. Sakaki and M. Ieki, *J. Am. Chem. Soc.*, 1991, **113**, 5063.
- 40 S. Sakaki and M. Ieki, *J. Am. Chem. Soc.*, 1993, **115**, 2373.
- 41 S. Shimada, M. Tanaka and K. Honda, *J. Am. Chem. Soc.*, 1995, **117**, 8289.

CHAPTER 6

EXPERIMENTAL



6.1 GENERAL METHODS

All syntheses and manipulations were carried out under argon using standard Schlenk and high vacuum techniques. All preparative solvents (Fison AR grade) were dried over sodium/benzophenone and distilled under argon (chlorinated solvents were dried over P_2O_5 , ethanol was dried over magnesium metal turnings and iodine). NMR solvents were obtained from Aldrich, Apollo or Goss Scientific and were dried over potassium metal under argon and distilled on a high vacuum line prior to use (chlorinated solvents were dried over molecular sieves or P_2O_5).

Chemicals were obtained from the following sources and used without further purification:

Gases: Argon, carbon dioxide, ethene, nitrogen and oxygen (BOC).

Silanes: $(CH_2=CHSiMe_2)_2O$, (Aldrich or donated by Dow Corning, Barry). $HSiMe_2Et$, $(HSiMe_2)_2C_6H_4$, $HSiClMe_2$, $HSiMe(OSiMe_3)_2$, (Aldrich). $HSiMe_2CH_2CH=CH_2$, $HSi(OMe)CH_2CH=CH_2$ (Gelest), $(HSiPh_2)_2O$ (donated by Fabien Delpech, Toulouse).

Azo compounds: EtO_2CNNCO_2Et , $Pr^iO_2CNNCO_2Pr^i$, $Bu^iO_2CNNCO_2Bu^i$ and 1,1'-(azodicarbonyl)dipiperidine (Aldrich).

Phosphines: PPh_3 , PCy_3 , (Aldrich). *dppe* (Aldrich or Lancaster). PMe_3 (Strem).

Other reagents: $PtCl_2$ (donated by Dow Corning). K_2PtCl_4 , $K_2C_2O_4$, $Na_2(O_2C)_2CH_2$, $Na_2(O_2C)_2C_6H_4$, $AgNO_3$, $PhOCNHNHCOPh$, $MeOCNHNHCOME$, $CH_2=C(Me)CH_2OH$, 1,5-cyclooctadiene, diphenylacetylene, 1-hexene, 1-octene, celite, molecular sieves, sodium, potassium, triethylamine (Aldrich). Na_2CO_3 , $NaOH$, KOH , Mg , $MgSO_4$, P_2O_5 , Iodine (Fisons). Sodium dispersion (Strem).

UV/Visible spectra were recorded on a Perkin-Elmer Lambda 7 spectrophotometer. Infrared spectra were recorded on a Mattson RS FTIR instrument at York or on a Nicolet FTIR instrument at Dow Corning, Barry. Mass Spectra were recorded on a VG Auto-Spec mass spectrometer by the University of York analytical services. X-Ray data were collected on a Rigaku AFC6S diffractometer by Leroy Cronin at the University of York. Elemental analyses were performed by Elemental Microanalysis Ltd, Devon, UK.

The work on platinum catalysed hydrosilation reaction was carried out at Dow Corning in Barry, on a Hewlett Packard capillary GC with FID detection. The instrument was fitted with a BP1 column and temperature ramping was employed.

GC-MS work on organosilane products from the decomposition of *cis*- $Pt(PCy_3)_2(H)(SiMe_2CH_2CH=CH_2)$ **16** was carried out by the Laboratoire de Chimie de Co-ordination analytical services in Toulouse, on a Hewlett Packard HP 5890 capillary GC, using a 12 m column packed with methylsilicone, connected to a Hewlett Packard HP 5970 mass spectrometer. Elemental analysis on *cis*- $Pt(PCy_3)_2(H)(SiPh_3)_2$ **15** was

also carried out by the Laboratoire de Chimie de Co-ordination analytical services in Toulouse.

NMR spectra were recorded on a Bruker MSL 300 (^1H , 300.13 MHz; ^{13}C , 75.47 MHz; ^{31}P 121.49 MHz; ^{195}Pt , 64.41 MHz; ^{29}Si , 59.62 MHz) and AMX 500 (^1H , 500.13 MHz; ^{13}C , 125.78 MHz; ^{31}P 202.46 MHz; ^{195}Pt , 167.57 MHz; ^{29}Si , 99.36 MHz) spectrometers in York, and on a Jeol EX400 spectrometer in Dow Corning (^1H , 399.65 MHz; ^{29}Si , 79.38 MHz; ^{195}Pt , 85.28 MHz), and on a Bruker AC200 (^1H , 200.13 MHz; ^{31}P 81.02 MHz) or AC250 (^1H , 250.13 MHz; ^{31}P 101.26 MHz) spectrometers in Toulouse. ^1H NMR spectra were referenced relative to the peaks of the residual protio solvents: benzene (δ 7.15), chloroform (δ 7.30), dichloromethane (δ 5.30), tetrahydrofuran (δ 1.73), toluene (δ 2.10). ^{31}P $\{^1\text{H}\}$ NMR spectra were referenced to external H_3PO_4 (85%). ^{13}C $\{^1\text{H}\}$ NMR spectra were referenced to the solvent peak: benzene (δ 28.0), dichloromethane (δ 54.5), chloroform (δ 77.7) and tetrahydrofuran (δ 25.2), toluene (δ 21.1). ^{195}Pt $\{^1\text{H}\}$ NMR were referenced to external $\text{Pt}(\text{COD})\text{Cl}_2$ in CDCl_3 (δ -3361).¹

Photolysis of samples was carried out in Pyrex NMR tubes ($\lambda > 290$ nm) using a Philips HPK 125 W medium pressure mercury lamp at room temperature. Typically, both a cut-off filter (295-410 nm) and a water filter were placed in front of the lamp output. For low temperature photolysis, samples were immersed in a partially silvered Dewar containing a dry-ice/acetone mixture (*ca.* -77 °C). ^1H NMR spectroscopy with *in situ* photolysis was performed by John Lowe at York on a Bruker 300 MSL NMR spectrometer. Generally, samples were kept for 24 hours at room temperature and shielded from ambient light prior to photolysis. Their NMR spectra were then recorded in order to check for competing thermal reaction at room temperature.

6.2 SYNTHESIS AND REACTIONS OF PLATINUM BIS(PHOSPHINE) AZODICARBONYL COMPLEXES

The complexes *cis*- $\text{Pt}(\text{PPh}_3)_2\text{Cl}_2$,² *cis*- $\text{Pt}(\text{PMe}_3)_2\text{Cl}_2$ ³ and $\text{Pt}(\text{PPh}_3)_2(\text{C}_2\text{H}_4)$ ⁴ were prepared according to literature procedures. Mass spectral peaks are quoted only when they have a major contribution from ^{194}Pt .

6.2.1 Preparation of $\text{Pt}(\text{PPh}_3)_2(\text{PhOCNNCOPh})$ 1

This synthesis follows the procedure of Dilworth and Kasenally.⁵ $\text{Pt}(\text{PPh}_3)_2\text{Cl}_2$ (0.20 g, 0.2 mmol) and PhOCNHNHCOPh (0.06 g, 0.2 mol) were suspended in ethanol (20 mL) with sodium hydrogen carbonate (0.06 g). The mixture was refluxed under argon for 4 h. During this time the white suspension gradually dissolved yielding a yellow solution. The solvent was removed under vacuum. The crude product was re-

dissolved in benzene, and hexane was added until precipitation began. Yellow crystals were formed overnight (Yield 1.30 g, 70%). Mass spectrum (FAB): m/z 956 (M^+ , ^{194}Pt , 63 %), m/z 957 (M^+ , ^{195}Pt and $[M + \text{H}]^+$, ^{194}Pt , 100 %). ^1H NMR spectrum (300.13 MHz, CDCl_3 , 295 K): δ 7.00-8.00 (m, Ph). ^{13}C $\{^1\text{H}\}$ NMR spectrum (75.47 MHz, CDCl_3 , 295 K): δ 127.1-135.2 (Ph), δ 163.2 [dd, $\underline{\text{CO}}$, $J(\text{PC}) = 10$, 3 Hz], δ 171.7 [d, $\underline{\text{CO}}$, $J(\text{PC}) = 4$]. ^{31}P $\{^1\text{H}\}$ NMR spectrum (121.94 MHz, CDCl_3 , 295 K): δ 3.1 [d, P^{O} , $^2J(\text{PP}) = 22$ Hz, $J(\text{PtP}) = 3685$ Hz], δ 17.5 [d, P^{N} , $^2J(\text{PP}) = 22$ Hz, $J(\text{PtP}) = 3261$ Hz]. ^{195}Pt $\{^1\text{H}\}$ NMR spectrum (107.52 MHz, CD_2Cl_2 , 300 K): δ -4291 [dd, $J(\text{PtP}) = 3302$ Hz, 3680 Hz]. IR (KBr): $\nu(\text{CO}, \text{CN})$ 1565, 1595 cm^{-1} .

6.2.2 Preparation of $\text{Pt}(\text{PPh}_3)_2(\text{Et}_2\text{OCNNCO}_2\text{Et})$ 2

$\text{Pt}(\text{PPh}_3)_2(\text{C}_2\text{H}_4)$ (0.64 g, 0.9 mmol) and $\text{Et}_2\text{OCNNCO}_2\text{Et}$ (0.60 g, 3.4 mmol) were dissolved in benzene (20 mL) under an atmosphere of argon at room temperature. On mixing the two compounds together a gas was evolved and the solution changed from yellow to red. Within 1 hour of addition, a yellow precipitate began to form. The mixture was shielded from ambient light and left stirring for 12 h. The product was collected and recrystallised from ethanol to form yellow crystals (0.63 g, 69 % yield) (Found: C, 56.1; H, 4.6; N, 3.1. Calc. for $\text{C}_{42}\text{H}_{40}\text{N}_2\text{O}_4\text{P}_2\text{Pt}$: C, 56.4; H, 4.5; N, 3.1). Mass spectrum (FAB): m/z 892 (M^+ , ^{194}Pt , 18 %), m/z 893 (M^+ , ^{195}Pt and $[M + \text{H}]^+$, ^{194}Pt , 79 %). ^1H NMR spectrum (300.13 MHz, C_6D_6 , 295 K): δ 1.14 (3H, br t, CH_2CH_3), δ 1.35 [3H, t, CH_2CH_3 , $J(\text{HH}) = 7.0$ Hz], δ 4.12 (2H, br, CH_2CH_3), δ 4.57 [2H, quart, CH_2CH_3 , $J(\text{HH}) = 7.0$ Hz] δ 7.00-8.00 (30H, m, Ph). ^{31}P $\{^1\text{H}\}$ NMR spectrum (121.94 MHz, C_6D_6 , 295 K): δ 6.2 [br d, P^{O} , $J(\text{PtP}) \approx 3790$ Hz], δ 16.6 [d, P^{N} , $^2J(\text{PP}) = 23$ Hz, $J(\text{PtP}) = 3166$ Hz]. IR (KBr): $\nu(\text{CO}, \text{CN})$ 1610, 1621, 1629, 1648, 1668 cm^{-1} .

6.2.3 Preparation of $\text{Pt}(\text{PMe}_3)_2(\text{PhOCNNCOPh})$ 3

This complex was prepared by the same procedure as **1** using *cis*- $\text{Pt}(\text{PMe}_3)_2\text{Cl}_2$ (0.2 g, 0.5 mmol). The product was recrystallised by addition of hexane to a benzene solution until precipitation began. The benzene/hexane mixture gave light yellow crystals (Yield 0.20 g, 68 %) (Found: C, 40.3; H, 4.5; N 4.5. Calc. for $\text{C}_{20}\text{H}_{28}\text{N}_2\text{O}_2\text{P}_2\text{Pt}$: C, 41.0; H, 4.8; N, 4.9). Mass spectrum (FAB): m/z 584 (M^+ , ^{194}Pt , 55 %), m/z 585 (M^+ , ^{195}Pt and $[M + \text{H}]^+$, ^{194}Pt , 100 %). ^1H NMR spectrum (300.13 MHz, CDCl_3 , 295 K): δ 1.80 [9H, d, PCH_3 , $^2J(\text{PH}) = 11.0$ Hz], δ 1.90 [9H, d, PCH_3 , $^2J(\text{PH}) = 11.3$ Hz], δ 7.00-8.00 (10H, m, Ph). ^{13}C $\{^1\text{H}\}$ NMR spectrum (75.47 MHz, CDCl_3 , 295 K): δ 16.6 [d, PCH_3 , $J(\text{PC}) = 38$ Hz, $J(\text{PtC}) = 33$ Hz], δ 19.7 [dd, PCH_3 , $J(\text{PC}) = 44$ Hz, $^2J(\text{PC}) = 2$ Hz, $J(\text{PtC}) = 43$ Hz], δ 124.2-131.8 (Ph), δ 163.4 [dd, $\underline{\text{CO}}$, $J(\text{PC}) = 9$, 3 Hz], δ 174.6 [d,

$\underline{\text{CO}}$, $J(\text{PC}) = 4$]. ^{31}P $\{^1\text{H}\}$ NMR spectrum (121.94 MHz, CDCl_3 , 295 K): $\delta -20.1$ [d, P^{O} , $^2J(\text{PP}) = 26$ Hz, $J(\text{PtP}) = 3435$ Hz], $\delta -10.9$ [d, P^{N} , $^2J(\text{PP}) = 26$ Hz, $J(\text{PtP}) = 3028$ Hz]. ^{195}Pt $\{^1\text{H}\}$ NMR spectrum {107.52 MHz, CD_2Cl_2 , 300 K}: $\delta -4257$ [dd, $J(\text{PtP}) = 3028$ Hz, 3458 Hz]. IR (KBr): $\nu(\text{CO}, \text{CN})$ 1561, 1586 cm^{-1} .

6.2.4 Preparation of $\text{Pt}(\text{PMe}_3)_2(\text{MeOCNNCOMe})$ 4

This complex was prepared by a procedure similar to that of **1** using *cis*- $\text{Pt}(\text{PMe}_3)_2\text{Cl}_2$ (0.2 g, 0.5 mmol). The product was recrystallised by addition of hexane to a benzene solution of **4** until precipitation began. The benzene/hexane mixture yielded light brown crystals (Yield 0.15 g, 65 %) (Found: C, 26.3; H, 5.4; N, 6.1. Calc. for $\text{C}_{10}\text{H}_{24}\text{N}_2\text{O}_2\text{P}_2\text{Pt}$: C, 26.0; H, 5.2; N, 6.1). Mass spectrum (FAB): m/z 460 (M^+ , ^{194}Pt , 53 %), m/z 461 (M^+ , ^{195}Pt and $[M + \text{H}]^+$, ^{195}Pt , 100%). ^1H NMR spectrum (300.13 MHz, CDCl_3 , 295 K): δ 1.70 [9H, d, PCH_3 , $^2J(\text{PH}) = 10.7$ Hz], δ 1.80 [9H, d, PCH_3 , $^2J(\text{PH}) = 11.2$ Hz], δ 2.01 [3H, d, COCH_3 , $^5J(\text{PH}) = .9$ Hz], δ 2.23 (3H, COCH_3). ^{13}C $\{^1\text{H}\}$ NMR spectrum (75.47 MHz, CDCl_3 , 295 K): δ 16.3 [d, PCH_3 , $J(\text{PC}) = 38$ Hz, $^2J(\text{PtC}) = 33$ Hz], δ 16.5 [d, OCH_3 , $^4J(\text{PC}) = 5$ Hz], δ 19.6 [dd, PCH_3 , $J(\text{PC}) = 45$ Hz, $^3J(\text{PC}) = 2$ Hz, $^2J(\text{PtC}) = 45$ Hz], δ 22.1 [d, OCH_3 , $^4J(\text{PC}) = 5$ Hz], δ 165.4 [dd, $\underline{\text{CO}}$, $J(\text{PC}) = 9$, 4 Hz], δ 175.4 [d, $\underline{\text{CO}}$, $J(\text{PC}) = 3$, $J(\text{PtC}) = 67$ Hz]. ^{31}P $\{^1\text{H}\}$ NMR spectrum (121.94 MHz, CDCl_3 , 295 K): $\delta -38.0$ [d, P^{O} , $^2J(\text{PP}) = 26$ Hz, $J(\text{PtP}) = 3435$ Hz], $\delta -29.0$ [d, P^{N} , $^2J(\text{PP}) = 26$ Hz, $J(\text{PtP}) = 3028$ Hz]. ^{195}Pt $\{^1\text{H}\}$ NMR spectrum {107.52 MHz, CD_2Cl_2 , 300 K}: $\delta -4260$ [dd, $J(\text{PtP}) = 3010$ Hz, 3446 Hz]. IR (KBr): $\nu(\text{CO}, \text{CN})$ 1576, 1612 cm^{-1} .

6.2.5 Preparation of $\text{Pt}(\text{PPh}_3)_2(\text{Pr}^{\text{I}}\text{O}_2\text{CNNCO}_2\text{Pr}^{\text{I}})$ 5

This complex was prepared as for **2** using *cis*- $\text{Pt}(\text{PPh}_3)_2\text{Cl}_2$ (0.2 g, 0.2 mmol). The product was recrystallised from THF giving orange crystals (Yield 0.12 g, 70 %) (Found: C, 57.3; H, 4.8; N, 3.0. Calc. for $\text{C}_{44}\text{H}_{44}\text{N}_2\text{O}_4\text{P}_2\text{Pt}$: C, 57.3; H, 4.8; N, 3.0). Mass spectrum (FAB): m/z 920 (M^+ , ^{194}Pt , 12 %), m/z 921 (M^+ , ^{195}Pt and $[M + \text{H}]^+$, ^{194}Pt , 73 %). ^1H NMR spectrum {300.13 MHz, $[\text{H}_8]\text{THF}$, 295 K}: δ 0.75 [6H, d, $\text{CH}(\text{CH}_3)_2$, $J(\text{HH}) = 6.2$ Hz], δ 1.06 [6H, d, $\text{CH}(\text{CH}_3)_2$, $J(\text{HH}) = 6.2$ Hz], δ 4.08 [1H, sept, $\text{CH}(\text{CH}_3)_2$, $J(\text{HH}) = 6.2$ Hz], δ 4.12 [1H, sept, $\text{CH}(\text{CH}_3)_2$, $J(\text{HH}) = 6.2$ Hz], δ 7.00–8.00 (30H, m, Ph). ^{13}C $\{^1\text{H}\}$ NMR spectrum {75.47 MHz, $[\text{H}_8]\text{THF}$, 295 K}: δ 23.8 (s, CH_3), δ 24.1 (s, CH_3), δ 67.6 (s, $\underline{\text{CH}}$), δ (s, $\underline{\text{CH}}$), δ 128.8–136.6 (Ph). ^{31}P $\{^1\text{H}\}$ NMR spectrum {121.94 MHz, $[\text{H}_8]\text{THF}$, 295 K}: δ 5.8 [d, P^{O} , $^2J(\text{PP}) = 23$ Hz, $J(\text{PtP}) = 3859$ Hz], δ 16.5 [d, P^{N} , $^2J(\text{PP}) = 23$ Hz, $J(\text{PtP}) = 3158$ Hz]. ^{195}Pt $\{^1\text{H}\}$ NMR spectrum {107.51 MHz, $[\text{H}_8]\text{THF}$, 300 K}: $\delta -4168$ [dd, $J(\text{PtP}) = 3118$ Hz, 3871 Hz]. IR (KBr): $\nu(\text{CO}, \text{CN})$ 1613, 1635 cm^{-1} .

6.2.6 Preparation of Pt(dppe)(EtO₂CNNCO₂Et) **6**

Pt(dppe)(EtO₂CNNCO₂Et) **6** was prepared *in situ* by reacting Pt(PPh₃)₂-(EtO₂CNNCO₂Et) **2** with excess dppe in C₆D₆ in an NMR tube. ¹H NMR spectrum (300.13 MHz, C₆D₆, 295 K): δ 0.97 [3H, t, CH₂CH₃, *J*(HH) = 7.2 Hz], δ 1.35 [3H, t, CH₂CH₃, *J*(HH) = 7.2 Hz], δ 4.00 [2H, br, CH₂CH₃, *J*(HH) = 7.2], δ 4.57 [2H, quart, CH₂CH₃, *J*(HH) = 7.2 Hz], δ 7.00-8.00 (30H, m, Ph). ³¹P {¹H} NMR spectrum (121.94 MHz, C₆D₆, 295 K): δ 31.1 [d, P^O, ²*J*(PP) = 11 Hz, *J*(PtP) = 3839 Hz], δ 38.1 [d, P^N, ²*J*(PP) = 11 Hz, *J*(PtP) = 3041 Hz].

6.2.7 Preparation of Pt(dppe)(PrⁱO₂CNNCO₂Prⁱ) **7**

This complex was prepared by reacting Pt(PPh₃)₂(PrⁱO₂CNNCO₂Prⁱ) **5** with excess dppe *in situ* in C₆D₆, in an NMR tube. ¹H NMR spectrum (300.13 MHz, C₆D₆, 295 K): δ 1.10 [6H, d, CH(CH₃)₂, *J*(HH) = 6.2 Hz], δ 1.36 [6H, d, CH(CH₃)₂, *J*(HH) = 6.2 Hz], δ 4.79 [1H, sept, CH(CH₃)₂, *J*(HH) = 6.2 Hz], δ 5.40 [1H, sept, CH(CH₃)₂, *J*(HH) = 6.2 Hz], δ 7.00-8.00 (30H, m, Ph). ³¹P {¹H} NMR spectrum (121.94 MHz, C₆D₆, 295 K): δ 31.0 [d, P^O, ²*J*(PP) = 12 Hz, *J*(PtP) = 3843 Hz], δ 38.1 [d, P^N, ²*J*(PP) = 12 Hz, *J*(PtP) = 3023 Hz].

6.2.8 X-ray crystallographic study of **5**

Crystals of compound **5** were grown at ambient temperature by the slow evaporation of a 2:1 THF/benzene solution. The resulting crystal was cut to size and mounted on a glass fibre using epoxy cement. The structure of compound **5** was solved using Patterson methods with SAPI91 and expanded using Fourier techniques with DIRDIF. Full-matrix least squares refinement on *F*² was carried out with SHELXL 93. Programs.^{6,7} All non hydrogen atoms were refined anisotropically. The hydrogen atoms were refined on all structures using a riding model with isotropic temperature factors 1.2 times that of their carrier atoms (1.5 times for methyl groups). The crystal data of **5** were collected, solved and refined by Leroy Cronin at the University of York.

6.2.9 Photolysis of Pt(PPh₃)₂(PhOCNNCOPh) **1**, Pt(PMe₃)₂(PhOCNNCOPh) **3** and Pt(PMe₃)₂(MeOCNNCOME) **4** with ethene or diphenylacetylene in C₆D₆

NMR samples of **1**, **3** and **4** were photolysed in C₆D₆ with either excess diphenyl acetylene or under an 1 atmosphere of ethene. Photolysis of these samples was stopped periodically and checked by ¹H and ³¹P {¹H} NMR spectroscopy for signs of reaction. No signs of reaction were detected after 4 days of irradiation.

6.2.10 Photolysis of Pt(PPh₃)₂(PhOCNNCOPh) **1**, Pt(PMe₃)₂(PhOCNNCOPh) **3** and Pt(PMe₃)₂(MeOCNNCOMe) **4** with ethene or diphenylacetylene in CDCl₃

NMR samples of **1**, **3** and **4** were photolysed in CDCl₃ with either excess diphenylacetylene or under 1 atmosphere of ethene. Photolysis of these samples was stopped periodically and checked by ¹H and ³¹P {¹H} NMR spectroscopy for signs of reaction. After two days of photolysis, the major product formed with **1** was *cis*-Pt(PPh₃)₂Cl₂, and for **3** and **4** was *cis*-Pt(PMe₃)₂Cl₂.

6.2.11 Photolysis of Pt(PPh₃)₂(EtO₂CNNCO₂Et) **2** and Pt(PPh₃)₂(PrⁱO₂CNNCO₂Prⁱ) **5** with ethene or diphenylacetylene in C₆D₆

NMR samples of **2** and **5** were photolysed with excess diphenylacetylene or under an atmosphere of ethene. After two days of photolysis, either Pt(PPh₃)₂(η²-C₂H₄) or Pt(PPh₃)₂(η²-PhC≡CPh) was formed as determined by their ¹H and ³¹P {¹H} NMR spectra.^{4,8}

6.2.12 Thermal reaction of Pt(PPh₃)₂(EtO₂CNNCO₂Et) **2** and Pt(PPh₃)₂(PrⁱO₂CNNCO₂Prⁱ) **5** with ethene or diphenylacetylene in C₆D₆

NMR samples of **2** and **5** were heated at 60 °C with excess diphenylacetylene or under an atmosphere of ethene. The samples were shielded from light with aluminium foil. After 1 day, either Pt(PPh₃)₂(η²-C₂H₄) or Pt(PPh₃)₂(η²-PhC≡CPh) was formed as determined by their ¹H and ³¹P {¹H} NMR spectra.^{4,8}

6.3 SYNTHESIS AND REACTIONS OF AZO INHIBITED PLATINUM HYDROSILATION CATALYSTS

6.3.1 Synthesis of [(Pt{η⁴-(CH₂=CHSiMe₂)₂O})₂(μ-(CH₂=CHSiMe₂)₂O)] **8**

The synthesis of **8** follows the procedure reported by Lappert and co-workers,⁹ with minor modifications. H₂PtCl₆ (5.0 g) was added to a 250 mL round bottom flask. To this degassed water (0.6 g) and (CH₂=CHSiMe₂)₂O (50.0 g) was also added, the mixture was stirred and refluxed under a nitrogen atmosphere for 10 h. The reaction vessel was then allowed to cool to room temperature and the volatiles removed under vacuum to yield a yellow oil. The yellow oil was dissolved in hexane and NaHCO₃ (0.8 g) was added in small portions with continuous stirring. The mixture was then filtered through Celite, using hexane as an eluant. A majority of the oligomeric siloxanes and free (CH₂=CHSiMe₂)₂O can be removed by eluting a hexane solution of **8** through a

column of silica. Complex **8** was removed from the silica by eluting with acetone. The yield of **8** was calculated to be 74 %, *via* quantitative ^{29}Si { ^1H } NMR spectroscopy using an inverse gated pulse sequence.¹⁰ The preparation of **8** was carried out in minimal lighting.

6.3.2 Synthesis of $\text{PtCl}_2(\text{CH}_2=\text{CHPh})_2$

$\text{PtCl}_2(\text{CH}_2=\text{CHPh})_2$ was prepared as described by Pregosin and co-workers.¹¹ A 250 mL round bottom flask was charged with PtCl_2 (3.0 g), and styrene (60 mL) and stirred for 4 days at room temperature. An intensely red solution and a yellow precipitate was formed over this period. The yellow precipitate was collected and washed with toluene (2 x 10 mL) and then hexane (2 x 10 mL). The yellow solid of $\text{PtCl}_2(\text{CH}_2=\text{CHPh})_2$ was dried under vacuum for 2 h (yield 50 %).

6.3.3 Synthesis of **8** with $\text{PtCl}_2(\text{CH}_2=\text{CHPh})_2$

This was prepared as described in Section 6.3.1, using $\text{PtCl}_2(\text{CH}_2=\text{CHPh})_2$ instead of H_2PtCl_6 relaxed in toluene.

6.3.4 Inhibition of **8** with $\text{RO}_2\text{CNNCO}_2\text{R}$ to form **9** (R = Et), **10** (R = Prⁱ) and **11** (R = Bu^t)

Typically a two-fold excess of the azo dicarboxylate inhibitor, $\text{RO}_2\text{CNNCO}_2\text{R}$, is stirred with **8** (0.5 g) in toluene (10 mL). The mixture was then eluted through a column of silica with toluene to remove excess vinylsiloxanes, oligomers and free azo inhibitors. Azo inhibited **8** was then obtained by eluting the silica column with a 50:50 acetone:toluene mixture. Removal of solvent under vacuum yielded a yellow/brown oil which precipitated a light brown solid upon addition of hexane (10 mL). The light brown solid was collected, washed with hexane and dried under vacuum (yield 10-15 %).

6.3.5 Model hydrosilation system using 1-octene and 1,1,1,3,5,5,5,-heptamethyl-trisiloxane and azo inhibited **8**

A typical model hydrosilation involved dissolving **8** in 1-octene (12.2 g) (1 % wt. Pt). To this solution a 40 fold excess, relative to platinum, of the azo dicarboxylate inhibitor $\text{RO}_2\text{CNNCO}_2\text{R}$ was added. Equal molar quantities of 1,1,1,3,5,5,5,-heptamethyl-trisiloxane (24.2 g), relative to 1-octene, was then added to the rest of the reaction mixture. The reaction mixture was left at room temperature for up to 4 h and

checked by GC to ensure no hydrosilation has taken place. Equal quantities (*ca.* 2 mL) of the reaction mixture were then transferred into two Pyrex sample tubes, one of which was shielded with foil. The sample tubes were immersed in water and photolysed for a measured amount of time (up to 5 minutes). Once photolysis had finished, 1 μL samples were taken from the photolysed and the control reaction mixture and were then subsequently monitored by GC. Further GC samples were taken at regular intervals and the progress of the increase in hydrosilation product was monitored with respect to time.

GC conditions employed: oven temperatures were at 100-250 $^{\circ}\text{C}$ at 20 $^{\circ}\text{C}$ / min, injection temperature and detector temperature were at 300 $^{\circ}\text{C}$. A 1 m long OV 101 packed column was used.

6.4 SYNTHESIS AND REACTIONS OF PLATINUM BIS(PHOSPHINE) CARBOXYLATES COMPLEXES

The compounds *cis*-Pt(PMe₃)₂Cl₂,³ Pt(dppe)Cl₂,¹² Pt(COD)Cl₂,¹³ Ag₂(O₂CCH₂-CO₂)¹⁴ and Ag₂[O₂C(C₆H₄)CO₂]¹⁴ were prepared according to literature procedures.

6.4.1 Preparation of Pt(dppe)(O₂CCH₂CO₂) 12

The complex Pt(dppe)(O₂CCH₂CO₂) was prepared with minor modifications to the procedure reported by Anderson and co-workers.¹⁵ Pt(dppe)Cl₂ (1.00 g, 2 mmol) was dissolved in a minimum amount of dichloromethane or chloroform. An excess of the silver malonate salt, Ag₂(O₂CCH₂CO₂) (3.0 g, 6 mmol), was then added to the solution. The reaction mixture was left stirring for 72 h at room temperature, whilst shielded from light. The mixture was then filtered and the resultant solution concentrated under reduced pressure to *ca.* 5 mL. Addition of ether at this point precipitated the white complex Pt(dppe)(O₂CCH₂CO₂) **12**. The complex was collected, washed with ether and dried under vacuum (Yield 1.2 g, 83 %). Mass spectrum (FAB): *m/z* 696 {*M*⁺, [¹⁹⁵Pt + H]⁺ and [*M* + 2H]⁺, ¹⁹⁴Pt, 100 %}. ¹H NMR spectrum (300.13 MHz, CD₃CN, 295 K): δ 2.58 [d, PCH₂, ²*J*(PH) = 17.3 Hz], δ 3.34 (s, O₂CCH₂CO₂), δ 7.60-7.50 (m, Ph). ¹³C {¹H} NMR spectrum (75.47 MHz, CD₂Cl₂, 295 K) δ 27.5 [d, PCH₂, *J*(PC) = 51 Hz], δ 51.1 (s, O₂CCH₂CO₂), δ 126.4-133.7 (Ph), δ 174.0 (s, O₂CCH₂CO₂). ³¹P {¹H} NMR spectrum (121.94 MHz, CD₃CN, 295 K): δ 32.7 [s, *J*(PtP) = 3665 Hz]. IR (KBr): ν (C=O) 1649 cm⁻¹, ν (C-O) 1354 cm⁻¹.

6.4.2 Preparation of Pt(PMe₃)[O₂C(1,2-C₆H₄)CO₂] **13**

Complex **13** was prepared from *cis*-Pt(PMe₃)₂Cl₂ (1.0 g, 2.4 mmol) and Ag₂[O₂C(1,2-C₆H₄)CO₂] using the same procedure as for complex **12** (Yield 0.73 g, 60 %). (Found: C, 32.7; H, 4.3. Calc. for C₁₄H₂₂O₄P₂Pt: C, 32.9; H, 4.3). Mass spectrum (FAB): *m/z* 512 {M⁺, [¹⁹⁵Pt + H]⁺ and [M + 2H]⁺, ¹⁹⁴Pt, 100 %}. ¹H NMR spectrum (300.13 MHz, CD₃CN, 295 K): δ 1.51 [d, PCH₃, ²J(PH) = 11.7 Hz, J(PtH) = 36.2], δ 7.35-7.50 [m, O₂C(C₆H₄)CO₂]. ¹³C {¹H} NMR spectrum (75.47 MHz, CD₂Cl₂, 295 K) δ 14.6 (m, PCH₃), δ 127.4-139.2 [m, O₂C(*o,m*-C₆H₄)CO₂], δ 175.3 [s, O₂C(*o,m*-C₆H₄)CO₂]. ³¹P {¹H} NMR spectrum (121.94 MHz, CD₃CN, 295 K): δ -27.4 [s, J(PtP) = 3564 Hz].

6.4.3 Preparation of Pt(COD)(O₂CCH₂CO₂) **14**

Complex **14** was prepared from Pt(COD)Cl₂ (1.0 g, 2.7 mmol) and Ag₂(O₂CCH₂CO₂) using the same procedures as for complexes **12** and **13** (Yield 0.9 g, 81 %). Mass spectrum (FAB): *m/z* 406 {M⁺, [¹⁹⁵Pt + H]⁺ and [M + 2H]⁺, ¹⁹⁴Pt, 100 %}. ¹H NMR spectrum (300.13 MHz, CD₂Cl₂, 295 K): δ 2.30, 2.73 [br. m, CH₂CH₂ (COD)], δ 3.37 (s, O₂CCH₂CO₂), δ 5.39 (br. s, CH=CH (COD)), J(PtH) = 66.5 Hz]. IR (CH₂Cl₂): ν(C=O) 1674 cm⁻¹, ν(C-O) 1340 cm⁻¹.

6.4.4 Photolysis of Pt(dppe)(O₂CCH₂CO₂) **12**

Photolysis of **12** in CD₃CN for up to 4 days with either diphenylacetylene or ethene (1 atm) resulted in low conversion to an unidentified yellow compound **A4**. ³¹P {¹H} NMR spectrum (121.94 MHz, CD₃CN, 295 K): δ 47.6 [J(PtP) = 3625 Hz].

6.4.5 Photolysis of Pt(PMe₃)₂(PMe₃)₂[O₂C(C₆H₄)CO₂] **13**

Prolonged photolysis of **13** in CD₃CN with either diphenylacetylene or ethene (1 atm) yielded small amounts of two products, Pt(PMe₃)₂[O₂C(C₆H₄)CO₂] **B4** and the unassigned product **C4**. ¹H NMR spectrum (300.13MHz, CD₃CN, 295 K) of **B4**: δ_H 1.78 [d, PCH₃, J(PH) = 11.2 Hz], δ 1.86 [d, PCH₃, J(PH) = 11.0 Hz]. ³¹P {¹H} NMR spectrum (121.94 MHz, CD₃CN, 295 K) of **B4**: δ -11.2 [d, P^C, J(PP) = 19 Hz, J(PtP) = 1849 Hz], δ -29.7 [d, P^O, J(PP) = 19 Hz, J(PtP) = 3712 Hz]. ¹H NMR spectrum (300.13MHz, CD₃CN, 295 K) of **C4**: δ 1.62 [d, PCH₃, J(PH) = 9.8 Hz]. ³¹P {¹H} NMR spectrum (121.94 MHz, CD₃CN, 295 K) of **C4**: δ -28.2 [s, J(PtP) = 3960 Hz].

6.5 SYNTHESIS AND REACTIONS OF PLATINUM BIS(PHOSPHINE) SILYL HYDRIDE COMPLEXES

6.5.1 Preparation of Pt(PCy₃)₂

Pt(PCy₃)₂ was prepared with a slight variation to the procedure described in the literature.¹⁶ Crude *trans*-Pt(PCy₃)₂Cl₂ (2.22 g, 2.69 mmol), PCy₃ (0.02 g) and a magnetic stirrer bar were placed in a 100 mL Schlenk tube. To this a 0.33 M tetrahydrofuran solution of sodium naphthalene solution [prepared from sodium (0.5 g) and naphthalene (2.2 g) in THF (50 mL)] was added dropwise with stirring under an atmosphere of argon. The mixture gradually changed colour to red-brown and addition of the sodium naphthalene solution was stopped when the reaction mixture sustained a brown-green colour. The mixture was then stirred for a further 1-2 h, and the solvent was removed under vacuum leaving a brown-green residue. The brown-green residue was extracted with hexane (2 x 25 mL) and filtered under argon to give a yellow solution. The yellow hexane solution was concentrated under vacuum leaving behind the yellow complex of Pt(PCy₃)₂ which was contaminated with naphthalene. The unwanted naphthalene was removed by sublimation. Pt(PCy₃)₂ was used without further purification, since attempts on recrystallisation in hexane often resulted in the formation of phosphine oxide and the platinum oxygen complex Pt(PCy₃)₂(O₂) (Yield 0.86 g, 42 %). ¹H NMR spectrum (500.13 MHz, C₆D₆, 300 K): δ 1.30-2.40 (m, C₆H₁₁). ³¹P {¹H} NMR spectrum (202.46 MHz, C₆D₆, 300 K): δ 61.5 [s, *J*(PtP) = 4163 Hz].

6.5.2 Preparation of *trans*-Pt(PCy₃)₂(H)₂

The complex *trans*-Pt(PCy₃)₂(H)₂ was prepared by N. Jasim at York, using the following procedures. Pt(PCy₃)₂ (0.50 g, 0.66 mmol) was dissolved in hexane, then carbon dioxide and oxygen were bubbled simultaneously through the solution. The white platinum peroxy carbonato complex precipitated out of solution and was collected and dried under reduced pressure. The platinum peroxy carbonato complex was stirred with excess NaBH₄ in ethanol for 10 min to give *trans*-platinum bis(phosphine) dihydride *trans*-Pt(PCy₃)₂H₂. Excess solvent was removed under vacuum. The platinum dihydride complex was extracted from the solid with benzene and recrystallised from a 1:1 methanol/benzene solution (Yield 0.2 g, 45 %). ¹H NMR spectrum {500.13 MHz, [²H₈]toluene, 300 K}: δ -3.08 [t, PtH₂, ²*J*(PH)_{cis} = 17.2 Hz, *J*(PtH) = 793.1 Hz]. ³¹P {¹H} NMR spectrum {202.46 MHz, [²H₈]toluene, 300 K}: δ 52.4 [s, *J*(PtP) = 2887 Hz].

6.5.3 Preparation of *cis*-Pt(PCy₃)₂(H)(SiPh₃) **15**

Pt(PCy₃)₂ (0.10 g, 0.15 mmol) was dissolved in pentane or hexane (15 mL). To this triphenylsilane (0.07 g, 0.26 mmol) in pentane or hexane (10 mL) was added dropwise with stirring. The reaction mixture was then left stirring in an ice bath for 12 h and a white precipitate was formed. The white solid of *cis*-Pt(PCy₃)₂(H)(SiPh₃) **15** was collected and washed with 3 x 10 mL of cold pentane or hexane (Yield 0.70 g, 47 %) (Found: C, 63.8; H, 8.1. Calc. for C₅₄H₈₂P₂SiPt: C, 63.1; H, 8.1). Mass Spectrum (FAB): *m/z* 1014 {*M*⁺, ¹⁹⁴Pt, 18 %}, *m/z* 1015 {*M*⁺, ¹⁹⁵Pt and [*M* + H]⁺, ¹⁹⁴Pt, 79 %}. ¹H NMR spectrum {500.13 MHz, [²H₈]toluene, 250 K}: δ -3.95 [1H, dd, PtH, ²*J*(PH)_{*cis*} = 23.3 Hz, ²*J*(PH)_{*trans*} = 141.8 Hz, *J*(PtH) = 784.2 Hz], δ 1.12-2.50 (22H, m, PC₆H₁₁), δ 7.20-8.40 (10H, m, PC₆H₅). ³¹P {¹H} NMR spectrum {202.46 MHz, [²H₈]toluene, 250 K}: δ 37.3 [d, P^H, *J*(PP) = 13 Hz, *J*(PtP) = 2642 Hz], δ 41.1 [d, P^{Si}, *J*(PP) = 13 Hz, *J*(PtP) = 1560 Hz]. ¹⁹⁵Pt {¹H} NMR spectrum: δ -5205 [dd, *J*(PtP^{Si}) = 1555 Hz, *J*(PtP^H) = 2650 Hz]. IR (KBr): ν(Pt-H) 2078 cm⁻¹.

6.5.4 Preparation of *cis*-Pt(PCy₃)₂(H)(SiMe₂CH₂CH=CH₂) **16**

Complex **16** was prepared using the same procedure as for *cis*-Pt(PCy₃)₂(H)(SiPh₃). Pt(PCy₃)₂ (0.43 g, 0.57 mmol) and HSiMe₂CH₂CH=CH₂ (0.33 μL, 2.27 mmol) was dissolved in hexane and left stirring in an ice bath for 5 h. The white solid formed was collected and wash with 3 x 10 mL of cold hexane (Yield 0.20g, 41 %) (Found: C, 56.3; H, 9.1. Calc. for C₄₁H₇₈P₂SiPt: C, 57.5; H, 9.2). Mass Spectrum (FAB): *m/z* 854 {*M*⁺, ¹⁹⁴Pt, 18 %}, *m/z* 855 {*M*⁺, ¹⁹⁵Pt and [*M* + H]⁺, ¹⁹⁴Pt, 79 %}. ¹H NMR spectrum {500.13 MHz, [²H₈]toluene, 240 K}: δ -3.46 [1H, dd, PtH, ²*J*(PH)_{*cis*} = 26.1 Hz, ²*J*(PH)_{*trans*} = 144.1 Hz, *J*(PtH) = 853.3 Hz], δ 1.05 [6H, d, SiCH₃, ⁴*J*(PH) = 1.6 Hz, ³*J*(PtH) = 26.5 Hz], δ 1.10-2.30 (22H, m, PC₆H₁₁), δ 2.41 [2H, d, SiCH₂CH=CH₂, *J*(HH) = 8.3 Hz, ³*J*(PtH) = 30.8 Hz], δ 5.16, δ 5.25 (2H, m, SiCH₂CH=CH₂), δ 6.52 (H, m, SiCH₂CH=CH₂). ³¹P {¹H} NMR spectrum {202.46 MHz, [²H₈]toluene, 240}: δ 41.6 [d, P^H, *J*(PP) = 12 Hz, *J*(PtP) = 2677 Hz], δ 42.8 [d, P^{Si}, *J*(PP) = 12 Hz, *J*(PtP) = 1420 Hz]. IR (KBr): ν(PtH) 2085 cm⁻¹.

6.5.5 Preparation of *cis*-Pt(PCy₃)₂(H)(SiMe₂Et) **17**

Complex **17** was prepared *in situ* in an NMR tube by reacting Pt(PCy₃)₂ with an excess amount of HSiMe₂Et in [²H₈]toluene at -77 °C. Attempts to obtain a solid by reacting Pt(PCy₃)₂ and HSiMe₂Et in hexane only resulted in an oily residue. ¹H NMR spectrum {500.13 MHz, [²H₈]toluene, 240 K}: δ -3.54 [1H, dd, PtH, ²*J*(PH)_{*cis*} = 25.8 Hz, ²*J*(PH)_{*trans*} = 144.0 Hz, *J*(PtH) = 858.3 Hz], δ 0.85 [6H, d, SiCH₃, ⁴*J*(PH) = 1.6 Hz,

$^3J(\text{PtH}) = 26.7 \text{ Hz}$], δ 1.10 - δ 2.40 [27H, m, PC_6H_{11} , SiCH_2CH_3]. ^{31}P $\{^1\text{H}\}$ NMR spectrum {202.46 MHz, [$^2\text{H}_8$]toluene, 240}: δ 42.2 [d, P^{H} , $J(\text{PP}) = 12 \text{ Hz}$, $J(\text{PtP}) = 2704 \text{ Hz}$], δ 43.1 [d, P^{Si} , $J(\text{PP}) = 12 \text{ Hz}$, $J(\text{PtP}) = 1387 \text{ Hz}$].

6.5.6 Preparation of $\text{HSiMe}_2\text{OCH}_2\text{C}(\text{Me})=\text{CH}_2$

$\text{CH}_2=\text{C}(\text{Me})\text{CH}_2\text{OH}$ (5.4 mL, 64.0 mmol) and NEt_3 (9.0 mL, 63.0 mmol) were added to 175 mL of ether in a 1 L two necked round bottom flask and cooled in an ice bath. HSiMe_2Cl (7.4 mL, 66.6 mmol) was added dropwise to the mixture with vigorous stirring over the course of 20 minutes, where upon a white precipitate of ammonium chloride was formed. The mixture was left stirring for 15 h and then filtered through Celite. Volatiles were removed under vacuum leaving an opaque liquid. The product was collected in a liquid nitrogen trap on a high vacuum line. Small amounts of ether were detected as impurities in the final product. ^1H NMR spectrum (300.13 MHz, C_6D_6 , 295 K): δ 0.11 (6H, d, SiCH_3 , $^3J(\text{HH}) = 2.9 \text{ Hz}$), δ 1.58 [3H, m, $\text{CH}_2\text{C}(\text{CH}_3)=\text{CH}_2$], δ 3.93 [2H, m, $\text{CH}_2\text{C}(\text{CH}_3)=\text{CH}_2$], δ 4.82 [1H, m, $\text{CH}_2\text{C}(\text{CH}_3)=\text{CH}_2$], δ 4.84 [1H, sept, SiH , $^3J(\text{HH}) = 2.9 \text{ Hz}$], δ 5.10 [1H, m, $\text{CH}_2\text{C}(\text{CH}_3)=\text{CH}_2$].

6.5.7 Preparation of *cis*- $\text{Pt}(\text{PCy}_3)_2(\text{H})[\text{SiMe}_2\text{OCH}_2\text{C}(\text{Me})=\text{CH}_2]$ 18

This complex was prepared by reacting $\text{Pt}(\text{PCy}_3)_2$ and excess $\text{HSiMe}_2\text{OCH}_2\text{C}(\text{Me})=\text{CH}_2$ in [$^2\text{H}_8$]toluene *in situ* at $-78 \text{ }^\circ\text{C}$. Attempts at obtaining a solid product only yielded an oily residue. ^1H NMR spectrum {500.13 MHz, [$^2\text{H}_8$]toluene, 250 K}: δ -4.15 [1H, dd, PtH , $^2J(\text{PH})_{\text{cis}} = 27.7 \text{ Hz}$, $^2J(\text{PH})_{\text{trans}} = 140.5 \text{ Hz}$, $J(\text{PtH}) = 888.5 \text{ Hz}$], δ 1.16 [6H, s, SiCH_3 , $^3J(\text{PtH}) = 29.9 \text{ Hz}$], δ 1.20-2.40 [25H, m, PC_6H_{11} , $\text{CH}_2\text{C}(\text{CH}_3)=\text{CH}_2$], δ 4.52 (2H, br., SiOCH_2); δ 5.24, δ 5.51 [2H, br., $\text{C}(\text{CH}_3)=\text{CH}_2$]. ^{31}P $\{^1\text{H}\}$ NMR spectrum {202.46 MHz, [$^2\text{H}_8$]toluene, 250 K}: δ 41.9 [d, P^{H} , $J(\text{PP}) = 13 \text{ Hz}$, $J(\text{PtP}) = 2658 \text{ Hz}$], δ 42.0 [br., P^{Si} , $J(\text{PtP}) = 1369 \text{ Hz}$].

6.5.8 Preparation of *cis*- $\text{Pt}(\text{PCy}_3)_2(\text{H})[\text{Si}(\text{OMe})_2\text{CH}_2\text{CH}=\text{CH}_2]$ 19

Complex **19** was prepared by reacting $\text{Pt}(\text{PCy}_3)_2$ and excess $\text{HSi}(\text{OMe})_2\text{CH}_2\text{CH}=\text{CH}_2$ in C_6D_6 in an NMR tube at room temperature. Attempts to isolate this product only produced an oily residue. ^1H NMR spectrum (200.13 MHz, C_6D_6 , 295 K): δ -4.00 [1H, dd, PtH , $^2J(\text{PH})_{\text{cis}} = 28.0 \text{ Hz}$, $^2J(\text{PH})_{\text{trans}} = 141.8 \text{ Hz}$, $J(\text{PtH}) = 863.4 \text{ Hz}$], δ 0.80 - δ 2.77 (22H, m, PC_6H_{11}), δ 2.40 [2H, d, $\text{SiCH}_2\text{CH}=\text{CH}_2$, $J(\text{HH}) = 8.9 \text{ Hz}$], δ 3.84 [6H, s, $\text{Si}(\text{OCH}_3)_2$], δ 5.13 - δ 5.30 (2H, m, $\text{SiCH}_2\text{CH}=\text{CH}_2$), δ 6.50 (1H, m, $\text{SiCH}_2\text{CH}=\text{CH}_2$). ^{31}P $\{^1\text{H}\}$ NMR spectrum (81.02 MHz, C_6D_6 , 295 K): δ 41.9 [d, P^{Si} , $J(\text{PP}) = 14 \text{ Hz}$, $J(\text{PtP}) = 1408 \text{ Hz}$], δ 42.4 [br. d, P^{H} , $J(\text{PtP}) = 2638 \text{ Hz}$].

6.5.9 Preparation of *cis*-Pt(PCy₃)₂(H)(SiPh₂OSiPh₂H) **20**

Complex **20** was prepared by reacting Pt(PCy₃)₂ and HSiPh₂OSiPh₂H in a 1:1 ratio in C₆D₆ in an NMR tube at room temperature. ¹H NMR spectrum (200.13 MHz, C₆D₆, 295 K): δ -4.00 [1H, dd, PtH, ²J(PH)_{cis} = 27.2 Hz, ²J(PH)_{trans} = 140.7 Hz, J(PtH) = 851.4 Hz], δ 0.71 - δ 2.79 (22H, m, PC₆H₁₁). δ 6.06 [1H, s, SiH, J(SiH) = 213.0 Hz], δ 7.04-7.15 (20H, m, SiC₆H₅). ³¹P {¹H} NMR spectrum (81.02 MHz, C₆D₆, 295 K): δ 43.1 [d, P^{Si}, J(PP) = 15 Hz, J(PtP) = 1428 Hz], δ 43.4 [d, P^H, J(PP) = 15 Hz, J(PtP) = 2612 Hz].

Using a 2:1 ratio of Pt(PCy₃)₂ and HSiPh₂OSiPh₂H in the reaction at room temperature only resulted in the formation of *cis*-Pt(PCy₃)₂(H)(SiPh₂OSiPh₂H) **20**. Chelating disilyl complexes or dimeric species were not detected.

6.5.10 Reaction of Pt(PCy₃)₂ with HSiMe₂(C₆H₄)SiMe₂H

Pt(PCy₃)₂ and HSiMe₂C₆H₄SiMe₂H were reacted in [²H₈]toluene in an NMR tube at -77 °C to form an unidentified platinum hydride phosphine complex **A5**. Attempts to isolate **A5** only resulted in an oily residue. ¹H NMR spectrum {500.13 MHz, [²H₈]toluene, 295 K}: δ -1.89 [br, J(PtH) = 675.2 Hz], δ 0.94 [s, Si(CH₃)₂, J(PtH) = 28.3 Hz]. ¹H NMR spectrum {500.13 MHz, [²H₈]toluene, 200 K}: δ -1.89 [d, J(PH) = , J(PtH) = 675.2 Hz], δ 0.94 [s, Si(CH₃)₂, J(PtH) = 28.3 Hz]. ³¹P {¹H} NMR spectrum {202.46 MHz, [²H₈]toluene, 295 K}: δ 56.1 [br, J(PtP) = 1531 Hz]. ¹⁹⁵Pt {¹H} NMR spectrum {107.52 MHz, [²H₈]toluene, 200 K}: δ -5700 [d, J(PtP) = 1538 Hz].

At room temperature, reaction of Pt(PCy₃)₂ and HSiMe₂C₆H₄SiMe₂H formed a new unidentified platinum species **B5**, along with **A5** which was initially formed at low temperature. Warming a sample of **A5** to room temperature only resulted in gradual decomposition to the *trans*-platinum dihydride, no formation of **B** was detected. ³¹P {¹H} NMR spectrum {81.02 MHz, C₆D₆, 295 K} of **B5**: δ 33.5 [s, J(PtP) = 1437 Hz].

6.5.11 Thermolysis of *cis*-Pt(PCy₃)₂(H)(SiMe₂CH₂CH=CH₂) **16**

Complex **16** (ca. 30 mg) was dissolved in 5 mL of C₆D₆ under an argon atmosphere. Immediate GC analysis of this sample showed that only one volatile species was present which corresponded to HSiMe₂CH₂CH=CH₂ in C₆D₆. Over a period of 30 minutes, GC analysis of the sample showed the disappearance of HSiMe₂CH₂CH=CH₂ and the formation of three new products with retention times of 7.2, 19.0 and 33.9 minutes. GC/MS analysis of the three major products contains the following dominant mass spectral peaks: 7.2 min [*m/z* = 73 (15 %), 133 (100 %), 173 (33 %), 175 (23 %)]. 19.0 min [*m/z* = 41 (36 %), 55 (56 %), 81 (24 %), 83 (25 %), 115

(25 %), 116 (27 %), 117 (100 %), 198 (89 %), 199 (36 %), 280 (25 %)]. 33.9 min [m/z = 41 (25 %), 55 (42 %), 132 (40 %), 133 (54 %), 214 (100 %)].

GC conditions employed: oven temperatures were at 40-200 °C at 15 °C / min, injection temperature and detection temperature were at 250 °C. A 12 m long methylsilicone packed column was used.

6.5.12 Photolysis of *cis*-Pt(PCy₃)₂(H)(SiR¹₂R²) [R¹ = R² = Ph (15); R¹ = Me, R² = CH₂CH=CH₂ (16)]

NMR samples of complexes **15** and **16** in [²H₈]toluene were photolysed for 4 h at -78 °C and partially yields *trans*-Pt(PCy₃)₂(H)(SiPh₃)₂ **21** and *trans*-Pt(PCy₃)₂(H)(SiMe₂CH₂CH=CH₂) **22**. ¹H NMR spectrum of **21** {500.13 MHz, [²H₈]toluene, 250 K}: δ -3.00 [t, PtH, ²J(PH) = 16.6 Hz, J(PtH) = 584.2 Hz]. ³¹P {¹H} NMR spectrum of **21** {202.46 MHz, [²H₈]toluene, 250 K}: δ 37.5 [s, J(PtP) = 2656 Hz]. ¹H NMR spectrum of **22** {500.13 MHz, [²H₈]toluene, 250 K}: δ -2.64 [t, PtH, ²J(PH) = 18.1 Hz, J(PtH) = 584.2 Hz]. ³¹P {¹H} NMR spectrum of **22** {202.46 MHz, [²H₈]toluene, 250 K}: δ 37.5 [s, J(PtP) = 2747 Hz].

6.5.13 Photolysis of *trans*-Pt(PCy₃)₂(H)₂ with HSiMe₂Et

An excess amount of HSiMe₂Et was added to an NMR sample of *trans*-Pt(PCy₃)₂(H)₂ in C₆D₆ at room temperature. The sample was monitored by ¹H and ³¹P{¹H} NMR spectroscopy and no reaction was observed between the silane and the platinum dihydride complex. A small amount of *trans*-Pt(PCy₃)₂(H)(SiMe₂Et) **23** was formed after 1 day of photolysis. ¹H NMR spectrum of **23** {500.13 MHz, C₆D₆, 300 K}: δ -2.85 [t, PtH, ²J(PH) = 18.5 Hz, J(PtH) = 552.1 Hz]. ³¹P {¹H} NMR spectrum of **23** {202.46 MHz, C₆D₆, 250 K}: δ 37.5 [s, J(PtP) = 2747 Hz].

An NMR sample of *trans*-Pt(PCy₃)₂(H)₂ with an excess amount of HSiMe₂Et in [²H₈]toluene was prepared at room temperature. NMR spectroscopy of the sample with *in situ* photolysis, performed by John Lowe at the University of York, was carried out at 250 K. After 1 h of *in situ* photolysis, a small amount of *cis*-Pt(PCy₃)₂(H)(SiMe₂Et) was detected in the ¹H NMR spectrum.

6.5.14 Thermodynamic and kinetic measurements of dynamic processes in *cis*-Pt(PCy₃)₂(H)(SiR¹₂R²) [R¹ = R² = Ph (15); R¹ = Me, R² = CH₂CH=CH₂ (16); R¹ = Me, R² = Et (17)]

NMR samples of complexes **15** and **16** were prepared by distillation of [²H₈]toluene into a Pyrex NMR tube, using a liquid nitrogen trap, containing complexes

15 or **16** on a high vacuum line. NMR samples of complex **17** were prepared by distillation of a solution of HSiMe₂Et (1 equivalent relative to Pt) in [²H₈]toluene into a Pyrex NMR tube containing Pt(PCy₃)₂. All samples were kept cold in liquid nitrogen prior to NMR spectroscopy. For each complex, quantitative ¹H and ³¹P {¹H} NMR spectra were recorded in the range of 250-300 K. Samples were left for 30 minutes at each temperature prior to obtaining the spectrum. The ¹H NMR resonance of the Si-H group on the free silanes was found to have a long relaxation time of up to 8 seconds at room temperature. A 60 seconds delay between acquisition was therefore used to allow for reliable integration analysis of the proton spectrum. Quantitative ³¹P {¹H} NMR spectra were acquired using an inverse-gated pulse.¹⁰

Integration values of the hydride and Si-H signals in the ¹H NMR spectra, and the Pt(PCy₃)₂ and the Pt(PCy₃)₂(H)(SiR₃)₂ signals from the ³¹P {¹H} NMR spectra were used to determine the thermodynamic parameters for complexes **15-17**. Kinetic data were obtained by simulation of the hydride resonance using the computer programme DNMR-SIM, see Chapter 5, Section 5.2.6.¹⁷

6.6 REFERENCES

- 1 P. S. Pregosin, *Coord. Chem. Rev.*, 1982, **44**, 247.
- 2 F. R. Hartley, *Organomet. Chem. Rev. A*, 1970, **6**, 119.
- 3 J. G. Evans, P. L. Goggin, R. J. Goodfellow and J. G. Smith, *J. Chem. Soc. (A)*, 1968, 464.
- 4 J. Cook, *J. Am. Chem. Soc.*, 1968, **90**, 1464.
- 5 J. R. Dilworth and A. S. Kasenally, *J. Organomet. Chem.*, 1973, **60**, 203.
- 6 (a) F. Hai-Fu, *SAPI91, Structure Analysis Programs with Intelligent Control*, Rigaku Corporation, Tokyo, Japan, 1993; (b) P.T. Beurskens, G. Admirral, G. Bosman, W. P. Garcia-Granda, H. O. Gould, J. M. Smits and C. Smykalla, *The DIRDIF Program System, Technical Report of the Crystallographic Laboratory*, University of Nijmegen, the Netherlands, 1992; (c) G. M. Sheldrick, *SHELXL 93, Program for Crystal Structure Refinement*, University of Göttingen, Germany, 1993.
- 7 C. K. Johnson, *ORTEP, Report ORNL-5138*, Oak Ridge National Laboratory, Oak Ridge, TN, 1976.
- 8 J. A. Davies, C. T. Eagle and D. E. Otis, *Organometallics*, 1989, **8**, 1080.
- 9 G. Chandra, P. Y. Lo, P. B. Hitchcock and M. F. Lappert, *Organometallics*, 1987, **6**, 191.
- 10 S. Braun, H. -O. Kalinowski and S. Berger, *100 and More Basic NMR Experiments: A Practical Course*, VCH, Cambridge, 1996, 99.

- 11 A. Albinati, W. R. Caseri and P. S. Pregosin, *Organometallics*, 1987, **6**, 788.
- 12 G. K. Anderson, H. C. Clark and J. A. Davies, *Inorg. Chem.*, 1981, **20**, 3607.
- 13 J. X. McDermott, J. F. White and G. M. Whitesides, *J. Am. Chem. Soc.*, 1976, **98**, 6521.
- 14 A. K. Galways, P. J. Herley and M. A. Mohamed, *J. Chem. Soc., Faraday Trans. 1*, 1988, **84**, 729.
- 15 G. K. Anderson and G. J. Lumetta, *Inorg. Chem.*, 1987, **26**, 1291.
- 16 T. Yoshida and S. Otsuka, *Inorganic Synthesis*, 1989, **28**, 113.
- 17 G. Hägele and R. Fuhler, *DNMR-SIM, Simulation for Dynamic NMR Spectra VI.00*, Heinrich-Heine University of Düsseldorf, Germany, 1994.